



University
of Glasgow

Feeney, Andrew (2014) *Nitinol cymbal transducers for tuneable ultrasonic devices*. PhD thesis.

<http://theses.gla.ac.uk/5805/>

Copyright and moral rights for this thesis are retained by the author

A copy can be downloaded for personal non-commercial research or study, without prior permission or charge

This thesis cannot be reproduced or quoted extensively from without first obtaining permission in writing from the Author

The content must not be changed in any way or sold commercially in any format or medium without the formal permission of the Author

When referring to this work, full bibliographic details including the author, title, awarding institution and date of the thesis must be given

NITINOL CYMBAL TRANSDUCERS
FOR TUNEABLE ULTRASONIC
DEVICES

Andrew Feeney

A thesis for the degree of Doctor of Philosophy (PhD)

Submitted to the College of Science and Engineering,
University of Glasgow

December 2014

Declaration

I declare that this thesis is a record of the original work carried out by myself under the supervision of Professor Margaret Lucas in the School of Engineering at the University of Glasgow, United Kingdom, during the period of October 2010 to October 2014. The copyright of this thesis therefore belongs to the author under the terms of the United Kingdom Copyright acts. Due acknowledgement must always be made of the use of any material contained in, or derived from, this thesis. The thesis has not been presented elsewhere in consideration for a higher degree.

Signature:

Printed Name: Mr Andrew Feeney

Signature:

Printed Name: Prof Margaret Lucas

Abstract

In recent years, there has been notable interest in the integration of smart and active materials, such as shape memory alloys, in the design of tuneable and multiple frequency devices. There is a growing desire to be able to tune transducers for a range of applications. As an example, surgical procedures could be enhanced by using an ultrasonic device whose performance could be tailored to penetrate more than one material, such as bone and soft tissue. Research conducted on cymbal transducers, a type of Class V flexensional transducer developed at Pennsylvania State University in the early 1990s, has been largely limited to low power applications, such as for hydrophone systems, and their performance in high power applications has only recently been studied. As such, the integration of smart materials to expand the useful applications of this type of transducer has not been fully explored. In this investigation, a shape memory alloy (SMA) called nickel-titanium, or Nitinol, has been adopted in two forms, one being superelastic and the other shape memory, as the end-cap material in the classical cymbal transducer configuration. The resonant frequencies of these transducers can be tuned by changes to the temperature of the Nitinol, which alters the microstructure, and the modulus, of the material. The microstructure of Nitinol can also be controlled by changes in applied stress. The phases present in the Nitinol microstructure are relatively hard cubic austenite and comparably soft monoclinic martensite. An intermediate phase, called the R-phase, can also appear. This is a rhombohedral distortion of austenite, and has been known to be a source of inconvenience for those who wish to avoid multiple stage transformations. An advantage of using Nitinol end-caps in the classical cymbal transducer configuration is that they are very small, hence minimal thermal energy is required to generate a phase transformation. Also, cymbal transducers are very simple and inexpensive to fabricate.

The first part of this research focuses on the development of a dual resonance cymbal transducer using steel and titanium as the end-cap materials. Dynamic analysis techniques comprising electrical impedance measurements, experimental modal analysis (EMA) and vibration resonance response characterisation (VRRC) using laser Doppler vibrometry are introduced and form the dynamic characterisation process. The experimental data is supported in part by finite element analysis (FEA). It is demonstrated that a major problem in cymbal transducer fabrication is the difficulty in controlling the deposition of epoxy resin which is used to create the mechanical coupling in the transducer. This means that the bond layers in a transducer will likely be dissimilar, thereby introducing asymmetry into the transducer. This asymmetry can contribute to the dual resonance in a cymbal transducer.

The cymbal transducer is designed to be actively tuneable by the incorporation of Nitinol end-caps in the transducer assembly. The characterisation of Nitinol transducers is performed using the dynamic characterisation methods in conjunction with differential scanning calorimetry (DSC). This is a thermoanalytical technique which has been adopted to estimate the transformation temperatures of Nitinol, and hence the temperatures at which each transducer must be driven to generate the desired operating frequencies. It is demonstrated that in certain cases, particularly with respect to superelastic Nitinol, the estimations of the transformation temperatures from the DSC analysis of Nitinol can be misinterpreted.

The dynamic performance of Nitinol vibrating at ultrasonic frequencies has not before been the subject of detailed investigation, including the influence of superelasticity on the vibration response of an ultrasonic transducer. Superelasticity occurs in the austenite phase of Nitinol, where austenite reorients to martensite after a characteristic stress threshold is passed, thereby accommodating very large strains. The results show that whilst Nitinol can be used to fabricate cymbal transducers with tuneable resonant frequencies, there is no evidence that superelasticity contributes to the vibration response of the transducers. The incorporation of shape memory Nitinol in a simple prototype actuator device is also considered, where it appears that the transformation of the shape memory Nitinol is affected by the affixed cylinders used to create the device.

This thesis is for my grandparents.

Acknowledgements

There are many people who have helped me through this research, without whom I would not have finished. Firstly, I want to thank my supervisor, Professor Margaret Lucas, for her expert guidance and confidence in me, and also for sparking my interest in the field of ultrasonics. I have learned so much from her in my time as her PhD student, and I am grateful for all the opportunities she has given me to publish my research and attend international conferences. I also want to acknowledge the Engineering and Physical Sciences Research Council (EPSRC) for the funding of this project.

There are three other people who deserve special thanks for providing me with valuable support and encouragement over the last four years. The first is Dr Fernando Bejarano. We spent many long days, and sometimes nights, in the early stages of our respective investigations working together through experiments and trying to solve the many problems which we encountered. He has become a close friend, and I am very appreciative that I had someone with his ingenuity and knowledge around to help me out when I needed it. Secondly, I want to thank Dr Trevor Hodgkiess for being so helpful and approachable, and especially for giving up much of his valuable time to help me decipher the intricacies of Nitinol. Lastly, and certainly not least, I want to say thanks to Dr Andrew Mathieson. He has become one of my closest friends in the last four years, and in addition to the runs by the River Kelvin, circuit training in the gym and coffee in the morning, he has always made himself available to help me out when I needed it, and I am very grateful for the time he has given to support me with my work during this process.

I am indebted to the technical staff at the University of Glasgow for helping me out so much over the last four years, especially Denis Kearns, George Silvie and Wilson MacDougall. I am particularly grateful for all the hard work Wilson did in fabricating

some of my experimental materials. I must also thank Bernie Hoey and Neil Owen for their assistance with all of my electrical/electronic problems, and Andrew Monaghan of the School of Chemistry for sharing with me his expert knowledge of DSC and XRD.

Although this has been a challenging endeavour, I have found the last four years immensely enjoyable. I have made many friends during this process, and I want to especially thank Malcolm McRobb, Chris Murray, Eimear Neeson and John Russell. I shared an office with John for nearly four years, and he has become a good friend. I want to sincerely thank him for the many interesting discussions, the research troubleshooting, and the sampling of the delights of nearly every lunch establishment in the West End of Glasgow.

I want to thank Kelly for putting up with me through this, and Daniel and Rachel for their interest and always being able to give me new perspectives on what I was doing. My family have been a constant source of encouragement from the very start, and I want to thank my Dad for helping me out, especially for the proof-reading of the thesis in the latter stages, and for being there to discuss aspects of my work when I needed it. Finally, I want to make a special mention of thanks for my Mum, who has always motivated me to try and do the best that I can, and without whom none of this would have been possible.

Nomenclature

Symbol	Definition	Base Unit
a_o	Displacement amplitude	m
A_F	Austenite finish temperature	°C
A_P	Austenite peak temperature	°C
A_S	Austenite start temperature	°C
ADP	Ammonium dihydrogen phosphate	-
$ASDIC$	Allied Submarine Detection Investigation Committee	-
$ATVA$	Adaptive tuned vibration absorber	-
CAD	Computer-aided design	-
$COTS$	Commercial off-the-shelf	-
$Cyl_{L/S,1/2}$	Cylinder (Large/Small), (1,2)	-
d_{31}	Piezoelectric radial charge coefficient	C/N
d_{33}	Piezoelectric longitudinal charge coefficient	C/N
d_h	Hydrostatic piezoelectric charge coefficient	C/N
dT	Change in temperature	°C

$d\sigma$	Plateau stress change	Pa
<i>DIC</i>	Digital image correlation	-
<i>DSC</i>	Differential scanning calorimetry	-
E	Young's modulus	Pa
E_A	Young's modulus of austenite	Pa
E_M	Young's modulus of martensite	Pa
E_R	Young's modulus of the R-phase	Pa
<i>EMA</i>	Experimental modal analysis	-
f	Frequency	Hz
f_a	Anti-resonant frequency	Hz
f_D	Frequency shift	Hz
f_{HT}	Resonant frequency at high temperature	Hz
f_{LT}	Resonant frequency at low temperature	Hz
f_r	Resonant frequency	Hz
<i>FEA</i>	Finite element analysis	-
<i>FEM</i>	Finite element modelling	-
<i>FFT</i>	Fast fourier transform	-
<i>FRF</i>	Frequency response function	-
ΔH	Transformation latent heat	J/kg
<i>HT</i>	High temperature	-
I	Light intensity	Candela

IA	Impedance analysis	-
IR	Infrared	-
k_{eff}	Effective electromechanical coupling factor	%
l	Length	m
$LVDT$	Linear Voltage Differential Transducer	-
LDV	Laser Doppler vibrometer	-
LT	Low temperature	-
LV	Low viscosity	-
m	Mass	m
M_D	Martensite desist/deformation temperature	°C
M_F	Martensite finish temperature	°C
M_P	Martensite peak temperature	°C
M_S	Martensite start temperature	°C
NOL	Naval Ordnance Laboratory	-
NRL	Naval Research Laboratory	-
$PMNT$	Lead magnesium niobate-lead titanate	-
PZT	Lead zirconate titanate	-
Q_m	Mechanical quality factor	-
r	Path length of light	m
R	Radius	m
R_F	R-phase finish temperature on cooling	°C

R_P	R-phase peak temperature on cooling	°C
R_S	R-phase start temperature on cooling	°C
R'_F	R-phase finish temperature on heating	°C
R'_P	R-phase peak temperature on heating	°C
R'_S	R-phase start temperature on heating	°C
s	Displacement	m
SBC	Stress-biased cymbal	-
SMA	Shape memory alloy	-
SME	Shape memory effect	-
T	Temperature	°C
T_{ra}	Reflected apparent temperature	°C
$UMAT$	User material	-
UTS	Ultimate tensile strength	Pa
v	velocity	m.s ⁻¹
V_{p-p}	Peak-to-peak voltage	V
$VRRC$	Vibration resonance response characterisation	-
XRD	X-ray diffraction	-
α	Mass coefficient	-
β	Stiffness coefficient	-
$\Delta\%$	Percentage change	-
ε	Emissivity	-

ε_0	Transformational strain	-
λ	Wavelength	m
ν	Poisson's ratio	-
ξ	Damping ratio	-
ρ	Density	kg.m ⁻³
σ	Stress	Pa
σ_{AF}	Stress required to complete austenite transformation	Pa
σ_{AS}	Stress required to start austenite transformation	Pa
σ_F	Stress finish	Pa
σ_{MF}	Stress required to complete martensite transformation	Pa
σ_{MS}	Stress required to start martensite transformation	Pa
σ_S	Stress start	Pa
ϕ	Diameter	m
ϕ_c	End-cap cavity base diameter	m
ω_a	Angular frequency	rad.s ⁻¹

Contents

Declaration	ii
Abstract	iii
Acknowledgements	vi
Nomenclature	viii
1 Introduction	1
1.1 Cymbal transducers	2
1.1.1 Piezoelectric transduction	3
1.1.2 Transducer Fabrication	4
1.1.3 Applications of cymbal transducers	6
1.1.4 Interest in multiple frequency applications	9
1.2 Nitinol and its characteristics	11
1.3 Nonlinear dynamic behaviour	21
1.4 Original contributions to knowledge	23
1.5 Summary	24
2 Review of the literature	25
2.1 A brief history of ultrasound	25
2.2 Flextensional transducers	27
2.2.1 Early developments in transduction	27
2.2.2 Evolution of flextensional transducers	31
2.2.3 Cymbal transducer research and development	34
2.3 Nitinol and tuneable transducer technology	43

2.3.1	Development of SMAs and understanding nitinol	43
2.3.2	Tuneable and multiple frequency transducers and devices	47
3	A study of an asymmetric cymbal transducer	51
3.1	Transducer design	53
3.1.1	End-cap design and fabrication	53
3.1.2	Piezoceramic selection	56
3.2	Transducer assembly	56
3.3	Dynamic characterisation	59
3.3.1	Thermal loading	59
3.3.2	Resonant frequency characterisation	60
3.3.3	Experimental modal analysis	65
3.3.4	Vibration resonance response characterisation	70
3.4	Finite element modelling and analysis	74
3.4.1	Model development and optimisation	75
3.4.2	Resonant frequency estimation	80
3.4.3	Displacement amplitude estimation	81
3.5	Chapter conclusions	82
4	Recommendations for design with nitinol	84
4.1	Material selection	84
4.2	Transformation temperature identification	85
4.3	Analysis of commercial nitinol	91
4.3.1	Sample preparation	92
4.3.2	Programming and test control	93
4.3.3	Calibration process	94
4.3.4	Results	95
4.4	Transducer assembly	98
4.5	Experimental testing considerations	99
4.5.1	Temperature measurement	99
4.5.2	Mechanical behaviour	103
4.6	Numerical simulation considerations	105

4.7	Chapter summary	106
5	Shape memory nitinol cymbal transducers	108
5.1	Transducer fabrication	108
5.1.1	DSC analysis of the shape memory nitinol	110
5.2	First transducer characterisation	113
5.2.1	Resonant frequency characterisation	114
5.2.2	Vibration resonance response characterisation	116
5.2.3	Modal behaviour	120
5.3	Second transducer characterisation	122
5.3.1	Resonant frequency characterisation	123
5.3.2	Modal behaviour	124
5.3.3	Vibration resonance response characterisation	125
5.4	Finite element analysis	128
5.5	Chapter conclusions	133
6	Superelastic nitinol cymbal transducers	134
6.1	Transducer fabrication	135
6.1.1	DSC analysis of the superelastic nitinol	136
6.2	Dynamic characterisation	138
6.2.1	Resonant frequency characterisation	138
6.2.2	Modal behaviour	141
6.2.3	Vibration resonance response characterisation	141
6.3	Effect of annealing	144
6.3.1	Heat treatment by annealing	145
6.3.2	Resonant frequency characterisation	150
6.3.3	Modal behaviour	152
6.3.4	Vibration resonance response characterisation	152
6.4	Evidence of the superelastic effect	154
6.4.1	Resonant frequencies and modal behaviour	155
6.4.2	Vibration resonance response characterisation	157
6.5	Chapter conclusions	159

7	A tuneable prototype device	161
7.1	Characterisation of the transducer	162
7.1.1	Resonant frequency characterisation	162
7.1.2	Modal behaviour	163
7.2	Characterisation of the prototype device	164
7.2.1	Resonant frequency characterisation	166
7.2.2	Modal behaviour	167
7.2.3	Vibration resonance response characterisation	170
7.3	Chapter conclusions	175
8	Conclusions	176
9	Future research and development	182
A	List of publications	185
	References	187

List of Tables

2.1	Features of the seven flextensional transducer classes	32
3.1	Chemical composition of silver steel	53
3.2	Selected mechanical properties of silver steel and titanium	54
3.3	Chemical composition of titanium T5	54
3.4	End-cap dimensions of the asymmetric cymbal transducer	55
3.5	Data comparison	82
4.1	Transformation temperatures of Flexinol [®]	95
4.2	Emissivity measurements	102
5.1	Chemical elements and quantities used for end-cap fabrication	109
5.2	Geometrical dimensions of the shape memory Nitinol end-caps	109
5.3	Transformation temperatures of shape memory Nitinol	112
5.4	Resonant frequency shifts of the first shape memory transducer	115
5.5	Resonant frequency shifts of the second shape memory transducer	123
5.6	Epoxy resin bond layer properties	129
5.7	Resonant frequency comparison	130
5.8	Material damping in each phase	131
6.1	Geometrical dimensions of the superelastic Nitinol end-caps	135
6.2	Selected superelastic Nitinol properties	136
6.3	Transformation temperatures of superelastic Nitinol	136
6.4	Resonant frequency shifts of the first superelastic transducer	139
6.5	Transformation temperatures of annealed superelastic Nitinol	147
6.6	Resonant frequency shifts of the annealed transducer	152

6.7	Resonant frequency shifts of the third superelastic transducer	157
7.1	Resonant frequency shifts of the transducer	163
7.2	Dimensions of the larger steel cylinders	164
7.3	Dimensions of the smaller steel cylinders	165
7.4	Resonant frequency shifts of the smaller prototype device	170
7.5	Resonant frequency shift comparison	171

List of Figures

1.1	Cutaway schematic of the classical cymbal transducer	3
1.2	The piezoelectric effect	3
1.3	FEA mode shapes of a symmetric cymbal transducer	5
1.4	Transdermal drug delivery designs	7
1.5	Modified cymbal transducer devices	8
1.6	Reorientation of crystal structure for the superelastic effect	14
1.7	The superelastic effect	15
1.8	The superelastic region	16
1.9	The shape memory effect	17
1.10	Nitinol crystal structures	20
1.11	Nonlinear hardening and softening behaviour	22
2.1	The seven flextensional transducer classes	31
2.2	Moonie and cymbal transducers	35
2.3	Timeline of shape memory alloy discovery	44
3.1	Cymbal transducer end-cap geometry	55
3.2	Cymbal transducer assembly rig	57
3.3	Dehydrator chamber	60
3.4	Impedance and phase plots of a cymbal transducer	62
3.5	Impedance and phase plots of the asymmetric transducer	63
3.6	End-cap constraint data of the asymmetric cymbal transducer	64
3.7	A schematic of the LDV	66
3.8	EMA test set-up	67
3.9	EMA measurement grid for a cymbal transducer	69

3.10	EMA results of the asymmetric cymbal transducer	70
3.11	VRRC test set-up	71
3.12	Vibration responses of the symmetric mode	72
3.13	Vibration responses of the asymmetric mode	72
3.14	Dynamic characterisation comparison for the asymmetric transducer . .	73
3.15	Bond layer condition of the asymmetric cymbal transducer	74
3.16	Mesh convergence study of the asymmetric cymbal transducer	77
3.17	Cutaway schematic of the asymmetric transducer FEM	78
3.18	FEA and EMA comparison of the asymmetric cymbal transducer . . .	81
3.19	Displacement amplitude response of each mode from FEA	82
4.1	The active A_F technique	86
4.2	The constant load technique	87
4.3	Analysis of DSC data	89
4.4	Sensitivity and accuracy of DSC data	91
4.5	DSC sample preparation	93
4.6	Placement of test material in DSC	93
4.7	DSC thermograms of low temperature Flexinol [®]	96
4.8	DSC thermograms of high temperature Flexinol [®]	97
4.9	Infrared images of phase transformation	101
5.1	The shape memory Nitinol cymbal transducer	110
5.2	DSC thermograms of shape memory Nitinol	111
5.3	Impedance and phase plots of the first transducer	114
5.4	Vibration responses of mode 1	116
5.5	Initial vibration responses of mode 2	117
5.6	Repeated vibration responses of mode 2	118
5.7	Vibration responses of the small peak	119
5.8	Repeated impedance and phase plots of the first transducer	120
5.9	EMA results of the first shape memory cymbal transducer	120
5.10	Dynamic characterisation comparison for the first transducer	121
5.11	Bond layer condition of the first shape memory transducer	122

5.12	Impedance and phase plots for the second transducer	123
5.13	EMA results of the second shape memory cymbal transducer	124
5.14	Vibration responses of the asymmetric mode	125
5.15	Vibration responses of the symmetric mode	126
5.16	Dynamic characterisation comparison for the second transducer	127
5.17	Vibration response at raised input voltages	127
5.18	Stress distribution in a cymbal transducer from FEA	132
5.19	Normalised stress distribution from FEA	132
6.1	DSC thermograms of superelastic Nitinol	137
6.2	The superelastic nitinol cymbal transducer	138
6.3	Impedance and phase plots of the superelastic transducer	139
6.4	EMA results of the first superelastic cymbal transducer	141
6.5	Vibration responses of the asymmetric mode	142
6.6	Vibration responses of the symmetric mode	142
6.7	Dynamic characterisation comparison for the first transducer	144
6.8	Bond layer condition of the first superelastic transducer	144
6.9	Three conditions of superelastic Nitinol end-cap	147
6.10	DSC thermograms of superelastic Nitinol annealed for one hour	148
6.11	DSC thermograms of superelastic Nitinol annealed for two hours	149
6.12	Initial impedance and phase plots of the annealed transducer	151
6.13	Final impedance and phase plots of the annealed transducer	151
6.14	EMA results of annealed cymbal transducer	152
6.15	Vibration responses of the symmetric mode	153
6.16	Vibration responses of the asymmetric mode	153
6.17	Dynamic characterisation comparison for the annealed transducer	154
6.18	Impedance and phase plots of the third superelastic transducer	156
6.19	EMA results of the third superelastic transducer	156
6.20	Maximum displacement amplitude at 2V of the third transducer	157
6.21	Vibration response of the third transducer at raised voltages	158
7.1	Impedance and phase plots of the transducer	162

7.2	EMA results of the transducer	163
7.3	The prototype device with larger cylinders	164
7.4	Impedance and phase plots of the larger prototype device	165
7.5	The prototype device with smaller cylinders	166
7.6	Impedance and phase plots of the smaller prototype device	166
7.7	EMA measurement grid	167
7.8	EMA results of the prototype device	168
7.9	EMA results of the bending modes	168
7.10	Change in frequency compared to cylinder length	169
7.11	Repeated impedance and phase plots of the smaller prototype device	170
7.12	Vibration responses of the symmetric mode of the prototype	172
7.13	Vibration responses of the asymmetric mode of the prototype	172
7.14	Measurement points on the apex surface of the steel cylinder	173
7.15	Displacement amplitude comparison	174
7.16	Dynamic characterisation comparison for the prototype device	174

Chapter 1

Introduction

There has been a distinct interest in the design and development of transducers and devices in recent years which exhibit tuneable and multiple frequency capability. The improved understanding of the materials which enable these functions has meant that significant progress has been made in the development of such devices. This research is concerned with the design and vibration characterisation of tuneable cymbal transducers, whose resonant frequencies are able to be switched by modest changes to transducer temperature. This has been achieved by the incorporation of nickel-titanium shape memory alloys (SMA) as the end-cap materials in ultrasonic cymbal transducers.

Ultrasound is the name given to the range of frequencies which lie above those of human hearing [1]. The range of human hearing is commonly accepted to be between approximately 20Hz and 20kHz [2], and sounds below this are termed infrasound [3]. Power ultrasonics is the scientific discipline concerned with the administration of ultrasound waves in applications such as surgical or industrial cutting, cavitation generation, welding and drilling, among many others. Ultrasound can also be used at low power levels, for example in medical diagnostics or in sonar and hydrophone systems. Generally, low power ultrasound is non-destructive to the subject and is normally used for imaging and non-destructive testing processes, whereas high power ultrasound procedures impart irreversible changes to the subject material, for example permanent deformation.

In its most basic configuration, a standard ultrasonic system requires a power generator to produce the desired signal. This generator is connected to a transducer

which is designed to produce a specific amplitude output suitable for the designated application. A transducer converts one type of energy into another, and for the transducers studied in this research, this energy conversion takes the form of electrical input energy into the mechanical output energy which is required to drive a particular load. It is common for the displacement amplitude output of a transducer to be amplified by the addition of a tuned horn fixed to the end, depending on the application [4]. This is because very often the transducer alone cannot produce the amplitude that is required at that frequency. A Langevin-type transducer with a tuned horn connected is one type used in a wide range of applications ranging from rock drilling to orthopaedic surgery. The displacement amplitude and resonant frequency requirements for each differ, and so the ability to tune and optimise such a device is essential. This research is concerned with a specific type of flextensional transducer which is not limited by the dimensions of the attached horn or tool, unlike for Langevin-type transducers. Cymbal transducers are particularly advantageous for ultrasonic device design because they are not constrained by the fact that these attachments must be in a resonant or high gain configuration.

1.1 Cymbal transducers

The cymbal transducer, a schematic of which is shown in Figure 1.1 produced using CAD software (SolidWorks 2010), is a Class V flextensional-type transducer. The design was developed in the 1990s by Newnham et al. at the Materials Research Laboratory of the Pennsylvania State University, and was an evolution of the moonie design [5–7].

The cymbal transducer assembly consists of a piezoceramic driver, usually in the form of a disc or ring poled in the thickness direction, which is sandwiched between cymbal-shaped metal end-caps. The piezoceramic driver converts electrical input energy into mechanical output energy. The mode of vibration depends upon how the piezoceramic is manufactured, and those which are used in cymbal transducers tend to possess a small radial displacement as a result of the thickness mode which is sufficient to induce high axial displacement of the cymbal end-caps. A common piezoceramic

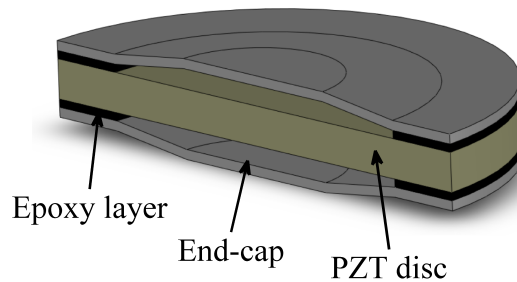


Figure 1.1: Cutaway schematic of the classical cymbal transducer

material used in the assembly of cymbal transducers is lead zirconate titanate (PZT).

1.1.1 Piezoelectric transduction

Ultrasonic transducers commonly incorporate piezoelectric materials which convert electrical input energy into mechanical motion. Piezoelectric materials exhibit the *piezoelectric effect*. The word ‘piezoelectricity’ is derived from the Greek word *piezein*, which can be literally translated as ‘pressure electricity’ [8]. The piezoelectric effect was discovered by the Curie brothers in the 1880s [9], after they demonstrated that certain materials, such as Rochelle salt, quartz and topaz, produced an electric charge in response to a pressure loading. This behaviour was not identified for all crystal specimens, and it was soon discovered that only asymmetric crystal configurations permitted the piezoelectric effect to take place. The piezoelectric effect is commutative [8], meaning that the application of an electric charge will cause mechanical movement, and hence stress, in the crystal. This was mathematically demonstrated using thermodynamics by Lippmann in 1881, and after that, the Curie brothers showed that the piezoelectric effect was indeed commutative, as illustrated in Figure 1.2 [9].

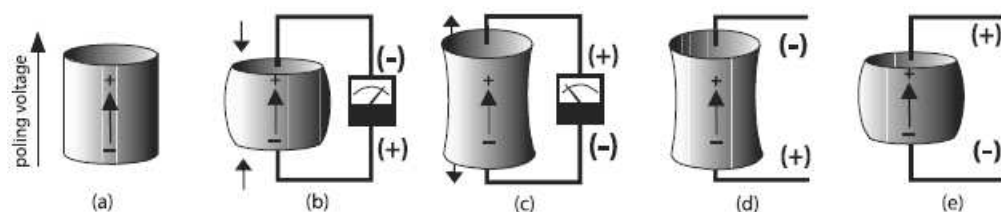


Figure 1.2: The piezoelectric effect [9]

A piezoceramic is an arrangement of perovskite crystals [9]. Any mechanical stress which is applied to a piezoelectric material is in direct proportion to the displacement of the electric field [8], and if this stress is switched from being tensile to compressive, then the electric charge reverses [8]. From this, it can be observed that tension or compression creates a voltage via alteration of the dipole moment [9]. If the material (shown in an unloaded state in Figure 1.2(a)) is compressed in the polarisation direction, or subjected to tension perpendicularly, then a voltage will be produced of equal polarity to the poling voltage [9], as shown in Figure 1.2(b). The contrasting scenario is also true based on the commutative nature of the phenomenon, where a tensile force in the polarisation direction will incur a voltage with inverted polarity [9], as exhibited in Figure 1.2(c). This condition is appropriate for sensing applications. For a piezoceramic to be used as an actuator, a voltage with a polarity equalling that of the poling voltage can be applied to the material in the polarisation direction, where the material will extend lengthways but reduce in diameter, as displayed in Figure 1.2(d) [9]. If the polarity of this voltage is reversed, the material compresses where it increases its diameter and decreases its length, as shown in Figure 1.2(e) [9]. The cyclic application of voltage, for example by using an alternating input voltage, will generate a repeated expansion and contraction cycle [9]. The frequency of the cyclic motion of the piezoceramic corresponds to the applied voltage frequency [9].

1.1.2 Transducer Fabrication

The mechanical coupling of the transducers is traditionally achieved by an insulating epoxy resin. This is because insulating epoxy resins commonly possess higher bond strengths compared to conductive epoxy resins [6, 10]. The low displacement radial motion of the piezoceramic driver is converted to high displacement axial motion of the end-caps by the influence of the cavity of each end-cap [10, 11]. Two piezoelectric coefficients of significance are the d_{31} parameter which relates to the radial contraction and expansion of the ceramic, and the d_{33} parameter which governs the axial motion [12]. For ultrasound applications such as underwater hydrophone arrays, the size of the classical cymbal transducer can be around 12mm in diameter [13]. The resonance response of the transducers can be controlled by changes to the geometrical dimensions

of each end-cap cavity and the elastic properties of the end-cap material [14]. Materials such as brass, titanium and steel are commonly used in the fabrication of the end-caps [15, 16]. These metals can be easily formed into the cymbal shape, and so are suitable for fast and repeatable production. The material elastic properties and the geometrical dimensions of the end-cap govern the displacement amplitude output which is achievable. For example, titanium is stiffer than brass and so will result in a transducer with a higher resonant frequency, but lower displacement amplitude. It has been reported that the manufacture of cymbal transducers is straightforward and low cost [6]. This is especially true where the end-caps can be punched from sheet metal, such as brass, titanium or steel. However, complications arise when using advanced materials whose properties must be carefully controlled.

Cymbal transducers exhibit up to two fundamental modes of vibration which are of interest to this research. The first is an out-of-phase symmetric mode. The second is an in-phase asymmetric mode, although this is generally undesirable. The asymmetric mode results in the bending of the piezoceramic driver which will generate stress. An example of a finite element analysis (FEA) of a symmetric titanium cymbal transducer is shown in Figure 1.3 to illustrate that symmetric and asymmetric modes exist for a cymbal transducer which is designed to be completely symmetric [6].

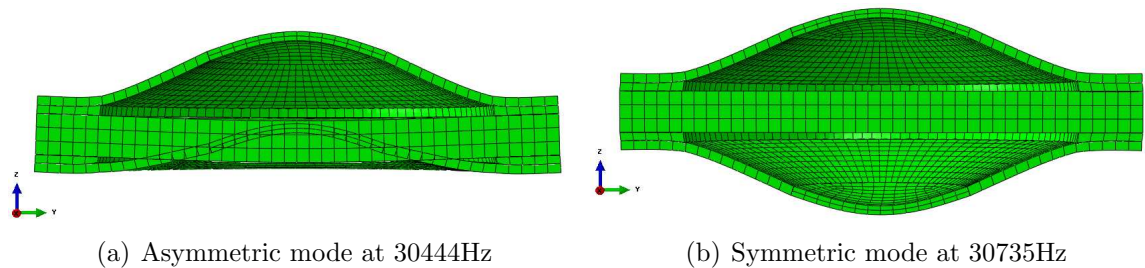


Figure 1.3: Mode shapes from the FEA of a symmetric titanium cymbal transducer configuration, showing (a) the asymmetric mode at 30444Hz and (b) the symmetric mode at 30735Hz

In addition to the vibration behaviour, it is often useful to be aware of the amount of electrical input energy which is transformed into usable mechanical output energy. This is a parameter which is commonly used in electromechanical analysis, and is called the effective electromechanical coupling factor (k_{eff}). This can be expressed by Equation 1.1.1 [17, 18].

$$k_{eff} = \sqrt{\frac{f_a^2 - f_r^2}{f_a^2}} \quad (1.1.1)$$

The series resonant frequency is the name often given to the resonant frequency [18] and is the low impedance, high admittance response. This is indicated by f_r . The parallel resonant frequency can also be referred to as the anti-resonant frequency [18] which represents the high impedance, low admittance response, and is denoted by f_a in Equation 1.1.1. The k_{eff} is the efficiency, where its maximum value is 1 and its minimum is 0 [17].

1.1.3 Applications of cymbal transducers

Considerable research has been conducted to establish the ways in which the cymbal transducer can be utilised and adapted for a range of applications. The cymbal transducer is commonly used in medium to low power applications such as hydrophone systems, principally as an underwater sonar device [19]. Cymbal transducers have found prominence in underwater applications, although they are small in comparison with the wavelength in the resonance condition, and are thus integrated into array formations [10]. For low power underwater and hydrophone applications, the cymbal transducer exhibits reasonable efficiency and Q factor, where the Q (quality) factor signifies the extent of system damping [20]. Cymbal transducers cannot individually produce the output power required for these applications, hence the necessity for array configurations. This improves the overall radiation efficiency as well as the power and the directivity compared to configurations containing only one cymbal transducer [19,21].

Problems associated with the quality of the mechanical coupling conferred by the epoxy bond layers are well known [6,22], and it has been suggested that cymbal transducers in their classical configuration are unsuitable for high power applications which place the epoxy bond layers under stress levels which cause them to crack or fail [23]. Consequently, efforts have been made to modify and improve the cymbal transducer design for integration into a greater number of applications, especially those

of high power [23–25].

One of the applications in which the cymbal transducer array formations have been successfully implemented is for transdermal drug delivery, where the transducer array generates a sonophoretic effect to enable the administration of the drug [26–30]. Even though the mechanisms are still not fully understood, it is probable that the ultrasound wave causes cavitation which alters the permeability of skin, thus permitting fluids consisting of large molecules such as insulin to pass. Figure 1.4 shows a selection of cymbal-type devices which have been adopted in practice.

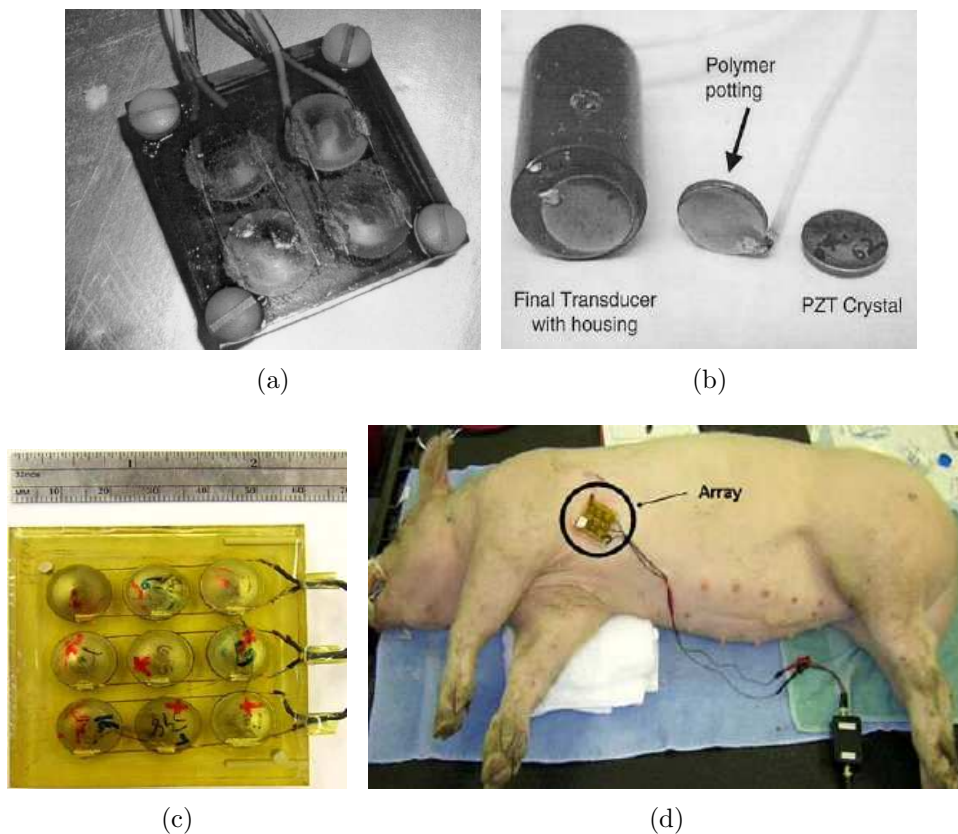


Figure 1.4: A selection of the cymbal transducer configurations used in transdermal drug delivery, including (a) the array delivery device constructed by Maione et al. [26], the portable transdermal drug delivery device developed by Smith et al. [27], and (c),(d) an array delivery device fabricated by Park et al. used to administer insulin to a pig [29]

There has been interest in the development of low weight and inexpensive sonicators due to the fact that transdermal drug delivery usually requires cumbersome equipment. The studies which have been published in recent years have shown success in achieving comparable levels of sonication intensity using lightweight cymbal transducer arrays,

despite the fact that the principle of sonophoresis is still not completely understood for these applications.

Cymbal transducers have also been studied and employed as accelerometers [31–33], but they have been more popular for research and integration in energy harvesting applications [34–40]. It has been found that vibration energy in ambient conditions can be collected and converted into electrical energy by using cymbal transducers. The transducers which have been adopted for this application are suitable because they can generate sufficient useful energy whilst being resilient to high levels of force [37].

A number of the recent developments in cymbal transducer technology relate to its adaptation for high power applications [23–25], because it has been recognised that the limitations of the classical cymbal transducer configuration principally relate to the mechanical coupling conferred by the epoxy bond layers. Figure 1.5 shows the modified devices which are based on the cymbal transducer configuration [23, 25].

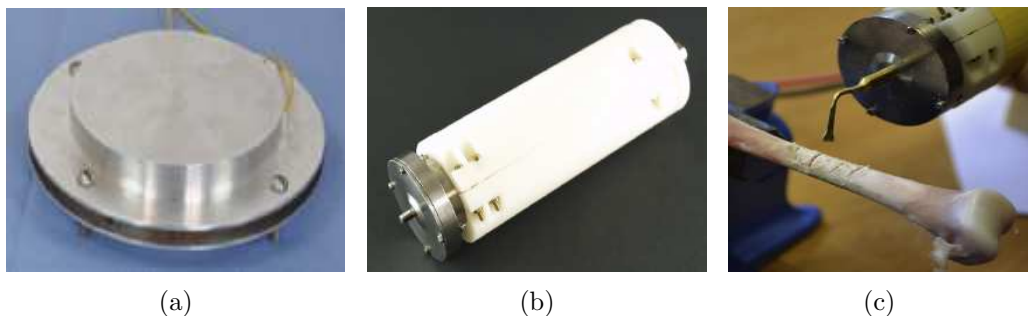


Figure 1.5: Modifications of the cymbal transducer configuration for applicability to (a) high power underwater sound projection and ultrasonic radiation in liquid and air [23], and (b),(c) a prototype orthopaedic surgical device [25]

These devices have improved the level of achievable displacement amplitude and eliminated the epoxy bond layer limitation. In each case, the mechanical coupling is formed by a metal ring fixed through the cymbal end-cap flanges. This removes the need for an epoxy bond layer, except to isolate the piezoceramic driver from the metal end-caps. The improved symmetry also means that in practice, there is a significantly reduced likelihood of an asymmetric mode appearing in the transducer vibration response. These recent attempts at improving the performance of cymbal transducers for high power applications indicates that there is a growing interest in utilising this technology for a wider range of applications.

1.1.4 Interest in multiple frequency applications

Substantial research and development has been conducted in the design and application of the classical cymbal transducer. In spite of this, there has been a distinct lack of activity in the incorporation of this transducer into applications other than low power underwater or energy harvesting. There is a wide variety of applications in which a tuneable flexensional configuration, such as a Nitinol cymbal transducer, would be advantageous. The attractive aspects of the cymbal transducer include its small and compact configuration, the relative simplicity and inexpense of manufacture, and the fact that an attached tool does not need to be tuned to the transducer. Another important feature is that it can be tuned with relative ease to a wide range of ultrasonic frequencies. This is achieved through alterations to the end-cap cavity dimensions and the end-cap material. Transducers have been constructed which are dual frequency by incorporating end-caps fabricated from two different materials [41]. In these transducers, the dual resonance is exhibited by the presence of two fundamental modes of vibration. This multiple frequency transducer demonstrates the ease by which more than one resonance can be introduced into a cymbal transducer.

Ultrasonic devices have also become popular in the field of surgery. The increased precision and control of ultrasonic devices for surgical applications such as bone cutting can result in a minimisation of tissue damage and improved tissue recovery time [42]. However, it is acknowledged that limited research has been conducted in recent years on the influence of a range of ultrasonic resonant frequencies on the cutting ability of such devices [42]. It is also clear that many medical and industrial applications may benefit from a multiple resonant frequency capability. An example of this is selectable-frequency ultrasonic cutting. In surgical procedures, a device which permits improved penetration into different materials could minimise unwanted effects such as necrosis of tissue. This is because the parameters that directly affect ablation and cutting procedures are the frequency and the amplitude of the applied ultrasonic vibration [43]. It has been reported that piezosurgery, which is an ultrasonic micro-vibration technique, minimises the damage to surrounding soft tissue in osteotomy [44], compared to conventional bone saws [20,44]. Micro-saws are known to visually obscure the operating area due to the presence of blood in the cutting zone [44]. In ultrasonics,

different surgical blade designs are often required for the coagulation and reshaping of soft tissue and those which are commonly used for bone surgery [45, 46]. If the device attachments are of different geometrical dimensions or mass, then the driving frequency will be different in order to enable the attachments to be resonant. Therefore the ability of a transducer to accommodate a number of different attachments would be beneficial. In addition, if different attachments are to be used on the transducer, then being able to change the resonant frequency of the transducer accordingly is desirable [47]. Therefore, being able to tune the resonant frequency of a surgical or dental device would be advantageous.

Another area in which a device with selectable resonant frequency would be desirable is in ultrasonic probes for medical imaging applications [48, 49]. It is known that there are problems associated with acoustic impedance mismatch between human tissues and the transducer, and therefore it would be useful to enable improved and effective acoustic coupling between the transducer and the patient [49]. It is also appreciated that because PZT-based devices are commonly used in these procedures [48, 49], the acoustic mismatch arises from the significant difference in acoustic impedance between PZT and human tissue. For example, the acoustic impedance of PZT is in the order of $33 \times 10^6 \text{kg/m}^2\text{s}$ compared to around $1.5 \times 10^6 \text{kg/m}^2\text{s}$ for human tissue [49]. This is complicated by the fact that different parts of the human anatomy are characterised by different acoustic impedances, and so the need to be able to match a single transducer to these tissues is evident. It has also been stated that due to the fact there is acoustic inhomogeneity in the human body, it would be advantageous to be able to operate a device at different resonant frequencies [49]. Therefore, the advantage of being able to operate at multiple frequencies is clear. Commercial ultrasonic probes and arrays are generally made to operate at one resonant frequency [49], and this can incur greater cost if a number of different conditions are to be observed and treated.

It is also known that cavitation activity can be enhanced by dual and multiple frequency sonication, and that the cavitation yield can be greatly increased [50–55]. It has been demonstrated that cavitation can be enhanced from a dual-sonication system, consisting of an ultrasonic transducer operating at a low ultrasonic frequency (for example between 20-30kHz) and a transducer vibrating at high (MHz) frequencies

[50]. The high frequency transducer accelerates the mass transfer and enhances the cavitation. The enhancement in cavitation activity has been reported to be synergistic [53], where the observed activity is greater for the dual-frequency system than the combined activity from individual sonications.

In contrast to many of the applications and approaches outlined in this section, and in Chapter 2, one of the more novel ways in which a tuneable or multiple frequency capability can be incorporated into transducer and device design is by making use of an advanced functional material. These smart materials include those which are piezoelectric, and SMAs. Scientific advances are enabling them to be incorporated into a wider range of technologies, and one of the most popular SMAs in recent years is nickel-titanium, also known as Nitinol.

1.2 Nitinol and its characteristics

Nickel-titanium (Ni-Ti) is a type of SMA whose interesting material properties were first recognised and recorded at the Naval Ordnance Laboratory in the 1960s. It became known as Nitinol [56] due to the initials of the place of discovery and the binary chemical composition. Materials which exhibit the shape memory effect (SME) are classified as either ferrous or non-ferrous [57]. Nitinol is a non-ferrous alloy [57], and can be referred to as a binary alloy due to its near-equiatomic composition of nickel and titanium. Due to the fact that Nitinol is a binary alloy, very fine control of chemical composition is required in the fabrication process in order to produce the desired material behaviour, for example in response to a change in temperature.

Nickel-titanium based SMAs have been shown to exhibit good corrosion resistance, due to the passive titanium-rich oxide layer which can form on the surface of the material, and are biocompatible. They can also endure relatively high stress levels [58, 59] with favourable strain recovery performance, exhibit a high level of damping capacity [60], and are operational to around 100°C [61]. Nitinol is commonly produced in wire, ribbon and plate forms, and has been successfully utilised in applications as diverse as biomedical stents [62], spectacle frames, orthodontic arch-wires and minimally invasive surgical devices [63]. Drills have also been manufactured using

Nitinol for dental surgery because of the resilience of the material to large-angle deformation, thus improving precision [63].

Phase transformations

Nitinol experiences a phase transformation between the highly symmetric [64], cubic CsCl B2 austenite at higher temperatures [65], and the lesser-ordered monoclinic B19' martensite [66] at lower temperatures. The martensite microstructure can be triclinic, monoclinic, tetragonal, orthorhombic, or rhombohedral depending on the alloy [59]. The phases are characterised by different elastic properties, electrical resistivity and crystal structure. The Young's modulus can typically be between 28-41GPa in the martensite phase and 60-90GPa in the austenite phase [67], and as such, SMAs harden as their temperature is raised. This is contrary to the behaviour of most metals. The martensite to austenite transition is called the reverse transformation [66], whilst the forward transformation represents the transition from austenite to martensite. The phase transformations are stimulated by changes in either stress or temperature [56].

The transformation between each phase of Nitinol occurs via shear lattice distortion [63] and not by atomic diffusion. The phase transitions are often termed in the literature as 'martensitic transformations' where up to 24 variants, or orientations, of the martensite can be generated [63]. The martensite which is formed after a transformation will exist in one of two forms [63]. The first is twinned martensite in which the variants are self-accommodated. This means that there is no observable change in shape. The second is detwinned martensite, where a particular variant is dominant. Detwinned martensite can be induced by applying a sufficient deformation load to the Nitinol in its martensitic state. The transformation behaviour is governed by the transformation temperatures which are normally designated as the start (s) and finish (F) of the martensite (M), rhombohedral R-phase (R) and austenite (A) phases. The R-phase is described in more detail later, but in general it is an intermediate phase which can appear in either cooling or heating cycles. It is more commonly observed on cooling, but in the event of encountering this phase on heating, the transformation temperatures R'_s and R'_F [68] are designated.

Superelasticity

Superelasticity, also known as pseudoelasticity [63], is a unique property of an SMA which is exhibited above the final austenitic transformation temperature, A_F . It is characterised by a high elasticity, around ten times that of stainless steel [69], recoverable deformation under high stress. This is because the strain can be reversed in a lower stress condition than loading, due to the mechanical hysteretic nature of the material [69]. Even though it is often referred to as pseudoelasticity, superelasticity is in strict terms one of two forms of pseudoelastic behaviour [63]. This is because pseudoelasticity can also be used to describe the rubber-like response of martensite due to reversible martensitic reorientation. Martensite ageing can cause a reversal of the martensitic detwinning when unloading the material below M_F [63]. This behaviour is often referred to as rubber-like [63]. Superelasticity is an isothermal process which occurs when Nitinol at a temperature above A_F experiences a stress which causes the austenite phase to transform to martensite [59, 63]. This occurs because the transformation temperatures are stress dependent [56, 63], which causes the material to undergo a change in microstructure which reorients the austenite phase to the martensite phase. Upon unloading, this effect is reversed since the martensite phase is unstable at temperatures suitable for austenite formation. The thermal behaviour of Nitinol is hysteretic, as is the stress-strain response [70]. The mechanism behind the reorientation of the crystal structure is best illustrated by comparison to a classical Hookian elastic response as exhibited by most metals such as stainless steel, as shown in Figure 1.6 [71].

When a stress is applied to a superelastic material when it is 100% austenite, the austenite reorients to martensite on the upper plateau [72]. The ‘upper plateau’ refers to the loading of the material, and the unloading part is called the ‘lower plateau’. The difference between these paths on a stress-strain diagram is referred to as the mechanical hysteresis. As an example, the force required for superelastic Nitinol stent compression is linked to the upper plateau stress, where the greater the upper plateau stress the more force is needed, and the release of the stent is related to the lower plateau stress, where the magnitude of the lower plateau stress influences the radial force. The relationship between temperature and stress for stable phases of

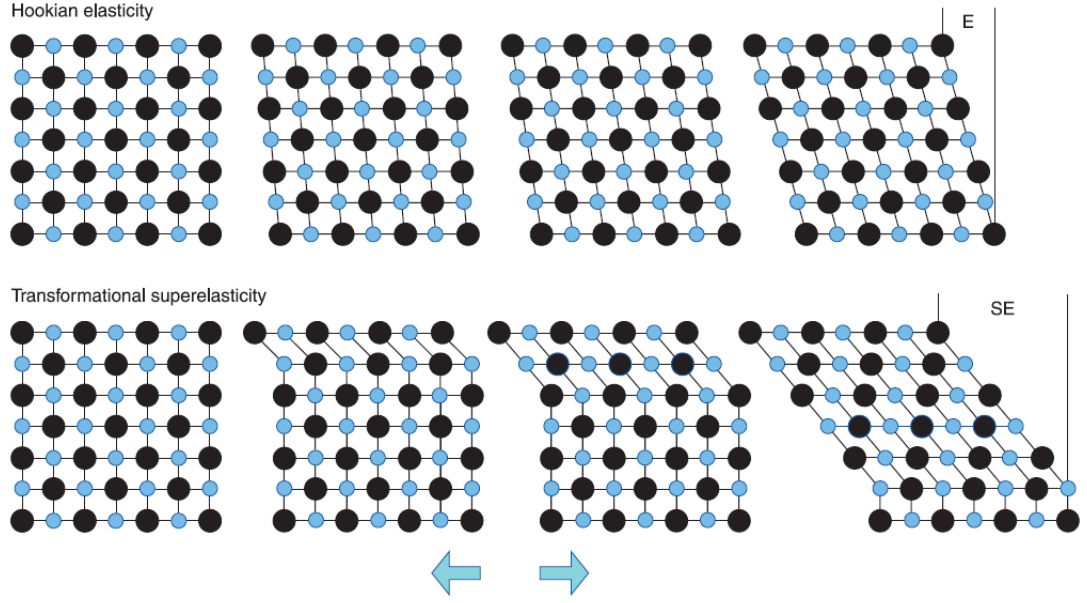


Figure 1.6: Reorientation of crystal structure for the superelastic effect [71]

austenite and martensite is a dependence governed by a form of the Clausius-Clapeyron equation. This equation, when applied to stress-strain data, allows an approximation for the reversible elastic strain permissible by the Nitinol to be determined [71, 73]. In general terms, Equation 1.2.1 shows how the mechanical behaviour of Nitinol depends on temperature and also the transformation temperatures [71].

$$\frac{d\sigma}{dT} = \frac{-\Delta H}{T\varepsilon_0} \quad (1.2.1)$$

In Equation 1.2.1, $d\sigma$ is the change in plateau stress, ΔH is the transformation latent heat, T is temperature, and ε_0 is the transformational strain [71]. Due to the latter two parameters being effectively constant, as they are dependent on the transformation crystallography [71], this relationship provides an expression for the stress-rate of transformations which are stress-induced, such as can be observed via the superelastic effect, and governs the stress required to generate stress-induced martensite [74]. It may be necessary to understand the stress at which superelastic Nitinol in a given application will transform. For devices incorporating superelastic Nitinol, A_F should ideally be lower than the intended operational temperature in order to properly exploit the superelastic properties of the material. Figure 1.7 shows two typical superelastic

cycles in an SMA [63].

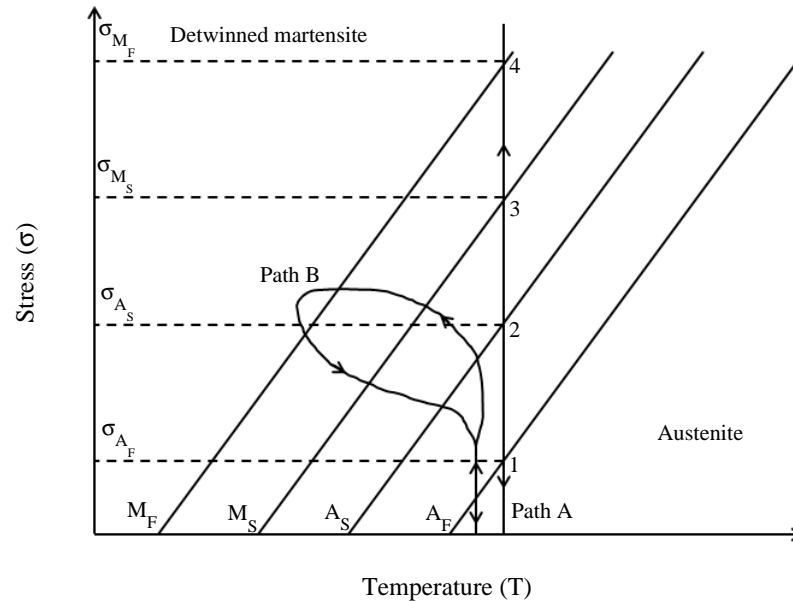


Figure 1.7: The superelastic effect and the σ - T dependency of alloy transformation [63]

The temperatures required to transform to each phase increase as the mechanical loading of Nitinol is raised. This is displayed in Figure 1.7 by the inclusion of the four diagonal lines. Nominal transformation temperatures M_F , M_S , A_S and A_F are marked around the zero-stress region, and it is shown how these transformation temperatures change with applied stress. The detwinned martensite which forms from austenite by the applied stress in both Path A and Path B is a form of stress-induced martensite, and there are multiple loading paths which can cause stress-induced martensite to form. Path B in Figure 1.7 shows how detwinned martensite can be generated from mechanical loading. Path A is included to illustrate that superelastic loading experiments are usually performed at a constant temperature above A_F . The material deforms elastically from Step 1 to Step 3, where σ_{M_S} is reached. This is the stress at which martensite begins to form. The transformation completes at Step 4, at σ_{M_F} , which represents the stress at which there is only martensite. After σ_{M_F} , the martensite phase experiences elastic loading. Upon unloading, the material elastically unloads to Step 2, at σ_{A_S} which is the start of the martensite to austenite transformation. Strain is recovered until Step 1 is reached, which corresponds to the stress at which there is only austenite, σ_{A_F} . A final elastic unloading process will then be observed until the

stress level is zero. The plateau stress levels will be able to be observed clearly from a stress-strain response curve. It is evident from Figure 1.7 that Nitinol is hysteretic in terms of stress-strain response. The reason for this hysteresis is the dissipation of energy in the complete transformation cycle of the material. It is also known that the hysteresis and the stresses required to transform between phases are dependent on the material and the experimental conditions [63].

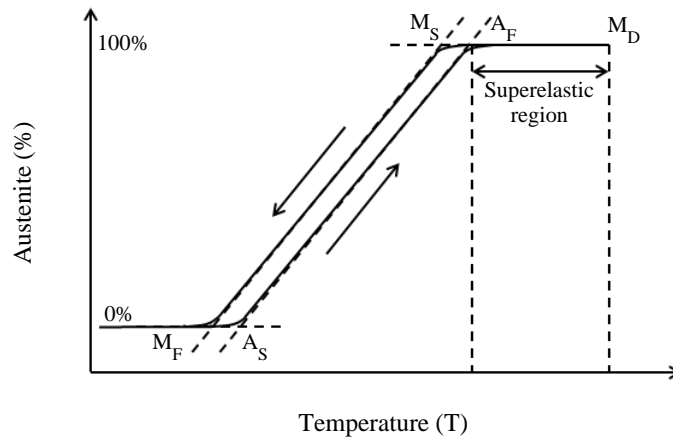


Figure 1.8: The superelastic region [56]

Figure 1.8 shows the relationship between austenite content of Nitinol and transformation temperature [56]. The range in which the superelastic effect emerges is clearly depicted, and identifies the temperature at which it stops, termed the martensite desist, or martensite deformation temperature, designated by M_D . The superelastic effect is known to disappear around 50°C above the A_F temperature [69], indicating that Nitinol can be superelastic over a reasonably wide temperature range. The hysteresis of the Nitinol transformation can also be observed in Figure 1.8, where the arrows indicate the difference between the heating and cooling of the material.

The shape memory effect

The second interesting property of Nitinol is called the shape memory effect (SME), which is the shape recovery of the material from a deformed state back to the original configuration. In order to achieve this, the Nitinol must be exposed to a thermal stimulus [72]. As an example, if Nitinol starts as austenite, above A_F , it can be allowed

to cool to form pure martensite, below M_F , where it is now twinned martensite. A deformation can now be applied to the material, where it is now detwinned as the microstructure has been distorted, assuming sufficient stress has been imposed on the material. If the Nitinol is then heated, it will progress through its transformation temperature stages until it is above A_F , where it will recover the original configuration, and once again exist as 100% austenite. The SME is shown in Figure 1.9 [63].

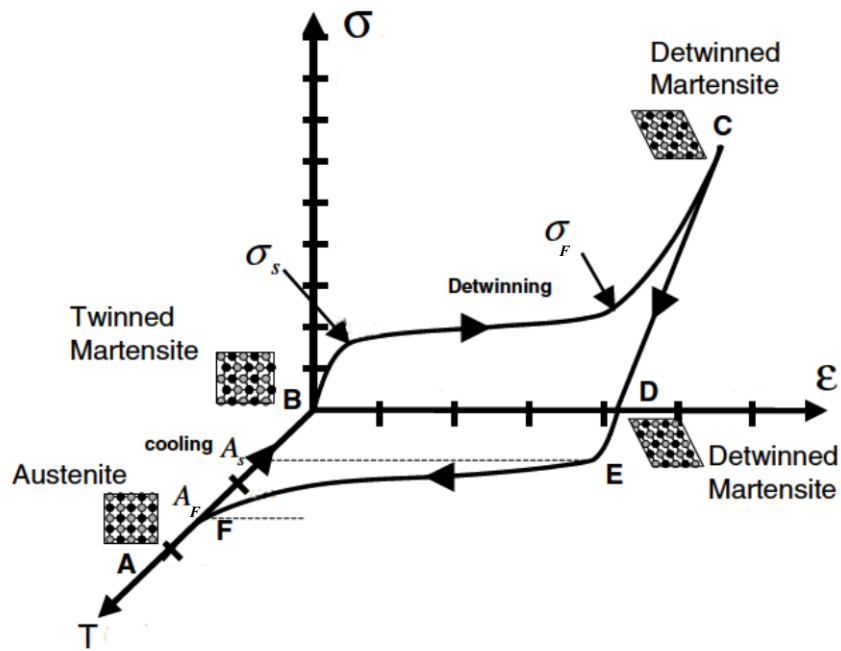


Figure 1.9: The shape memory effect [63]

Figure 1.9 represents the SME for a Nitinol sample under uniaxial loading [63]. In the diagram, point A represents the parent austenite phase. The term ‘parent’ is often used to describe the phase in which the set shape can be recovered. When cooling in the zero-stress condition takes place, the material undergoes a transition through M_S and M_F to point B, assuming it is a direct austenite to martensite transition, where twinned martensite is formed. If the material is mechanically loaded in the martensite state, then detwinned martensite will begin to form once the stress level is sufficient for the dominant variants to form. This is represented by σ_S and completes at σ_F . The σ_F limit is much lower than that required to plastically deform the martensitic Nitinol. The final detwinned martensite condition is at point C, and if the deformation load is removed, as shown elastically to point D, the material remains deformed. The original

set shape can now be fully recovered by heating the Nitinol through point E which is at the A_S transformation temperature, before reaching point F, the A_F transformation temperature. As long as no permanent deformation is experienced by the Nitinol in the detwinned martensite state, the original shape can be fully recovered. It is known that the SMA can experience a plastic strain, such that the material can no longer recover the parent austenite shape [63], therefore this loading level should be avoided. The material can be cooled once more back to twinned martensite with no further shape change of the Nitinol, thereby completing the SME cycle.

Nitinol is very sensitive to variations in strain and temperature [74] and can react very quickly to changes in these conditions. Two reasons why SMAs such as Nitinol have been adopted so widely are both the reliability of these phase transformations and also the speed at which they occur. The SME has been used to repair damaged transducers [67], and could be used to repair larger SMA structures. In addition, studies have been conducted on Nitinol under the influence of ultrasonic vibrations [75, 76], demonstrating that the SME can be activated. An SMA can also exhibit the two-way SME [63]. This is the repeatable change in shape of an SMA in response to a temperature cycle, for no mechanical loading [63]. The process of inducing this behaviour is called training, and it requires the thermomechanical cycling of the material. [63]. For each individual training cycle, the material is mechanically loaded and exposed to a temperature cycle. After each thermomechanical cycle, a very small strain remains which decreases as the number of cycles increases. The internal residual stress of the material grows, such that specific martensite variants are formed when the material is cooled from austenite under zero mechanical loading [63].

Transformation control

The thermomechanical processing history of Nitinol has a great impact on its mechanical behaviour and the transformation temperatures [59, 77]. The transformation temperatures of Nitinol can be tuned via a range of methods. The first is by the control of the chemical composition [59, 78], where an increase in nickel content reduces the transformation temperatures [63]. Also, alloying elements such as copper, aluminium and manganese can be used to increase the transformation temperatures [61]. The

transformation temperature range of Nitinol can generally be set from approximately -200°C to around $+110^{\circ}\text{C}$ [79]. For example, a nickel content of just 1% over 50at% nickel can reduce the transformation temperatures by more than 100°C [59]. Alloying elements can also be used to increase the strength of the material in the austenitic phase and either raise or lower the strength of the material in the martensite phase [80]. Other methods of controlling the transformation temperatures include ageing in the range $350\text{--}500^{\circ}\text{C}$ and cold working, such as by cyclic loading [59,71]. As a consequence, metallurgists can fabricate alloys for a range of purposes to suit strength, strain or cyclic repeatability requirements, among many others. For example, it has been quoted that the final transformation temperatures can be tuned to within $\pm 3^{\circ}\text{C}$ of specification [71]. This is a high level of tolerance considering the numerous factors which affect the transformation temperatures. Cold working can also be used to tune mechanical properties and to shape the component [78]. Nitinol which has been cold worked usually has to be fully annealed at around $600\text{--}800^{\circ}\text{C}$ because it work hardens very quickly [78]. There can be further difficulties when attempting to control the transformation temperatures of Nitinol. For example, Nitinol has been successfully deposited as thin films in recent years [81–83]. This can be achieved by magnetron sputtering [84]. However, the relatively poor transformation temperature reproducibility and the difficulty of tuning high transformation temperatures have been identified as limiting factors for their use in actuation systems [82].

Thermomechanical cycling can be used to train an SMA to exhibit the two-way SME [63]. It has been demonstrated that by subjecting Nitinol to thermomechanical cyclic loading, a saturation of the strain takes place [63], and the hysteresis is altered for each new cycle as a result of changes to the material microstructure [63]. Thermal as well as mechanical cycling has been shown to produce dislocations in the microstructure, resulting in fatigue, and can impose shifts in the temperature at which transformation between phases occurs [85–87]. Also, the change in transformation temperatures becomes more significant when the number of cycles is increased [85].

The R-phase

The third crystal microstructure in Nitinol is an intermediate phase called the R-phase [88], often referred to as the pre-martensite phase. The crystal structure is rhombohedral, and can be considered as a martensitic phase [74], because it possesses both shape memory and superelastic characteristics. The superelastic effect in the R-phase is very small compared to that which can be generated in the austenite phase, being approximately 0.5% strain distortion [74]. The R-phase is a distortion of the parent austenite phase [59]. It can also be stress-induced [89], and can appear in twinned and detwinned modes [59]. To illustrate the difference between the phase microstructures, Figure 1.10 shows the crystal structures of austenitic, R-phase and martensitic Nitinol [59].

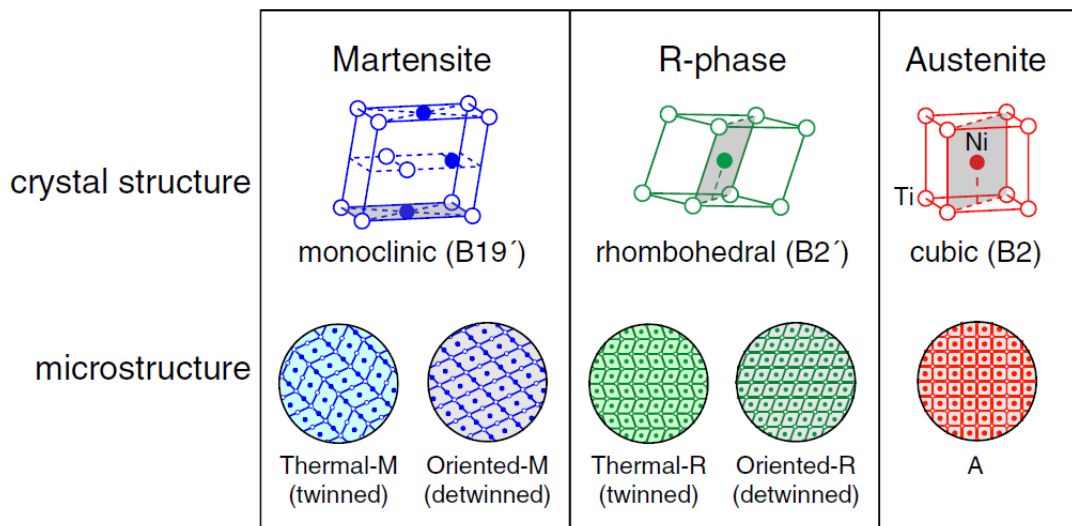


Figure 1.10: The crystal structures of the three primary phases of Nitinol [59]

The R-phase can appear when cooling from austenite to martensite, however, the R-phase can also appear intermediately in the transition from martensite to austenite [59, 68]. Often, the R-phase does not appear in a transformation between austenite and martensite [74], and this is referred to as a direct transformation. However, the R-phase is much more likely to occur in alloys that are nickel-rich [59] or have been subjected to certain heat treatments, solution treatments or cold working procedures [90]. Specifically, thermal cycling, increasing nickel content in the alloy and ageing heat treatments have been shown to contribute to the presence of the R-phase [90]. The R-phase can be induced in Nitinol by suppressing the transformation to martensite from

austenite by appropriate ageing and solution treatments which result in the appearance of nickel-titanium precipitates which cause the R-phase to grow [91]. Conversely, the R-phase can be suppressed by annealing at a temperature greater than around 600°C [92].

The appearance of the R-phase can lead to misinterpretation of experimental data [59, 74]. For example, a transformation event may be recorded at a temperature where it is expected martensite will form. However this may in fact be the R-phase. One significant difference between the R-phase and martensite is that the thermal hysteresis between the heating and cooling cycles is very low for an R-phase transformation, being as low as 2°C [59]. An attractive quality of the austenite to R-phase transformation is that it exhibits high cyclic stability compared to the austenite to martensite transformation [59]. This is because the R-phase exhibits kinematic compatibility with cubic austenite, unlike the monoclinic martensite structure [59], where internal twinning in the martensite must occur in the transformation between austenite and martensite. Therefore, if lower strain and stress levels are permissible, utilising this transformation may be an attractive opportunity for transducer design.

1.3 Nonlinear dynamic behaviour

Nonlinear dynamic behaviour has been identified in many ultrasonic transducers and devices, and the manifestations of these nonlinearities are relevant to the study of cymbal transducers. Real systems often exhibit behaviours which cannot be predicted or characterised by classical linear approximations [20]. Transducers and devices which incorporate piezoceramic drivers often exhibit nonlinear behaviour when the driving input voltage is high [93, 94]. The nonlinearities are present as shifts in resonant frequency and as hysteretic behaviour, and there has been significant research to investigate and model this behaviour for piezoelectric transducers [95]. Nonlinear behaviour is a phenomenon which appears in real dynamic systems, where a system input will produce a disproportionate system output [20, 96]. Nonlinearity in dynamic systems can be attributed to a number of sources [96]. Material or structure configuration such as the effect of nonlinear damping can cause nonlinear behaviour, as can the geometrical configuration or the behaviour of one or more materials in a

system [96].

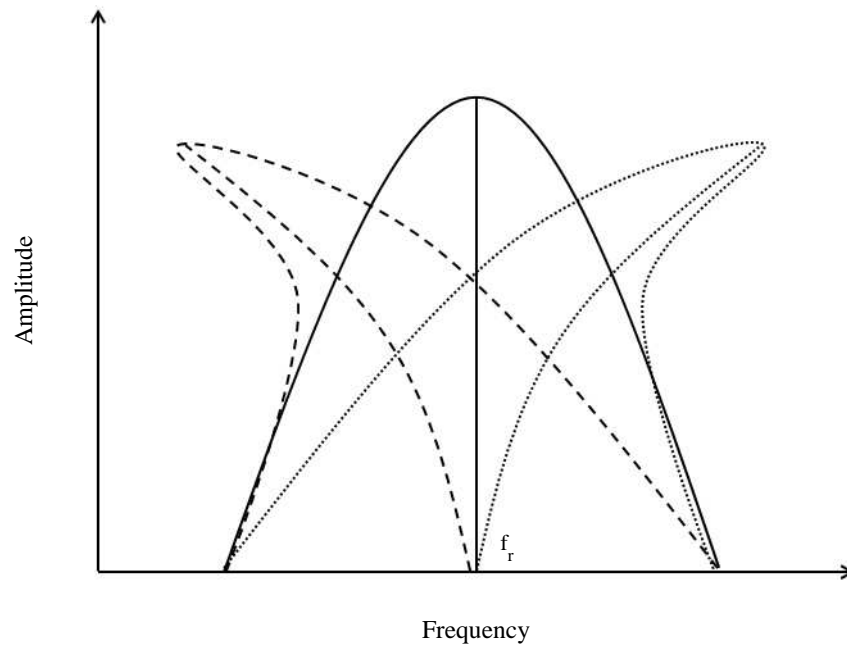


Figure 1.11: Nonlinear softening (dash) and nonlinear hardening (dot) behaviour in comparison to a standard linear response (solid)

It is known that the resonant frequency can decrease for PZT under increasing vibration amplitude [97], and this is demonstrated in Figure 1.11. This is referred to as softening, and is illustrated as the dash curve. The linear response of a system is represented by the solid curve, where there is no increase or decrease in resonant frequency as the amplitude, for example voltage or vibration, is increased. The dot curve shows a hardening nonlinearity, in which a system exhibits an increase in resonant frequency as the amplitude is increased.

In addition to the resonant frequency, the Q factor, which is an indicator of the system damping [20], has been observed to reduce as the amplitude of vibration is increased [97]. These changes in resonant frequency and Q factor have also been associated with increase in temperature [97]. It is therefore important to be aware that nonlinearities will affect the cymbal transducers, particularly at raised input voltages and vibration amplitudes.

1.4 Original contributions to knowledge

While there have been many studies conducted into the successful industrial and medical applications of cymbal transducers, they are generally limited to energy harvesting, sonar, underwater hydrophone array systems, and for transdermal drug delivery. However, there are many applications which would benefit from tuneable or multiple frequency cymbal transducers, and yet incorporation of SMAs such as Nitinol remains largely undeveloped. This is due to difficulties in understanding how Nitinol behaves in this application, and in particular under the influence of ultrasonic excitation. The original contributions to knowledge are:

1. An extension of the current knowledge of how the cymbal transducer behaves under ultrasonic excitation. This is achieved by vibration characterisation using electrical impedance measurements, experimental modal analysis (EMA) and vibration resonance response characterisation (VRRC). In addition, a finite element model of this transducer has been developed, showing a high level of correlation with natural frequency and displacement amplitude measurements for both the symmetric and asymmetric modes of vibration.
2. A framework of recommendations which can be implemented for the practical design and characterisation of Nitinol cymbal transducers and devices.
3. An investigation of the vibration responses of cymbal transducers fabricated using two different types of Nitinol, comprising shape memory and superelastic material. The shape memory Nitinol is martensitic or R-phase at room temperature, and the superelastic Nitinol is manufactured to be austenitic at room temperature. The differential scanning calorimetry (DSC) technique is utilised as a method of correlating the transformation temperatures of Nitinol to changes in the vibration response of the transducers at those temperatures.
4. A verification of the limitations of DSC for the analysis of superelastic Nitinol using new experimental evidence.
5. A study into how Nitinol behaves when loaded at a low ultrasonic frequency. The nonlinear vibration responses of transducers fabricated using Nitinol are

measured.

6. The demonstration, using dynamic characterisation methods, that the resonant frequencies of both the symmetric and asymmetric modes of a cymbal transducer, incorporating Nitinol as the end-cap material, can be tuned via a modest change in thermal loading.
7. An analysis of the limitations of the cymbal transducer configuration for device design, but also a demonstration that in principle, a tuneable and multiple frequency prototype device can be developed using Nitinol.

1.5 Summary

This chapter has discussed how SMAs can exhibit superelasticity, and that they can also recall a previous set configuration due to a phenomenon called the shape memory effect. Both of these phenomena derive from the fundamental phase transformation capability of SMAs, where the microstructure of the material changes as a function of stress or temperature. The purpose of the research presented in this thesis is to provide an account of the characterisation and development of tuneable and multiple frequency cymbal transducers using Nitinol, and to extend this knowledge to a novel prototype device. The transducers and devices which have been developed possess selectable vibration behaviours which can be tuned by changes to temperature. This research can therefore provide a foundation for the future development of tuneable and multiple frequency ultrasonic transducers incorporating Nitinol.

Chapter 2

Review of the literature

2.1 A brief history of ultrasound

The detection and understanding of sound has always interested scientific minds. Pythagoras (c.580–c.500 B.C.) reportedly became fascinated with the nature of sound after passing the forge of a blacksmith, hearing the impact of hammers on anvils [98]. Pleasing sounds were termed as consonant and unattractive sounds as dissonant. It was found that consonant sounds could be produced by the hammers at weight ratios of small numbers which were whole, a discovery that led to the development of the monochord. This was a device with a string which could be tuned to create different notes depending on the length ratio which was chosen. Among Pythagoras' many contributions to science and the scientific process, this can be considered as one of the most significant, because of the realisation that sound could be treated as a mathematical concept. In another very early account, Aristotle (384–322 B.C.) is known to have understood the nature of sound with respect to its propagation [98], and concluded that the air must vibrate in a particular way whenever sound is generated.

There was not a significant amount of progress made in the understanding of sound propagation, and the generation of sound, until the 16th century, when Galileo recognised that sound waves could be produced in water [98]. In 1636, the French mathematician Mersenne described sound in terms of movement, and consequently indicated that certain sounds may be too small to detect. Galileo and Mersenne both investigated the relationship between frequency and pitch, and Mersenne managed to

compute the frequency of a wire. Hooke also had an interest in this relationship, and demonstrated it with the creation of a device which could produce sounds of different frequency [98]. Hooke is also recorded to have postulated the potential use of sound in medical diagnosis [99], but it was Laplace in the early 19th century who developed the first precise formula for sound velocity in air [100], extending the work of Newton in 1687 [98]. Poisson also contributed to the understanding of sound propagation by the investigation of the propagation of sound waves in a solid which is isotropic [100].

In 1826, Colladon and Sturm made a successful attempt to measure the speed of sound in fresh-water [101]. Since they had no electroacoustic transducer with which to generate a signal, they opted to strike a bell which was positioned underwater. In one experiment, the sound was received approximately 13km away after indication of the strike time using a light flash. The signal was detected by a metal tube placed in the water. Lord Rayleigh, who is one of the most important figures in the history of sound and acoustics for his work on sound propagation, confirmed their very high accuracy for the techniques they had at their disposal, as did Beyer.

One of the earliest accounts of the concept of ultrasound comes from the work of the eighteenth-century physiologist and priest Spallanzani [102]. In 1793 he showed that bats could find their way around certain obstructions in the dark even when their sight was impeded, but could not do this when their mouths were covered. The work Spallanzani did with Jurine led them both to conclude that bats relied on their hearing capability to move in the real world, and that they could navigate their way around obstacles using sound waves rather than light waves [103]. At the time, the concept that there could be sound levels out-with the range of human hearing was not well received, and so despite the work and experiments Spallanzani performed, it took a long time for his results and ideas to be accepted. In 1883, Galton demonstrated that the upper limit of human hearing lay anywhere between 10-18kHz [104], which meant that for the first time, a proper marker could be set for ultrasonic frequencies. Galton himself developed the eponymous ‘Galton Whistle’ to show that there were indeed animals which could detect sounds at ranges humans cannot. Up until this point, ultrasound had commonly been detected by the use of sensitive flames. However, the advent of piezoelectricity meant that constructing devices which could accurately and

effectively generate and detect ultrasonic waves was possible [103]. By now, ultrasound was an established and accepted concept, and the Curie brothers were responsible for discovering the piezoelectric effect in 1880 [104]. They found that crystals which do not possess a centre of symmetry will produce positive and negative charges of a magnitude proportional to the pressure applied to certain axes. It was in 1881 that they discovered that this phenomenon was commutative, confirming Lippmann's prediction that same year [105], therefore giving rise to a wide range of possibilities for advances in technology. It implied that certain crystals exhibited an electric potential when subjected to a mechanical stress. This phenomenon was called the piezoelectric effect, and resulted in the opportunity to develop ultrasonic transducers.

2.2 Flexensional transducers

The scientific discoveries which took place in the 19th and early 20th centuries meant that new technologies could be developed. The principles were applied to a number of different applications culminating in the ultrasonic transducers in use today. The first notable attempt at ultrasonic transduction after the discovery of the piezoelectric effect by the Curie brothers was by Langevin, and was followed by numerous ultrasonic transducer designs to suit a variety of applications.

2.2.1 Early developments in transduction

Around thirty years after the discovery of the piezoelectric effect, the Titanic sank after a collision with an iceberg. The resulting widespread reforms in maritime law led to the need for a method of detecting these obstructions, and consequently Richardson and Maxim independently postulated the use of ultrasound detection systems at sea [103]. Langevin found a solution by developing a novel hydrophone system [103]. As well as a number of maritime disasters at this time, the outbreak of World War I meant that it was imperative that submarines could be not only navigated with a high level of control and accuracy, but that enemy submarines and ships could be detected at a great distance and with high accuracy and precision [103]. In 1917, Langevin developed the method of stimulating a quartz crystal into resonance with a tuned circuit, forming

the foundation of many future oscillator designs [104]. Langevin is commonly regarded as the father of ultrasonics due to his contributions in the early 20th century [100]. However, this could not have been possible without the work conducted by earlier researchers, in particular the Curie brothers and Lippmann.

It is important to appreciate that although the need for these devices was spurred on by the onset of international conflict, the designs were never ready in time for the detection of enemy submarines, and so they were instead later used to quantify depths of water [100]. The outbreak of World War I meant that the application of these new ultrasonic devices was limited by the need to detect submarines. The use of these devices was seen as ideal and the only real option because of the problem electromagnetic waves have in penetrating sea water due to the high electrical conductivity [100]. Ever since, ultrasonic transducers have been extremely popular in underwater environments. By the end of World War I, Langevin and Chilowsky collaborated to develop echo ranging technology which used piezoelectric transducers in water, making submarine detection possible [99]. It was also recorded that during the testing and operation of these devices, scores of dead fish were observed, showing that the effect of this technology on nature was understood at this time. As a result, efforts were undertaken to establish the safety of ultrasound [99].

In 1934, Sokolov made significant advances when he showed that it was possible to utilise ultrasound technology to allow flaw detection in different structures, meaning that it would be possible for potential structural failure zones, such as cracks within a material, to be accurately located [105]. However it was only when the pulse technique was developed through the advent of radar that ultrasonic flaw detection became feasible in practice. By the time World War II had begun, investigations were already taking place into new forms of piezoceramics that could be used in the transducer designs. Up to that point, Rochelle salt piezoelectric crystals were used in the devices [100,104]. Nickel magnetostriction was also a popular choice for generating ultrasonic waves, but Langevin-type transducers tended to utilise the piezoelectric effect. More sophisticated devices and applications were being developed, and it was found that using ammonium dihydrogen phosphate (ADP) crystals resulted in a far better performance than the Rochelle salt [100]. ‘Ultrasonic listening devices’ were even

attached to torpedoes and used to destroy enemy submarines [100]. The principle by which this worked was that the sound emitted from a submarine in the vicinity would control torpedo direction, and it had an impressive range for the time, being about 200 yards. It is testament to the work of Langevin that by the start of World War II, his underwater ultrasound detection system design had evolved into standard naval equipment called ASDIC, named after the Allied Submarine Detection Investigation Committee [103]. Mason made the argument that applications for technology increase during times of war or conflict [100], and progress made in technology such as radar systems certainly accelerated in this period. The development of radar also had great implications for technology such as ASDIC since it allowed transducers to be situated in arrays, improved visual display and allowed specific sections of space to be scanned. The term sonar, which is derived from the term *sound navigation and ranging*, was then adopted for systems used for underwater detection [103].

After the end of World War II, significant progress was made in the field of ultrasonic technology, partially due to the breaking down of international barriers between countries previously in conflict. For example, much of the significant work Japan did in this field during and up to the end of World War II was largely unknown to the West, and future collaboration enabled the field of ultrasonics to evolve at a much quicker rate. The pulse technique, which has such importance in medical diagnosis and non-destructive testing methods, was only realised because of the development of the radar system [105]. In 1945, materials called ferroelectrics which could naturally polarise were first used as ceramics in ultrasonic transducers [100]. It was found that these ceramics could polarise when a high voltage at a high temperature was applied and so acted like a piezoelectric crystal suitable for use in ultrasonic transducers. The USA (Von Hippel) and USSR (Vul and Goldman) independently developed barium titanate at the same time [100]. It was found that certain properties of the ceramic, such as the Young's modulus and the piezoelectric and dielectric constants, exhibited large deviations at the phase limits between crystalline structures. For this reason, lead-titanate and lead-zirconate were used, most notably by Jaffe et al. [100]. The difference with these new ceramics was that they could be manufactured to possess far higher magnitudes of piezoelectric and dielectric constants through grain boundary

impurity inclusion. In current ultrasonic technology, they are among the most popular and common ceramics, and can be used for a wide variety of transduction applications in many different industries.

Up to this point, most of the ultrasonic technology explored possessed a low amplitude capability. High power ultrasonics quickly became of great interest to many scientists and engineers, and it became clear that new phenomena occurred when the amplitude of motion increased. Wood and Loomis are credited with discovering that high amplitude or high intensity sound waves could produce cavities and fogs in liquids [100], which has led to the development of many new technologies such as ultrasonic cleaning and liquid food degassing [103,106]. At the same time, interest was growing in using ultrasound in medical applications [99]. More specifically, the use of the pulse-echo method for imaging the human body was postulated, and technology was developed by a number of scientists and engineers to allow this to happen. In 1940, the pulse-echo technique was also applied by a supersonic reflectoscope to detect flaws in metal in the form of a compact device [99].

The need for high resolution was now recognised as an important factor affecting the performance of an ultrasonic diagnostic system. Dussik was an Austrian psychiatrist interested in being able to diagnose brain tumours using non-invasive procedures [99]. In the 1940s, he undertook imaging experiments on patients using ultrasound, which were termed hyperphonograms. The resultant ultrasound images were among the first of their kind, and the first to be used to diagnose medical conditions. Many other scientists also used ultrasound technology in the 1940s and 1950s to diagnose medical conditions, such as Ludwig, who was able to identify conditions such as gall stones [99]. His work allowed the recording of the speed of sound waves as they propagated through different materials such as muscle, different organs and cavities [99]. The eminent University of Glasgow academic Donald showed how effective ultrasound could be in obstetrics [107, 108], but this was not his only contribution, as his work also led to further development of sonar [108]. At this time, power ultrasonics was not given as much attention as using ultrasound for low power or non-destructive techniques.

2.2.2 Evolution of flextensional transducers

The name *flextensional* first appeared in a publication by Toulis in the early 1960s [109], and combines the words ‘flexural’ and ‘extensional’, which describe the mode of operation of this type of transducer design. At its most basic and fundamental level, a flextensional transducer can be regarded as a mechanical shell driven by an internal piezoelectric stack [110]. A flextensional system can be considered to be made of three sub-systems, namely the shell, the stack and the surrounding medium. Flextensional transducers tend to comprise the same basic components, but the significant differences in performance arise from the variations in geometrical and material design configuration. Today, flextensional transducers can be divided into seven distinct classes, shown in Figure 2.1 [101]. These designs evolved throughout the 20th century to address a variety of different applications.

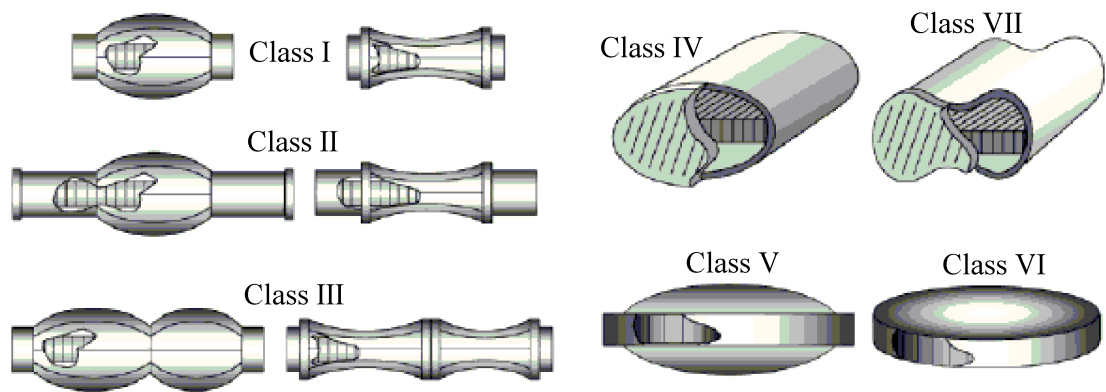


Figure 2.1: The seven flextensional transducer classes [101]

Even though it is accepted that the first flextensional transducer patent was filed in 1966 by Toulis [109, 112], it was actually in 1929 when research conducted by Hayes resulted in the fabrication of the first flextensional transducer [109]. This work, which remained forgotten and unacknowledged for a significant period of time, involved the development and assembly of a large-scale air transducer at the Anacostia Naval Research Laboratories (NRL). In 1936, a patent was filed termed ‘Sound Generating and Directing Apparatus’ [109, 112] and described the design and assembly of a transducer type which resembled the bow of an archer. Today this flextensional transducer is known as a Class IV transducer, and it has arguably been the most popular and best understood flextensional transducer configuration available [112].

Class	Distinguishing Features
I	Short, cylindrical end sections, rotational symmetry Low frequency, high power and omnidirectional radiation
II	Longer cylindrical end sections Higher frequency than Class I, around 1-15kHz, greater power output
III	Different resonance for each shell, broadband capability
IV	Oval shell design Uses piezoelectric bars instead of discs
V	Two bonded, shallow, spherical shells Contains a thin, electrically-isolated, piezoceramic disc
VI	Two concave end-caps Can operate at greater underwater depths than Class V
VII	‘Dog-bone’ shell, omnidirectional radiation, functional at greater depths Lower effective coupling coefficient than Class IV

Table 2.1: Features of the seven flextensional transducer classes [101, 110, 111]

Flextensional transducers have historically ranged from only a few centimetres to many metres in length, and can consequently be very heavy [112]. For certain low frequency applications, the miniaturisation of these designs was critical [112], and this contributed to the eventual development of the Class V moonie and cymbal transducers. The differences between the seven classes principally arise from the different transducer shell designs which can be affixed to a piezoceramic stack [110], and Table 2.1 briefly summarises a number of the features of each transducer class [101, 110, 111].

The inventiveness of Hayes’ design was that a high mechanical or acoustical impedance magnetostrictive component was used to drive a low impedance shell [109]. This principle applies to all of the transducer classes illustrated in Figure 2.1. It is known that Hayes developed a cylindrical transducer which was more durable than the original flextensional design [109], and both were used in a range of applications in the first half of the 20th century. The flextensional transducer was adopted in foghorns used by the Lighthouse Service, and the cylindrical ring design was incorporated into altitude and drift meters as a result of US Navy funding [109]. However, due to a lack of

funding and the fact that the cylindrical design performed better for the applications for which it was designed, research and development into flextensional transducers ceased in 1933. Even though Hayes' work remained largely unnoticed until the late 1980s, a publication by Pallas in 1937 outlined the possible uses of flextensional transducers, for example in microphone and telephone systems [109].

The design which Hayes developed was too advanced for the time, primarily because the sonar capabilities at the time would not have been able to cope with the demands of the technology [109]. It is known that flextensional transduction in an underwater environment experienced significant development around the 1950s [11]. The flextensional transducer Toulis created in the 1960s was the same as that developed by Hayes, except that the Toulis design incorporated a piezoceramic driver and was used in an underwater environment [109]. Merchant and Abbott both also developed flextensional transducers around this time [109], and from this point it is clear that the revival of flextensional transducer research started. The differences between the designs again were in the geometry of the shell, and so in an attempt to categorise new and upgraded designs along with the traditional, a classification system was set up by Brigham and Royster in the 1960s which are known as the flextensional classes [109]. Initially, only five classes were identified, with Classes VI and VII added later [113]. The broad differences between these classes are detailed in Table 2.1, but it is important to state that Abbott's flextensional transducer was a Class V [109], the design of which resulted in the cymbal transducer known today. After that, significant work was conducted into different flextensional transducer designs and also the modelling of their performance [114]. The literature on the different types of flextensional transducer and their evolution and applications throughout the latter half of the 20th century is substantial. As an example, there has been a significant amount of research conducted on the Class IV configuration in recent years. However, the focus of this review now shifts to the design and development of a variation of the Class V design, the cymbal transducer.

2.2.3 Cymbal transducer research and development

The cymbal transducer was originally developed as a miniaturised actuator which linked bimorph and multilayer actuation [11, 115], and was an extension of the ring-shell projector design developed by the Defense Research Establishment Atlantic (DREA) in the 1970s [6]. In 1998, it was patented by Newnham and Dogan [6], but it was not the first evolution of the Class V design. In the late 1980s, the moonie transducer was developed at the Materials Research Laboratory at Pennsylvania State University [11]. This design was created in order to lower the financial cost and improve the ease of assembly and mass production of the Class V configuration [11]. The design was named for its half-moon shaped end-cap cavities [116]. A second design called the cymbal transducer was developed to produce greater displacement amplitude and generative force than the traditional Class V configuration [11, 117]. Generative force is the term used to describe the force limit to avoid permanent deformation of the transducer [117]. The change in geometry of the end-cap ensured that the stress concentration in the end-cap was reduced, thus permitting higher displacements to be achieved compared to the moonie design [23]. A method of measuring the displacement of a cymbal transducer is by using a linear voltage differential transducer (LVDT) [115]. Generative, or blocking, force can also be determined using this technique [115]. The cymbal transducer commonly possesses thinner end-caps than the moonie, in a cymbal-type shape, hence the eponym. Another reason that transducer miniaturisation was required was to enable transducers to be used in low frequency sonar systems [113]. The Langevin-type transducer was found to be limited because as the mass loading increased, there was a reduction in resonant frequency. The solution was to develop a transducer with a raised effective compliance, either by using softer driver materials, or by changing the design of the transducer [113]. It was found that a suitably high compliance could be attained by using a flextensional design [113], hence the development of the moonie and cymbal transducers. Figure 2.2 illustrates the difference between the two Class V variations of flextensional transducer [116].

The cymbal transducer has been found to be suitable for sensing and actuation systems [115], and it possesses a displacement around 40 times the magnitude of the single piezoceramic [6, 115]. Cymbal transducer end-caps are commonly produced using

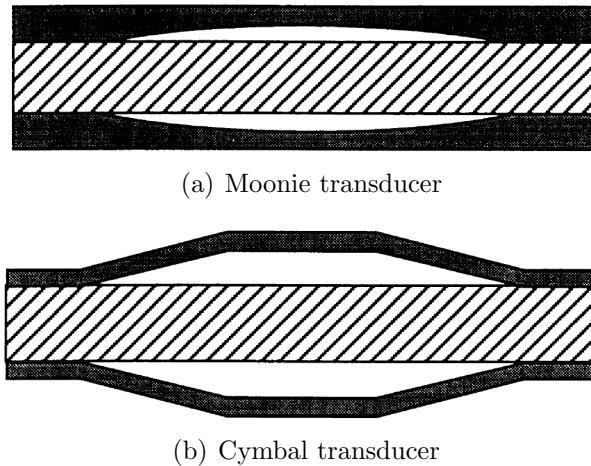


Figure 2.2: Moonie and cymbal transducers [116]

a punching technique [115] on sheet metal. The transducer can also be tuned first by adopting numerical modelling techniques before the end-cap geometrical dimensions and the end-cap material are chosen [118]. Cymbal transducers are omnidirectional with low radiation resistance with high reactance [6], and they have been integrated in both single and array formations for underwater applications [6]. For a cymbal transducer of about 12.7mm in diameter, the first resonant frequency can be in the order of 20kHz, and so the size of the transducer is very small in comparison to its wavelength in water [6, 10], being an acoustic monopole [119]. The cymbal transducer has a high Q but a relatively low radiation efficiency when acting as a sound projection system [10]. Due to the small size of the cymbal transducer, any mass loading lowers the ability of it to effectively radiate power if it is acting as a single element [6]. This is why they are usually situated in an array configuration for projection systems at low frequencies [6]. A number of studies have been subsequently carried out on array configurations, both numerical and experimental [5, 7, 10, 19, 21, 28, 120, 121]. Not long after the cymbal transducer was developed, there was interest in increasing the achievable displacement amplitude. One method was to fix multiple cymbal transducers on top of one another in a multi-stack formation [115]. It was demonstrated that this configuration exhibited high stability for an axisymmetric, uniaxial loading condition, and that for a configuration of five stacked cymbal transducers, a displacement amplitude of $175\mu\text{m}$ could be achieved.

In 1997, a paper was published on the design and characterisation of a dual

resonance cymbal transducer [41]. A cymbal transducer was assembled in an asymmetric configuration using one brass end-cap and one steel end-cap. The end-caps were of equal dimensions, and it was of interest to observe the resonance response as a result of differences between the elastic properties of the end-cap materials. It was found that two fundamental modes of vibration could be produced, each associated with the resonance of a particular end-cap [41]. The acknowledged benefits were the production of different vibration behaviours and an increased bandwidth of operation [41]. A similar response was also observed for a transducer assembled and characterised which consisted of end-caps made from the same material, but different dimensions, where one was a moonie end-cap and the other was a cymbal end-cap [41].

Around this time, finite element software was becoming more commonly used in the design of cymbal transducers. From this stage, both analytical and numerical modelling methods began to be widely used to optimise cymbal transducer performance [14, 118]. The resonant frequency, in addition to the displacement amplitude, generative force and the response time of a cymbal transducer can all be tuned by the appropriate selection of end-cap material and transducer geometry [6, 122, 123]. For example, if the diameter of the transducer is changed from 3mm to 40mm, the resonant frequency changes from around 100kHz to 1kHz [6]. The resonant frequency can also be tuned by changes to the geometrical dimensions of the cavity [6]. The effects of these changes can be accurately simulated in FEA software, for example as demonstrated in an investigation by Tressler et al. [14].

It has been reported that the classical cymbal transducer is unsuitable for underwater operation at depths exceeding approximately 200m [124]. The end-cap cavities were found to collapse under the influence of the high hydrostatic pressure, and so another design was developed in 1999 to enable the transducer to endure higher pressure loading [124]. The new design was called the concave transducer, or double-dipper, and replaced the piezoceramic disc with a ring. The end-caps were also formed as concave shapes by inverting the cymbal end-caps. It was found that the pressure tolerance was greatly improved compared to the cymbal transducer, and the end-caps and driver vibrated in-phase with one another [124]. In addition, FEA was used by the developers of the technology to complement the experimental data, demonstrating

consistent use of FEA in the design and analysis of transducers [124]. From this point, numerical simulation was used more extensively, including for modal analysis [112], and an analytical model aiming to represent the dynamics of cymbal transducer vibration was also produced [125], indicating an increasing focus on correlation between modelling and experimental data in the characterisation of transducers.

The next major development in the design of the cymbal transducer was in 2000. A tuneable cymbal transducer was proposed using shape memory alloy end-caps [67]. A cymbal transducer was constructed using Nitinol end-caps, where the resonant frequency could be tuned by exploiting the alloy modulus change as a result of the martensite to austenite phase transformation. The resonant frequency change was monitored using electrical impedance analysis in the appropriate thermal environments. It was noted in this work that not only can the elastic modulus change, but also the sound speed and the level of acoustic impedance matching [67]. A controllable resonant frequency was exhibited for the one symmetrically-configured cymbal transducer used in this study, and also that damaged end-caps could be repaired via the shape memory effect (SME). It was also shown that at a hydrostatic pressure of around 2MPa, the end-caps were elastically deformed, but could be actively repaired by generating the SME through heating [67]. Subsequent research into the effects of high levels of hydrostatic pressure [126] indicates that this capability would in general be very useful. In addition to the observed recovery of the resonant frequency after the SME was activated, the hydrostatic piezoelectric charge coefficient (d_h) was also shown to be recovered, demonstrating a completely reversible process [67]. This study was the first to employ an SMA in a flextensional transducer, and indicated great potential for the technology. It has been reported that further benefits of an actively tuneable cymbal transducer using SMA-type materials are a greater control of the displacement amplitude and also the achievable force [16, 67]. FEA was employed for modelling, but it was accepted that due to the highly nonlinear characteristics of the phase moduli and the fact that they significantly depend on the amount of annealing conferred to the material [67], the modulus parameters were incrementally altered until the simulated response accurately represented the experimental results [67]. It is clear that much research is required to be able to accurately simulate and predict the dynamic behaviour of SMAs such as

Nitinol as a result of specific heat treatments and cold work processes.

In 2001, the cymbal transducer configuration was modified once more to incorporate controllability of the radiation direction into the functionality of the transducer [119]. This design was called the double-driver, and was developed to address the problem of omnidirectionality [119]. The patent for this design was filed in that year before being granted in 2003 [127]. This omnidirectionality meant that sound transmission in one direction was difficult to achieve. At the time, multiple transducer arrangements were used, which were all prepared to be in phase with one another to generate the desired radiation pattern [119]. This was judged to be costly, and so a solution was required. The desired directional beam pattern was shown to be exhibited by the double-driver transducer by using two piezoceramic drivers to generate a bending mode in the PZT and a flexural mode in the end-caps, which causes a cancellation of the sound pressure in one direction, but an addition in the other [119]. At the same time, research was being conducted into the amplification of the displacement of a cymbal transducer using a range of electroactive materials [12]. Different compositions of PZT were used in the transducer configuration, and it was found that the piezoelectric coefficients, in addition to elastic properties, significantly influenced the obtainable displacement [12]. It was also stated that single crystal ceramics would confer advantages for cymbal transducer performance such as a significant reduction in response hysteresis [12], and further work was later conducted into single crystal cymbal transducers and arrays [121]. A study in 2006 into the incorporation of a lead-free driver into the transducer assembly [128], showed an increased interest in the integration of different ceramics into cymbal transducers for improved performance, for example relating to the electromechanical properties. It was shown that the performance of the actuator fabricated using the lead-free driver was similar to that of the transducer assembled using a hard PZT driver, albeit with a lower d_{33} coefficient [128]. Another study conducted in 2005 showed how improving the bonding technique, for example by abrasion of the end-cap flanges before bonding, improved the displacement amplification performance and the resonance behaviour [18].

More detailed research began to be conducted in 2002 into the optimisation of cymbal transducer design and production [6] and also the causes and influences of

asymmetry in the performance of the transducer [6, 129]. The report by Meyer, Jr. et al. [6] was one of the first to discuss in depth the undesirable effects of asymmetric behaviour as a result of low quality manufacture [6]. Any asymmetry in the design, such as differences between the geometrical dimensions of the two end-cap cavities, can cause other modes of vibration to appear in the resonance response spectrum, and it is stated that the cavity depth tolerance is potentially as small as $5\mu\text{m}$ [6]. This makes the assembly process very uneconomical. The resonance response of the transducer is very sensitive to changes in the geometrical dimensions of the end-cap cavities, as even very minor alterations can result in a resonant frequency shift in the order of kilohertz [6]. Not only that, but any non-uniformity can stimulate other undesirable modes of vibration to appear in the frequency response spectrum, again indicating the very small tolerances which limit the repeatable fabrication of these transducers [6]. The research offered one solution to the appearance of extraneous modes, and that was to adopt a thicker piezoceramic driver in the design [6].

Meyer, Jr. et al. demonstrated via FEA that a ‘double-peak’ could be observed in the resonance response of a cymbal transducer with unequal or uneven epoxy bond layers. It was also shown that the asymmetric mode could appear at a lower or higher frequency than the symmetric mode in the measured resonance response spectrum, the order being dependent on the geometrical dimensions, especially of the end-cap [6]. The study was also one of the first to analyse the response of a cymbal transducer using laser Doppler vibrometry, where the vibration velocity was measured as a function of frequency [6]. The results were correlated with electrical admittance measurements, the inverse of impedance. There was an indication that conducting only experimental impedance analysis may not be sufficient, since this method often does not reveal the effects of the small asymmetries which may exist in the configuration [6]. A proposed solution to the unevenness in the epoxy resin was to use a piezoceramic driver which had a greater diameter than the end-caps, so that the wires could be affixed without distorting the epoxy bond layers, coupled with a screen printing bonding technique [6]. One other very important observation from the work of Meyer, Jr. et al. was that shifts in resonant frequency of the symmetric and asymmetric modes are not always in proportion [6]. In their FEA, the resonance response of a cymbal transducer in air

was compared to that in water. The resonant frequency of each mode decreased as expected, but the resonant frequency of the asymmetric mode was found not to change by the same percentage as the symmetric mode [6]. It was noted later on in 2005 that typically only 20% of the cymbal transducers constructed in a study possessed a single peak resonant frequency response [17], showing how difficult it is to produce single-resonance response cymbal transducers. Research into the double-peak response, resonance characterisation, and debonding (bond failure) was continued in 2006 [130] and 2007 [22].

Further research into maximising the displacement and the transmission of energy was conducted in 2004 [131]. Even though developments of the cymbal end-cap design had addressed the problem of high concentration of stresses around the cavity edges, it was noticed that tangential stress remained a problem, exacerbated by the flexural motion of the transducer end-caps [131]. Radial slots were cut in the cymbal end-caps to reduce the influence of stresses in the tangential direction. FEA was used to help quantify the impact of these slots, and it was demonstrated that the performance, especially relating to the energy transmission and displacement, was improved [131]. Further research into the reduction of stress in the end-caps was conducted in 2008 with the development of a wagon-wheel flextensional transducer [132], which addressed the problem by the removal of more end-cap material. The wagon wheel design exhibited a distinct improvement in the displacement response [132].

In 2005, the concept of resonant frequency and device performance tuneability was considered once again, although not in relation to SMAs [17]. Instead, two approaches were adopted for each end-cap. The first was to apply a mass loading to the apex of the end-cap, and the other was to supply fluid into the cavity [17]. In principle, the addition of mass to the system lowers the resonant frequency of each mode, and it was demonstrated that a single resonance condition could be produced by the addition of the correct mass on each side of the transducer [17]. The study also shows that mass addition is much more practical than controlling the fluid volume in each end-cap cavity [17]. Nevertheless, it highlights progress that was made in the consideration of tuneable transducers at this time.

From this point, there have been several different avenues of research which have

been active relating to cymbal transducer design and application. Another study which incorporated an SMA in the design and fabrication of a cymbal transducer was published in 2007, and again adopted Nitinol as the end-cap material [79]. This research was performed in order to further improve the performance of the transducer by utilising the SME to impose a radial pre-stress on the configuration which is opposed by the epoxy bond layers. The transducer was called a stress-biased cymbal (SBC) and a patent was filed in 2008, being accepted the following year [133]. The end-caps are heated after bonding, transforming from martensite to austenite, and the radial force creates a tensile stress in the PZT disc [79]. Properties such as the dielectric constant and effective d_{33} were shown to increase [79]. In 2007, the cymbal transducer configuration was modified into a rectangular shape and constructed with a single crystal lead magnesium niobate-lead titanate (PMNT) driver to maximise displacement amplitude [134]. A new variation of the cymbal transducer, called the spherical-cymbal transducer was developed in 2009 which was intended to improve the frequency performance of the transducer configuration [135]. In this design, the cymbal-shaped end-cap cavity profile is replaced by one which is a crescent shape. The major contribution from the research was that the spherical-cymbal transducer was observed to possess lower resonant frequencies than for a cymbal transducer with comparable geometrical dimensions, which improves its applicability for underwater acoustic systems [135]. However, it is clear that a cymbal transducer can be tailored to produce lower resonant frequencies, but the effect of the stress concentrations in the spherical-cymbal transducer are not yet fully understood.

A patent filed in 2008 but published in 2011 showed how cymbal transducers could be situated in an array formation in between plates which could produce electrical energy from external mechanical vibrations [136]. This recent patent demonstrates the potential that small cymbal transducers exhibit for cost-effective and lightweight energy harvesting. It is clear that despite the many efforts to improve the performance of cymbal transducers, both singular and in array formations, they have principally been adopted for low power functionality. The investigations into increasing displacement and force have in many cases been very successful, but the technology has still largely remained in the field of sonar. It is known that cymbal transducers are limited when

operating at resonance, particularly with respect to the effect of increasing stress on the epoxy bond layers [130,137], and so in recent years research has been conducted into adapting them for high power ultrasonic applications [23–25], for integration into systems such as surgical cutting devices. It is known that the mechanical coupling of cymbal transducers at medium to high power levels due to the fact that the chosen bond agent possesses a finite strength [23]. At very high displacement amplitudes and input voltage or power levels, there is an increased risk of debonding taking place [23]. Lin reported that due to this limitation, classical cymbal transducers have been restricted to sensing, actuation and low power projection systems [23]. The mechanical coupling of the transducer has to be improved, and it can either be achieved by using a stronger bonding agent, which is currently difficult [23], or by completely modifying the coupling mechanism to remove the reliance on a finite-strength bonding agent. This is the approach both Lin and Bejarano et al. followed [23,24]. In these improved transducers, the end-caps were fixed to an intermediate metal ring via screws. The metal ring enclosed the piezoceramic driver meaning that the mechanical coupling was focused on the interface between the metal ring and the end-cap flanges, thereby raising the maximum displacement amplitude and input voltage. This was successfully demonstrated by Bejarano et al. and a prototype cutting device was later constructed and tested using the same principle [25]. It was also found by Bejarano et al. that the asymmetric response was eliminated [24], showing how much of an effect an epoxy resin coupling mechanism contributes to an asymmetric vibration response.

Even though the limitations of the cymbal transducer at resonance have been extensively discussed in the literature [130,137], it is clear from the research conducted in this thesis that repeatable actuation is achievable for modest input voltage levels. When correctly assembled, a cymbal transducer can operate as intended, providing the resulting displacement amplitude or input voltage does not cause the epoxy bond layers to fail. The cymbal transducer is also a relatively simple configuration by which to investigate more complex behaviour which is likely to be caused by using an advanced functional material such as an SMA, an area which has not received much attention in the literature. In addition, the progress which has been made in the modification of the classical cymbal transducer configuration for implementation in high power applications

means that there is a new branch of technology in which a more robust cymbal-type flexensional transducer could be useful. It also indicates that a range of new materials not extensively studied in power ultrasonic transducer technology can be adopted for the design and fabrication of these transducers, one of which is the SMA Nitinol.

2.3 Nitinol and tuneable transducer technology

When the piezoelectric effect was first identified, it was one of the first recorded observations of smart material behaviour. Since the discovery of the first SMA, which is another class of smart material, the number of composite materials which exhibit smart characteristics has considerably grown. This section outlines the evolution and progress made in SMA technology, and also the different applications for which they have been most successful, in particular in the aerospace and medical industries.

2.3.1 Development of SMAs and understanding nitinol

Martensite was discovered in steels the 1890s by Martens [63, 138]. It was initially thought that the transformation to a martensitic state, as identified in the Fe-C system, was irreversible [63]. The first documented observation of shape memory behaviour was in 1932, when Ölander identified the pseudoelastic phenomenon exhibited by the Au-Cd alloy [139]. However, it was not until 1949 that Kurdjumov and Khandros explained how a reversible transformation was possible, through the concept of thermoelasticity observed in Cu-Zn and Cu-Al alloys [63]. This led to a greater understanding of the mechanisms of the martensitic transformation, and over the next few years, reversible martensitic transformations were observed in other alloys such as In-Tl [63]. This sparked great interest, and in the 1950s pseudoelastic behaviour was observed in alloys including Cu-Al-Ni, Cu-Zn, and In-Tl [139]. The first signs of the SME were found by Greninger and Mooradian in 1938 [139], only a short time after the revelation of pseudoelasticity. They noticed that when they raised and lowered the temperature of a Cu-Zn alloy, the martensitic phase disappeared and reappeared respectively. Due to the fact that the effect of temperature on the martensite phase was also studied in depth by Kurdjumov and Khandros a decade later, they also receive credit for their work in

discovering the SME [139]. In 1951, Chang and Read first observed the SME of $\text{Au}_{47.5}\text{-Cd}$ [138], but it was not until 1963 with the discovery of the smart material properties of Ni-Ti by Buehler et al. at the US Naval Ordnance Laboratory [63, 138, 139] that using this reversible martensitic transformation phenomenon started to be extensively exploited in engineering applications [63]. Buehler et al. were investigating materials which could be used for heat shielding for missiles which would experience re-entry into the atmosphere [140], and noticed a material which showed an ability to recover its shape after deformation [63, 140]. This material was eponymously called Nitinol, as it was a nickel-titanium alloy (Ni-Ti) discovered at the Naval Ordnance Laboratory (NOL). The recoverable behaviour it demonstrated was called the shape memory effect (SME). This discovery led to extensive research by many engineers and scientists into alloys displaying shape memory behaviour, experimenting with composition changes in different alloys, heat treatments and different microstructures. Figure 2.3 shows the timeline of SMA discovery [59].

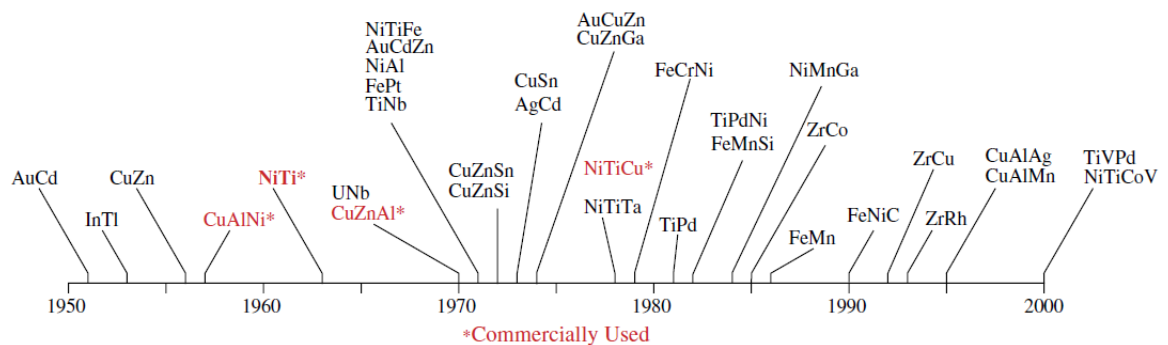


Figure 2.3: Timeline of shape memory alloy discovery [59]

In 1965 it was found that adding a third element to Nitinol, such as iron or cobalt, reduced the transformation temperatures of the material [63]. This had significant implications as it meant the number of engineering applications in which the materials could be implemented radically increased. As an example, the first major commercial SMA application was in 1971 with the development of Cryofit, which was used for F-14 fighter plane pipe couplings [63, 141]. The transformation temperatures for this SMA were extremely low and the pipes had to be transported in liquid nitrogen to prevent actuation of the material before the assembly process was underway. It was not until 1989 that Nitinol was combined with niobium to create a Ni-Ti-Nb alloy with

a large temperature hysteresis [63]. This was a significant development as the new alloy composition showed a remarkable ability to behave like Cryofit, but did not need to be transported in liquid nitrogen due to the vast temperature hysteresis inherent in the alloy. Research into the performance of different alloy compositions and other types of SMA was also conducted, for example in the development of high temperature SMAs [63]. These SMAs possessed transformation temperatures exceeding 100°C, such as Ti-Pt, Ti-Pd and Ti-Au, and were popular in the 1970s [63]. In 1978, Melton and Mercier demonstrated that alloying Nitinol with copper did not significantly alter its transformation temperatures, but instead decreased the stress hysteresis. The effect of copper in improving the fatigue life of Nitinol was reported in 1999 by Miyazaki [63], and showed that Nitinol was suitable for a wide range of applications in engineering, and especially for its relatively low cost [63]. For example, the use of Nitinol in biomedical applications began around the 1970s, and in the 1990s the material started to be exploited commercially for stents [63]. Nitinol alloys are commonly used for industrial, dental, and medical applications [141]. They have been employed in applications as wide ranging as valves, dental and orthodontic arch-wires (first attempted in the 1970s by Andreasen and Hilleman [56,142]), spectacle frames, vents in air conditioners, active control of acoustics, switches, as a method of improving the buckling characteristics of certain composite panels, actuators and as connectors for electrical cables [63,141].

It is desirable to be able to optimise the performance of Nitinol for high temperature actuation conditions [63]. In recent years, the most popular and common research and application activities for Nitinol have been in the medical industry, where they are incorporated into devices such as stents [62,71,142–147]. Nitinol can be more expensive to fabricate than rival SMAs such as Cu-Zn-Al alloys, but are generally preferred for commercial applications [61]. Part of the reason Nitinol became more widely accepted in this industry was the shift to less invasive medical procedures [143]. Not only that, but material fabrication processes have greatly improved [143], and much of the recent research into Nitinol and other types of SMA focuses on a range of material characterisation and property optimisation techniques available for both mechanical and thermal behaviours [59,71,148–150]. These procedures include differential scanning calorimetry (DSC), electrical resistivity measurement and x-ray diffraction (XRD), and

are relevant for tuneable transducer and device design. However, it is important to note at this stage that there is still a significant amount which is unknown about Nitinol, particularly in relation to its mechanical behaviour. In 2006, several of these unresolved problems were outlined in a detailed publication by Duerig [151]. There is not the scope to discuss them all in depth, but those which have some relevance to this investigation are briefly outlined. It was indicated that the R-phase can be stress-induced from the martensite phase [151]. This would have great implications for Nitinol-based actuators which rely on high-stress actuation in both low temperature and high temperature phases. A distinct nonlinear response would likely be observed for an actuator activated in the martensite phase which at some stage experiences contributions from a stress-induced R-phase. This was of course purely hypothetical, but is important to consider for future research. The elastic modulus of Nitinol in its various states is also confirmed as an area of poor understanding [151]. It is accepted that the changes in elastic modulus, as can be identified from the stress-strain responses of Nitinol, are not well understood [151]. For example, due to variations in loading and unloading stiffnesses, an actuator cannot accurately be described by taking into account only the Young's moduli of austenite, martensite and R-phase. Over a temperature range, the volume mixtures between each alloy phase change, and hence so does the apparent stiffness. This means that to accurately represent actuator behaviour in a finite element simulation, it may be more sensible to inversely determine the moduli using dynamic methods. This is the approach which was followed by Meyer, Jr. and Newnham in 2000 [67]. The logical question arising from this relates to the value obtained from the numerical simulations if the accuracy of acquired stiffness data for an operational actuator is very difficult to ensure. The answer is that if geometrical dimensions of the actuator are known with confidence, as well as the operating conditions, then finite element simulations offer a unique opportunity to be able to identify the modulus of Nitinol at a particular stress and temperature, for each phase. This modulus can then be applied to other geometrical configurations of transducer or device which incorporate an SMA such as Nitinol, to improve the accuracy of predictions of its behaviour. Nevertheless, there is much scope for further investigation concerning the material and mechanical properties of Nitinol, and also in the improvement of the modelling of the

material, even though the understanding of its behaviour has significantly improved in recent years. There have been recent studies which have focused on the martensitic transformations in Nitinol as a result of ultrasonic vibrations [75,76]. It has been found that phase transformations can be induced by the application of ultrasonic energy in Nitinol to produce the SME [75,152], and that application of ultrasonic vibrations which cause the Nitinol specimen to experience cyclic stress can result in a reduction in the A_F temperature. The implementation of SMAs in ultrasonic devices therefore needs to be based on observation and an understanding of the effect of ultrasonic vibrations on the phase transformation behaviour of the material, especially the transformation temperatures.

2.3.2 Tuneable and multiple frequency transducers and devices

It is clear that Nitinol has received much attention for medical applications. In 1999, a paper was published which emphasised the importance of expanding the number of applications in which SMAs are used [60]. It is known that the development of devices incorporating Nitinol has been hindered by the fact that the material exhibits behaviour which has taken a very long time to be well understood, and that knowledge about the mechanical behaviour has not been of the required standard [142,143]. In recent years, the understanding of this material has improved, but it is commonly being exploited, especially in medical applications, for its superelastic effect rather than the SME due to the higher permissible tolerance of the transformation temperatures [142]. The requirement of precise transformation temperatures for the SME has clearly limited its development in actuation applications, however the research presented in this thesis does not attempt to exploit the SME, but instead the changes in elastic modulus associated with the phase transformations. In terms of Nitinol in transducer design, there has not been a significant amount published in the field, and this also applies to the field of ultrasonics. However, notable examples include the development of a tuneable ultrasonic transducer which incorporated Nitinol in 1995 which could be used for applications such as imaging [48]. In 2008, a Nitinol linear actuator was developed which made use of the two-way SME, where the actuation performance for compression

and unloading tests was observed [153]. It was explained that for actuators utilising the one-way SME, a residual strain must be imposed, whereas this is not required for the two-way SME [153]. In 2012, reports of the triple SME were published [154] which exploits the R-phase in the operation.

Generally, the benefits of tuneable and multiple frequency technology have been known for a number of years, and are outlined in Chapter 1. In terms of multiple frequency technologies, there have been many advances since the 1970s. An early multiple frequency transducer was produced in 1976 which comprises both low frequency and high frequency elements in array formations [155]. Not long after that in 1983, Lindberg patented a parametric wide bandwidth dual mode transducer for underwater applications [156], and in 1986 two further multiple frequency transducers were developed. One was a radial vibrator which comprised different composite structures within the design which resonate at separate frequencies [157], and the other was a multi-resonant longitudinal transducer [158]. In 1996, a dual frequency transducer was produced which incorporated tonpilz-type transduction elements, and could operate at two different resonant frequencies individually or together [159], and in 1997 research into dual resonance cymbal transduction was successfully conducted [41]. Research in this area continued, including the creation of a multiple frequency array device in 2003 which can be used for medical purposes [160], and a multiple frequency transducer which can resonate at three different frequencies depending on the assembly components being resonated [161], which was developed in 2009. It is clear that there has been activity and interest in producing multiple frequency transducers and devices for many years, and it is now appropriate to outline the progress made in tuneable technology.

There was interest in the use of smart materials such as SMAs in transducer design as far back as 1992 [57]. In the same year, research was published on the deposition of lead zirconate titanate films on Nitinol to create smart composite materials which would be beneficial for optimised tuneable transducer design [162]. Later in that year, a tuneable Langevin-type transducer was patented by Newnham et al. whose resonant frequency could be controlled by the compressive stress on the composite material [67,163]. Research was published in 1996 on the tuneability of two transducer

configurations which could operate at ultrasonic frequencies, one being a sandwich-type and the other a two-plate design [164]. The resonant frequency could be controlled by short-circuiting one of the ceramics [164]. In 1999, research was conducted into adaptive tuned vibration absorbers (ATVAs) using Nitinol [165], and in 2000 the tuneability of the elastic properties of the magnetostrictive material Terfenol-D was exploited in a tuneable vibration absorber in order to control the resonant frequency [166]. Also in 2000, Meyer, Jr. and Newnham produced and characterised a Nitinol cymbal transducer, and demonstrated how the SME could be exploited to repair damaged end-caps [67]. In 2002, a patent was published which demonstrated the design of an SMA actuator which could transform between the R-phase and the austenite phase [167]. The advantage of this was that the temperature change required was much lower than for a martensite to austenite transition [167]. In 2003, an ultrasonic cutting device with tuneable capability was patented [168], where the principle of operation was that a change in resonant frequency could be induced by the adjustment of the length of specific assembly components [168]. This technology demonstrates that there is a clear interest in tuneable medical and surgical devices. In 2007, Narayanan and Schwartz showed how Nitinol can be used to pre-stress a transducer to improve its performance [79], and in 2008 Mertmann and Vergani discussed the development of SMA actuators [169], and in particular those utilising Nitinol in wire form. Also in 2008, Peters et al. conducted research on a tuneable transducer for energy harvesting purposes which exploited the ability to change the structure stiffness via the geometrical moment of inertia by using piezoelectric actuators [170]. Demonstrating even further interest in the energy harvesting application, a tuneable energy harvester was created in 2011 based on the magnetic coupling in a magnetoelectric transducer [171]. In 2012, a proposal was published on the use of Nitinol in the design and application of an active surgical needle [172], where Nitinol in wire form was proposed as an actuation mechanism for the device in order to control the location of the needle tip.

Due to the fact that there are many different transducer configurations available, it appears that the development and design evolution of multiple frequency and tuneable transducers and devices has generally focused on the functional requirements, and many of these systems are created for either medical or underwater applications. It is now

of interest to be able to characterise the dynamic performance of tuneable, multiple frequency transducers and devices in greater depth. One further interesting observation from the published research of Meyer, Jr. and Newnham was that a resonant frequency difference in a Nitinol cymbal transducer could be increased even further by altering material parameters such as the annealing and composition of the alloy [67]. However, since this paper was published, there has not been any extensive research into the development or characterisation of this technology which was shown to have great potential. The dynamic characterisation was generally limited to resonant frequency identification via measurement of electrical impedance, and there was little focus on the thermal response of the Nitinol used in the study. It is for these reasons that the thermal and dynamic characterisation procedures have to be introduced in depth using a number of case studies as examples in Chapters 3 and 4, before the thermal and dynamic characterisation of Nitinol cymbal transducers are performed, as reported in Chapters 5 and 6. The research culminates in the development of a tuneable and multiple frequency prototype device, shown in Chapter 7.

Chapter 3

A study of an asymmetric cymbal transducer

The resonant frequency and displacement amplitude of a cymbal transducer can be tailored by the appropriate selection of end-cap material and the control of the geometrical dimensions of each end-cap. Many of the studies in the literature report on the resonant frequency response of cymbal transducers which are fabricated using end-caps with identical geometrical dimensions and materials. These are single frequency if fabricated with precision. However, the research into dual resonance cymbal transducers [41] was conducted with the intention of creating asymmetry, which appears as a double-peak in the frequency response spectrum of the transducer due to the difference in resonant frequency between the symmetric and asymmetric modes. Sources of asymmetry in a cymbal transducer include differing end-cap materials, variations between the geometry of the end-caps (in particular the cavity), and also differences between the two epoxy bond layer profiles. As a result, the transducer will exhibit two fundamental modes of vibration. It has been found that the fabrication of single frequency, symmetric cymbal transducers is very difficult. However, there is a difference between transducers exhibiting dual resonance as a result of small asymmetries as a result of fabrication tolerances, and transducers where asymmetry has been deliberately introduced in order to control the dual resonance in the design process. This chapter outlines the dynamic characterisation of an asymmetric cymbal transducer which is assembled using one steel and one titanium end-cap. The

transducer has been designed to exhibit a dual resonance by using different end-cap materials and geometrical dimensions.

In order to ensure consistency with the later investigations of Nitinol cymbal transducers, the effects of temperature above room temperature, such as between 60-80°C, on the dynamic behaviour of the asymmetric cymbal transducer are studied. This was also an attempt to identify any common dynamic behaviour between the asymmetric cymbal transducer and the Nitinol cymbal transducers, for example relating to the mechanical coupling at high temperature. Therefore, the asymmetric cymbal transducer is tested at two temperatures, one being room temperature (around 20-25°C) and the other around 60-80°C. This upper temperature limit was chosen to be consistent with that which is required later for the characterisation of the cymbal transducers with shape memory Nitinol end-caps in the austenite phase. The experimental results are complemented by numerical simulations of the displacement amplitude and resonant frequency for both symmetric and asymmetric modes of vibration.

Recent research has demonstrated how classical cymbal transducers are being modified to enable them to be used for high power applications [23–25], which can include actuators for surgical and dental cutting devices. Consequently, it is desirable to be able to assess both the modal behaviour and the displacement amplitude of transducers constructed for such applications. It was not until recently [6, 24, 25] that LDV measurements were applied to cymbal transducers. As an example, Meyer, Jr. et al. were able to employ two LDV systems to simultaneously view the vibration of both end-caps of a cymbal transducer [6]. The displacement amplitude can be measured using a 1-D LDV system in a procedure called vibration resonance response characterisation (VRRRC), whereas the modal behaviour can be studied using 3-D laser vibrometry, called experimental modal analysis (EMA). These techniques are employed in this chapter, and are supported by electrical impedance measurements which are used to evaluate the resonant frequencies of the transducer. This characterisation process extends that used by Tressler et al. [41] in their study on a dual resonance cymbal transducer in 1997, where an admittance spectrum was used to measure the resonant frequencies.

3.1 Transducer design

The three primary components of a cymbal transducer are the end-caps, the mechanical coupling mechanism, and the piezoceramic driver. Transducers can be constructed which resonate at different frequencies depending largely on both the size and the type of end-cap material. The achievable displacement amplitude of such transducers is also dependent on the end-cap material.

3.1.1 End-cap design and fabrication

The elastic properties of the chosen end-cap material will affect the vibration response of a cymbal transducer, whose first axial mode acts as the operating mode. The fundamental resonant frequency, f_r , in air can be determined using shell theory, and is primarily dependent on the geometrical dimensions and the elastic properties of the end-caps [173]. Equation 3.1.1 shows this relationship [173].

$$f_r \propto \sqrt{\frac{E}{\rho} \left[\frac{1}{\phi_c^2(1-\nu^2)} + \frac{1}{R^2} \right]} \quad (3.1.1)$$

In Equation 3.1.1, ϕ_c is the end-cap cavity base diameter, and R is the radius of the end-cap [173]. The materials chosen for the end-caps were titanium T5 (Ti-6Al-4V), made to ASTM B265, and high-carbon bright steel, or silver steel, fabricated to BS 1407 with chemical composition as shown in Table 3.1 [174].

Element	C	Mn	Si	S	P	Cr
Min. (%)	1.10	0.25	0.00	0.00	0.00	0.35
Max. (%)	1.20	0.45	0.40	0.035	0.035	0.50

Table 3.1: Chemical composition of silver steel

In principle, the steel and titanium end-caps should resonate at different frequencies for equal geometrical dimensions because their stiffnesses are not the same. Steel and titanium were chosen as the end-cap materials because of the significant difference between the Young's modulus of each. This difference is shown in Table 3.2, in addition to the other mechanical properties required for the FEA simulation of the complete

asymmetric cymbal transducer [175–178].

Property	Silver Steel	Titanium T5
Young's modulus (GPa)	200	110
Density ($\text{g}\cdot\text{cm}^{-3}$)	7.85	4.043
Poisson's ratio	0.3	0.33

Table 3.2: Selected mechanical properties of silver steel and titanium

These properties can vary depending on factors such as the grade of the material. The Young's modulus used for each material in the simulation is as close as possible to that which is accepted in the literature. In Equation 3.1.1, the resonant frequency is shown to be dependent on specific modulus of the end-cap (E/ρ). By using the properties shown in Table 3.2, the specific modulus of the steel is $25.48 \text{ GPa}/\text{g}\cdot\text{cm}^{-3}$, and the specific modulus of the titanium is $27.21 \text{ GPa}/\text{g}\cdot\text{cm}^{-3}$. This shows that the differences in Young's modulus between the end-cap materials will not contribute a significant influence on the asymmetry. The differences in the geometrical dimensions between the fabricated end-caps will likely impart a greater effect on asymmetry. For reference, Table 3.3 shows the chemical composition of T5 from ASTM B265 [179].

Element	Ti	C	Al	V	Fe	H	N	O
ASTM B265 (%)	Bal.	<0.08	5.5-6.75	3.5-4.5	<0.30	<0.015	<0.03	<0.25

Table 3.3: Chemical composition of titanium T5

Selection of end-cap material and the tuning of geometrical dimensions can be undertaken using FEA to ensure that the transducer behaves as desired. Figure 3.1 shows a side-view schematic of a cymbal transducer end-cap, and Table 3.4 summarises the dimensions of the end-caps which are used in the assembly of the asymmetric cymbal transducer, measured with Mitutoyo digital callipers.

The geometrical dimensions shown in Table 3.4 were chosen to ensure the resonance of the transducer at ultrasonic frequencies. End-cap fabrication requires very high precision and accuracy, and differences in geometrical dimensions were found between the two end-caps. The impact of small changes in these dimensions, and also the effect of applying a scaling factor to each geometrical dimension of the transducer on the first resonant frequency, have previously been studied [130, 173]. Consequently, the

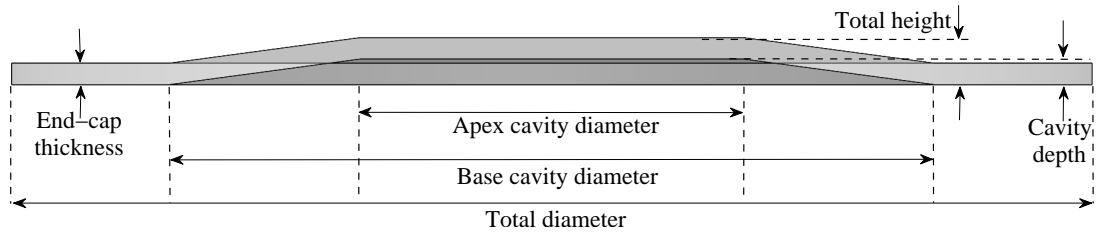


Figure 3.1: Cymbal transducer end-cap geometry

Parameter	Silver steel (mm)	Titanium T5 (mm)
Apex Cavity Diameter	4.56 ± 0.02	4.25 ± 0.01
Base Cavity Diameter	9.74 ± 0.02	9.55 ± 0.03
Cavity Depth	0.31 ± 0.02	0.30 ± 0.02
End-Cap Thickness	0.21 ± 0.01	0.22 ± 0.01
Total Diameter	12.71 ± 0.02	12.71 ± 0.02
Total Height	0.52 ± 0.01	0.52 ± 0.01

Table 3.4: End-cap dimensions of the asymmetric cymbal transducer

manufacturing tolerances are very small if precise geometrical dimensions are required. The resonant frequency of a cymbal transducer is dependent on parameters such as the base cavity diameter and the end-cap thickness [14], meaning that the manufacturing process requires very high precision and accuracy. For the steel end-cap used in this research, screw threads were first machined into a rod specimen to create a holding fixture from which the complete cymbal end-cap shape could be cut. The screw thread, which sat on the top surface, was then removed in the final step. There was a difficulty in ensuring the thickness of the end-cap remained the same as the flange thickness. The titanium end-cap was cut from sheet material. As shown in Table 3.4, it was found that the steel and titanium end-caps possessed marginally different geometrical dimensions after fabrication. Very minor changes to the dimensions shown in Table 3.4 can produce significant alterations to the resonant frequency of the transducer. This was shown in a study by Tressler et al. where they demonstrated how each parameter affected the frequency response using FEA [14].

3.1.2 Piezoceramic selection

The type and geometry of the piezoceramic both depend on the application and the geometry of the transducer. Piezoelectric drivers are commonly used in ultrasonic transducers because of the low dielectric loss [180] and due to their suitability at relatively high mechanical loading and input voltages [180]. A cymbal transducer incorporates a piezoceramic disc or ring which is poled in the thickness direction. Traditionally, either hard or soft piezoceramics can be used as the driver material, but a hard Navy Type I ceramic called Sonox[®] P4 (CeramTec) was chosen for this study due to its low dielectric and mechanical losses, and also its suitability for high power acoustic applications [181]. A high piezoceramic Curie temperature is also required for transducer assembly. This must be greater than the temperature conferred by soldering, or those of the environment in which the transducer operates. The Curie temperature of Sonox[®] P4 is approximately 325°C [182], and so the temperature required to apply small solder spots to the ceramic for conductivity between the end-caps and the piezoceramic must be much lower than this.

Some material properties, required for the FEA simulations, were not provided by CeramTec. For this reason, properties from Morgan Electro Ceramics Ltd were used to complete the FEA model, using their Navy Type I data. The Sonox[®] P4 class is a hard, Navy Type I piezoceramic which is similar to a Morgan Type 4 [183]. From the data available, PZT-402 from Morgan represented a close match to Sonox[®] P4.

3.2 Transducer assembly

One of the most significant limitations of classical cymbal transducers concerns the epoxy bond layers used to form the mechanical coupling, where the repeatable and consistent deposition of epoxy resin is very difficult to achieve. Devices based on the cymbal transducer have used different coupling techniques. These include producing end-caps with larger flanges which can accommodate bolts [23–25]. The asymmetric cymbal transducer was fabricated using small amounts of epoxy resin on the flanges of the end-caps in contact with the edge of the piezoceramic disc. A thin layer of insulating epoxy resin in the form of Eccobond[®] (Ellsworth Adhesives Ltd), at a ratio

of three parts 45 LV epoxy resin to one part 15 LV resin catalyst hardener, was applied to the flange of each end-cap before careful assembly. This resin must be cured at room temperature over a period of approximately 24 hours, and so a rig was required to hold the assembly in place, which is shown in Figure 3.2.

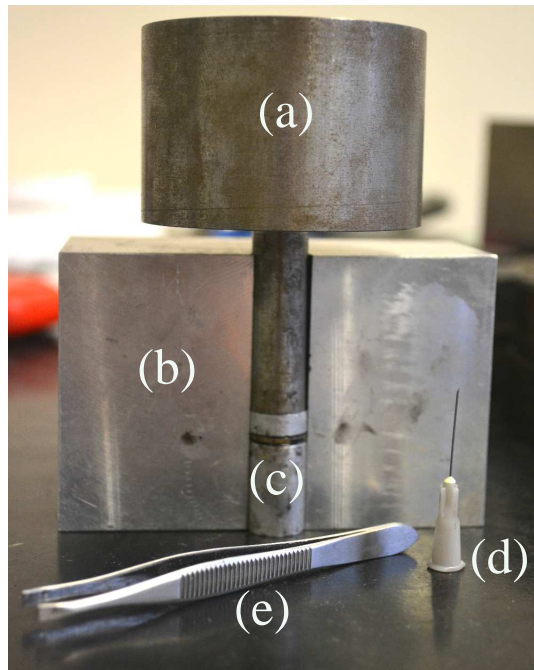


Figure 3.2: The rig used for transducer assembly, comprising (a) the top-weight, (b) support weight, (c) transducer assembly support, (d) the epoxy resin applicator and (e) the tweezers used for the transducer assembly

The transducer is carefully assembled using tweezers (e) and placed in the support cylinder (c). The epoxy resin is applied using the applicator (d), and the assembly is clamped in place using two support weights (b). To minimise the likelihood of epoxy resin entering the end-cap cavities, pressure was applied via a top weight (a), only around the end-cap flanges. The transducer is held in place as shown in Figure 3.2 at (c). It is very difficult to deposit exactly enough epoxy resin to hold the transducer together, but not an excessive amount so as to risk allowing epoxy resin into the end-cap cavity, because of the size of the transducer and the width of the end-cap flanges. The support rig was mainly used to ensure that the bonds contained as few defects as possible, such as small air bubbles. However, the elimination of every small defect and air bubble would be very difficult because this adhesive must be cured at room

temperature. These inhomogeneities in the bond layers can be a result of surface roughness, local menisci and a non-uniformity in the deposition which is difficult to control, all of which can affect the final resonant frequency [22, 130]. The deposited layers were $40\mu\text{m}$ thick in nominal terms, but this quantity is variable, because it is very difficult to precisely control the thickness of the deposited adhesive due to its viscous nature. This is an ongoing problem in the assembly of this type of transducer. Techniques such as screen printing can be used, but there remains the high possibility of adhesive moving over the 24-hour curing process. The reason that an insulating and not a conductive epoxy was chosen is that in general, conductive epoxies possess a relatively low bonding strength [10]. For this investigation, it was also important to ensure that an epoxy resin which can operate effectively around $60\text{-}80^\circ\text{C}$ is chosen, as that is the temperature range to which the Nitinol transducers will be subjected.

In a cymbal transducer, the electromechanical coupling between the piezoceramic driver and the metal end-caps must contain no possible sources of short or open-circuiting, and the type of adhesive to be used requires careful consideration. Insulating epoxy resins, such as Eccobond[®], tend to be stronger than conductive epoxies [10], many of which are silver-filled and do not provide the coupling performance required, especially at high displacement amplitudes. Therefore to ensure that effective electrical contact could be achieved between the end-cap flanges and the piezoceramic disc, six small solder spots were applied to each flat surface of the piezoceramic disc. Depositing these solder spots around the circumference minimises the risk that the end-cap would be unevenly affixed to the piezoceramic disc, and increases the likelihood that one of these spots would make electrical contact with the end-cap. The heat was applied for the minimum amount of time possible, and the integrity of the piezoceramic disc was verified using electrical impedance analysis to ensure it was operational, and that the temperature conferred by soldering did not cause damage or impede its functionality. Once the bonding was completed, wires were connected to the transducers, forming the electrodes. Commonly, this is achieved using a standard soldering technique. However, because of the sensitivity of Nitinol to temperature, and the fact that there would be a possibility that the phase transformations of the Nitinol would be permanently affected, conductive epoxy (Chemtronics CW2400) was chosen instead. The conductive

epoxy resin requires appropriately four hours at room temperature to fully cure, where room temperature is regarded as being approximately 20-25°C.

3.3 Dynamic characterisation

The dynamic characterisation process which has been implemented consists of electrical impedance measurement which allows the resonant frequency of a transducer to be evaluated, EMA for extracting the modal parameters through measurements using a 3-D LDV, and VRRC which allows the displacement amplitude of an oscillating surface to be measured as a function of frequency using a 1-D LDV. The dynamic characterisation measurements provide more than just resonant frequency and displacement amplitude information. The Q factor, any softening or hardening nonlinearities in the displacement amplitude responses, and the electromechanical coupling coefficient (k_{eff}) can all be evaluated if required.

3.3.1 Thermal loading

The transducers were characterised at two temperatures, one being room temperature, around 20-25°C, and the other around 70-80°C. This is because the Nitinol transducers and prototype device analysed in Chapters 5-7 are also analysed in this range. All materials are affected in some way by changes in the temperature to which they are exposed, and can soften when heated [184]. In addition, certain epoxy resins have been known to experience decreases in flexural and storage moduli at raised temperatures [185]. The thermal loading is a variable which was controlled using a commercial dehydrator. Using a dehydrator enabled an LDV laser beam to be directly focused on a transducer end-cap surface, but also provided suitable shielding from temperature fluctuations which would distort measurements. Measurement at the higher temperatures was difficult, because there had to be a way to measure the displacement amplitude responses using the LDV with minimum error. It is possible to conduct accurate LDV experiments through flat, transparent surfaces such as glass [186], providing the detection angles are properly calibrated, and that reflections and refraction of the laser light are not contributing to either noise or measurement errors.

However, many industrial ovens have very thick windows which make it difficult to use an LDV to measure the response of the transducer. A COTS dehydrator (Andrew James, Model: AJ-991) was selected because the transformation temperature range of both types of Nitinol lay within the operating range of the dehydrator, and there was opportunity for LDV measurement. The dehydrator is shown in Figure 3.3.

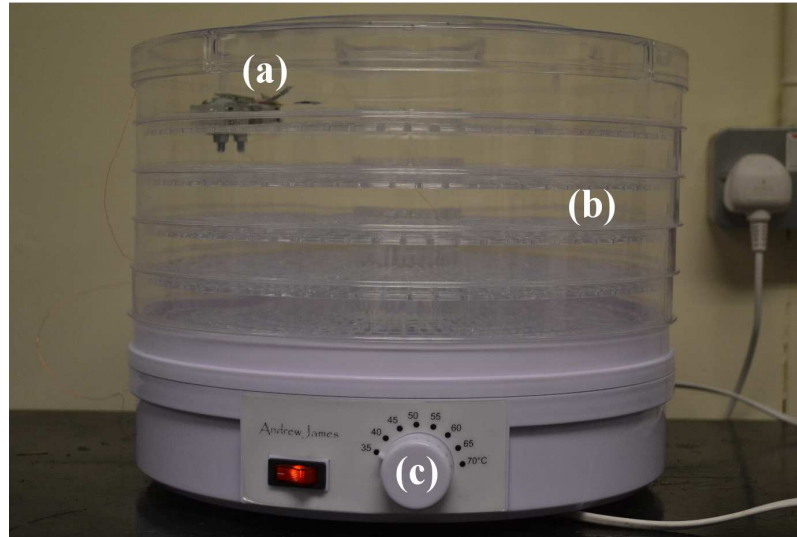


Figure 3.3: The dehydrator chamber used to change the transducer temperature, showing (a) the location of the transducer fixed in the chamber, (b) the different chamber sections, and (c) the thermostat for temperature control

The chamber could be controlled via a thermostat with an approximate 35-70°C temperature range. There were very small apertures in the chamber through which the laser beam of the LDV could be directed. The temperature within the thermal chamber was measured and monitored using a type-K thermocouple, and all resonant frequency and VRRC measurements were made after the transducer was allowed to thermally equilibrate in the heated environment for a minimum of around twenty minutes.

3.3.2 Resonant frequency characterisation

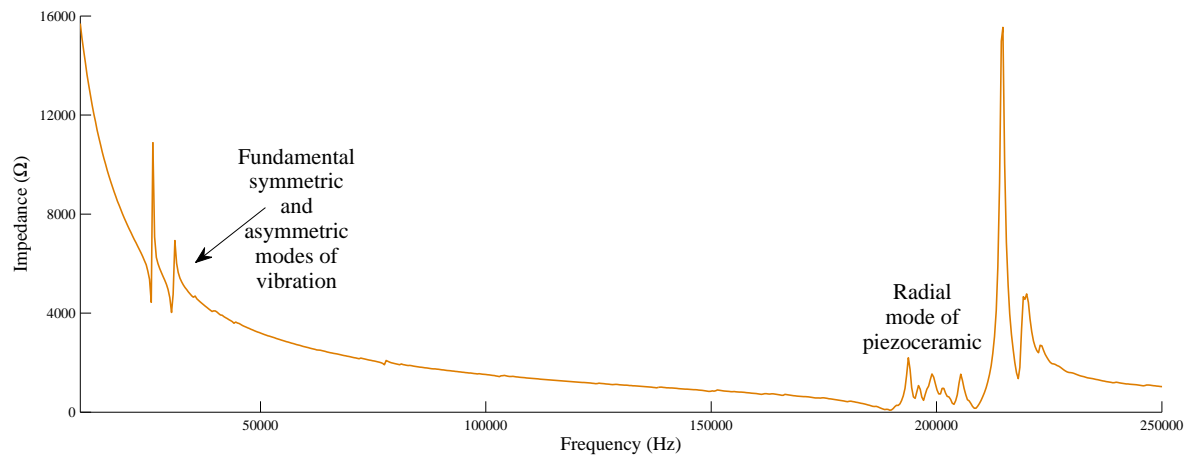
Resonant frequency characterisation is commonly performed by using an impedance gain/phase analyser. Impedance-frequency and phase-frequency spectra can provide important information about a transducer such as the quality of the assembly, the resonant frequencies and the associated phase angles. The spectra can also provide sufficient data to calculate the effective coupling coefficient (k_{eff}). Electrical impedance

measurements have a number of useful purposes. In many applications, it is desirable to be able to produce a cymbal transducer which resonates only in a symmetric mode. If not, then energy can be shared between multiple modes [130]. Measurements can be used to verify the presence of asymmetry, to assess the assembly quality of the transducer and also to check for open or short-circuiting between the piezoceramic driver and the end-caps. Problems associated with the epoxy bond layers can also contribute to asymmetry in transducer, which can be detected in an impedance-frequency spectrum as a double-peak. If there is a double-peak, then one frequency represents a symmetric mode, and the other an asymmetric mode.

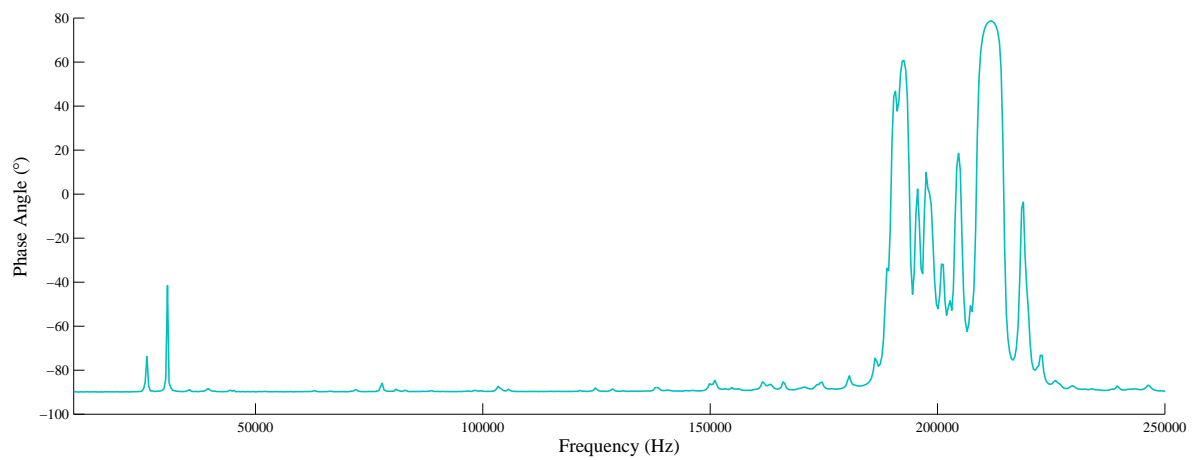
The Agilent 4294A Impedance/Gain Phase Analyser, with an Agilent 42941A probe, was used to generate impedance-frequency and phase-frequency spectra for the transducer. To ensure measurement accuracy and reliability, the impedance analyser is first calibrated by attaching two load-heads to the probe, one of 0Ω , (called the ‘short’, Agilent HRM 504), and the other of 50Ω (called the ‘load’, Agilent HRM 601). The component fixture, to which the cymbal transducer is connected, is then calibrated by configuring the open and short response of the impedance probe with the fixture attached but without the transducer connected. The cymbal transducer can then be tested in the dehydrator chamber, where it is excited at $0.5V_{p-p}$ by the impedance analyser. The temperature was monitored using a type-K thermocouple connected to a 10V power supply.

The resonant frequency of the fundamental mode and the frequency of the piezoceramic mode are both observable from the impedance-frequency and phase-frequency spectra. An example of each is shown in Figure 3.4, measured from the asymmetric cymbal transducer at 21.7°C . The location of minimum impedance, or maximum admittance, represents the resonant frequency of the transducer. It is clear that two fundamental modes exist for this transducer, indicating an inherent asymmetry in the design. Figure 3.5 shows the resonant frequency response response for two different temperatures in the 20-40kHz frequency range.

When the transducer was heated, the resonant frequency response was monitored in real-time using the impedance analyser. The resonant frequency decreased almost instantly after the heating function was activated. The elastic compliance of



(a) Impedance-frequency spectrum



(b) Phase-frequency spectrum

Figure 3.4: Standard impedance-frequency and phase-frequency spectra of the asymmetric cymbal transducer indicating both the fundamental modes of vibration and the piezoceramic mode of vibration, measured at 21.7°C, showing the measured (a) impedance-frequency and (b) phase-frequency spectra

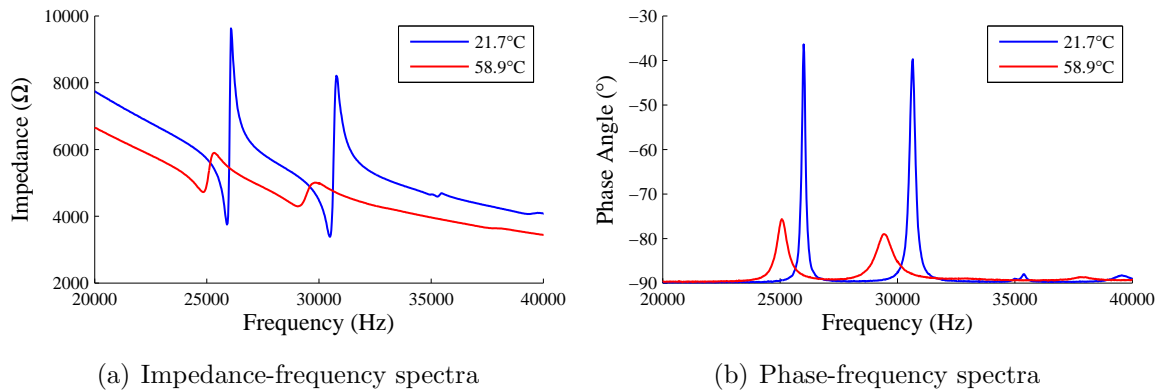
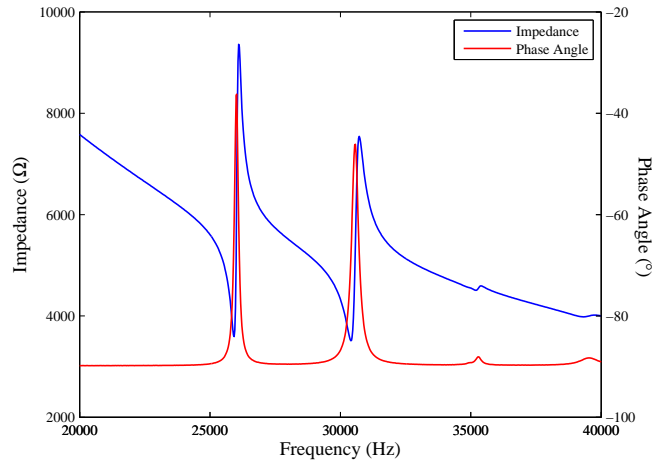


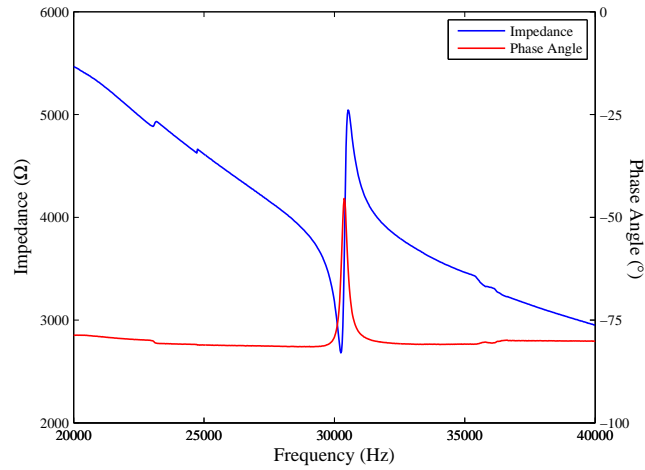
Figure 3.5: Resonant frequency characterisation of the asymmetric cymbal transducer fundamental modes of vibration, showing the measured (a) impedance-frequency and (b) phase-frequency spectra

piezoceramics can be affected by temperature [20, 187]. The end-cap materials and the epoxy bond layers are likely to be softening as a result of the temperature increase. In an asymmetric cymbal transducer, one frequency is associated with the symmetric mode, and the other with the asymmetric mode. Figure 3.6 shows the effect of imposing a physical constraint on the apex of each end-cap on the impedance-frequency response. This shows the contribution of the vibration of each end-cap to the frequency response of the transducer, demonstrating the asymmetry.

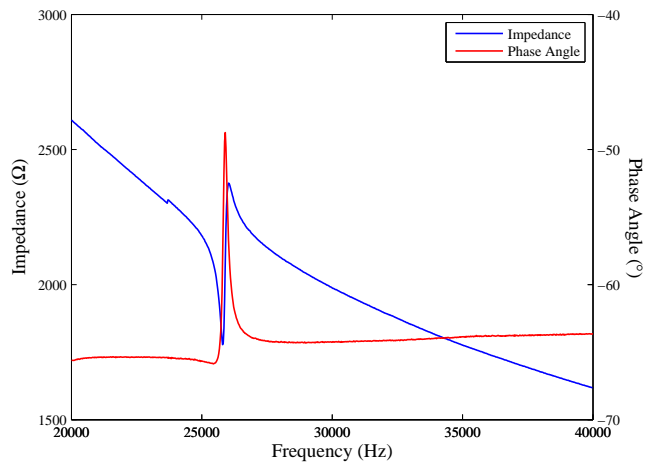
This data illustrates that the end-caps will vibrate at different frequencies if there is asymmetry in the transducer. One frequency will represent a symmetric mode of vibration, and the other an asymmetric mode. This is important in order to detect the displacement amplitude of the transducer in each mode of vibration. For example, to measure the displacement amplitude of the symmetric mode, the end-cap associated with that mode must be identified. Electrical impedance analysis allows resonant frequencies to be measured. However, due to the fact that impedance measurements do not give an accurate indication of whether a mode is symmetric or asymmetric, the modal behaviour of the cymbal transducer must be characterised, and this is performed using experimental modal analysis (EMA).



(a) Without constraint



(b) Steel end-cap constrained



(c) Titanium end-cap constrained

Figure 3.6: Resonant frequency characterisation of the asymmetric cymbal transducer showing (a) no constraint, (b) steel end-cap constrained and (c) titanium end-cap constrained, all measured at 22.3°C

3.3.3 Experimental modal analysis

Finite element analysis (FEA) packages such as Abaqus/CAE are powerful and time-effective tools for determining modal behaviour of structures. However, validation of these models in terms of accuracy and reliability must be undertaken. This is to ensure the assumptions and inputs in the numerical simulation process are acceptable. It is also helpful to be able to complement resonant frequency response measurements, such as those found using electrical impedance analysis, with the modal response at each resonant frequency. This is to provide information about the shapes of the modes, which can also be simulated using FEA. Experimental modal analysis (EMA) is often used as a method of validating numerical models, for example those used in modal analysis simulations.

In the 1930s, aircraft technology was becoming more important as the dynamics of flight were becoming better understood [188]. Because of this, it was important to be able to understand the dynamics of specific critical structures on an aircraft such as the wing section. Even though the technology available to do this was limited, analysis of the free vibrations at the tip of a wing was possible using a free decay curve, and from that the eigenvalues and damping ratios could be extracted [188]. When EMA was first being used, simple shakers were used to force the structure under test into a state of resonance. This soon evolved into a more intricate process called normal mode testing, which allowed the determination of the mode shape associated with each resonant frequency. This was achieved by situating shakers at different points on the structure [188]. In the 1960s, progress was made due to the development of the fast fourier transform (FFT) algorithm, which enabled the transformation between time and frequency domains to be faster with improved efficiency [188]. Computer technology, for example with respect to software complexity and processing speed, has since improved such that very complex structures can be studied using EMA.

The modal parameters are natural frequencies, damping factors, and mode shapes. For cymbal transducers, symmetric and asymmetric modes need to be differentiated. When a double-peak appears in the frequency response spectrum of a cymbal transducer, one of the peaks will represent the in-phase asymmetric mode and the other will be the out-of-phase symmetric mode. It has been reported that the

symmetric mode can be detected at either a higher or lower resonant frequency than the asymmetric mode [6]. The geometrical dimensions of the transducer are a contributing factor, and this requires experimental verification. This section introduces EMA, and reports an EMA study of the asymmetric cymbal transducer.

EMA set-up and procedure

The main components of an EMA test set-up are a method of excitation, technique for response measurement and a method for data extraction. The modal behaviour of transducers can be assessed by using a 3-D LDV, which operates by splitting a laser beam into a measurement beam and a reference beam. After splitting, the two beams are recombined once they are reflected back to the LDV, as shown in Figure 3.7 [189].

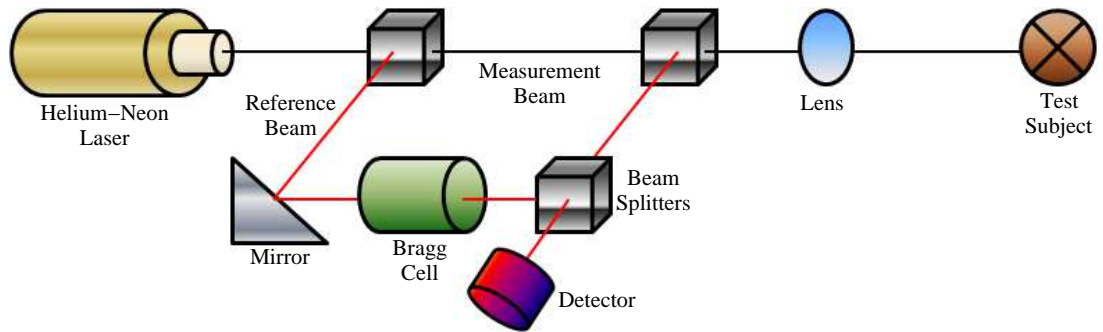


Figure 3.7: A schematic of the LDV [189]

Laser Doppler vibrometry is a non-contact optical technique comprising two phenomena. The first is the Doppler Effect, which is the frequency shift of a wave in relation to the source frequency, described by Equation 3.3.1 [189].

$$f_D = 2 \left(\frac{v}{\lambda} \right) \quad (3.3.1)$$

A source wave with wavelength λ is reflected by an object with velocity, v . The Doppler-shift can be used to find the velocity of the object relative to the source with a wavelength which is known. This is achieved by the LDV making use of the interferometry principle, shown by Equation 3.3.2, where I represents the light intensity of a particular laser beam [189].

$$I_{TOT} = I_1 + I_2 + 2\sqrt{I_1 I_2 \frac{\cos 2\pi(r_1 - r_2)}{\lambda}} \quad (3.3.2)$$

As shown in Figure 3.7, the laser beam is split to form a measurement beam and a reference beam. The measurement beam is ultimately reflected by the test object, where it is focused on to the detector [189]. The vibration of the object creates a bright and dark fringe pattern on the detector as a result of the interferometry principle [189]. A half-wavelength displacement of the test object is represented by a full dark-to-bright cycle. The modulation frequency of this pattern is in proportion with the velocity of the test object vibration due to the Doppler effect, however the direction of movement cannot be determined. This is the reason for the inclusion of a Bragg Cell, which is an acousto-optic modulator [189]. It applies a shift to the frequency of the light when the test object is not moving, and so when a change is detected, for example test object position, the direction of movement can be identified [189]. The LDV can then be used to determine the velocity and displacement amplitudes of a point on a test surface, by counting the fringes on the detector. In conjunction with displacement demodulation, the displacement amplitude is measured, as governed by Equation 3.3.3 [189].

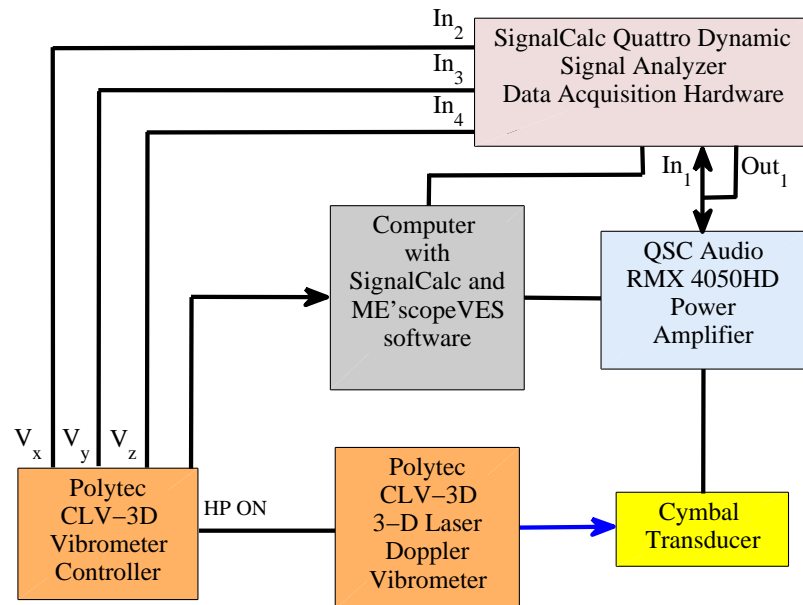


Figure 3.8: EMA test set-up

$$v = 2\pi fs \quad (3.3.3)$$

When using a laser Doppler vibrometer it must be ensured that the laser signal to the test object surface is precisely focused to minimise inaccuracy. For EMA, a 3-D LDV (Polytec CLV) is connected to a power amplifier via a SignalCalc Ace (Quattro) Signal Analyzer (Data Physics Corporation). Figure 3.8 shows the complete EMA set-up.

Experimental considerations and measurements

A frequency response function (FRF), which is the ratio of an output amplitude response to an input signal as a function of frequency [20], for each measurement point is recorded. After curve-fitting, the individual FRFs can be processed to create a complete modal response measurement for a set of data points. The measured data can then be used in data processing software whereby the modal behaviour can be extracted and analysed using a representative model of the real structure. The quality of data which is obtained from any experiment depends on careful experimental set-up. Factors which must be considered for EMA are [190]:

1. Mechanism of excitation.
2. Locations of measurement points, including the density of the measurement grid.
3. Boundary conditions, in particular the support mechanism for the transducer.
4. Quality of the signal.
5. The response measurement transducer, such as accelerometer, or laser Doppler vibrometer.

There is a range of input excitation signals which can be used including sinusoidal, chirp, burst and random [190]. In this case, the transducer was driven with a random input signal since the resultant FRFs were clear. Once the FRFs from each measurement point were acquired, they were curve-fitted and processed using

ME'ScopeVES (Vibrant Technology, Inc.) software. Figure 3.9 shows the cymbal transducer measurement grid in the ME'ScopeVES environment. There were 41 measurement grid points on the surface of each end-cap, totalling 82 for the transducer. Measurements were not made around the circumference face of the PZT disc in each case due to the fact that this vibration motion could be detected on the edges of the end-cap flanges. Figure 3.10 shows the EMA results measured in the out-of-plane axial z -direction for the transducer. The coordinate system used for the experiments is shown in Figure 3.10(d), where the z -direction is normal to the apex surface of the end-cap.

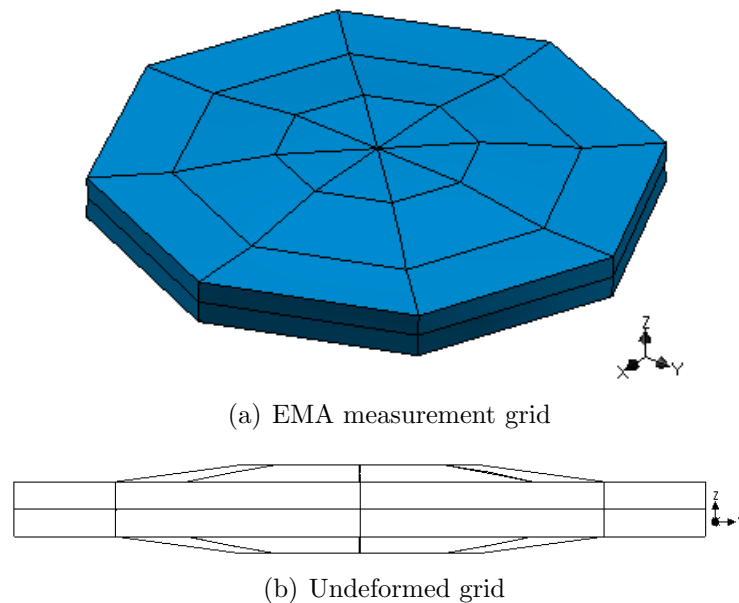


Figure 3.9: (a) The EMA measurement grid and (b) the side view of the undeformed grid

Vibrations from the environment were minimised by the use of an isolated optics table, but there were sources of noise from the poor reflectivity as a result of the surface condition of the material. Due to the small size of the end-caps, any abrasion of the material or addition of reflective tape to boost the reflectivity would have affected the thickness of the end-caps, and thus one or both of the resonant frequencies of the transducer. There was also noise in the lateral x -direction and y -direction measurements compared to that of the axial z -direction, so only the z -direction measurements are presented. However, the symmetric and asymmetric modes can be clearly distinguished. Also, the locations of conductive epoxy bonding spots

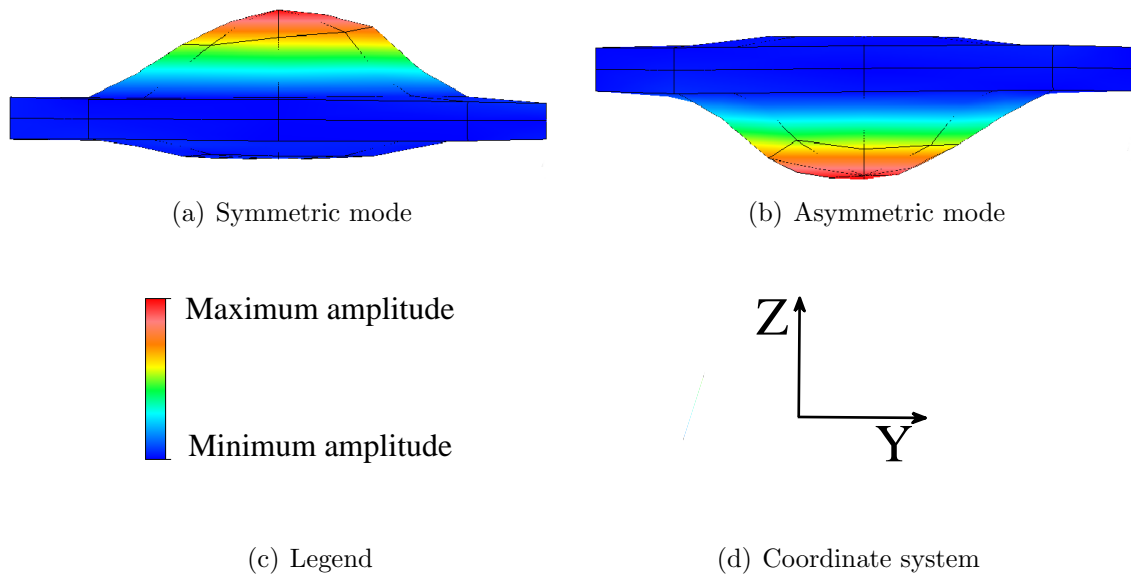


Figure 3.10: Modes of the asymmetric cymbal transducer, showing (a) the symmetric mode at 26056Hz, and (b) the asymmetric mode at 30648Hz, measured at 20.4°C, (c) shows the legend for the EMA results shown in this research where cool colours correspond to lower amplitudes and warm colours signify higher amplitudes, and (d) shows the coordinate system in which the mode shape results are presented

on the end-cap flanges for the electrodes restrict measurement at those points, but this is unavoidable. The frequencies of the symmetric and asymmetric mode shapes confirm a high level of agreement with the resonant frequencies found using the electrical impedance measurements. The displacement amplitudes of each mode around resonance can now be measured using the VRRC technique.

3.3.4 Vibration resonance response characterisation

The displacement amplitudes of cymbal transducers can be measured using laser Doppler vibrometry using a 1-D LDV. A measurement protocol was adopted in order to characterise the displacement amplitude for five voltage levels, from 2-10V in 2V steps around the resonant frequency of each mode of vibration. It was also used to detect nonlinear behaviour of the transducers at two different temperatures as the input voltage is increased, using LabVIEW software to control the excitation signal into the transducer. Figure 3.11 shows the schematic for the VRRC experimental set-up.

It is important to ensure that the laser beam is aligned perpendicular to the test surface for accurate measurement. Also, the displacement amplitude response

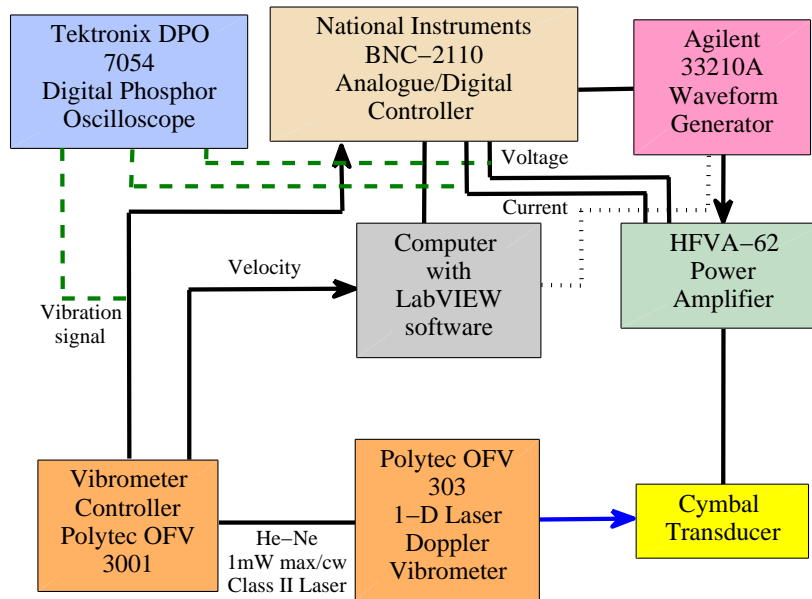


Figure 3.11: VRRC test set-up

should be measured at the same location for different temperatures. For each VRRC experiment, the laser beam was focused on the centre of the apex. The LDV and cymbal transducer under test were then both connected to the LabVIEW characterisation system via the NI GPIB data-card. The input voltage signal to the cymbal transducer could be controlled, and the vibration response was measured using the LDV. The data was collected and analysed in real-time using the LabVIEW software. A burst-sine excitation signal was applied with 2 or 4 seconds between these bursts depending on the voltage level, to minimise heating which could affect the frequency response at the lower of the two test temperatures. The cymbal transducer was subjected to bi-directional frequency sweeps around the resonant frequency of each mode so that any nonlinearity in the responses could be observed. The results for the asymmetric cymbal transducer are shown in Figures 3.12 and 3.13.

The displacement amplitudes of the symmetric and asymmetric modes of the transducer were measured at two different temperatures. At the higher temperature, the displacement amplitude of the titanium and steel end-caps and the resonant frequencies are lower. This behaviour can be attributed to a combination of the tendency of many materials to soften as their temperature is increased, including, importantly, the epoxy bond layer. Despite the fact that epoxy resin from Eccobond[®]

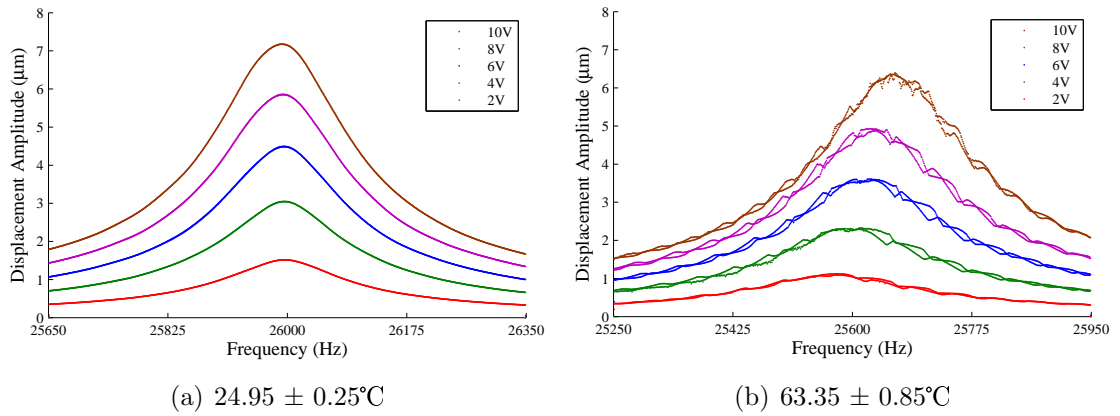


Figure 3.12: Plots showing the (a) low temperature and (b) high temperature vibration responses of the symmetric mode of the asymmetric cymbal transducer

is operational up to around 90°C , the material is clearly being affected. At the raised temperature, modulations in the vibration responses are evident which do not appear in the vibration responses at the lower temperature. This provides an indication that the bond layers have been compromised in some way at the higher temperature.

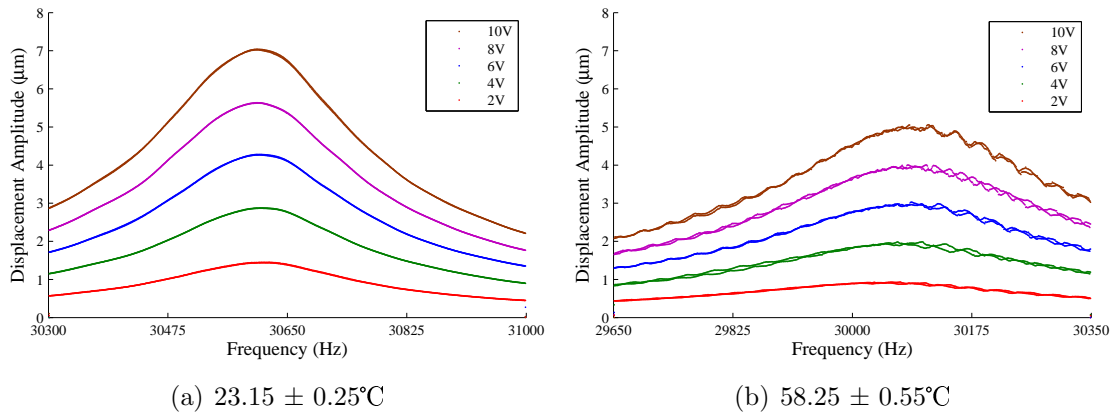


Figure 3.13: Plots showing the (a) low temperature and (b) high temperature vibration responses of the asymmetric mode of the asymmetric cymbal transducer

The difficulties surrounding the use of cymbal transducers in their classical form are exacerbated by exposing them to raised temperatures. It has already been established that methods of improving the cymbal transducer design for implementation in high power applications have focused on ameliorating the physical coupling mechanism. There is a further need for this if such a transducer is to be used over a wide temperature range, and it is evident that certain adhesives may not be sufficiently reliable. In addition, the epoxy bond layers have such a profound impact on the vibration response

of a cymbal transducer, that repeatable transducer assembly is very difficult. It is vital that the epoxy resin components are properly mixed, and in equal quantities, before the epoxy resin is then deposited equally in the transducer assembly. The epoxy resin could also be degassed before use to help eliminate air bubbles, although this was not performed in this research. It would be useful to be able to measure the vibration response of both transducer end-caps simultaneously, for example by using two 1-D LDV systems focused on both end-caps at the same time. This has previously been undertaken [6], but would be advantageous for transducer characterisation to be able to instantly detect a failure in one of the end-caps, rather than performing the experiments one after another.

Materials such as steel and titanium soften as they are heated, but the VRRC results show a reduction in displacement amplitude. The small reduction in resonant frequency is evident for both modes, but if this is a result of a reduction in stiffness, a corresponding increase in displacement would be expected [122]. This is not consistent with these results, and so the epoxy bond layers may be compromised by the thermal loading, thus limiting the achievable displacement amplitude at the raised temperature. The characterisation of cymbal transducers at different temperatures is not fully understood. However, the correlation between the measurement results from the dynamic characterisation techniques is evident for this transducer, and Figure 3.14 shows the comparison.

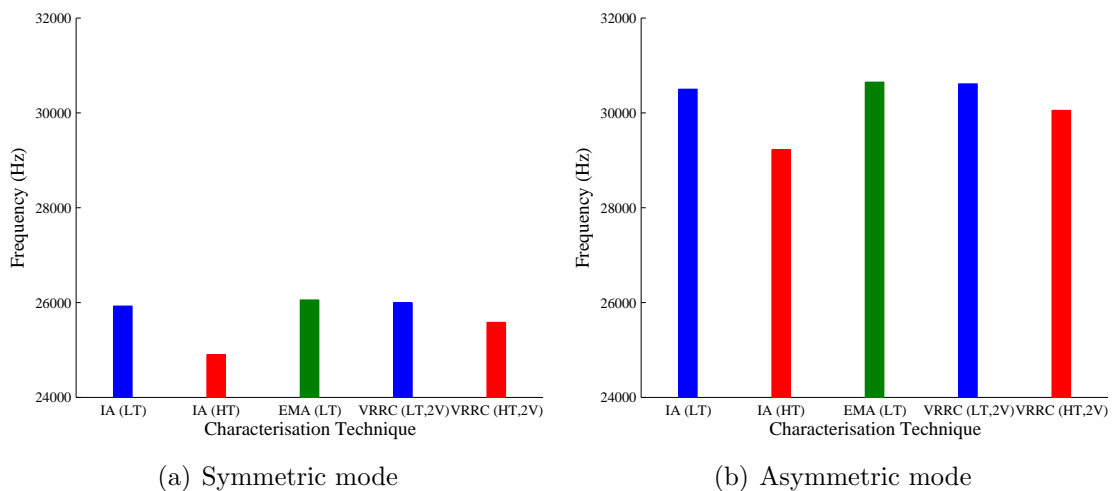


Figure 3.14: Resonant frequencies measured using the three dynamic characterisation techniques for the asymmetric cymbal transducer

The data in Figure 3.14 shows the comparison between resonant frequency measured from each measurement technique for both modes of vibration. This comprises electrical impedance analysis (IA) and vibration resonance response characterisation (VRRC) at the low temperature (LT) and high temperature (HT), and EMA at the low temperature. Only the 2V measurements from the VRRC tests were used in the comparison, since the resonant frequency changed for the higher temperature test for each mode of vibration.

The non-uniformities in the epoxy bond layers are shown in Figure 3.15 to illustrate the difficulty in controlling the profile of the mechanical coupling in cymbal transducers. The condition of each bond layer after the characterisation procedure is shown, and while the bond layers were likely affected when subjected to the higher temperature, they were not deposited uniformly in the transducer assembly process.

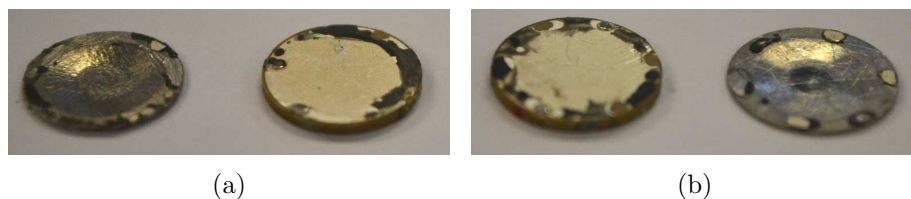


Figure 3.15: Condition of each epoxy bond layer in the asymmetric cymbal transducer after dynamic characterisation

3.4 Finite element modelling and analysis

In order to complement and correlate with experimental results, FEA can be conducted to predict the resonant frequencies, modal behaviour and displacement amplitudes around resonance of the transducer. Finite element analysis (FEA) is a numerical technique which is used to resolve a complex system into discrete components which can then be mathematically analysed. It is common to complement experimental data with results from a numerical model or simulation. There are a number of reasons for doing this, for example enabling the validation of a numerical model using experimental data, so that the model can then be used to predict behaviour for a range of boundary conditions. Modern computational tools and advanced simulation software mean that a very close correlation between experimental and numerical data is achievable, provided

that the simulation inputs are realistic. The numerical modelling undertaken in this investigation utilises the finite element analysis (FEA) software Abaqus/CAE v6.12-2. Two procedures have been implemented, the first being natural frequency extraction using a Lanczos eigensolver. This allows the natural frequencies and the mode shapes to be evaluated. A steady-state linear dynamics step has then been used to solve for the displacement amplitude of each mode. This step can also be implemented for von Mises stress analysis.

The literature provides many accounts of recent worldwide research to accurately model, simulate and represent flexensional and cymbal transducer behaviour. The epoxy bond layer significantly affects the resonance behaviour of the transducer [10], and so its inclusion in finite element simulations is necessary. There are ostensible difficulties with this, because there is difficulty in accurately measuring the bond layer in practice. Therefore, an iterative technique may be the most suitable option for correlating numerical and experimental data. It can be appropriate to model a half or quarter section of the cymbal transducer due to the intrinsic symmetry of the configuration [10, 113]. This is advantageous as it eases computation time, although it is often desirable to view the entire three-dimensional resonating structure, for example if there are asymmetries in the fabricated transducer. Despite the accuracy which is achievable, finite element simulations are mathematical approximations, and there will inevitably be inhomogeneities and inconsistencies in materials used for the experimental investigations which are not included in the simulations. These are sources of discrepancy between numerical and experimental data.

3.4.1 Model development and optimisation

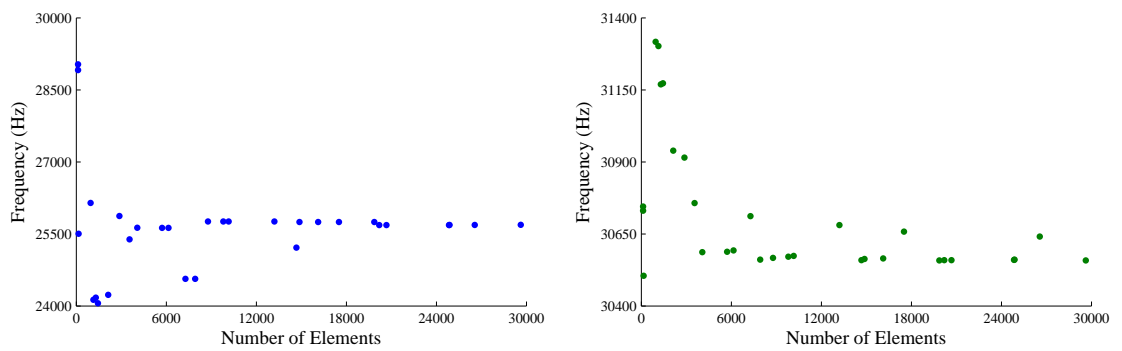
One of the major objectives of numerical modelling is the simulation of real systems such that the models can be used to predict behaviour for a range of conditions with high accuracy. A finite element model (FEM) is created from discrete elements, and a full model assembly is created from these elements by joining them at node points. Once this is achieved, material properties can be assigned to the elements, such as Young's modulus, density and Poisson's ratio. In this work, a cymbal transducer FEM was produced using the C3D20R element type with a hexagonal element shape. A

continuum element was chosen rather than a shell element so that both the natural frequency of each mode and the von Mises stress of the transducer could be accurately calculated, and also because they enable bending to be accurately simulated. This element type is a 20-node quadratic brick element with reduced integration. Reduced integration decreases computation time [191], and the simulations are solved either via linear or quadratic interpolation. In order for the correct mode shapes to be predicted, quadratic interpolation must be implemented. The natural frequency and steady-state linear dynamics steps are then conducted.

Mesh convergence study

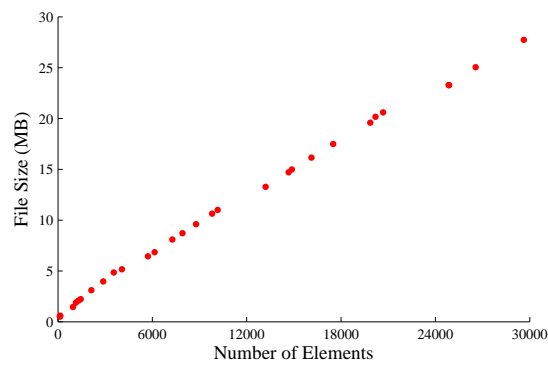
In FEA, it is common for a compromise to be made between simulation accuracy and computation time. To ensure the reliability of the computed results of each resonant frequency, and also to assess whether the modelled mesh density is sufficient to be able to simulate the transducer behaviour, a mesh convergence study was conducted on the cymbal transducer FEA model for both symmetric and asymmetric modes of vibration. The results are shown in Figure 3.16.

The file size, and hence computation time, for the FEM increased as the density of the mesh increased, as shown in Figure 3.16(c). In order to achieve a compromise between computation time and model accuracy, it was found that a mesh density of 9804 elements was sufficient for the entire assembly to be able to effectively simulate the response of each transducer mode. It is noticeable in Figure 3.16(b) that complete convergence of the resonant frequency has not been reached up to a mesh density containing 30000 elements. This is contrary to the results of the symmetric mode, shown in Figure 3.16(a). For an increase in overall FEM mesh density, the structure stiffness in each direction can be different, based on the distribution of the elements in the structure model. When the FEM mesh density is changed, the horizontal density of the elements in the model changes, as does the vertical density of the elements. As the mesh density of the complete FEM is increased, the distribution of the elements in each direction is changed to accommodate them within the geometry of the transducer. It was decided that a mesh density of 9804 elements was acceptable for an accurate simulation. The computation time required for simulation was significantly increased



(a) Symmetric mode

(b) Asymmetric mode



(c) Size of output file

Figure 3.16: Mesh convergence study of the asymmetric cymbal transducer finite element model, showing (a) convergence of the symmetric mode, (b) convergence of the asymmetric mode and (c) size of output file as a function of the number of elements in the finite element model

for the FEM with a denser element mesh, which produced results which were not significantly different to those obtained with less dense FEM element meshes. For example, from the results shown in Figure 3.16(a), the resonant frequency of the symmetric mode is around 26kHz where the FEM mesh density is 6000 elements. For a mesh density of 30000 elements, the computed resonant frequency remains around 26kHz. Although the computed resonant frequency of the asymmetric mode has not fully converged, as shown in Figure 3.16(b), the computation time at 30000 elements was found to be very high for only a marginal change in resonant frequency compared to FEM meshes with fewer elements. A cutaway schematic of the final FEM is shown in Figure 3.17.

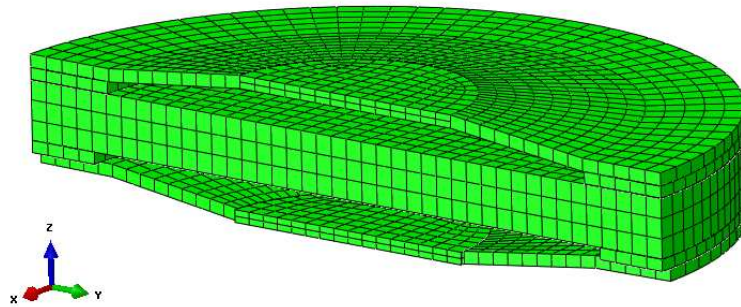


Figure 3.17: Cutaway schematic of the asymmetric transducer FEM

The model was constructed using the dimensions and material properties shown earlier in the chapter. The dimensions of the epoxy bond layer were altered in small steps until the numerical prediction of the resonant frequencies correlated with the experimental results. The thicknesses of the epoxy bond layers had to be adjusted in the model because it was not possible to acquire a precise measurement of thickness from the transducer by physical inspection. The thickness of each epoxy bond layer was defined as 0.2mm in the FEM. One difference between the two epoxy bond layers was set in the model. The inside diameter of the epoxy bond layer ring in between the steel end-cap and the piezoceramic disc was 10.2mm, and the inside diameter for the epoxy bond layer ring in between the titanium end-cap and the piezoceramic disc was 9.62mm. It would also be possible to use cohesive elements for modelling the epoxy resin bond layers, however due to the difficulty of the physical observation of debonding in the transducers, these elements were not adopted in this research.

Initially, material property data for the epoxy bond layers were obtained using

tensile testing. However, during VRRC measurements, the epoxy bond layer was softer. In the FEA, the Young's modulus of the epoxy bond layer was found to significantly affect the mode shapes. It was not possible to determine the stiffness properties of the epoxy bond layers in the transducer either during or post operation. As a consequence, the elastic properties of the epoxy bond layers in the FEM were tailored until the correct mode shapes were identified, ensuring that the resonant frequencies were also accurate.

Model damping

All real dynamic mechanical systems experience energy losses as a result of assembly component interactions and the environment in which they operate. Energy loss in the response of a dynamic system is governed by damping, of which there are three principal types. Viscous damping relates to the dissipation of energy in a fluid, friction damping can occur due to the physical interaction of different sub-structures or system components, and structural damping, for example from the material properties of a system [192]. In a transducer, damping is not uniform [20]. Damping was applied in two ways in the cymbal transducer FEM. In Abaqus/CAE, a global damping factor can be applied in the analysis step. The second is a viscous damping factor which is a proportional aggregate of the stiffness and mass matrices in the form of Equation 3.4.1 [192].

$$[C] = \alpha[M] + \beta[K] \quad (3.4.1)$$

In Equation 3.4.1, $[C]$ is the damping matrix, $[M]$ is the mass matrix, $[K]$ is the stiffness matrix, α represents the mass coefficient and β is the stiffness coefficient. The damping ratio, ξ , is related to both α and β via Equation 3.4.2 [192].

$$\xi = \frac{\alpha}{2\omega_a} + \frac{\beta\omega_a}{2} \quad (3.4.2)$$

The α coefficient decreases as frequency increases, whereas the β coefficient increases [180]. For this reason, at ultrasonic frequencies the α coefficient is assumed to be

negligible based on the dominance of the β coefficient [180]. The β coefficient can be expressed as shown in Equation 3.4.3 [192].

$$\beta = \frac{1}{\omega_a Q_m} \quad (3.4.3)$$

Damping can be calculated using the mechanical quality factor, Q_m . At frequencies far from resonance, the damping from the material will be less accurate [20]. This relates to the structural damping of the model. As shown later in the section, only the displacement amplitude at resonance for each mode of vibration has been computed. In Equation 3.4.3, ω_a can be calculated by $\omega_a = 2\pi f_r$, and the mechanical quality factor Q_m can be found by using the relationship shown in Equation 3.4.4 [193].

$$Q = \frac{f_r}{f_2 - f_1} \quad (3.4.4)$$

Q_m is in itself an expression of the damping in the system, as a ratio between the stored energy and the energy lost each cycle [193]. In Equation 3.4.4, f_1 and f_2 are determined by dividing f_r by $\sqrt{2}$ [193], and this relationship is therefore known as the half power bandwidth (HBW) [193]

3.4.2 Resonant frequency estimation

Abaqus/CAE was used to predict the mode shapes and resonant frequencies of the asymmetric cymbal transducer FEM. The computed results were also compared with the results of the EMA. The results are shown in Figure 3.18.

In the transducer models shown in Figure 3.18, the upper end-cap indicates the steel end-cap, and the lower is the titanium end-cap. The symmetric and asymmetric modes of vibration calculated from FEA are respectively identified from the out-of-phase and in-phase motion of the end-caps. Figure 1.3 also showed the symmetric and asymmetric modes of vibration for a cymbal transducer modelled in Abaqus/CAE. However, the FEM presented in this chapter is different, as there is asymmetry modelled into the transducer via differences in geometrical dimensions between the end-caps, and also

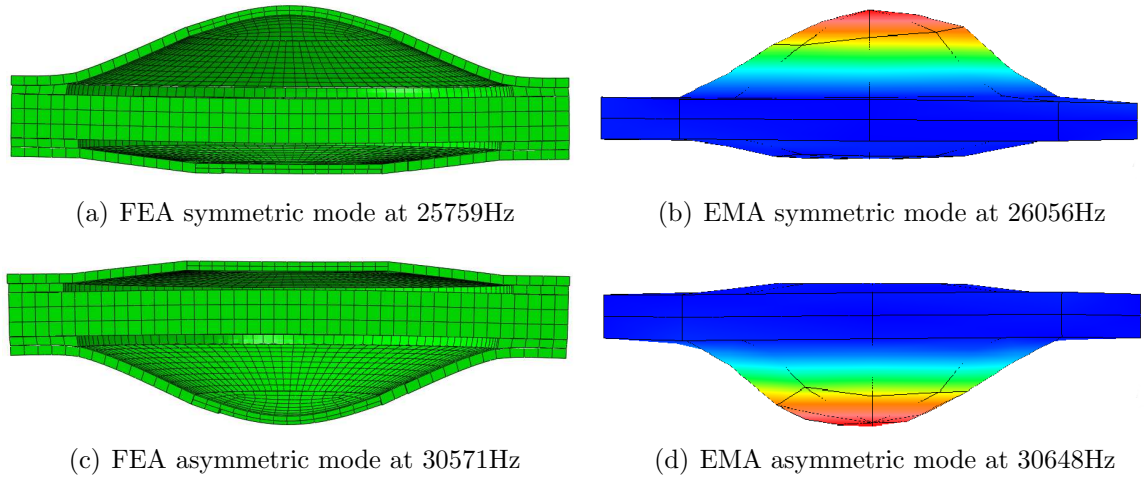


Figure 3.18: FEA and EMA comparison of the asymmetric cymbal transducer showing (a) the symmetric mode at 25759Hz from FEA, (b) the symmetric mode at 26056Hz from EMA, (c) the asymmetric mode at 30571Hz from FEA and (d) the asymmetric mode at 30648Hz from EMA

the epoxy bond layers. Therefore, whilst the phase relationship between the end-caps is preserved, one end-cap will resonate with higher amplitude compared to the other for each mode, due to the asymmetry. A very close correlation between FEA and EMA for both the mode shapes and the resonant frequencies of the modes has been achieved. There are only minor differences in the actual mode shapes of the symmetric and asymmetric modes. With this high level of correlation achieved between experimental and numerical data, the displacement amplitudes around the resonant frequency of each mode were then calculated.

3.4.3 Displacement amplitude estimation

In the computation of the displacement amplitude response of the cymbal transducer in each mode, a steady-state linear dynamics step was implemented in the FEM.

Only data for the 2V input voltage condition was computed to limit the response to the linear regime. Figure 3.19 shows the simulated displacement amplitude response for the symmetric and asymmetric modes of vibration for an input voltage of 2V. The peak displacement amplitude of each mode is shown in Table 3.5, with the experimental data being acquired from VRRC. A very high degree of correlation between the resonant frequencies and the peak displacement amplitudes of each mode between experimental

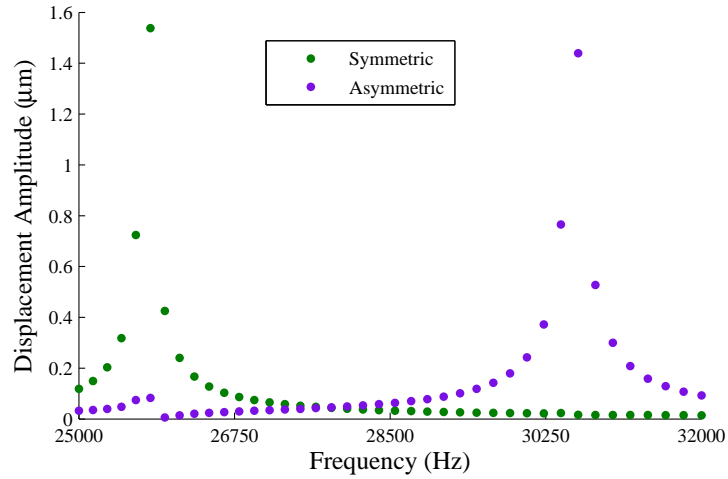


Figure 3.19: Displacement amplitude response of each mode from FEA for a 2V input voltage

and numerical techniques has been obtained. This is important for this research, because it increases confidence in the ability of the cymbal transducer FEM to be able to accurately predict the resonant frequency and displacement amplitude for the FEM with property adjustments, for example to material properties.

Mode	Symmetric		Asymmetric	
	f_r (Hz)	a_o (µm)	f_r (Hz)	a_o (µm)
Experimental	25996	1.52	30613	1.44
FEA	25759	1.54	30571	1.44
Difference	-237	+0.02	-42	0
Change (%)	-0.91	+1.32	-0.14	0

Table 3.5: Comparison between experimental and numerical data for the displacement amplitude response of the asymmetric cymbal transducer for a 2V input voltage

3.5 Chapter conclusions

This chapter has provided an overview of the design of an asymmetric cymbal transducer, and how the dynamic response can be tailored by careful end-cap material selection and end-cap geometry specification. A cymbal transducer has been successfully designed to operate at two resonant frequencies by adopting end-caps fabricated from two different materials. This transducer could be successfully

implemented as a tuneable transducer, in that an end-effector or tool could be attached to one side of the transducer to resonate at that frequency. The tool could then be driven at a different frequency using this transducer, but in order to achieve a sufficient amplitude, the tool would have to be attached to the other end-cap in order to achieve sufficient amplitude.

The dynamic characterisation process has also been introduced, and there have been a number of original contributions. Cymbal transducers have not before been driven and characterised in the VRRC configuration at raised temperatures. The raised temperature condition is likely conferring a softening effect on the epoxy bond layers, as there are modulations which appear in the displacement amplitude response of each mode in the higher temperature condition. It is possible that the mechanical coupling is softening when the temperature of the epoxy resin is increased closer to its maximum operational temperature, which is around 90°C, thus affecting its behaviour under the influence of ultrasonic vibrations. It is evident that this method of mechanical coupling is very difficult to control, and this is detrimental to an efficient and economical design process. Nevertheless, a high level of correlation has been achieved between the experimental data obtained from EMA and VRRC and the results of the FEA.

A dual frequency ultrasonic device could be developed using the transducer studied in this chapter, where a tool attachment could be operated at two different frequencies simply by affixing it to different sides of the transducer. However, the limitation of this is that the tool must be detached and connected to the other end-cap. This may be undesirable for some applications. For example, a medical device might require more than one resonant frequency to penetrate different materials during an operation, such as bone and muscular tissue. Removing the device to switch the attachment would be cumbersome and inconvenient. Therefore, a method of tuning the resonant frequency of the transducer would be an attractive capability. The forthcoming chapters discuss how this capability has been achieved using Nitinol as the transducer end-cap material.

Chapter 4

Recommendations for design with nitinol

Cymbal transducers can be fabricated which incorporate Nitinol as the end-cap material. The mechanical behaviour of Nitinol is complex, and guidelines are required to enable the reliable manufacture and testing of tuneable transducers using Nitinol. A thermal analysis technique, differential scanning calorimetry (DSC), is employed to identify the temperatures at which Nitinol transforms between phases, and is performed prior to the dynamic characterisation process. This chapter aims to provide advice for the design and fabrication of cymbal transducers with Nitinol end-caps.

4.1 Material selection

The loading conditions to which the material will be subjected are the first important considerations. Phase transformations are stress dependent, so that if Nitinol is subjected to high stress, then a higher temperature must be reached to transform the material. This has been illustrated previously in Figure 1.7. Two types of Nitinol can be used. The first is shape memory Nitinol, which possesses a final austenitic transformation temperature above room temperature. The Nitinol microstructure can either be switched with no associated observable shape change, or via the SME. Shape memory Nitinol is suitable for applications where the transducer is permitted to be heated above room temperature, with nickel-titanium alloys being operational

to approximately 100°C [61]. Recently it has been found that temperature increases in piezoceramic materials can cause an increase in the influence of nonlinearities in the vibration response of an ultrasonic device [20]. Nonlinearities in the vibration response of the transducer, and the stress and temperature limits of the Nitinol must therefore both be considered.

The second type of Nitinol is superelastic Nitinol. This possesses a final austenitic transformation temperature around or below room temperature. Traditionally widely used for biomedical stents [142–147], superelastic Nitinol has not received much attention in transducer design. The vibration behaviour of superelastic Nitinol cymbal transducers is studied in this research. It is unknown if sufficient stress can be generated in the cymbal transducer end-caps to cause the superelastic effect, and this is also investigated. The importance of understanding the influence of the superelastic effect is not restricted to superelastic Nitinol. If a transducer fabricated with shape memory Nitinol end-caps is operated at a temperature higher than the A_F transformation temperature of the shape memory Nitinol, then the influence of superelasticity at sufficiently high stress levels in the material would be significant, and therefore should be understood.

It is known that it is difficult to machine Nitinol [194], and so the effect on the tooling equipment of Nitinol fabrication should be considered. It is also possible to optimise or change the transformation temperatures of Nitinol by changes to chemical composition, heat treatments and cold working. Therefore, in the design of a Nitinol transducer, the type of Nitinol to be used, the fabrication of the Nitinol assembly component, including any heat treatments or cold working which would be required should all be considered.

4.2 Transformation temperature identification

There are a number of transformation temperature identification techniques which can be applied to Nitinol. There are advantages and limitations of each, such as the availability of sacrificial material for testing and the ability to accurately observe the transformation changes. Some of the techniques which can be applied to Nitinol are

described in this section [195].

Active A_F measurement

One of the simplest methods is called the Active A_F test. This is also commonly referred to as either the Water or Alcohol Bath Test [195]. First, the Nitinol sample is deformed when below its M_S temperature, after which it is heated. The shape recovery of the material is carefully monitored as it is heated, until a complete deformation-temperature relationship can be produced. A representation of this is shown in Figure 4.1 [195].

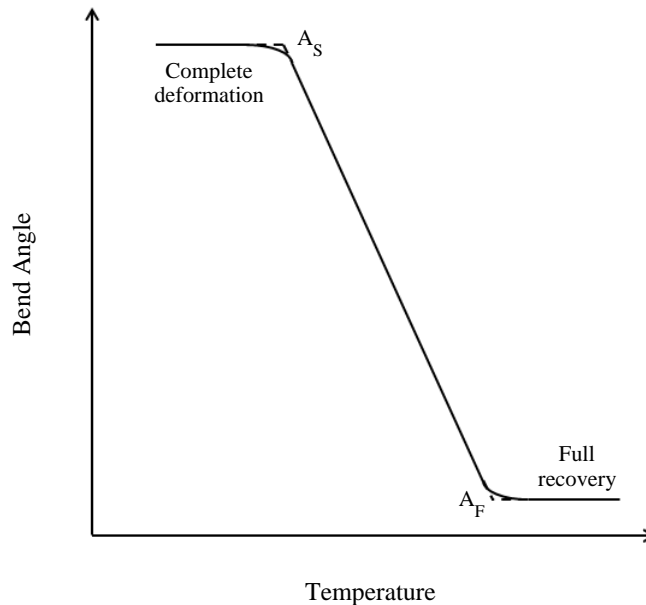


Figure 4.1: The active A_F technique [195]

A common example of this method is the testing of a sample of Nitinol wire. The sample is placed in a water or alcohol bath where the temperature can be carefully monitored using a thermocouple. The angle of bending as a function of temperature is recorded, and a bend angle versus temperature relationship can be produced. Johnson Matthey Medical Components specify a start temperature of around -50°C for testing superelastic Nitinol [195]. The technique requires prior knowledge of the temperature required for the material to exist in the pure martensite phase, and also whether the material is superelastic or shape memory at the test temperature. However, it is a straightforward method which allows for a fast and effective identification of the

transformation. This method was successfully adopted in determining the A_F for a shape memory Nitinol end-cap (Memry GmbH). The end-cap was deformed at room temperature before being placed in boiling water. It was observed to spring back into its original shape, indicating that the A_F transformation temperature had been passed. The reverse transformation was very fast, and the transformation temperatures of this material were therefore impossible to determine with accuracy using this technique.

Constant load method

The Constant Load technique is normally applied for Nitinol utilising the SME instead of superelasticity [195]. A load is applied to the material and then it is subjected to a thermal cycle, where the transformation temperatures can be extracted from the resulting deformation-temperature relationship. For example, a deformed sample of Nitinol in the martensite condition is heated until it is pure austenite, where shape recovery can be observed. After this, the Nitinol is cooled to below M_F where the set configuration is retained. The shape recovery is monitored at all stages in the thermal cycle, and the relationship can be plotted. Figure 4.2 shows sample data for this method [195].

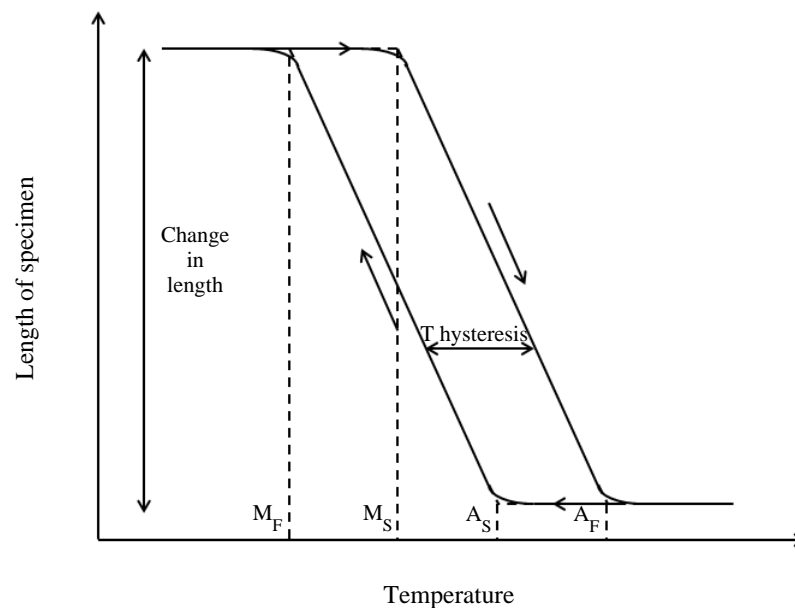


Figure 4.2: The constant load technique [195]

The hysteresis between the transformations on the heating and cooling curves is

indicated by the arrows on the hysteresis loop, their direction showing the thermal cycle. Whilst this method does give an indication of the four primary transformation temperatures, it is more suited to shape memory Nitinol than superelastic material. This is because where the M_S and M_F temperatures are well below 0°C , the experiment would require a setup which permits the temperature of the Nitinol to be decreased to a sub-zero temperature range.

The techniques described are relatively simple and inexpensive to perform. However, not all of the transformation temperatures can be accurately identified. Other techniques can be used to identify transformation behaviour because many of the properties of Nitinol are stress, temperature and phase dependent. As an example, monitoring changes in the electrical resistivity of Nitinol as a result of changes in stress or temperature can provide phase transformation information. This technique has had success for identifying the transformation temperatures of a nickel-titanium alloy exhibiting the R-phase [196,197]. The electrical resistivity technique has been found to be more sensitive to R-phase presence than DSC [196], despite concerns reported in the literature regarding the difficulty in data interpretation and that there are limitations surrounding the inability of the electrical resistivity method to provide specific or latent heat information [59].

Differential scanning calorimetry

An accurate and reliable transformation temperature identification method is differential scanning calorimetry (DSC). DSC is a thermo-analytical technique that records the difference in heat energy between a sample and a reference. A Diamond DSC (Perkin Elmer) was used to analyse the Nitinol samples. DSC can be very reliable and repeatable if used correctly, and significantly more accurate than the simpler rival techniques. Temperature is recorded as a function of heat flow in the sample of material for a designated temperature range, and the data is presented as a thermogram. The transformations between different microstructural phases can be identified from the thermogram, where the points of inflection on both the heating and cooling curves are the approximate locations of the transformation temperatures. As the response curve deviates from its natural baseline, the associated endothermic or exothermic reaction

is due to a transition between one of three possible phases to another. The start and finish temperatures of the martensite, R-phase and austenite phases are identified in the example thermogram in Figure 4.3.

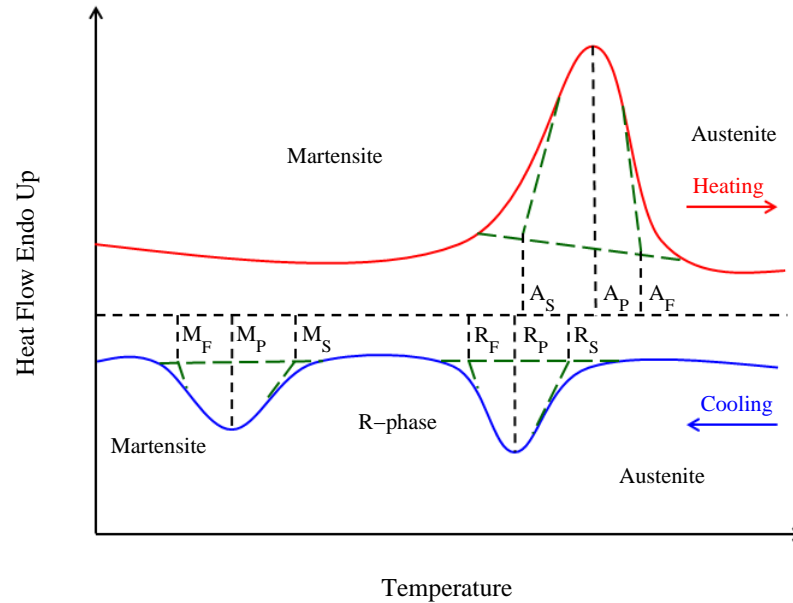


Figure 4.3: Analysis of DSC data

In the analysis of DSC thermogram data, the steepest slopes are extrapolated to the baseline for each transformation event. The associated transformation temperature is then estimated directly from the abscissa. The definitions of the baseline, the steepest slopes and the transformation temperatures incur human error, and so this is why the estimated transformation temperatures are all approximations. It is more accurate to estimate the transformation temperatures of a material which exhibits sharper peaks, and hence steeper slopes.

The phase transformations between austenite, the R-phase and martensite are thermally hysteretic between the heating and cooling cycles [59]. This means that the transformation events in the material can occur at different temperatures when the material is being heated compared to when it is being cooled. There are three types of thermal transformation response in Nitinol. The first is a direct transformation from one phase to the other, with no indication of a developing intermediate microstructure. Another is the asymmetric case, where the intermediate R-phase only appears on the cooling curve. The third is where the R-phase appears in both the heating and cooling

curves. In this case, the R-phase and austenite peaks on the heating curve are often either overlapped or closer together than the martensite and R-phase peaks on the cooling curve [59]. Consequently, there are up to eight transformation temperatures for a Nitinol alloy, being the finish and start temperatures of austenite (A_F , A_S), martensite (M_F , M_S), R-phase on cooling (R_F , R_S), and R-phase on heating (R'_F , R'_S). DSC allows all of these temperatures to be estimated with a high level of accuracy compared to rival techniques. Figure 4.3 is a characteristic thermogram for the asymmetric case, which has been found to be typical of the Nitinol alloys reported in this thesis.

There are further sources of error which can arise in the interpretation of data obtained from DSC thermograms [59]. The first is that material can move when it is inside the sample pan in the calorimeter [198], resulting in minor distortions in the DSC thermograms. It is therefore important not to mistake a distortion for a transformation event. It can also be easy to misinterpret the R-phase as the martensite phase. This can occur if the chosen temperature range is not large enough. The thermal hysteresis between the austenite and martensite phases is far greater, around 25-50°C [199] or higher, than the austenite to R-phase hysteresis, which can be as low as 2°C, or even less [59]. All Nitinol samples used to conduct the experiments in this research were analysed for two DSC scan rates, one being 10°C/min and the other 20°C/min. The sensitivity and accuracy of the analysis are both affected by the chosen scan rate, as shown in Figure 4.4.

Figure 4.4 qualitatively shows how a transformation temperature, indicated by the abbreviation TT on the abscissa, is affected by the chosen scan rate. The red line indicates a low scan rate, the green line a higher scan rate, and the blue line a very high scan rate. As scan rate increases, the reactions in the thermogram become more distinct, but the accuracy of the data is reduced. Heat flow increases with scan rate because the material is subjected to the temperature range for a shorter duration. The power to both furnaces is monitored and adjusts in response to this change. Therefore a higher scan rate means that an increase in power is required. The resulting compromise is between sensitivity and accuracy [59]. A higher scan rate allows smaller peaks on the heating curve and troughs on the cooling curve to be detected, but will not be as

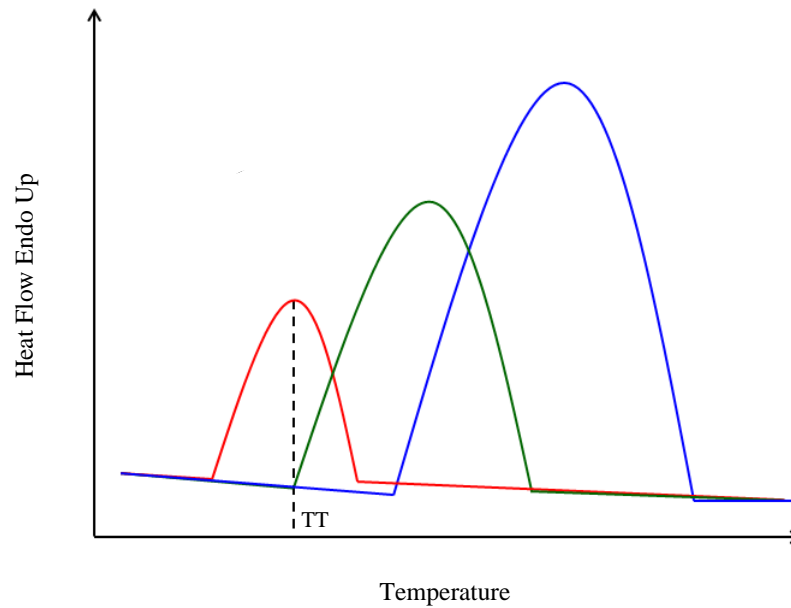


Figure 4.4: Sensitivity and accuracy of DSC data for 3 scan rates, showing red (lowest), green (middle) and blue (highest)

accurate as a test cycle conducted using a lower scan rate due to the increased thermal lag. This thermal lag arises from the delay of the DSC instrument to the change in heat flow. Two scan rates have therefore been implemented in this research, the higher scan rate experiments exhibiting higher heat flow in the samples. Even though studies reported in the literature have adopted $10^{\circ}\text{C}/\text{min}$ as a satisfactory scan rate [59, 200], the chosen scan rate is generally dependent on the need for accuracy or sensitivity.

4.3 Analysis of commercial nitinol

It is difficult to accurately tune the transformation temperatures for Nitinol which must be cold worked, for example to optimise superelasticity or as a result of shape-setting. This is because cold working, in addition to heat treatment and the chemical composition, affects the transformation temperatures [59, 201]. Nitinol is very sensitive to composition and treatments, and even very small adjustments can significantly affect the transformation temperatures. Cold working and heat treatments can also be used to tailor mechanical properties such as the plateau stress and ultimate tensile strength (UTS) [201]. When the transformation temperatures of the material are estimated

using DSC, the fabricated Nitinol cymbal transducers can be operated at temperatures which will generate the desired microstructure in the Nitinol end-caps.

DSC is introduced here for the analysis of two types of commercially available shape memory Nitinol wire (Flexinol[®], Dynalloy) for illustration. Wire specimens of low temperature (LT) and high temperature (HT) shape memory Nitinol alloy were acquired. The material exists as wire, and although there will be cold working caused by the fabrication process which may affect the transformation temperatures, this is not likely to be as severe as the cold working caused in the production of Nitinol end-caps. LT wire possesses a transformation temperature of 70°C, and HT wire a transformation temperature of 90°C. The materials will complete their transformation from martensite to austenite when heated past the respective transformation temperature.

A small sample of material in the order of milligrams is positioned in one of the two furnaces in the calorimeter, with the other furnace acting as the reference, containing an empty sample pan. A thermal cycle is then programmed, whereby the scan rate is defined, as well as the upper and lower temperature limits of the thermal cycle. The heat flow in the material is measured as a function of temperature by comparison with the reference. Endothermic and exothermic reactions are then identified to allow the transformation temperatures of the specimen to be estimated. An endothermic reaction signifies a transition from martensite to austenite, where heat is absorbed, whereas heat-releasing exothermic reactions signify the transformation from austenite to a martensitic microstructure [202].

4.3.1 Sample preparation

For both the calibration and the standard test procedures, 10 μ L or 50 μ L sample pans can be placed in the DSC furnaces. Samples of material must ideally be small, around 2mg in mass for melting-point temperature tests, and approximately 5mg for solid-to-solid phase transition experiments [203]. Material mass is taken into account by the calorimeter, but it is advisable to keep the mass within the specified range limits to ensure that the transformation events can be clearly identified. Since the Nitinol would not experience melting, the larger sample sizes were permitted, around 4-5mg in mass. Plastic deformation of samples during their preparation must be avoided, as residual

stresses can distort DSC thermogram data [59].

A sample was cut from the Nitinol to be tested and placed in a Perkin Elmer 50 μ L vented aluminium sample pan, which was then sealed with a lid in a sample pan press. Vented pans are used to prevent the DSC being damaged from pressure or out-gassing from the sample pan during a test. The pan is placed in the pan press which supports a crimping press holder, and the lid is forced together with the flange of the pan. The sample preparation procedure is illustrated in Figure 4.5.

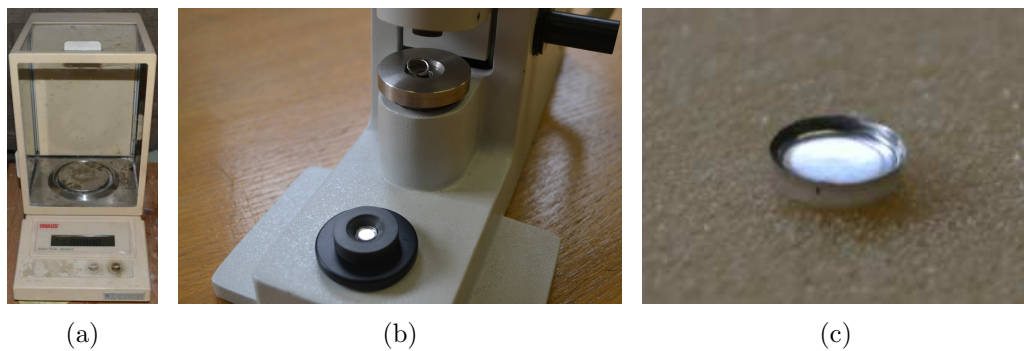


Figure 4.5: Sample preparation by (a) weighing the material, (b) sealing the material in a pan press and (c) resulting in the assembled vented sample pan

4.3.2 Programming and test control

A DSC intracooler controls the thermal environment within the DSC test chamber. All of the tests were conducted between -10 $^{\circ}$ C and +110 $^{\circ}$ C to enable the observation of as many of the transformation events as possible.



Figure 4.6: The placement of test material in DSC, showing the two furnaces in the centre covered with platinum lids where the sample pans are situated

For the superelastic Nitinol, the estimated start and finish temperatures of the martensite phase would likely be out-with the range of the calorimeter, requiring a liquid nitrogen DSC. However, the A_S - A_F range is of most significance, because those are the transformation temperatures at which the transition to austenite is exhibited. The scan rate was specified, and the furnaces were covered and protected by platinum lids, indicated by the small silver discs in the centre of Figure 4.6.

4.3.3 Calibration process

Transformation temperature information is inaccurate without proper calibration. However, the baseline is liable to drift, and this can arise from thermal imbalances between a sample and reference [204]. For this reason, a new baseline calibration was implemented for each experiment. The calorimeter was calibrated for the temperature range and scan rate before the analysis was conducted. The DSC remains calibrated until a different scan rate or temperature range is selected, for which a new calibration procedure must be undertaken. The calibration procedure was performed in four steps:

1. Baseline calibration

A test step is run where the DSC performs a calibration over the chosen temperature range. The baseline range was set to $\pm 50^\circ\text{C}$ of the temperature range used in the tests. Therefore, the baseline range was -60°C to $+160^\circ\text{C}$. The purpose of this step is to measure the noise in the system which is then subtracted from the final experiment scan.

2. Sample calibration

The sample calibration requires the heat flow of a standard reference sample of a single element, sealed in a vented aluminium pan, to be measured with respect to temperature. For this investigation, indium was used, but zinc can also be chosen. Indium and zinc are used because they can be tested many times without having to remake samples. The expected heat flow and the melt temperature of indium is defined, and for the calibration process to continue, the measurement must satisfy the acceptable limits governed by the DSC operating program. If it does not, then calibration should be repeated.

3. Furnace and heat flow calibrations

These are automated procedures performed by the DSC operating program which use the data obtained from the first two steps to ensure the DSC is ready for accurate and reliable experiments to be conducted.

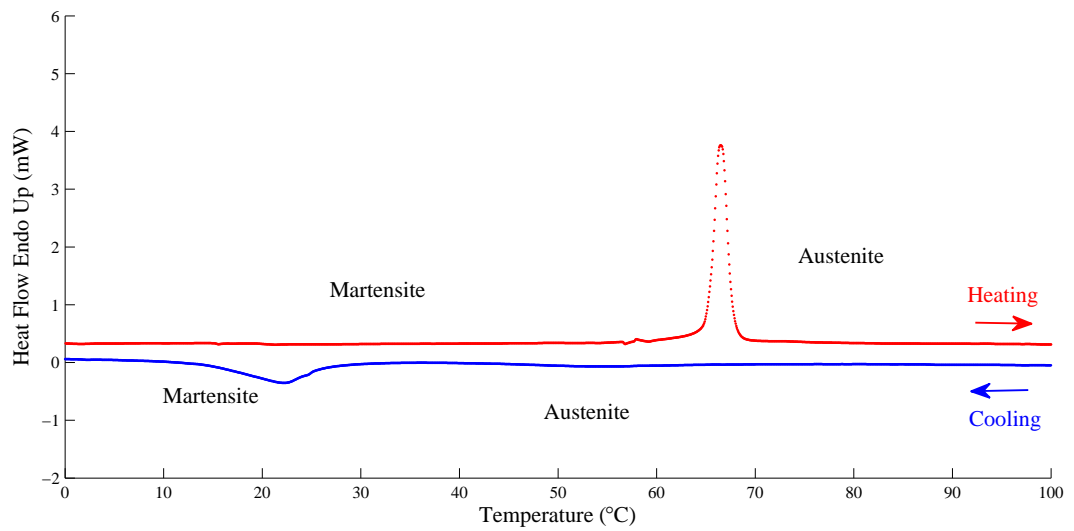
4.3.4 Results

The DSC thermograms of each sample at both scan rates are shown in Figures 4.7 and 4.8, and Table 4.1 summarises the estimated transformation temperatures. The results show that four transformation temperatures, which correspond to the M_F , M_S , A_S and A_F , have been found. As expected, there is a small variation in these temperatures between the two scan rates. From supplier information, the LT wire had a specified transformation temperature of 70°C, and the HT wire had a transformation temperature of 90°C. Both of these temperatures relate to the transformation to austenite, thus the A_F transformation temperature estimated from DSC can be used to assess the accuracy. It was found that the A_F results for both scan rates are closer to the commercially-specified transformation temperature for the LT wire compared to the HT wire. This is shown by the A_F results in Table 4.1. The reason for this is not clear, but one contributing factor will be that the material processing required to fabricate the HT wire, such as the heat treatment used to set the transformation temperatures, will be different to that required to fabricate the LT wire. Differences in processing history may then be affecting how accurately DSC can detect the transformation events in the material.

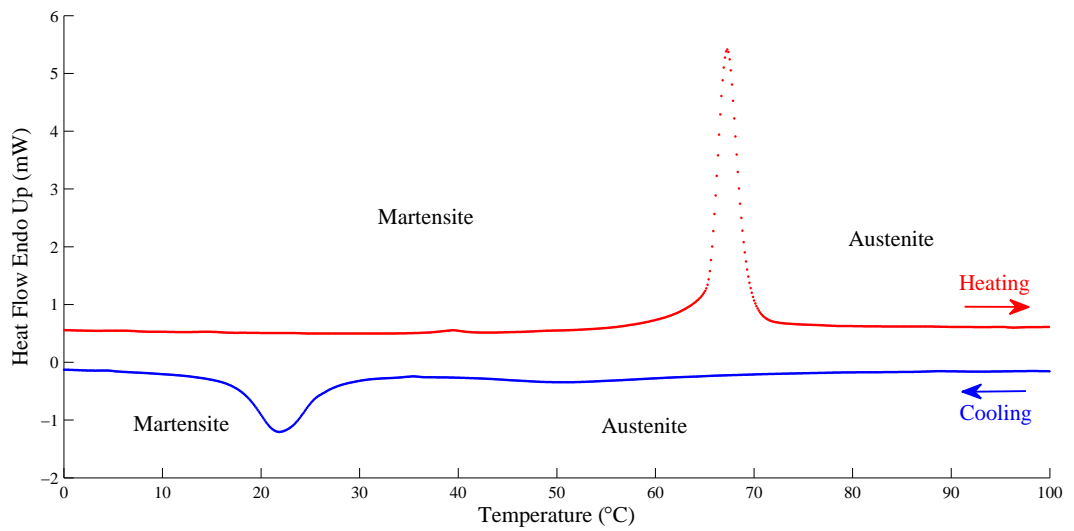
Scan rate	10°C/min				20°C/min			
Transformation temperature (°C)	A_F	A_S	M_F	M_S	A_F	A_S	M_F	M_S
LT Nitinol	68	65	15	25	70	65	18	25
HT Nitinol	82	78	42	47	82	77	40	47

Table 4.1: Transformation temperatures of the Flexinol[®] wire specimens from DSC analysis

The DSC thermograms were reproducible over a series of experiments with different samples cut from the as-received wire. Small distortions in the thermograms have been

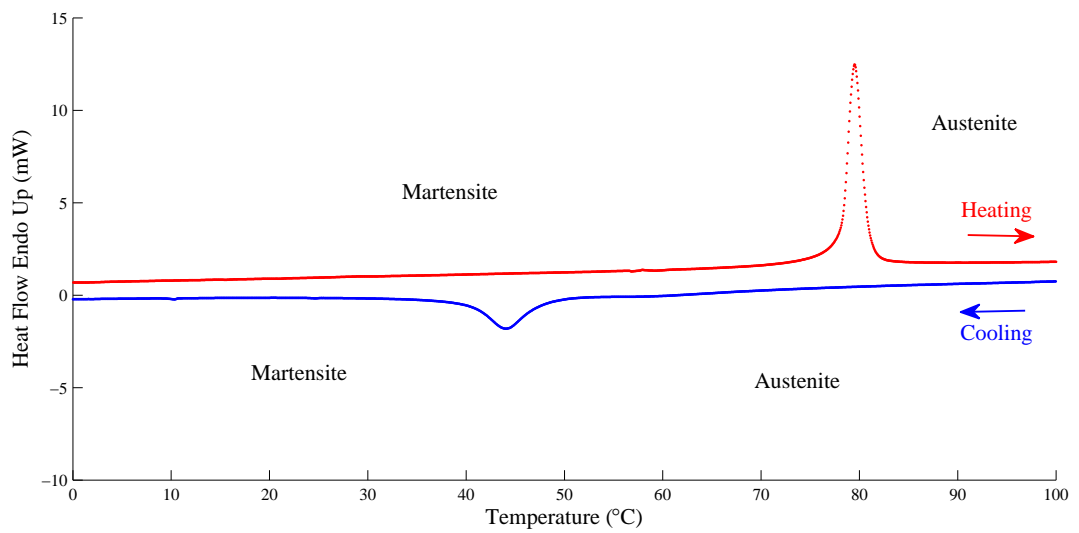


(a)

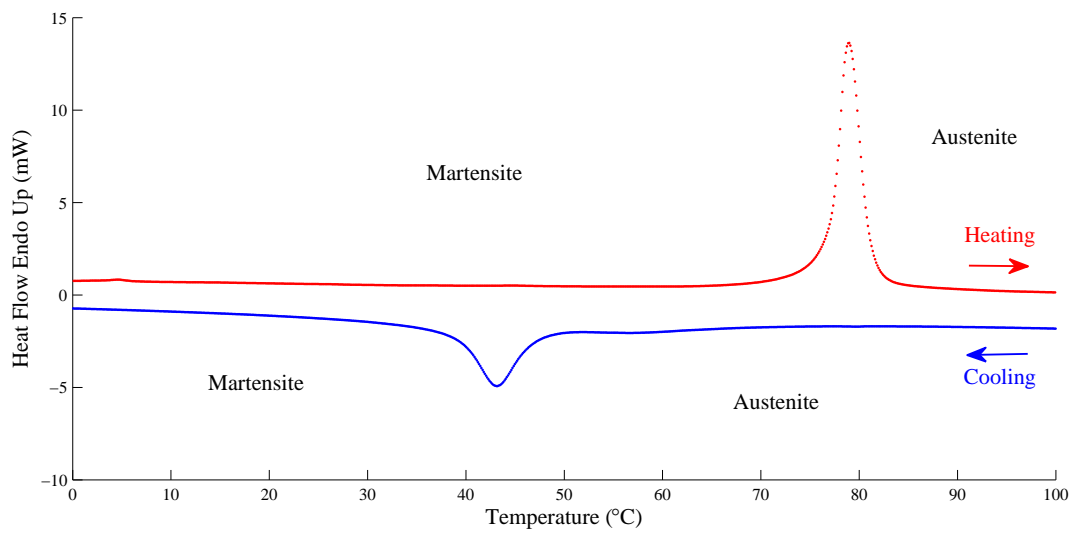


(b)

Figure 4.7: DSC thermograms of low temperature Flexinol[®] at scan rates of (a) 10°C/min and (b) 20°C/min



(a)



(b)

Figure 4.8: DSC thermograms of high temperature Flexinol[®] at scan rates of (a) 10°C/min and (b) 20°C/min

identified in these results, around 58°C on the heating cycle of Figure 4.7(a) and around 40°C on Figure 4.7(b), both attributed to material moving in the sample pan during the DSC test. It is imperative to conduct DSC tests over a wide enough range to ensure all transformation temperatures can be estimated, however there is no evidence of an intermediate R-phase transformation in the DSC results of Flexinol[®]. For the results shown in Figures 4.7 and 4.8, the austenite and martensite phases are clearly defined. The correlation of A_F for each material with the A_F specified by the manufacturer, as shown in Table 4.1, is evidence that DSC is a reliable technique for estimating the transformation temperatures of this shape memory Nitinol.

4.4 Transducer assembly

Nitinol cymbal transducers can be assembled as described in Chapter 3. Once the epoxy bond layers in the transducer have cured, wires have to be attached to the flange of each end-cap to create electrodes which allow a voltage to be applied across the piezoceramic disc. The wires could be soldered to the flanges of the end-caps, but Nitinol can be incredibly difficult to solder due to the titanium-rich oxide layer which forms on the surface [58]. It is well known that titanium is highly reactive with oxygen. This can result in a weaker electrode connection, thereby limiting the operational voltage input range of the transducer. Also, soldering may confer temperatures which adversely affect the Nitinol material properties [58], and based on the very small size of the Nitinol end-caps, any solder operation could rapidly confer an undesirable high temperature over the entirety of the Nitinol end-cap.

Two approaches can be used when soldering is difficult. The first is to mechanically abrade the surface area of interest to remove the oxide layer. There are risks associated with this option, as surface abrasion will affect the transformation properties of Nitinol. Due to the small size of the end-caps, it may also be very difficult to ensure that an excessive amount of end-cap material is removed. The second option is to apply a chemical solution prior to soldering, such as flux, to remove any material which could cause bonding problems. However, when this was attempted, it was noticed that the electrode connection was not strong enough, and the wires connecting the

transducer to the power supply were liable to detachment. To avoid affecting the material properties and to fabricate a transducer which is robust enough to withstand the dynamic characterisation experiments, a conductive epoxy resin was used, although this was more expensive than soldering. A conductive epoxy (Chemtronics CW2400) was used to create the electrodes. This epoxy resin can withstand temperatures up to approximately 100°C, similar to the Eccobond[®] insulating epoxy resin, whose limit is 90°C in its rigid form. The conductive epoxy resin can cure in around four hours at room temperature, providing an epoxy resin mixture containing equal parts of epoxy and catalyst is used.

4.5 Experimental testing considerations

This section presents a brief discussion of the experimental testing of Nitinol. The control of the test environment temperature is critical. In order to ensure the Nitinol device is being operated at the desired temperature, a reliable method of temperature measurement is required. In addition, for a Nitinol device in operation, the mechanical properties of the Nitinol must also be understood, and in particular how they respond to changes in temperature.

4.5.1 Temperature measurement

There are two temperature measurement techniques which have been employed. The first involves placing a thermocouple (type-K) in the thermal chamber, which itself is controlled with a thermostat. The thermocouple does not directly measure the temperature of the material, but rather the environment in which it is situated. The Nitinol end-caps are very small, and so by situating a Nitinol cymbal transducer in the chamber and controlling the temperature, a measurement should only be made when the temperature of the end-caps is assumed to have equilibrated with the temperature of the surrounding environment. A similar technique has been reported for the electrical impedance analysis of a Nitinol cymbal transducer in a temperature-controlled oven [67], where the temperature of the environment was increased in small increments and the frequency-temperature relationship was recorded. In this case, a thermocouple

was used to monitor temperature, and measurements of resonant frequency were taken approximately two minutes after the thermocouple settled on a set temperature. The analysed temperature range was from -5°C to $+80^{\circ}\text{C}$, with either 5°C or 10°C increments between measurements. A similar approach has been adopted for this research by using electrical impedance measurements in a temperature-controlled environment, although the transducer was permitted to equilibrate for twenty minutes instead of two, to ensure the transformation of the Nitinol was complete. Also, measurements were not taken in increments but rather two different temperatures. An alternative to the thermal chamber used for these experiments could be to heat or cool a fluid in which the transducer is submerged.

Temperature measurement was also conducted by using an infrared (IR) thermal imaging camera (FLIR T425). The use of IR measurement is particularly attractive for applications where the object is small in size such that using a thermocouple attached directly to the measurand surface is impractical. An example of this would be monitoring the temperature of a cymbal transducer, like those studied in this research, undergoing EMA testing. The transducer is small enough such that attaching a thermocouple to one of the end-caps would affect the vibration behaviour of the transducer.

IR was employed for temperature measurement for a number of experiments to support the thermocouple measurements. The emissivity (ε) is critical for accurate measurement of surface temperature of a sample using the IR camera. ε is a parameter that describes the ability of a material to emit radiation from its surface, and is temperature-dependent. The emissivity of metals increases with temperature, whereas the converse is true for non-metallic objects [205]. Emissivity is expressed as a value between 0 and 1. For accurate temperature measurement using an IR camera, the required parameters are [205]:

1. Emissivity of the object material, ε
2. Reflected apparent temperature, T_{ra}
3. Distance between the infrared source and the object
4. Relative humidity of the environment

5. Atmospheric/environment temperature

A thermocouple is inappropriate for the measurement of reflected apparent temperature, because intensity of radiation is not measured, and the thermal contact to the measurand requires a specialist bonding agent [205]. The emissivity of metals is generally low compared to non-metallic materials. The manufacturer recommends defaults for parameters which are unknown. For example, over short distances and for normal environmental humidity, the relative humidity can be set to 50% [205]. Figure 4.9 shows infrared images of a transformation between martensite and austenite for a low temperature Flexinol[®] shape memory Nitinol wire, where it is shown exhibiting the SME.

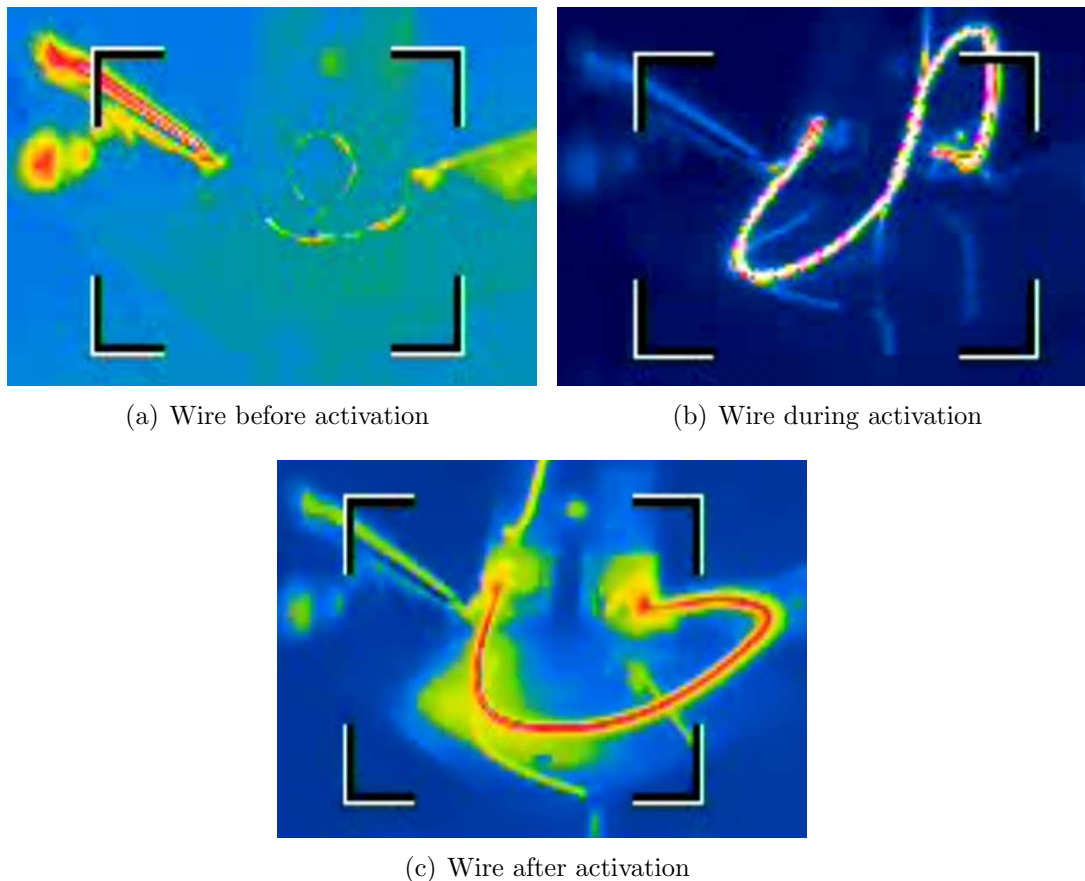


Figure 4.9: Infrared images of the phase transformation (a) before, (b) during and (c) after the thermal activation of low temperature Flexinol[®] shape memory Nitinol wire, where a current of 3A was passed through the wire to create enough heat to generate the SME

At room temperature, the wire exists as martensite because it is shape memory Nitinol. The wire was deformed and twisted, before being fixed at both ends. A

current of 3A was then passed through the wire in order to heat it and force the phase transformation to occur. As the temperature of the material has passed the A_S temperature and approached A_F , the wire has attempted to recover its original set shape. However, because it is constrained at its ends, it cannot recover its original configuration. In this case, the phase transformation occurred so quickly that the transformation temperature could not be recorded with accuracy. However, for a slower and controlled transformation such as that achieved by using the thermal chamber, the IR technique is suitable. Table 4.2 shows emissivity data measured for the materials used in the transducers in this research.

Sample	Measured Temperature (°C)	ϵ
Black oil paint (Gloss)	56.9	0.92
Shape memory Nitinol, <i>Memry GmbH</i>	56.9	0.64
Superelastic Nitinol, <i>Johnson Matthey Noble Metals</i>	56.9	0.67
PZT disc (silver electrode surface)	56.9	0.69

Table 4.2: Emissivity measurements

After some experimentation, it was found that the discrepancy in temperature measurement between using the type-K thermocouple and the thermal imaging camera was within 2-5°C. This means that the thermal chamber was providing a suitable controlled environment for the experiments. For the majority of the experiments, only the type-K thermocouple was used.

Nitinol cymbal transducers require a suitable protective enclosure, method of environmental temperature control and a support mechanism to enable the transducer vibration response characterisation at different temperatures. Impedance analysis has been commonly used for the characterisation of transducers, but using 1-D and 3-D LDVs to study the vibration response, at raised temperatures and with temperature control, is more complicated. This is because the transducer should be in a direct line of sight for the vibrometer laser beam, and the environment needs control to around 60-80°C. The laser beam must be perpendicular to the measurement surface for the 1-D LDV, with a strong signal. This minimises measurement error, which is important when detecting displacement amplitudes in the order of a few microns. It is possible to make LDV measurements through a transparent enclosure or window [186], but care

must be taken to minimise reflections or laser beam scattering which could distort the results, by using a suitable calibration procedure.

The thermal chamber for the experiments incorporated the type-K thermocouple. A drawback of the available thermal chamber was that the thermostat was not precise, as the temperature in the thermal chamber usually settled to around $\pm 10^\circ\text{C}$ of the desired temperature. However, it was possible to raise the temperature of the thermal chamber to a sufficiently high temperature to allow the Nitinol end-caps studied in this research to transform to austenite. The thermal chamber contains four very small apertures on the top surface which are just wide enough to permit a laser beam to pass through, but small enough so that the steady temperature is being maintained within the chamber. These apertures also allowed the use of the IR camera when required.

4.5.2 Mechanical behaviour

The lack of understanding of how the mechanical properties of Nitinol are affected by phase transformations and can be accurately measured is limiting the applications in which the material is being successfully exploited [206]. This also applies to mechanical properties at high strain rates, where lack of knowledge has limited the use of Nitinol in applications in defence and aerospace [207]. Physical properties such as electrical resistivity, thermal conductivity, thermal expansion and magnetic susceptibility all differ depending on the material microstructure [74]. Some of these properties experience a more significant change under a phase transition than others. For example, damping can exhibit a large change, whereas the change in electrical resistivity is much smaller, under a transition between austenite and martensite [74]. Tensile testing has been utilised to measure the stress-strain response of Nitinol as both martensite and austenite, and can be used in the determination of plateau stresses and the superelastic response [208]. Performing stress-strain tests on martensitic Nitinol, however, is problematic because the contributions from plastic deformation, material twinning deformation and elastic deformation can be very difficult to differentiate [209].

The elastic modulus is highly dependent on strain and temperature [74], in both phases. The lack of success of measuring elastic modulus via mechanical testing methods has been attributed to the propensity of Nitinol to exhibit a secondary

deformation during testing [206], where another phase or a microstructural change is stimulated in the material. For example, if tensile testing is being conducted above the A_F temperature, then a sufficient stress can generate stress-induced martensite [210]. Contributions to the stress-strain response of Nitinol from stress-induced martensite in the tensile testing of Nitinol has been reported in the literature [206]. Since using mechanical testing to determine the elastic modulus of austenite is ineffective [211], ultrasonic, electrical resistance and neutron diffraction techniques are alternative measurement techniques useful for elastic modulus measurement in the R-phase [211]. It is also the case that the measured SMA modulus and damping are sensitive to the type of test method used [212].

These measurement problems can significantly affect the accuracy of numerical models, unless the variability of mechanical properties such as elastic modulus is addressed. It has been suggested that elastic modulus is not important for practical applications, and that the apparent elasticity is more important as it is governed by both mechanical twinning and the transformation of the material [194]. Previous studies have confirmed that the moduli are very dependent on the annealing of the material [67], and this might explain why the moduli reported in the literature are inconsistent, where the reports of the moduli are occasionally contradictory [206]. A dynamic method therefore appears to be a more appropriate option for the determination of the moduli, because it enables the apparent modulus for each phase to be determined.

Tensile testing has not been conducted on the as-received material in this research. In fact, the mechanical properties cannot be extracted from cymbal end-caps easily due to their small size and geometrical configuration, and because the material must be in the as-received condition in order to acquire reliable properties data. For example, a Nitinol wire with the same chemical composition as a Nitinol end-cap cannot be used as a sacrificial sample for mechanical property investigation, because does not have the same material processing history as the end-cap. This is why a high level of understanding of the thermomechanical processing history of Nitinol is required for its reliable implementation in different applications [77]. Also, cyclic deformation of Nitinol can alter the mechanical response such that it experiences fatigue failure [77].

Determining at what stage this will occur would require repeated material prototype testing.

4.6 Numerical simulation considerations

There are studies in the literature which have reported on the generation of algorithms, called user material (UMAT) subroutines [213, 214], which can account for shape memory, thermomechanical and superelastic effects, and are embedded in an FEA code such as Abaqus. This has been reported for configurations such as helical springs and wires. Although a subroutine providing the ability to program smart material properties has not been employed in this research, it would be valuable to investigate in future. In this research, a finite element simulation of a shape memory Nitinol cymbal transducer has been produced. The resonant frequency and displacement amplitude of the transducer with Nitinol end-caps in each phase are predicted, using an estimate of the Young's modulus for each simulation. The FEM was tuned by changing the elastic modulus, and a similar approach has been reported in the literature [67].

In general, FEA cannot yet accurately simulate nonlinear vibration behaviour such as softening and hardening, or complex phase transformation behaviour of an SMA such as Nitinol. The strain and temperature dependent phase transformation behaviour of Nitinol provides further modelling complexities. For example, the elastic modulus of austenitic Nitinol is not constant with temperature [74]. However, despite these limitations, the FEA results shown later in this research demonstrate how a numerical model can be used to predict the modal response of a Nitinol transducer with end-caps in each microstructure phase, and also enable the regions of high stress concentration to be calculated.

There is evidently a need for material property data which is reliable and meaningful [210], and even though constitutive models have improved, there is still the need for experimental data [210]. Fabricators of Nitinol often specify the Young's modulus of each phase in terms of a range, such is the sensitivity of the properties of the material to heat treatments, chemical composition and cold working. This makes it very difficult to determine the elastic properties of a Nitinol end-cap which has

undergone both heat treatment and cold working in the fabrication process. Another complexity for the numerical simulation of Nitinol cymbal transducers is that the effect of higher temperatures on the epoxy bond layers is unknown, and the softening which is likely to occur is difficult to quantify. In a cymbal transducer FEM, the elastic properties of the materials and the cavity profile of the end-cap greatly affect the resonant frequency, whereas damping significantly affects the displacement amplitude. The source of asymmetries in the transducer between end-caps and epoxy bond layers are difficult to determine and accurately model, and so only the symmetric mode from FEA can reliably be compared with that found using EMA.

4.7 Chapter summary

This chapter has aimed to illustrate a number of important considerations which must be made in the design and experimental testing of Nitinol transducers. Some of this information would be applicable to other types of SMA, such as copper-zinc alloys, where DSC can also be adopted. As with any transducer design, material selection is important. The transformation temperatures of Nitinol are very sensitive to cold working, as well as chemical composition and certain heat treatments, and so the shape of the Nitinol assembly component should be carefully considered, in addition to whether it should be superelastic or shape memory. It is very difficult to predict the effect of cold working on the transformation behaviour of Nitinol. For SMAs to be adopted in different tuneable transducers, a greater understanding of how the fabrication of Nitinol affects transformation temperatures and material properties is required. There are different methods which can be used to estimate the transformation temperatures of Nitinol. Some of them are very simple and can be performed on a small sample of material in a very short period of time, with high reliability and repeatability. However, DSC is considered as a more rigorous and comprehensive method of transformation temperature estimation, although the results can be misinterpreted.

Nitinol is very sensitive to changes in temperature, and this is significant in the fabrication of Nitinol cymbal transducers. In the fabrication of cymbal transducers not

incorporating SMAs such as Nitinol, wires are soldered to the end-cap flanges to create the electrodes. However, in the assembly of Nitinol cymbal transducers, the avoidance of soldering is recommended because the effect on the transformation behaviour of the Nitinol would be unclear. Conductive epoxy resin can be used to connect the wires to the transducer, forming the electrodes. There are conductive epoxy resins available which have high operating temperatures, but it has to be ensured that the adhesive bond strength is sufficient for operation. Also, the use of an appropriate enclosure for temperature-sensitive experiments is vital, in addition to the accurate control and monitoring of the temperature. Temperature measurement can be conducted using a suitable thermocouple or IR thermal imaging camera.

The mechanical behaviour of Nitinol is very difficult to simulate using FEA. Manufacturers of Nitinol tend to specify the Young's modulus of each phase in terms of a range, due to the temperature dependency of the moduli. In this research, the elastic properties of each Nitinol phase are defined using experimental data as the input information for FEA simulations of the Nitinol cymbal transducers. However, it is clear that much research is required in future to develop FEMs which can accurately simulate the smart material properties. The forthcoming chapters demonstrate how these recommendations, coupled with the design and analysis methodology outlined in Chapter 3, can be used to fabricate and test two types of Nitinol cymbal transducer, and subsequently develop a simple Nitinol prototype actuator device.

Chapter 5

Shape memory nitinol cymbal transducers

Shape memory Nitinol exhibits the SME, but also superelasticity if it is heated above its A_F transformation temperature. The objective of this chapter is to identify the transformation of shape memory Nitinol between two microstructure phases, and to characterise the vibration behaviour of two different transducers fabricated using shape memory Nitinol end-caps. The end-cap shapes are set to be identical in each phase, and so no shape recovery will be exhibited, although the SME can be utilised in the event of end-cap deformation. The influence of the mechanical coupling of cymbal transducers and the sensitivity of Nitinol to changes in temperature are discussed.

5.1 Transducer fabrication

Shape memory Nitinol end-caps (Memry GmbH) were used to fabricate the transducers, with an A_F transformation temperature intended to be approximately $60\pm 10^\circ\text{C}$. The preparation of the Nitinol by the manufacturer comprises vacuum induction melting followed by vacuum arc melting to ensure that the transformation temperatures are as evenly distributed as possible in the ingot [215]. This can also be achieved by using a multiple-stage vacuum arc melting process. The Nitinol was fabricated to ASTM: F2063-05, and produced with a transformation temperature ingot with $A_S = 71.5^\circ\text{C}$ and $A_P = 83.5^\circ\text{C}$, was used to create the end-caps. The ingot A_S temperature provided by

the manufacturer will not be the same as the A_S transformation temperature estimated from DSC analysis, because of the effects of the subsequent annealing and cold working to produce the final end-cap shape. The chemical composition of the shape memory Nitinol is 55.11wt% nickel with a balance of titanium. Table 5.1 shows the quantities of other chemical elements present.

Element	Cr	Cu	Fe	Nb	Co
Composition (wt%)	< 0.01	0.0520	0.012	< 0.01	< 0.01

Table 5.1: Chemical elements and quantities used for end-cap fabrication

The elements carbon (256ppm), oxygen (233ppm) and hydrogen (3ppm) were also present in the shape memory Nitinol. The end-caps were produced via cold rolling, and the final hot die heat treatment was conducted in air before microblasting and pickling surface treatments were administered. The as-received end-caps could be deformed with no spring-back at room temperature, indicating that they were not in the austenitic state. Table 5.2 shows the sample average of each geometrical dimension of the end-caps, measured using Mitutoyo digital callipers.

Parameter	Dimension (mm)
Apex Cavity Diameter	4.00
Base Cavity Diameter	9.30
Cavity Depth	0.26
End-Cap Thickness	0.24
Total Diameter	12.70
Total Height	0.50

Table 5.2: Geometrical dimensions of the shape memory Nitinol end-caps

In Chapter 3, it was demonstrated that differences between the end-caps in a cymbal transducer contribute to a double-peak in the frequency response, where one mode is symmetric and the other is asymmetric. Asymmetry in the frequency response can also be caused by differences between the epoxy bond layers. The shape memory Nitinol end-caps were manufactured to a very high quality, with no significant variation in geometrical dimensions between them. The epoxy resin required to form the bond layers was deposited and distributed as evenly as possible on the flanges and

piezoceramic surfaces. Conductive epoxy resin was then used to form the electrodes, and a fully assembled shape memory Nitinol cymbal transducer is shown in Figure 5.1.

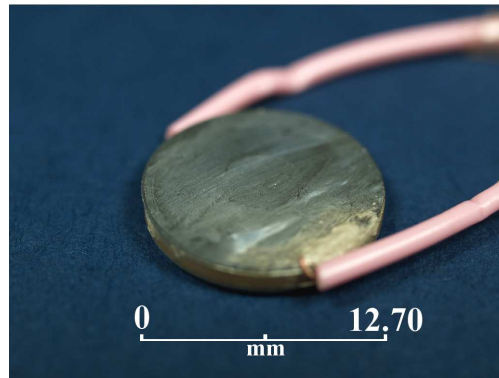
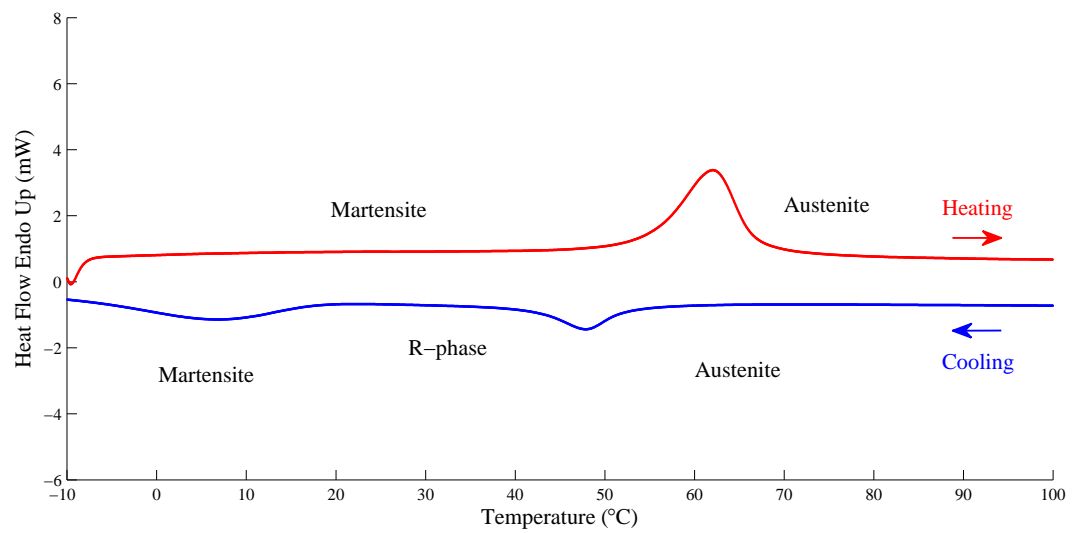


Figure 5.1: The shape memory Nitinol cymbal transducer

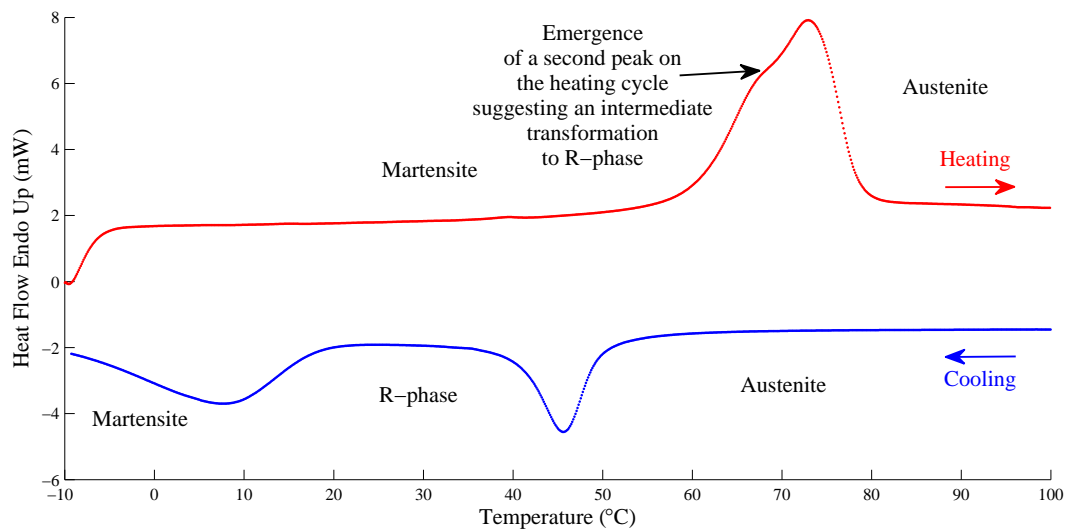
5.1.1 DSC analysis of the shape memory nitinol

One of the end-caps was used as sacrificial material for the DSC experiments. It is important to use material as similar as possible to that being used in the transducers for accuracy. The DSC thermograms for two scan rates are shown in Figure 5.2.

The thermograms show that the complete phase transformation cycle has been recorded through heating and then cooling. Both martensite and austenite phases have been detected, allowing the transformation temperatures at each stage of the transformation process to be estimated, in addition to an intermediate phase on the cooling cycle of both thermograms. This is the rhombohedral R-phase which can appear in the DSC thermograms of cold worked Nitinol alloys, or those which have been subjected to certain heat treatments. Chemical composition is also a significant factor, where nickel-rich alloys are more susceptible to the emergence of the R-phase. The shape memory Nitinol underwent cold rolling in the fabrication process, and is also rich in nickel, therefore likelihood of the R-phase appearing is increased [59]. For the 10°C/min scan rate, the shape memory Nitinol exhibits the asymmetric case, where there is one clear intermediate phase evident in the thermogram appearing in the cooling cycle, as shown in Figure 5.2(a). This means that the transformation from austenite to martensite is a multiple stage process over this temperature range. The material is assumed to exist as R-phase at room temperature, around 25°C. The



(a)



(b)

Figure 5.2: DSC thermograms of shape memory Nitinol at scan rates of (a) 10°C/min and (b) 20°C/min

hysteresis in the thermograms indicates that the material can exist as either R-phase (on cooling) or martensite (on heating) at this temperature. The material is assumed to be R-phase at 25°C because the processing history of the material means it has already been heated, and so a subsequent cooling cycle would form R-phase [59].

One consequence of heat treatment and cold working in end-cap fabrication is that an R-phase on the heating cycle can start to form, as shown in Figure 5.2(b). The symmetric case can be detected when the scan rate is increased to 20°C/min, as the heating cycle exhibits a double-peak at the transformation event. This is the R-phase overlapped with the endothermic austenite peak [59]. Therefore, the need for DSC analysis at more than one scan rate is evident to elicit this type of transformation behaviour. The lower scan rate exhibits a greater accuracy albeit with reduced sensitivity, whereas the higher scan rate results in a lower accuracy but higher sensitivity, meaning that the R-phase transformation on the heating cycle can be detected. Employing different scan rates will provide a clearer representation of the relationship between sensitivity and accuracy for DSC analysis, although this can be time-consuming and costly. Estimated transformation temperature data for the shape memory Nitinol is shown in Table 5.3, approximated from the DSC thermograms shown in Figure 5.2.

Scan Rate	A_F (°C)	A_S (°C)	M_F (°C)	M_S (°C)	R_F (°C)	R_S (°C)
10°C/min	68	55	-6	16	44	52
20°C/min	78	61	-5	17	40	50

Table 5.3: Transformation temperatures of the shape memory Nitinol from DSC analysis

As indicated by the manufacturer, the target transformation temperature criteria for the Nitinol are that A_P is approximately 10°C hotter than A_S , and the A_F is around 15°C higher than A_S , both determined by the manufacturer using DSC on fully annealed samples [216]. The results shown in Figure 5.2 and Table 5.3 demonstrate that this target has been achieved, especially with respect to the scan rate of 10°C/min.

It is possible to misinterpret DSC thermogram data. Figures 4.7 and 4.8 presented in Chapter 4 showed the DSC results of two shape memory Nitinol wires. No intermediate R-phase was detected in these results and so they are indicative of

direct single-step transformations. The R-phase was more likely to appear in the results shown in Figure 5.2. However, if the R-phase is not expected, or there is unfamiliarity with the material or its processing history, then the R-phase could be easily mistaken as the classical martensite phase. This could also occur if the designated temperature range for the DSC analysis is not large enough, and as a result only the austenite and R-phase transformation events are detected. For example, if the DSC thermograms shown in Figure 5.2 were recorded between 30°C and 100°C, then there would be no indication of the classical martensite phase, and the R-phase could easily be mistaken as the classical martensite phase. In practice, the thermal hysteresis between austenite and the R-phase is normally much smaller than for the austenite to martensite transition. Therefore with experience, good judgement and a high level of experimental capability with the DSC method, the likelihood of making this error is reduced. The thermal hysteresis between austenite and martensite can be around 40°C and sometimes higher [199], whereas the thermal hysteresis between austenite and the R-phase is lower, and can be as small as 2°C [59].

5.2 First transducer characterisation

The first transducer was assembled with the shape memory Nitinol end-caps. It had to be ensured that the temperature in the thermal chamber was carefully monitored and controlled. The upper temperature limit of the chamber was just below the A_F transformation temperature of the shape memory Nitinol, as indicated by the DSC analysis. The thermostat control on the chamber was not accurate, where the temperature could be set within around $\pm 10^\circ\text{C}$. For this reason, thermocouple measurements were used to ensure a suitable temperature was set within the chamber. It was found that the chamber settled on the desired temperature after around 15-20 minutes.

The transducer was characterised with the end-caps in both the R-phase state and the austenite phase, using the temperatures estimated from the DSC thermograms as reference. Complete (100%) austenite, martensite or R-phase Nitinol will not be generated unless the final transformation temperature of that phase has been

passed. For example, in between the R_S and R_F on cooling, there exists a mixture between austenite and R-phase. When the R_S temperature is reached, not all of the microstructure is reoriented to the R-phase until the R_F temperature is passed. This is a reason for the highly variable elastic modulus. If the A_F transformation temperature is around 60°C , then operating the thermal chamber at a higher temperature will ensure the Nitinol end-caps exist in the austenite phase.

5.2.1 Resonant frequency characterisation

The impedance-frequency and phase-frequency spectra were obtained using the Agilent 4294A Impedance/Gain Phase Analyser. The temperature was monitored using a type-K thermocouple in conjunction with an FLIR T425 thermal imaging camera, but as it was clear there was a close correlation between the thermocouple and thermal camera measurements, subsequent experiments were conducted using only the thermocouple. Impedance-frequency and phase-frequency spectra were generated for two different temperatures. The temperatures were defined based on the DSC thermogram results, to ensure Nitinol in each phase was generated. The impedance-frequency and phase-frequency spectra are shown in Figure 5.3.

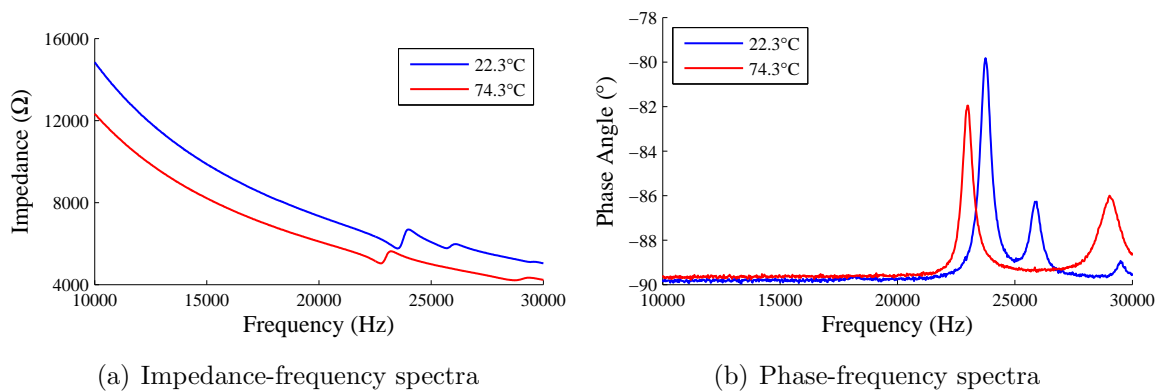


Figure 5.3: Resonant frequency characterisation of the first shape memory Nitinol transducer showing the measured (a) impedance-frequency and (b) phase-frequency spectra

The electrical impedance analyser allowed the shifts in the impedance-frequency spectra as a result of temperature change to be monitored in real-time. The resonant frequency of each mode marginally decreased at the start of the heating process before

sharply and rapidly increasing, likely once the A_S and A_F transformation temperatures were passed. This behaviour is consistent with that exhibited by the asymmetric cymbal transducer shown in Chapter 3. It is unclear what phenomena are occurring to cause the initial decrease in resonant frequency, but epoxy bond layer softening is likely a contributing factor. There have been reports of an initial reduction in modulus before the stiffening to the austenite phase on the heating cycle in Nitinol transformation [217, 218]. It has also been reported that in Nitinol, a softening of the Young's modulus occurs at the transformation between R-phase and martensitic Nitinol, in addition to the transformation between R-phase and austenitic Nitinol [219]. This softening may be a consequence of the instability in the crystal structure caused by the transformation from one phase to another. However, the DSC results are consistent with the temperature at which the measured resonant frequency of the transducer rapidly increases, being close to the A_S and A_F transformation temperatures.

A double-peak appears in the impedance-frequency response. The transducer has been fabricated with almost identical end-caps, meaning a significant proportion of the asymmetry is in the epoxy bond layers. The modes in Figure 5.3(a) comprise one symmetric and one asymmetric mode. It is unknown in which order they appear on the frequency axis, and so they are referred to as mode 1 and mode 2 until their shapes are verified. The modes started to sharply increase in frequency around 55°C, in close correlation with DSC analysis data for both scan rates, although the temperature at which this sharp resonant frequency increase occurred is an approximation. The resonant frequency (f_r) of each mode of the transducer, and also the resonant frequency shift associated with the transformation of Nitinol, are summarised in Table 5.4.

	f_r at 22.3°C (Hz)	f_r at 74.3°C (Hz)	Difference (Hz)	Change (%)
Mode 1	23525	22775	-750	-3.19
Mode 2	25650	28800	+3150	+12.28

Table 5.4: Resonant frequency shifts of the first shape memory Nitinol cymbal transducer

The transducer is exposed to low stress in the electrical impedance analysis, as the transducers are only excited by $0.5V_{p-p}$. This decreases the effect of stress on the Nitinol, which is desirable since the transformation temperatures are stress dependent.

The resonant frequencies of the transducer have shifted as a result of a change in temperature, and the temperature at which the rapid increase in frequency occurred is around the A_S and A_F transformation temperatures estimated from the DSC analysis of the shape memory Nitinol. It would be possible to conduct the dynamic characterisation experiments for the transducer end-caps existing in the martensite phase by cooling the transducer below M_F , for example by using a conventional freezer, before allowing it to return to ambient room temperature. From Figure 5.2, it is evident that the end-caps will remain as martensite on the heating cycle, before transforming to austenite. This is another avenue of interesting future research.

It is noticeable that the resonant frequencies do not change by the same proportion. This phenomenon has previously been observed [6], albeit for changes to the medium surrounding a cymbal transducer. The data presented in Table 5.4 show the change in frequency of each mode attributable to a temperature change. The resonant frequency of the first mode decreases which is contrary to the expected behaviour of Nitinol. The displacement amplitudes around resonance for each mode of the transducer were then measured using VRRC for further investigation.

5.2.2 Vibration resonance response characterisation

The displacement amplitudes of each mode for two temperatures were measured using the 1-D LDV system. The results for mode 1 are shown in Figure 5.4.

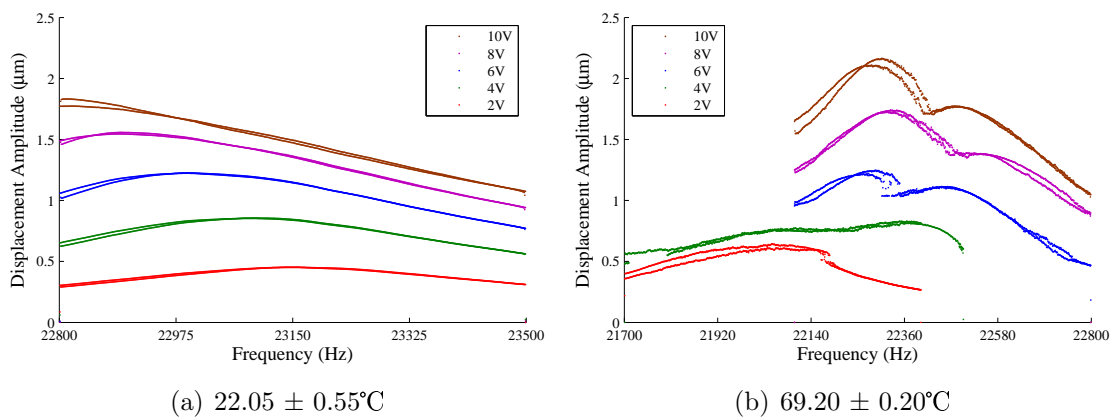


Figure 5.4: Plots showing the (a) R-phase and (b) austenite vibration responses of mode 1 of the first shape memory Nitinol cymbal transducer

The shift in resonant frequency from the lower to the higher temperature found

using the electrical impedance measurements correlates well with the change identified using VRRC. However, the resonant frequencies do not precisely match. As the voltage is increased, a higher displacement amplitude is produced by the cymbal transducer. Stress in the end-caps will increase as a result. Since the transformation of Nitinol is dependent on stress as well as temperature, then minor differences in resonant frequency between electrical impedance and VRRC measurements could be attributed to differences in stress on the cymbal transducer. Also, even very small changes in temperature affect the elastic properties of the shape memory Nitinol. Therefore, unless precisely the same temperature is used in each experiment, there may be small differences in modulus, and hence resonant frequency.

The epoxy bond layers will also be affected by cyclic vibration, thereby causing differences in resonant frequency. There is also evidence of nonlinear softening in Figure 5.4(a). The resonant frequency decreases as the input voltage level, and hence displacement amplitude, is raised. However, this was not found in the high temperature experiment shown in Figure 5.4(b), and so it is unclear how epoxy softening contributes to nonlinear behaviour. There is a higher displacement amplitude for each voltage level for the transducer with end-caps in the austenite phase compared to the R-phase. This is contrary to what was expected, as the cubic austenite phase is stiffer than the rhombohedral R-phase [220]. To investigate if this behaviour was detected in mode 2, the same characterisation procedure was conducted, the results of which are shown in Figure 5.5.

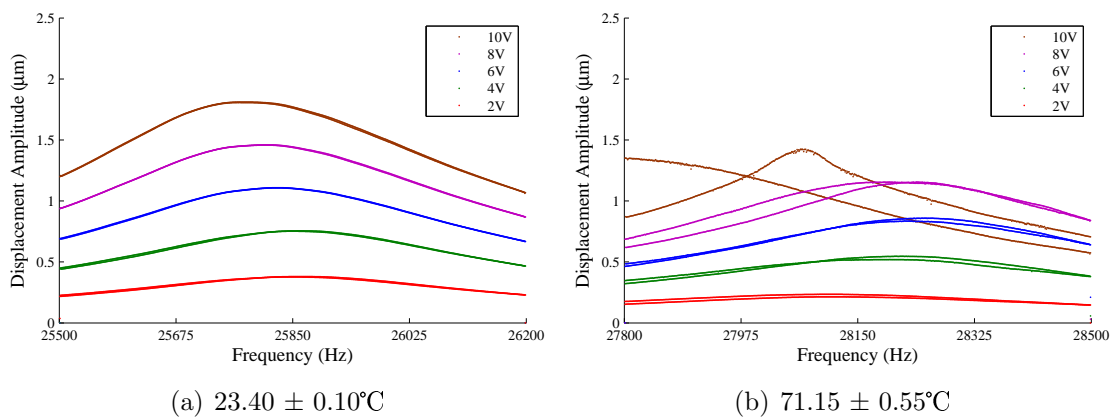


Figure 5.5: Plots showing the initial (a) R-phase and (b) austenite vibration responses of mode 2 of the first shape memory Nitinol cymbal transducer

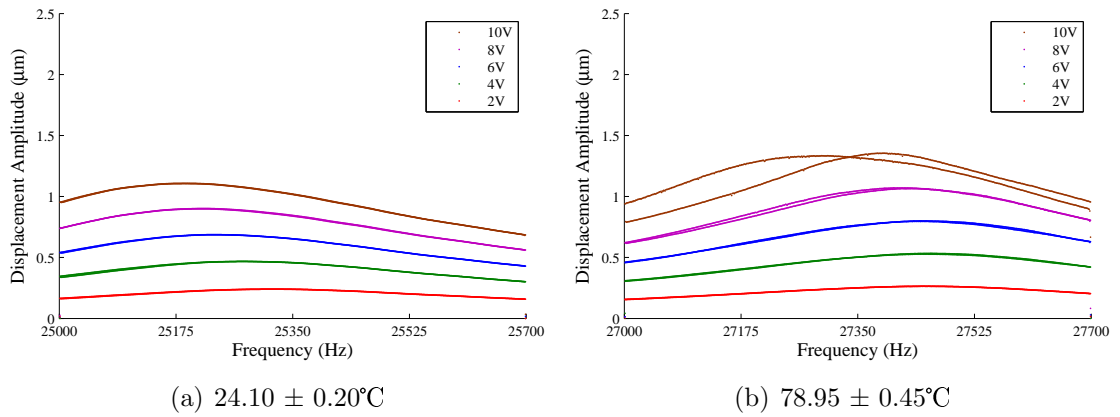


Figure 5.6: Plots showing the repeated (a) R-phase and (b) austenite vibration responses of mode 2 of the first shape memory Nitinol cymbal transducer

The displacement amplitudes were measured to be lower for the transducer with end-caps in the R-phase compared to the austenite phase. However, the transducer experienced a significant drop in resonance frequency at 10V, likely due to the mechanical behaviour of one of the epoxy bond layers at high temperature. A small crack may have developed in the bond layer, or the heating of the bond has caused it to soften. A difference between the upwards and downwards frequency sweeps for the 10V input voltage over the frequency range is clear, and there is a significant reduction in resonant frequency of mode 2. To assess the performance of the transducer after this reduction in resonant frequency, the tests on mode 2 were repeated, and it was found that both the resonant frequency and displacement amplitude had decreased for the transducer end-caps in both material phases, as shown in Figure 5.6. The mechanical coupling must be compromised for there to be a reduction in both resonant frequency and displacement amplitude. Both modes of vibration are still being detected, but it appears as though one or both of the epoxy bond layers in this transducer is not of sufficient quality at higher temperatures. If the epoxy bond layers around the end-cap flanges are heated and soften, they can crack or displace. The maximum operational temperature of the cured epoxy resin in its rigid form is above the test temperatures experienced by this transducer. It is likely that a small crack has formed in one of the epoxy bond layers as a result of the vibration, destabilising the mechanical coupling. The effect of cracks in epoxy bond layers on cymbal transducer performance have been reported in the literature [130]. A crack may be small enough to decrease the resonant

frequency, but not cause a complete failure of the mechanical coupling.

A small peak in the displacement amplitude response for the cymbal transducer operating in the second mode was detected in the repeated experiment. The displacement amplitude response around this small peak is shown in Figure 5.7. Small peaks such as these can be a consequence of asymmetry in the transducer causing another mode to appear, for example a bending mode of the end-cap. These small peaks appear frequently in assembled cymbal transducers which possess asymmetries, and it is important that they are not misinterpreted as either the symmetric or asymmetric modes of the transducer.

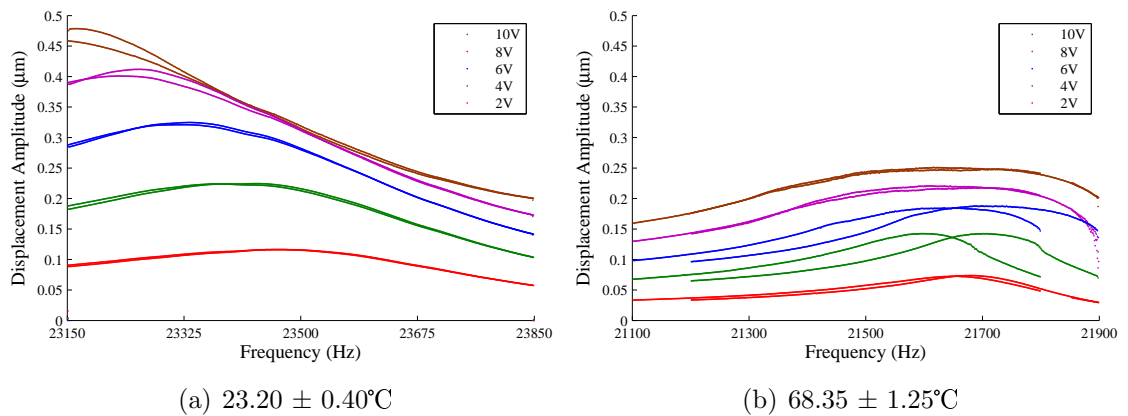


Figure 5.7: Displacement-frequency response of the small peak before the appearance of mode 2 of the first shape memory Nitinol cymbal transducer, showing the (a) R-phase and (b) austenite responses

The resonant frequency of each mode experienced a significant drop between 2V and 10V. The behaviour of the mechanical coupling appears to be important. The electrical impedance study was repeated to show the effect on the impedance-frequency and phase-frequency spectra for this transducer, as shown in Figure 5.8.

The results show that there is another peak in the frequency response of the transducer with end-caps in the high temperature state which is not shown in the first electrical impedance measurement results in Figure 5.3. This can be attributed to a change in one of the epoxy bond layers, for example a small crack. Also, mode 2 is in closer proximity to mode 1 for the low temperature state, showing that the frequency shift between the modes is unequal. This was also shown in Figure 5.3. It appears that the epoxy bond layers in this transducer have been insufficient, although the resonant frequencies from the electrical impedance measurements and the VRRC correlate well.

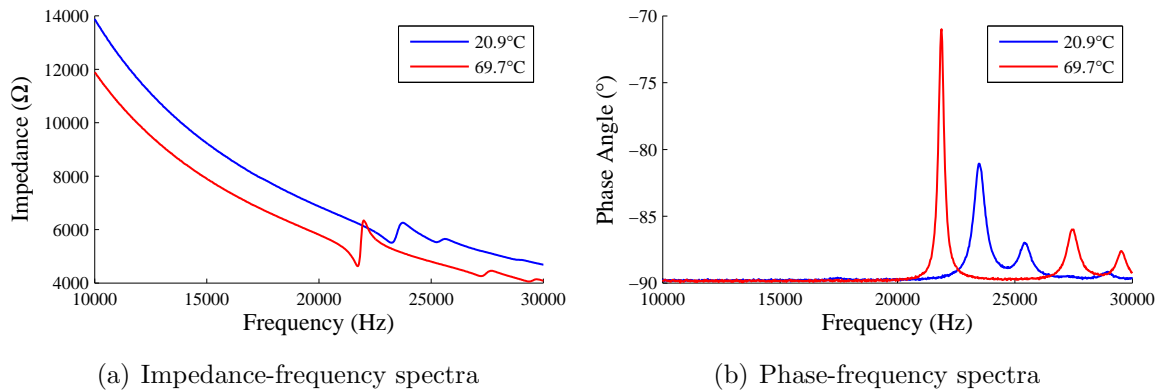


Figure 5.8: Repeated resonant frequency characterisation responses of the first shape memory Nitinol cymbal transducer, showing the measured (a) impedance-frequency and (b) phase-frequency spectra

5.2.3 Modal behaviour

The uncertainty in the mode shapes for the resonant frequencies measured in the previous section necessitates the use of EMA. A double-peak was found in the frequency response for this transducer, representing a symmetric mode and an asymmetric mode, and the EMA was conducted at room temperature only. This is because the apertures in the thermal chamber through which the laser beams of the 3-D LDV were focused were not large enough to enable the entirety of the cymbal transducer surfaces to be observed. Figure 5.9 shows the asymmetric and symmetric modes of the first transducer.

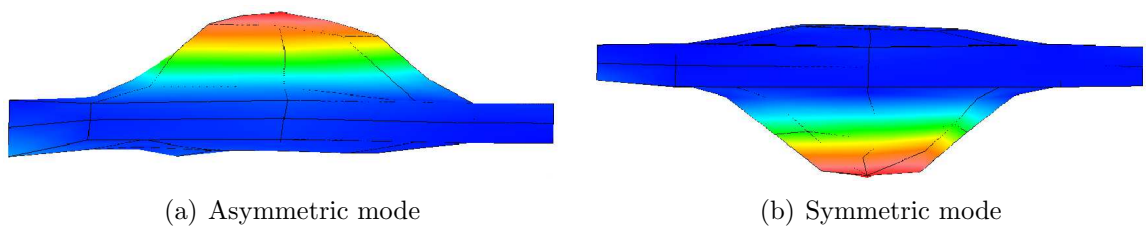


Figure 5.9: Modes of the first shape memory Nitinol cymbal transducer, showing (a) the asymmetric mode at 17302Hz, and (b) the symmetric mode at 24931Hz, measured at 20.8°C

During the experiment, it was found that the vibration response from two of the measurement points on the rim of the flange exhibited high levels of noise. The points were in the vicinity of the conductive epoxy resin used to create the electrodes, but were excluded from the analysis. The measurements on the end-cap faces were taken with the 3-D LDV normal to the object surface. This was set as the z-direction.

The measurements taken in the lateral x and y directions displayed very low levels of noise, and so a complete 3-D EMA is presented. The results show that mode 1 is the asymmetric mode, and mode 2 is the symmetric mode.

The resonant frequency of the symmetric mode is shown to correlate well with that obtained from the impedance measurements and the VRRC. However, the resonant frequency of the asymmetric mode has decreased, most likely because the EMA was conducted after VRRC. The epoxy bond layers experience higher stress from VRRC compared to electrical impedance measurement or EMA, and so any cracking or softening of these bond layers will affect subsequent measurements of the resonant frequency. Figure 5.10 shows the comparison between the resonant frequency data for the first shape memory Nitinol cymbal transducer.

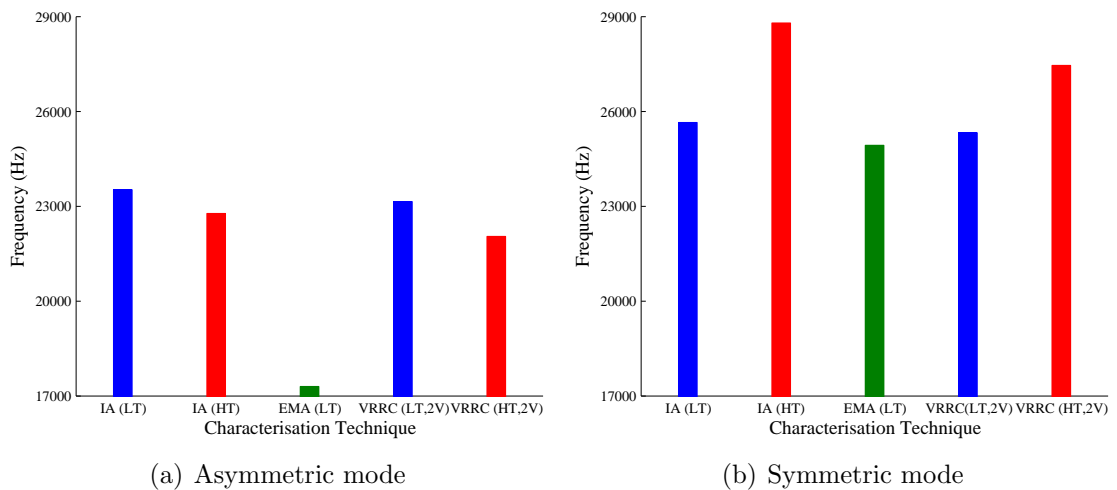


Figure 5.10: Resonant frequencies measured using the three dynamic characterisation techniques for the first shape memory Nitinol cymbal transducer

The symmetric mode exhibits the expected change in resonant frequency, which is due to a phase transformation of the Nitinol caused by an change in temperature. This change in resonant frequency is consistent for both the impedance analysis and the VRRC. The asymmetric mode also exhibits consistency between the impedance measurements and the VRRC, but the resonant frequency decreases for the phase transformation of Nitinol. The mechanical coupling conferred by the epoxy bond layers is suspected as the cause for this behaviour. To attempt to show this, once all the dynamic characterisation procedures were completed, the transducer was carefully dismantled to investigate the condition of the epoxy bond layers inside. The condition

of these layers are depicted in Figure 5.11.

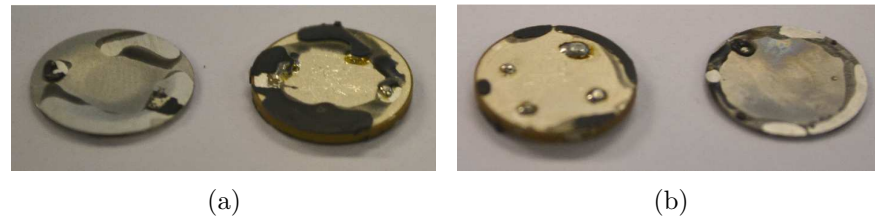


Figure 5.11: Condition of each epoxy bond layer in the first shape memory Nitinol cymbal transducer after dynamic characterisation

The epoxy resin distribution around the flanges of the end-caps and on the flat surfaces of the piezoceramic disc are shown in Figure 5.11. The uneven distribution, including the difference in the quantity of the deposited epoxy resin for each side of the piezoceramic disc, shows how difficult the equal and homogeneous deposition of epoxy resin is. There is more epoxy resin on one end-cap than the other, thereby enhancing transducer asymmetry. The small solder spots around the outer edge of the flat piezoceramic surfaces also affect the uniformity of epoxy resin deposition, and asymmetry can arise from the differing sizes of solder spot which are again difficult to control. Figure 5.11(a) shows the presence of epoxy resin in the cavity of the end-cap, and this will have had an impact on both the resonant frequency and the displacement amplitude of the transducer. Ideally, low stress experiments, such as electrical impedance measurements and EMA, should be performed before the VRRC experiments in the characterisation of a cymbal transducer. This is to reduce the chance of epoxy bond layer failure before displacement amplitude can be measured. Also, due to one of the epoxy bond layers being compromised, it could not be verified that the displacement amplitude of the transducer with end-caps in the R-phase were higher than in the austenite phase. In order to investigate all of these problems further, a second shape memory Nitinol cymbal transducer was fabricated and analysed.

5.3 Second transducer characterisation

It is a long process to conduct VRRC for upwards and downwards frequency sweeps over five voltage levels, from 2-10V. EMA was conducted prior to VRRC for this transducer, in contrast to the characterisation of the first transducer. Also, thicker epoxy bond

layers were deposited to attempt to improve the mechanical coupling.

5.3.1 Resonant frequency characterisation

Similar to the first transducer characterisation, impedance-frequency and phase-frequency spectra were produced for both temperatures required to generate the R-phase and austenite microstructures in the shape memory Nitinol end-caps. The results are shown in Figure 5.12.

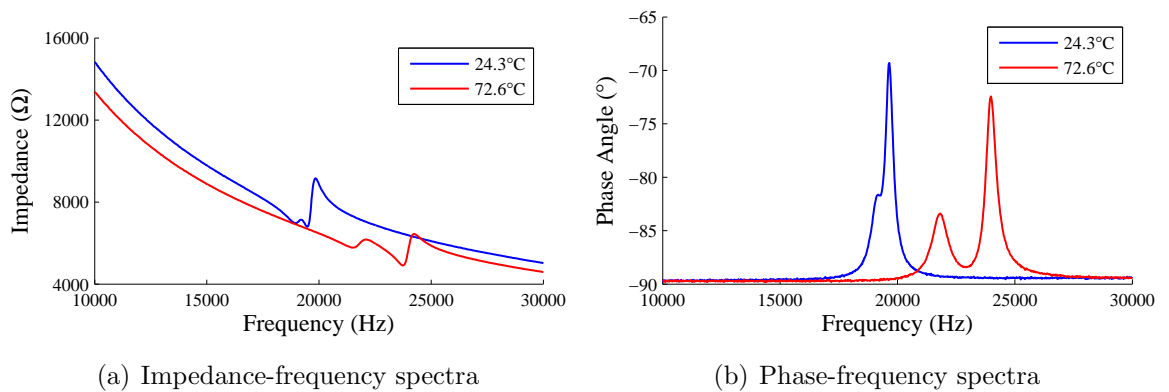


Figure 5.12: Resonant frequency characterisation of the second shape memory Nitinol transducer showing the measured (a) impedance-frequency and (b) phase-frequency spectra

A double-peak exists in the frequency response of the transducer. In addition, the temperature at which the rapid increase in resonant frequency occurred correlated well with the DSC analysis. The resonant frequencies of the transducer for two different temperatures are summarised in Table 5.5.

	f_r at 24.3°C (Hz)	f_r at 72.6°C (Hz)	Difference (Hz)	Change (%)
Mode 1	18950	21500	+2550	+13.46
Mode 2	19450	23750	+4300	+22.12

Table 5.5: Resonant frequency shifts of the second shape memory Nitinol cymbal transducer

The resonant frequencies are several kilohertz lower compared to the first shape memory Nitinol cymbal transducer. The differences can largely be attributed to the epoxy bond layers, since almost identical shape memory Nitinol end-caps were used to fabricate the transducer. The second mode exhibited the largest change in resonant

frequency. This transducer did not exhibit a reduction in resonant frequency of either mode as the temperature was increased. This suggests that the reduction in resonant frequency shown for the first shape memory Nitinol cymbal transducer was caused by the mechanical coupling.

5.3.2 Modal behaviour

Figure 5.13 shows the symmetric and asymmetric modes of the transducer. The noise levels for all three coordinates for each measurement point were sufficiently low, thus the EMA results are 3-D. Similar to the first shape memory Nitinol cymbal transducer, the measurements were taken with the transducer at room temperature. This means that the end-caps are in the R-phase condition. The resonant frequencies of the modes closely correlate with those measured using electrical impedance analysis.

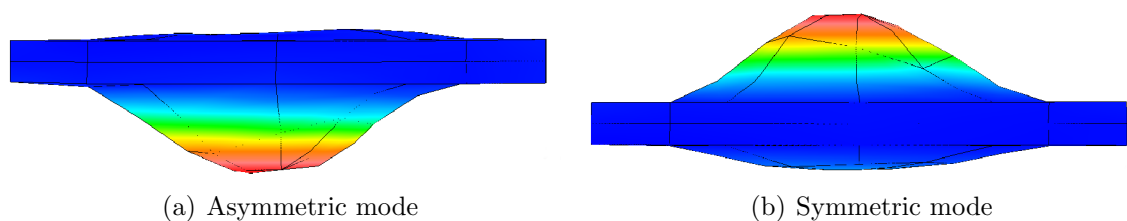


Figure 5.13: Modes of the second shape memory Nitinol cymbal transducer, showing (a) the asymmetric mode at 19270Hz, and (b) the symmetric mode at 20025Hz, measured at 20.9°C

EMA can be a time-consuming process, and this is an important consideration for the analysis of Nitinol cymbal transducers. The resonant frequencies of a Nitinol cymbal transducer are very sensitive to temperature, since the modulus of Nitinol is highly dependent on temperature. It has been found in the EMA studies presented in this chapter that the use of EMA for identifying the mode shapes of a Nitinol cymbal transducer can be successful if the setup of the experiment is carefully considered. Preventing temperature change of the Nitinol throughout the experiment is most important.

5.3.3 Vibration resonance response characterisation

There has been a good level of agreement between the resonant frequencies measured using electrical impedance analysis and those measured from EMA for the second transducer. Similar to the first transducer shown in this chapter, the asymmetric mode appears before the symmetric mode, and the EMA studies were conducted with no adverse noise effects.

The electrical impedance measurements and the EMA results demonstrate that the symmetric and asymmetric modes of this transducer are much closer together than those of the first shape memory Nitinol cymbal transducer. Figure 5.14 shows the displacement amplitudes for the asymmetric mode for the transducer with end-caps in R-phase and austenite states. The experiment was repeated for the symmetric mode, the results of which are shown in Figure 5.15.

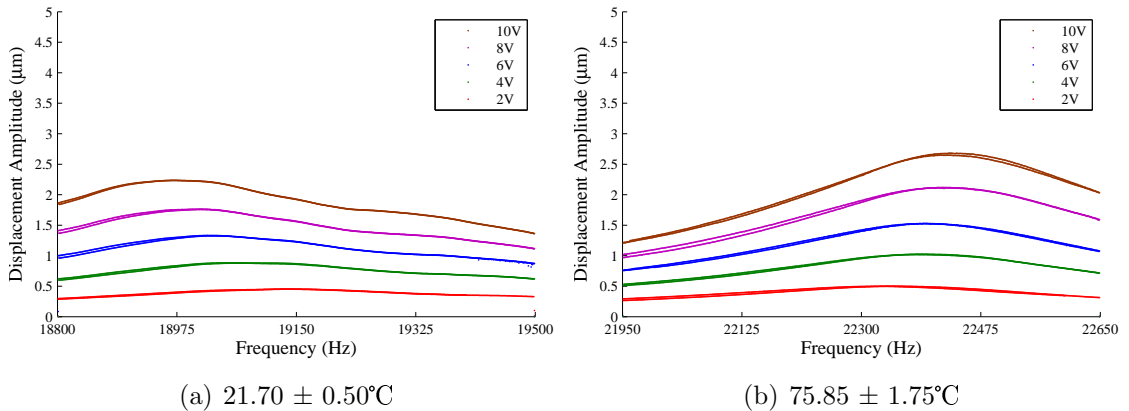


Figure 5.14: Plots showing the (a) R-phase and (b) austenite vibration responses of the asymmetric mode of the second shape memory Nitinol cymbal transducer

For both modes of vibration, the displacement amplitudes of the transducer with end-caps in the austenite phase are higher than the displacement amplitudes of the transducer with end-caps in the R-phase state. This was also detected for one of the vibration modes of the first transducer, as shown in Figure 5.4. It is known that the damping capacity of austenitic Nitinol is much lower than that of martensitic Nitinol [221]. For example, the very high energy dissipation property of martensitic Nitinol is a major reason why some vibration dampers are often made out of Nitinol in the martensite phase. It is known that R-phase can be considered as a martensitic microstructure [74]. For the displacement amplitudes shown in Figures 5.14 and 5.15,

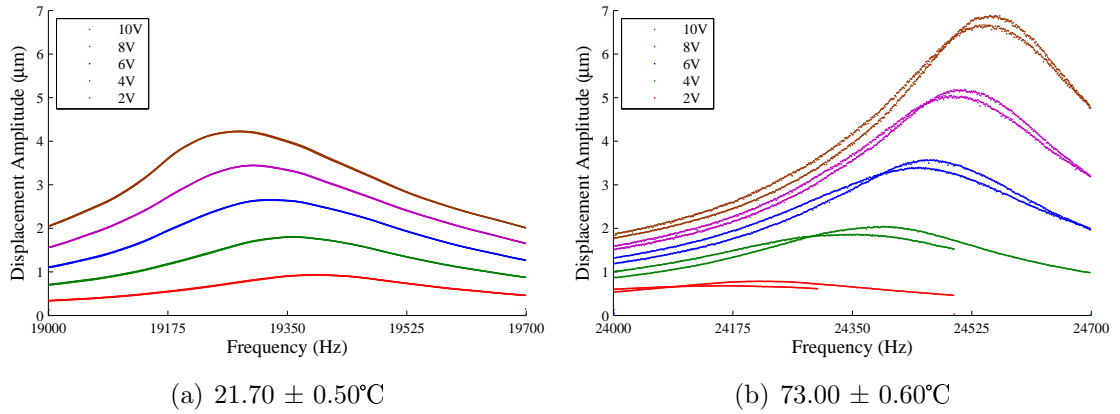


Figure 5.15: Plots showing the (a) R-phase and (b) austenite vibration responses of the symmetric mode of the second shape memory Nitinol cymbal transducer

it is likely that the energy dissipated is much greater in the Nitinol end-caps in the R-phase state compared to the Nitinol end-caps in the austenite phase. Therefore, the energy required to generate the same cymbal transducer displacement amplitude for Nitinol end-caps in the R-phase as the austenite phase is much greater. The large damping capacity of Nitinol in the R-phase compared to the austenite phase has been reported in the literature [222].

A high level of correlation between the resonant frequencies measured for the second shape memory Nitinol cymbal transducer using the different dynamic characterisation techniques has been demonstrated, and this is shown in Figure 5.16. A close correlation of resonant frequencies for different characterisation methods also suggests the repeatability of the phase transformations in the Nitinol end-caps. The transducer resonant frequencies for both the higher and lower temperatures could be reproduced for different characterisation techniques, and this would make it suitable and reliable for a practical application requiring a cymbal transducer with a tuneable frequency function.

Neither the first or the second transducer has displayed modulation behaviour in the displacement amplitude responses measured using VRRC. In Chapter 3, modulations were exhibited in the displacement amplitude response of the asymmetric cymbal transducer operated at the higher temperature. It was argued that the epoxy bond layers contributed to the modulation behaviour at the higher temperature. To investigate this further, the second transducer was driven at increasing voltage levels

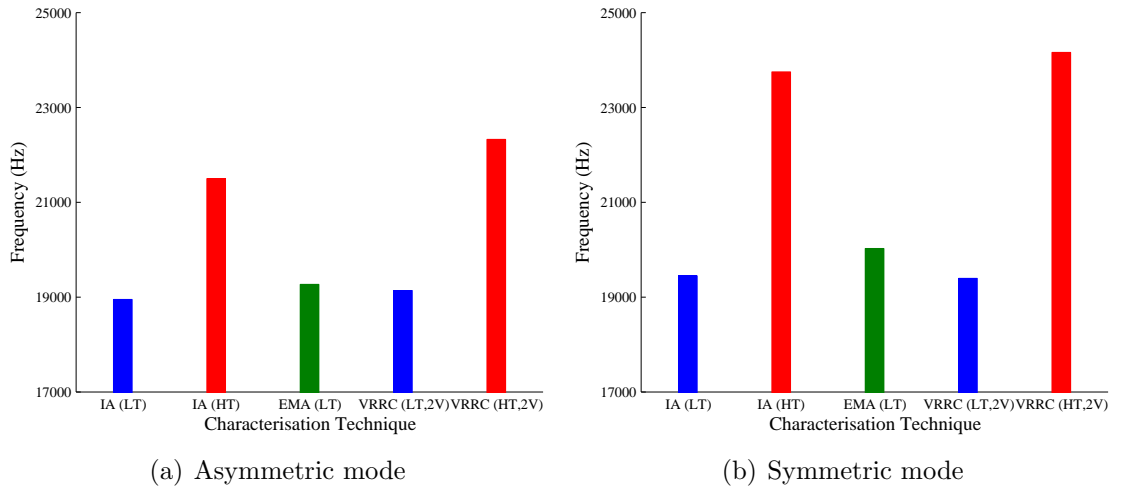


Figure 5.16: Resonant frequencies measured using the three dynamic characterisation techniques for the second shape memory Nitinol cymbal transducer

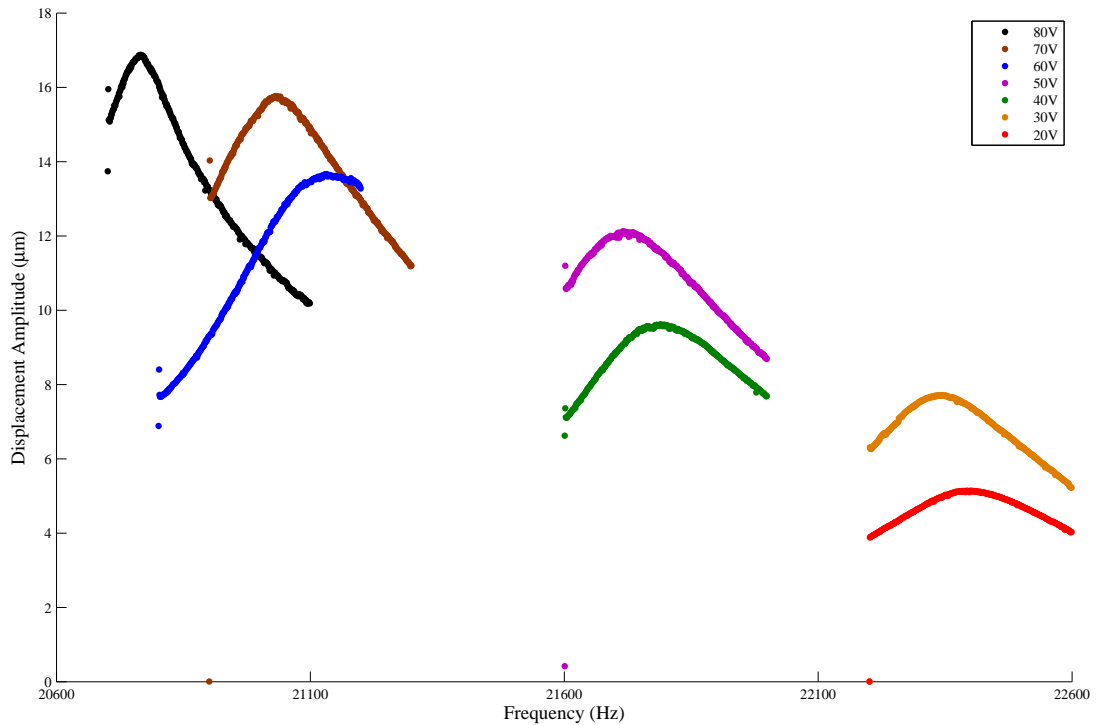


Figure 5.17: Vibration resonance response of the asymmetric mode of the second shape memory Nitinol cymbal transducer at raised input voltage levels, measured at $78.25 \pm 0.65^\circ\text{C}$

at a higher temperature than room temperature. The transducer was driven in only one mode of vibration for this experiment, since the displacement amplitude would be increased until the transducer was no longer operational. Figure 5.17 shows the displacement amplitudes of the asymmetric mode of the second shape memory Nitinol cymbal transducer with end-caps in the austenite phase for increasing voltage levels.

A steady LDV signal was monitored in the experiment, and from the results shown in Figure 5.17, there is no evidence that the modulations in the vibration response are caused by increasing the voltage, or the displacement amplitude, of the transducer. The transducer failed after the sweep at 80V was performed, likely due to a compromise of the mechanical coupling. The effect of voltages above 80V on the vibration response could therefore not be investigated. There was a very high level of nonlinear softening behaviour between 20V and 80V. It is probable that this softening occurred partly as a result of heating in the piezoceramic, and also because of the compromise of the mechanical coupling from the epoxy bond layers. However, the reasons for the modulations in the displacement amplitude responses shown in Chapter 3 are still unclear.

5.4 Finite element analysis

The symmetric mode of the second shape memory Nitinol cymbal transducer has been simulated. The resonant frequency of this mode has been calculated to investigate the modulus required for each phase of Nitinol to closely correlate with the experimental data. The asymmetric mode has not been computed, as it is very difficult to accurately quantify the asymmetry in the transducer. This numerical study has been conducted to demonstrate how FEA can be used to predict the resonant frequency and displacement amplitude of the transducer in the symmetric mode, for Nitinol end-caps in the R-phase state and the austenite phase, and to provide an estimation of the modulus of the Nitinol in each phase. The end-cap dimensions shown in Table 5.2 were used to produce the end-cap FEM, and Table 5.6 shows the epoxy bond layer properties used for both FEMs. Each epoxy bond layer was modelled as a ring, with internal and external diameters. The material properties were determined using tensile testing on

a dog-bone specimen of cured epoxy resin.

Property	Units	Magnitude
External diameter	mm	12.70
Internal diameter	mm	8
Bond layer thickness	mm	0.1
Density	kg.m ⁻³	1496
Poisson's ratio	-	0.35
Young's modulus	GPa	2.75

Table 5.6: Geometrical dimensions and material properties for the epoxy resin bond layer used in the FEA of the second shape memory Nitinol cymbal transducer

It has been reported that the Young's modulus of the R-phase is lower than the modulus of the martensite phase [77]. It has also been suggested that the elastic modulus of the R-phase, E_R , can be as low as 20GPa [211]. However, a reasonably accurate estimate of the R-phase elastic modulus remains unclear from the literature. The elastic properties of the shape memory Nitinol in either phase has not been determined by experiment. However, approximations for the Young's modulus and density of Nitinol, and the geometrical dimensions of the end-caps are all known. The manufacturer of the shape memory Nitinol state that Nitinol has a density of 6.5g/cc, an approximate E_M of 40GPa and that E_A is around 75GPa [223]. Whilst the exact modulus for the R-phase is unknown, it is probable that E_R is closer to E_M than that of E_A . This is because the R-phase is regarded as a martensitic microstructure [74].

Experimental and numerical comparison

The modulus in the FEM was changed until the resonant frequency of the symmetric mode of the transducer agreed with the experimental data for the Nitinol end-caps in each phase, giving an approximation for both E_A and E_R . An example of the symmetric mode shape is shown in Figure 1.3(b). The Young's moduli used in the FEM to calculate the resonant frequencies are shown in Table 5.7, complemented by both calculated and experimentally measured resonant frequencies. EMA data was only used for the resonant frequency of the transducer with Nitinol end-caps in the R-phase state, since EMA of the transducer with Nitinol end-caps in the austenite

phase was not performed. For the resonant frequency of the transducer with Nitinol end-caps in the austenite phase, the electrical impedance measurement result was used instead.

Phase	FEA E (GPa)	f_r (Experimental)	f_r (FEA)
Austenite	70	23750	23591
R-phase	48	20025	20060

Table 5.7: Resonant frequency comparison, in terms of Hz, for the symmetric mode of the second shape memory Nitinol cymbal transducer, with associated computed Young’s moduli for each Nitinol phase from FEA

The modulus required to simulate the symmetric mode of vibration of the transducer at a resonant frequency close to that measured using electrical impedance analysis was 70GPa for the Nitinol end-caps in the austenite phase. This is a 5GPa difference compared to the specification of the manufacturer, which was stated as 75GPa. This is a close estimation, since the modulus of Nitinol is dependent on both stress and temperature. The estimation of R-phase modulus from FEA, which was calculated to be 48GPa, is closer to the manufacturer’s specification of modulus for martensite, which is 40GPa, than to the austenite specification. The E_R has been reported to be as low as 20GPa [211], and it is evident that there remains much uncertainty in the definition of certain Nitinol material properties. Also, the precise epoxy bond layer geometry is not known, which affects the accuracy of the FEA simulations. However, the steady-state linear dynamics step was used in FEA to determine the damping of the Nitinol for each phase microstructure required to simulate the resonant frequency and peak displacement amplitude of the transducer in the symmetric mode of vibration for a 2V input voltage. The computed results are compared with experimental measurements from VRRC, and are shown in Table 5.8.

The material damping parameters have been normalised, and although the damping values are relatively close, the damping factor of the austenitic Nitinol phase has been found to be marginally higher than that of the R-phase Nitinol, which is not consistent with the literature. However, it is unknown how the material damping changes as the temperature of the Nitinol is raised. The difference in damping capacity between each phase of the Nitinol is very important to consider for the analysis of a shape memory

	R-phase		Austenite	
Analysis method	f_r (Hz)	a_o (μm)	f_r (Hz)	a_o (μm)
Experimental	19396	0.93	24215	0.79
FEA	20094	0.93	23628	0.79
Normalised material damping value (FEA)	0.97		1	

Table 5.8: Comparison between experimental and numerical data for the displacement amplitude response of the symmetric mode of the second shape memory Nitinol cymbal transducer for a 2V input voltage, showing the displacement amplitudes computed for each Nitinol phase from FEA

Nitinol transducer, and further research is required into the simulation of the material for the accurate prediction of displacement amplitude response.

Consideration of stress in the end-caps

The FEM was produced to simulate the vibration response of the transducer. However, the mechanical properties of the shape memory Nitinol have not been characterised by experiment. In addition, the profile of each epoxy bond layer is not accurately known.

The influence of stress on the phase transformation behaviour of Nitinol is important, particularly above the A_F transformation temperature, as a sufficient stress can generate regions of martensite due to the superelastic effect. To highlight the regions of a transducer end-cap which are susceptible to highest stress concentration, Figure 5.18 has been included to show the von Mises stress distribution in the transducer vibrating in the symmetric mode.

Cool colours indicate regions of low stress, and warm colours signify high stress. The regions of high stress concentration would become the most susceptible to localised phase transformation for changes in stress and temperature. Figure 5.19 shows the normalised von Mises stress distribution, as calculated over the surface of one of the end-caps at resonance in the symmetric mode, using FEA. The stress data is normalised by making use of the maximum stress, which was calculated to be 3.36MPa. The regions of high stress in the end-cap can clearly be identified as being around the circumference of each end-cap cavity base and also on the apex surface of the end-cap. The epoxy bond layers also experience increasing stress as the voltage, and hence displacement

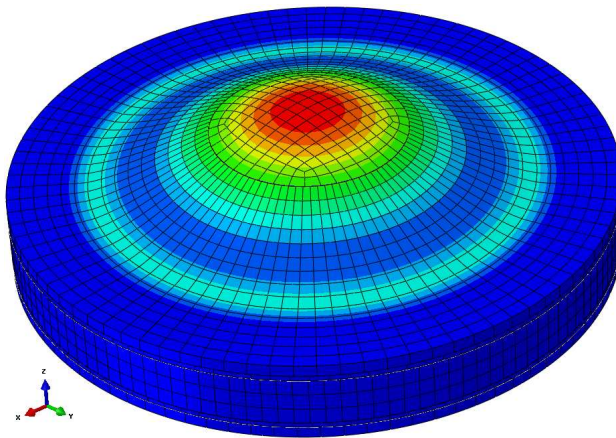


Figure 5.18: Locations of high stress concentration in a cymbal transducer, predicted from the FEA simulation of the shape memory Nitinol cymbal transducer with end-caps in the austenite phase of the symmetric mode at 24289Hz, with a 2V input voltage

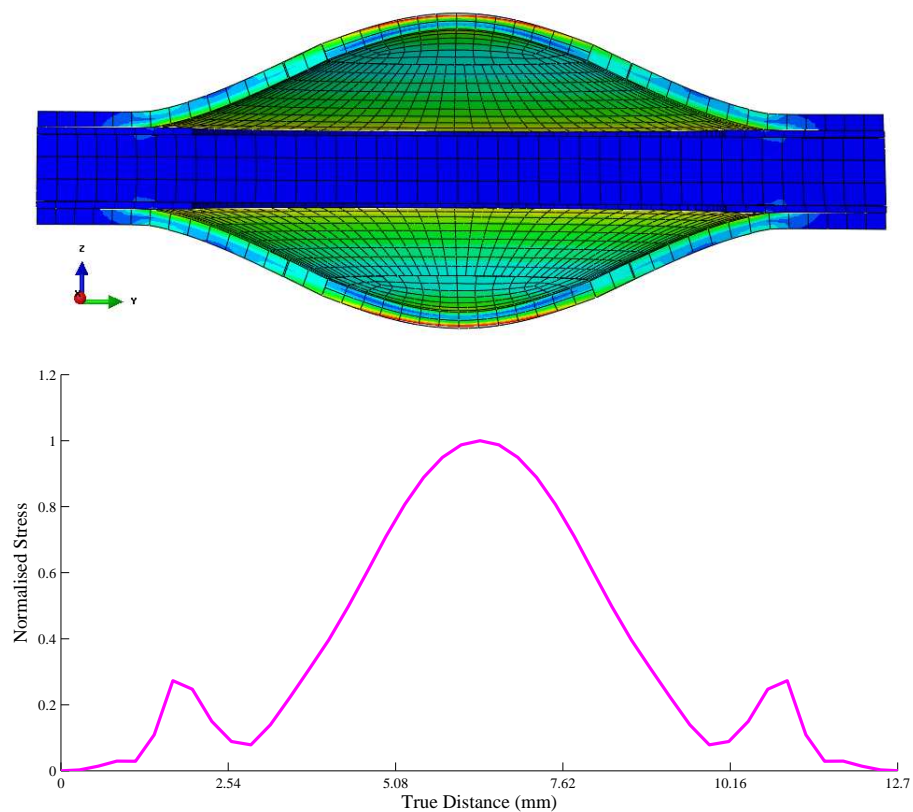


Figure 5.19: Normalised von Mises stress distribution for the shape memory Nitinol cymbal transducer end-cap in the austenite phase and in the symmetric mode, as calculated from FEA over the top of the end-cap surface

amplitude, is raised. A method of measuring the stress distribution in the end-caps by experiment would therefore be advantageous, for example by using digital image correlation (DIC) to map the stress, and also the evolution of stress over a defined time period.

5.5 Chapter conclusions

This chapter has shown that the two cymbal transducers which were assembled with shape memory Nitinol end-caps exhibited tuneable resonant frequency capability. The resonant frequency of each transducer could be controlled by changing the temperature of the end-caps. The lower temperature which was used in the experiments generated the R-phase microstructure in the Nitinol end-caps, and the higher temperature produced the austenite phase microstructure. The R-phase and austenite states each possess different elastic properties, resulting in different resonance responses. However, the poor controllability in the deposition of the epoxy resin used to create the bond layers caused asymmetries in the transducer to appear. There is little consistency between the frequency response of the transducers due to significant differences in the epoxy resin deposition. Also, the lack of suitable mechanical property data for Nitinol, and geometrical property information regarding the epoxy bond layers, are hindering the progress of the numerical analysis of Nitinol cymbal transducers.

Evidence has also been presented that the displacement amplitude of the transducer can be higher for end-caps in the stiffer austenite phase compared to those in the softer R-phase state. This has been attributed to the difference in damping capacity between the two phases. However, shape memory Nitinol is a suitable material for tuneable cymbal transducers, despite notable limitations of the cymbal transducer configuration.

Chapter 6

Superelastic nitinol cymbal transducers

The superelastic effect occurs in the austenite phase, above the A_F transformation temperature of Nitinol, but the stress required to generate martensite is unknown. At sufficient stress levels, there may be a local emergence of martensitic behaviour which affects the vibration response of a transducer fabricated with superelastic Nitinol end-caps. However, it is possible that the epoxy bond layers fail before this stress level is reached. Transformation temperature estimation of superelastic Nitinol is undertaken using DSC analysis. Although reports in the literature suggest that these can be misinterpreted from DSC measurements, the experimental evidence to support this is not substantial.

Three superelastic Nitinol cymbal transducers were fabricated. Two were constructed using untreated superelastic Nitinol end-caps. The other was fabricated using superelastic Nitinol end-caps which were heat treated. The heat treatment was performed to reduce residual stress within the end-caps from the manufacturing process, and investigate the suitability of the DSC method for transformation temperature estimation after heat treatment. Also, one of the transducers fabricated with the untreated superelastic Nitinol end-caps was driven above the A_F transformation temperature at increasing voltages to investigate any stress-induced phase change in the end-caps which may be exhibited in the displacement amplitude response of the transducer.

6.1 Transducer fabrication

The superelastic Nitinol end-caps (Johnson Matthey Noble Metals) were manufactured in an oxide-free condition utilising shape-set annealing, with geometrical dimensions shown in Table 6.1. The Nitinol exhibited high deformation resistance and spring-back at room temperature by physical inspection, indicating a stiff austenitic phase. The geometrical dimensions of the end-caps were measured with Mitutoyo digital callipers, and it was found that the dimensions of the end-caps were not all equal. A sample average is included for each parameter in Table 6.1 for a batch of 10 end-caps. Variations in these parameters can lead to resonance at different frequencies.

Parameter	Dimension (mm)
Apex Cavity Diameter	4.50
Base Cavity Diameter	9.10
Cavity Depth	0.31
End-Cap Thickness	0.24
Total Diameter	12.72
Total Height	0.55

Table 6.1: Geometrical dimensions of the superelastic Nitinol end-caps

The Nitinol was composed of 55.99wt% nickel with a balance of titanium. Small quantities of cobalt, chromium, copper, iron, manganese, molybdenum, niobium, silicon and tungsten made up under 0.20% of the total alloy composition, and were included to tune the transformation temperatures of the material, in conjunction with cold working and heat treatments. Carbon and oxygen, both in quantities of <0.05wt%, were also present. Superelastic Nitinol possesses a greater proportion of nickel than the shape memory Nitinol, and so the transformation temperatures can be expected to be lower [63]. Material information supplied by Johnson Matthey Noble Metals is shown in Table 6.2.

Typical tolerances for the ingot temperature are stated by the manufacturer to be from -5°C to +15°C [224]. The contribution of each alloying element to the strength, ductility and transformation temperatures of Nitinol has been reported [78]. A nickel content of just below 56wt% in the Nitinol means the A_F transformation temperature can be as low as 5°C [78]. However, due to the influence of heat treatment and cold

Property	Information
Temper	Shaped set annealed
Surface	Oxide free
Ingot A_P	2°C

Table 6.2: Selected mechanical and physical properties of the superelastic Nitinol

working on the end-caps, this is not an accurate estimate.

6.1.1 DSC analysis of the superelastic nitinol

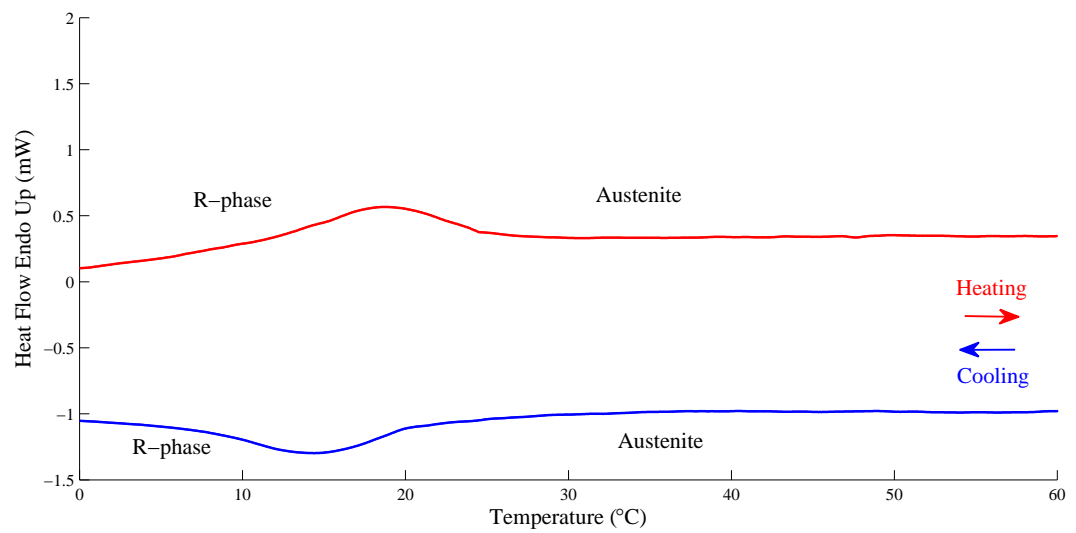
The transformation temperatures were not provided in the manufacturer's data. The thermograms for scan rates of 10°C/min and 20°C/min are shown in Figure 6.1.

It is known that for Nitinol optimised for superelastic performance, DSC can often provide unclear results [195]. However, the experimental evidence to support this is limited. Only two phases have been detected in the DSC results. The endothermic peak represents the transformation to austenite, but there is only one exothermic trough on the cooling cycle. Therefore, either there is no intermediate R-phase present, or the temperature range is not large enough to enable the lower temperature martensite phase to be measured. This is another example of why DSC thermograms can be difficult to interpret. It is very unlikely that for cold worked, nickel-rich and heat treated superelastic Nitinol that no intermediate R-phase exists. Also, the thermal hysteresis between the endothermic peak and the exothermic trough is very small, and therefore is unlikely to be a classical austenite-to-martensite transition [59]. The exothermic trough in the DSC thermogram is most likely the intermediate R-phase, and the estimated transformation temperatures are summarised in Table 6.3.

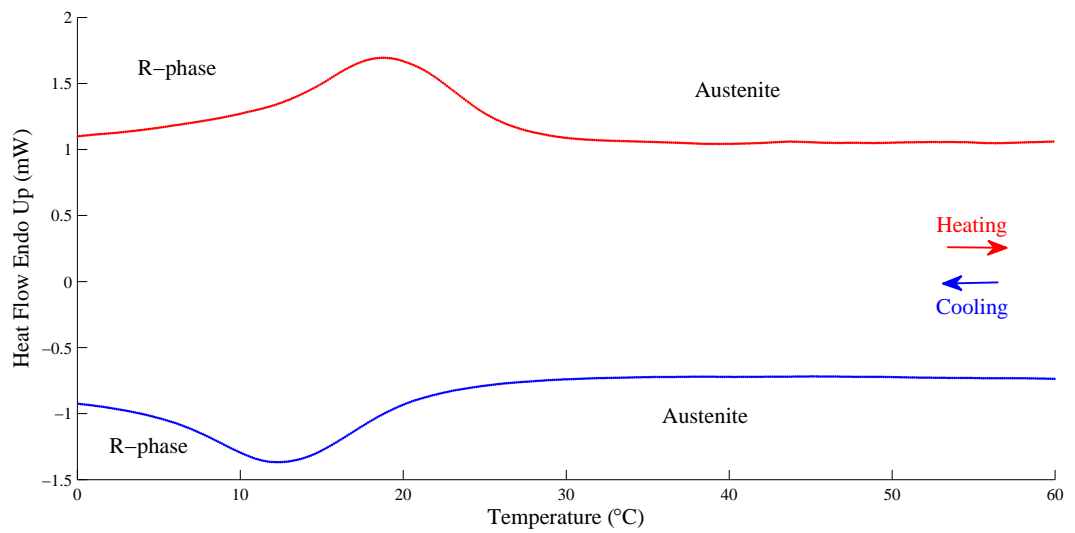
Scan Rate	A_F (°C)	A_S (°C)	R_F (°C)	R_S (°C)
10°C/min	23	16	9	19
20°C/min	25	15	7	19

Table 6.3: Transformation temperatures of superelastic Nitinol from DSC analysis

A wider temperature range would be required to verify the existence of the martensite phase, and at sub-zero temperatures. This would necessitate a method such as liquid nitrogen DSC. On first inspection, it appears that the superelastic Nitinol



(a)



(b)

Figure 6.1: DSC thermograms of superelastic Nitinol at scan rates of (a) 10°C/min and (b) 20°C/min

has been fabricated to be in the superelastic condition around room temperature, as desired. This is because the A_F transformation temperature estimated for both scan rates is approximately 25°C. A superelastic Nitinol cymbal transducer is shown in Figure 6.2. The red spots on the transducer were used as measurement markers for EMA.



Figure 6.2: The superelastic nitinol cymbal transducer

6.2 Dynamic characterisation

The Nitinol end-caps were initially assumed to exist in the austenite phase at room temperature. However, it was noticed that when the temperature of the first transducer was raised above room temperature, the resonant frequencies measured using electrical impedance analysis increased up until the temperature of the thermal chamber shown by the thermocouple, and hence the transducer, was approximately 45°C. This was significant, because despite the DSC analysis results, it was evident that the Nitinol had not completely transformed to austenite at 25°C.

6.2.1 Resonant frequency characterisation

Impedance-frequency and phase-frequency spectra were generated for two different temperatures, and are shown in Figure 6.3. The martensite phase, according to the DSC analysis, is likely to be far below -10°C, and therefore the transducer with Nitinol end-caps in the R-phase and austenite states is studied. The resonant frequencies of the transducer at two different temperatures have been measured, shown in Table 6.4, where the shifts of the transducer resonant frequencies are also summarised.

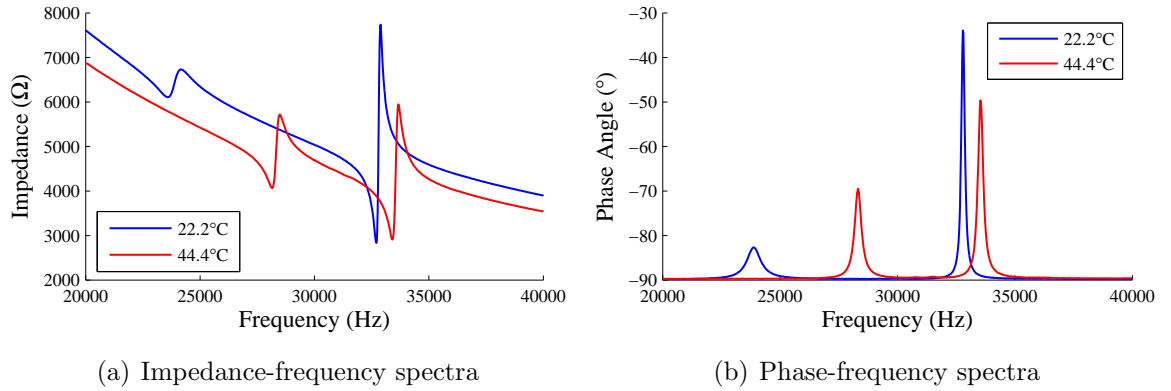


Figure 6.3: Resonant frequency characterisation of the first superelastic Nitinol cymbal transducer showing the measured (a) impedance-frequency and (b) phase-frequency spectra

	f_r at 22.2°C (Hz)	f_r at 44.4°C (Hz)	Difference (Hz)	Change (%)
Mode 1	23495	28137	+4642	+19.76
Mode 2	32698	33407	+709	+2.17

Table 6.4: Resonant frequency shifts of the first superelastic Nitinol cymbal transducer

The electrical impedance measurements confirmed the existence of a double-peak in the frequency response spectrum of the transducer. This signifies the presence of both a symmetric and an asymmetric mode. Consistent with the behaviour of the shape memory Nitinol cymbal transducers, the resonant frequencies of the modes do not change equally when the transducer is heated from the lower temperature to the higher temperature. However, during the measurement of the data shown in Table 6.4, it was found that the increase in the resonant frequencies completed at around 44.4°C, suggesting that the transformation of the Nitinol end-caps from the R-phase state to austenite phase also finished around this temperature. Therefore, the DSC estimate of the A_F transformation temperature of the superelastic Nitinol as shown in Figure 6.1 and Table 6.3 is not consistent with the temperature at which the resonant frequencies of the transducer stopped rising. In Chapter 5, the DSC estimation of the A_F transformation temperature was found to correlate well with the temperature required to increase the resonant frequencies of the shape memory Nitinol transducers. However, the DSC technique is clearly unsuitable for accurate determination of the transformation temperatures of the superelastic Nitinol.

DSC can be ineffective for Nitinol which has been either partially cold worked, or aged in the 400-600°C range [195]. Problems concerning the DSC analysis of superelastic Nitinol have been reported by Eaton-Evans et al. [91], where it was found that the estimation of the R_S transformation temperature was inaccurate, despite a high level of accuracy achieved for the A_F transformation temperature estimation. Distortions in the DSC results were attributed to residual stresses in the material as a result of cutting for sample preparation [91]. Other studies found that the estimated transformation temperatures were lower when the Nitinol was cold worked compared to annealed [172], and they could be as much as 20°C different to those measured by resistance and loading tests [225]. It was reported that the electrical resistance method yielded more accurate results which correlated well with the results of the applied loading method [225]. In this technique, the electrical resistance of the Nitinol is measured over a heating and cooling cycle. A decrease in resistance on cooling indicates a transition from austenite to martensite, and an increase of resistance on heating signifies a transformation to austenite [225]. It has been reported that although it is a simple method of transformation temperature estimation, changes in measured electrical resistance can exhibit poor correlation with phase changes in the Nitinol [225]. The temperatures required to produce the changes in electrical resistance can then be compared with DSC estimations. The inaccuracy of DSC measurements have been attributed to stress-induced transformation in the Nitinol, even though there is a distinct lack of experimental evidence available to support this [225]. In general, it has been acknowledged that experimental evidence in this area is limited [225]. However, it is known that cold working can cause residual stress [77], and that superelastic Nitinol alloys are often produced with significant cold working [226]. This suggests that cold working is a significant factor in the accurate estimation of transformation temperatures using DSC.

Many studies which focus on the behaviour and applications of superelastic Nitinol utilise relatively simple configurations of the material, such as wires or flat plates, rather than more complex geometry, typified by a cymbal-shaped end-cap. Cold working influences the transformation temperatures, but it has also been suggested that making the assumption that elastic modulus remains constant in both martensite and austenite

states is a common error [74]. This could mean that the superelastic Nitinol has not yet fully transformed to austenite at 25°C, but that it has passed the A_S transformation temperature, which would explain the stiff condition of the Nitinol. The superelastic Nitinol may exist as a mixture of austenite and R-phase at room temperature, the latter of which is not completely eliminated until it is heated past the A_F transformation temperature. The low temperature state likely possesses a high proportion of R-phase, and the high temperature state is assumed to be composed of mostly austenitic Nitinol. It is assumed that this is the nature of the phase transformation of the as-received superelastic Nitinol end-caps used in this research.

6.2.2 Modal behaviour

The mode shapes of the superelastic Nitinol cymbal transducer were found using EMA with the end-caps in the R-phase. Figure 6.4 shows both the asymmetric and symmetric modes of vibration. Similar to the transducers reported in Chapters 3 and 5, the measurements on the end-cap faces were taken with the 3-D LDV. The noise levels when recording the measurements in the lateral x-direction and y-direction were low enough such that the mode shapes were clear in 3-D. The asymmetric mode was found to exist at a lower resonant frequency than the symmetric mode.

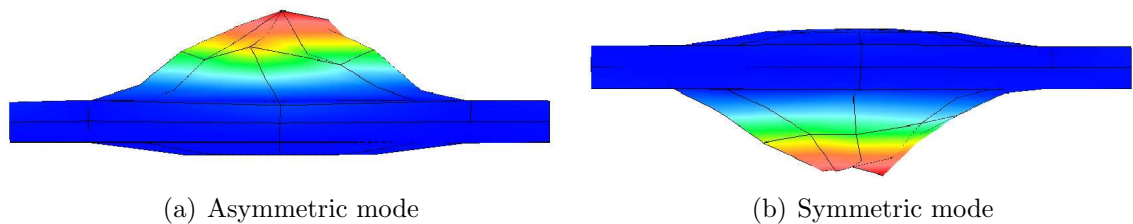


Figure 6.4: Modes of the superelastic Nitinol cymbal transducer, showing (a) the asymmetric mode at 23267Hz, and (b) the symmetric mode at 32594Hz, measured at 21.6°C

6.2.3 Vibration resonance response characterisation

VRRC was conducted for five voltage levels, from 2-10V, around the resonant frequency of each mode in bi-directional sweeps. The displacement amplitude data for the asymmetric mode is shown in Figure 6.5, and the displacement amplitude response

of the symmetric mode is shown in Figure 6.6. The temperature set for the end-caps in the austenite phase is much higher than the A_F transformation temperature estimated using DSC. This was performed in order to ensure the complete transformation of the Nitinol to the austenite phase, and so the Nitinol is assumed to be superelastic at the higher of the two temperatures.

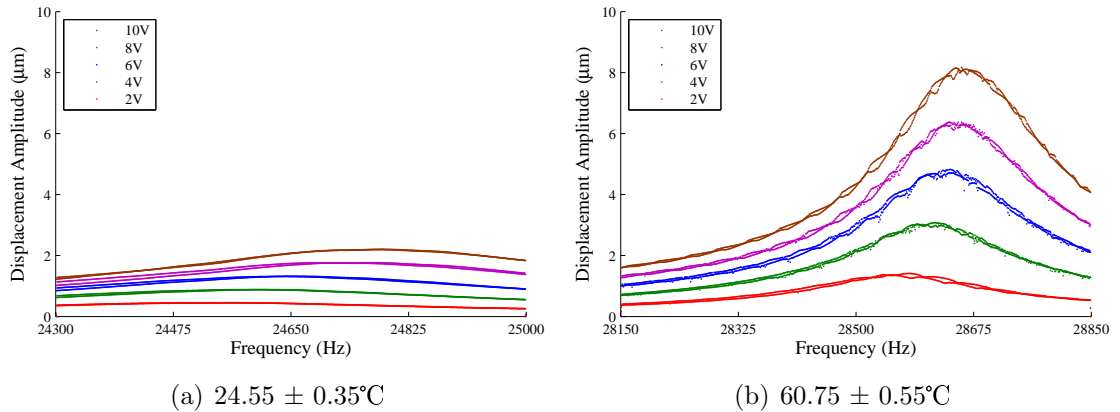


Figure 6.5: Plots showing the (a) R-phase and (b) austenite responses of the asymmetric mode of the first superelastic Nitinol cymbal transducer

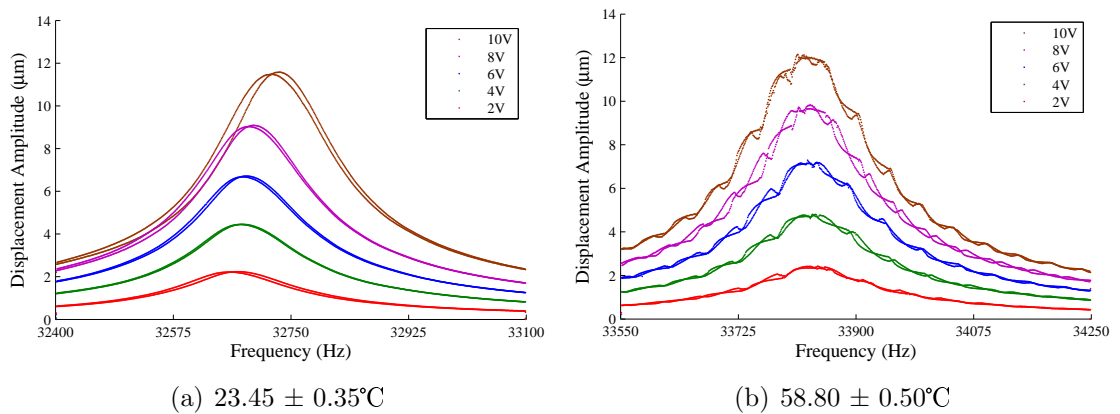


Figure 6.6: Plots showing the (a) R-phase and (b) austenite responses of the symmetric mode of the first superelastic Nitinol cymbal transducer

For the asymmetric mode, the displacement amplitude is lower for the transducer with end-caps in the R-phase than that exhibited by the transducer when the end-caps are in the austenite phase. Similar to the analysis in Chapter 5, the difference in damping capacity between the two microstructure phases is likely to be a significant contributing cause. However, for the symmetric mode, the displacement amplitude of the transducer with end-caps in the R-phase state is almost identical to the response

of the transducer with end-caps in the austenite phase. Further investigation into the displacement amplitude of each mode for the transducer with R-phase and austenitic Nitinol end-caps is required in order to understand this. In particular, the contributions from the damping capacity of the Nitinol in each phase and the condition of the epoxy bond layers in the transducer must be better understood, since it is very probable that damping and the condition of the epoxy bond layers are both contributory factors.

The transducer with end-caps in the austenite phase exhibits modulations in the vibration response of both modes of vibration, as shown in Figures 6.5(b) and 6.6(b). This behaviour was also observed in the vibration responses of the asymmetric cymbal transducer at the higher of the two temperatures used in the experiments. Therefore, it is not exclusive to the superelastic Nitinol transducer. However, this does not eliminate the possibility that the superelasticity of the Nitinol also contributes to this behaviour, in addition to the condition of the epoxy bond layers.

Nonlinear hardening is displayed in the response of the asymmetric mode of the transducer with end-caps in both the R-phase and austenitic states, showing an increasing frequency for increasing excitation level. This behaviour is also exhibited in the displacement amplitude response of the symmetric mode of the transducer, although only for the end-caps in the R-phase state. The displacement amplitude response of the transducer with end-caps in the austenite state is almost linear in the excitation range of the experiment. In addition to temperature, it is possible that a change in stress level could cause a nonlinear response, based on the dependency of Nitinol transformation temperatures on applied stress. This would also apply to the shape memory Nitinol cymbal transducers. The resonant frequencies obtained from the dynamic characterisation of the transducer are compared in Figure 6.7, showing a high level of correlation obtained between each technique.

The epoxy bond layers in the transducer were assumed to remain undamaged for all experiments, since no significant drops in displacement amplitude were observed for either mode of vibration at both the lower and higher temperatures. The condition of each epoxy bond layer of the transducer after the characterisation process was completed is shown in Figure 6.8. It is shown that a similar amount of epoxy resin has been deposited between each end-cap and the piezoceramic disc compared

to the first shape memory Nitinol transducer, although the deposition remains uneven. To minimise the chance of cracking in the epoxy bond layers during dynamic characterisation, a greater amount of epoxy resin can be used to reinforce the bond. However, this increases the likelihood of the epoxy resin entering an end-cap cavity.

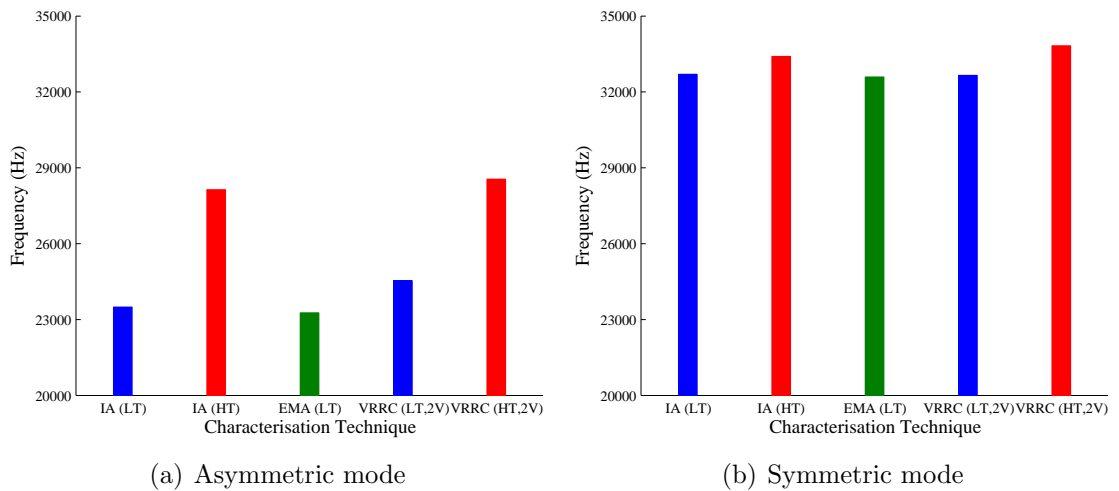


Figure 6.7: Resonant frequencies measured using the three dynamic characterisation techniques for the first superelastic Nitinol cymbal transducer



Figure 6.8: Condition of each epoxy bond layer in the first superelastic Nitinol cymbal transducer after dynamic characterisation

6.3 Effect of annealing

A specimen of Nitinol can be set in different shapes by constraining the material in the desired shape before heating. For example, heating to around 550°C or higher for only approximately two minutes is sufficient to set a shape in the material [74]. It is known that subjecting Nitinol to high enough temperatures for sufficiently long durations can result in the annealing of the material [78], which results in more precise shape setting and decreased spring-back [78]. The stress relief in Nitinol can be achieved at

temperatures as low as 300°C, and Nitinol can be heat treated in an air environment up to around 500°C [194]. Also, the superelasticity of Nitinol can be optimised using both heat treatment and cold working processes [71]. It has been suggested that annealing heat treatments could be used to increase the modulus difference between austenitic and martensitic Nitinol [67]. In addition to cold working, ageing is known to improve the superelastic performance of superelastic Nitinol and also change the A_F transformation temperature, where an increase in the A_F transformation temperature occurs after ageing at 450°C [78]. The duration of the heat treatment also affects the A_F transformation temperature, where 60 minutes can be required to induce significant change.

The DSC thermograms of superelastic Nitinol are liable to misinterpretation, because the superelastic Nitinol does not complete its phase transformation to austenite at the temperature estimated using DSC. The temperature required to complete the transition from R-phase to austenite is approximately 20°C higher in the dynamic characterisation experiments than has been estimated from the DSC thermograms. DSC was repeated to eliminate the possibility of random errors in the measurement, and it was found that the result was repeatable. DSC has been found to be very reliable for the estimation of the transformation temperatures of shape memory Nitinol, suggesting that DSC analysis is appropriate for shape memory Nitinol, but not superelastic Nitinol. However, it is known that DSC analysis is suitable for annealed Nitinol, and especially Nitinol which is fully annealed, for example at around 700°C [195]. Therefore, to improve the understanding of how the end-cap fabrication affects the suitability of DSC analysis for the characterisation of Nitinol, the superelastic Nitinol end-caps were annealed before DSC was conducted. A transducer was then fabricated using this material for dynamic characterisation.

6.3.1 Heat treatment by annealing

The effect of annealing on the transformation behaviour of superelastic Nitinol wires has been reported in the literature [68], where samples were annealed at a range of temperatures from approximately 300°C to 700°C for around 30 minutes. By using DSC analysis, it was shown that the annealing temperature significantly influenced

the transformation temperatures and the material behaviour [68]. More recently, the effects of annealing between 450-800°C for durations ranging from 20 minutes to 3 hours were demonstrated [92]. Annealing temperatures below 500°C were referred to as low annealing temperatures, and it was found again that the transformation temperatures, and the behaviour of the material, could be significantly affected by the annealing procedure [92]. At the same time, in a different study, the influence of annealing temperature on the transformation temperatures of Nitinol was investigated [202]. Whilst the changes in transformation temperature were clearly more significant for Nitinol in the martensite phase, it was concluded that much further investigation is required in order to improve the understanding of the material behaviour [202].

To investigate the effect of heat treatment on the superelastic Nitinol end-caps, a temperature of 450°C was chosen as the annealing temperature, which is within the common effective heat treatment temperature range which can be found in the literature. Only two different annealing durations were investigated due to the small number of available samples. Two of the Nitinol end-caps were annealed at 450°C in a temperature-controlled furnace for one hour and then immediately quenched in water. This process was repeated for another two end-caps, but for two hours.

Sacrificial end-cap samples were also given the same heat treatments for use in DSC analysis. After annealing, one of the end-caps (heat treated for one hour) was deformed out of shape at room temperature, and retained the applied deformation. The end-cap was then placed in boiling water, where it recovered its original shape. This suggests that the sample was not fully austenitic at room temperature. The end-cap did not exhibit the same level of spring-back as the untreated end-cap, appearing to be softer. The end-caps also changed colour as a result of the heat treatment processes. This can be attributed to oxidation of Nitinol which can occur after heat treatment, where colours can range from straw to blue [227].

The outer layer of the end-caps annealed for one hour were removed by mechanical abrasion to investigate the condition of the Nitinol underneath. Surface oxide layers as a result of machining and other processing can be a concern when applying a heat treatment. The end-caps were originally supplied in an oxide-free condition, and no oxide layer removal was performed before the heat treatment. The condition of the

end-caps after the different treatments is shown in Figure 6.9.

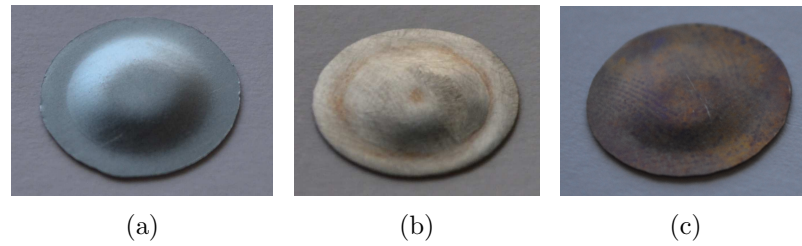


Figure 6.9: Three conditions of superelastic Nitinol end-cap, comprising (a) untreated, (b) annealed for one hour with surface abrasion, and (c) annealed for two hours, no surface abrasion

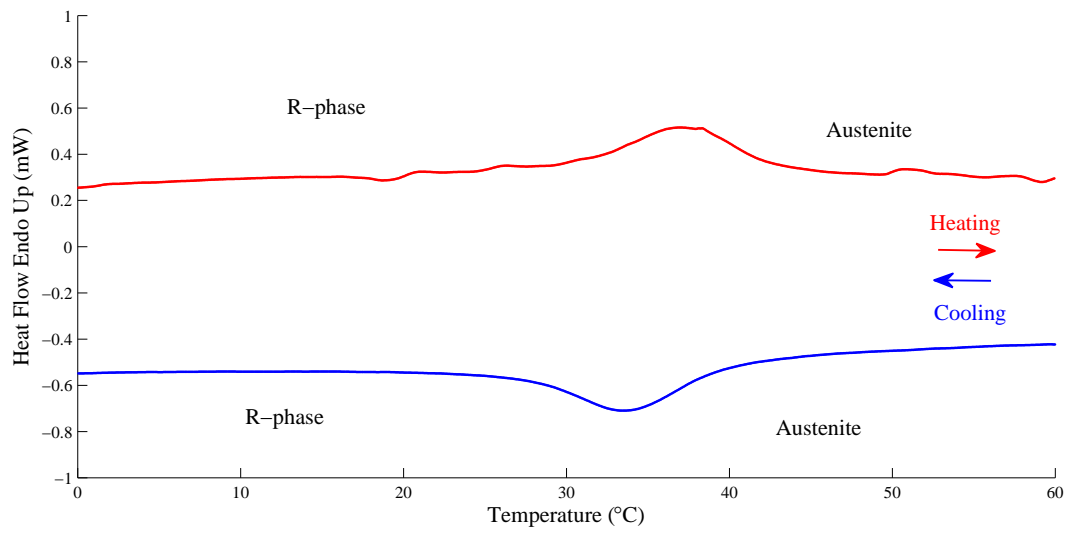
The DSC thermograms of the superelastic Nitinol annealed for one hour at scan rates of 10°C/min and 20°C/min are shown in Figure 6.10, and the DSC thermograms of the sample annealed for two hours at both scan rates are shown in Figure 6.11. The transformation temperatures estimated from DSC are summarised in Table 6.5.

Duration of anneal	Scan rate							
	10°C/min				20°C/min			
	A_F (°C)	A_S (°C)	R_F (°C)	R_S (°C)	A_F (°C)	A_S (°C)	R_F (°C)	R_S (°C)
1 hour	41	33	30	38	43	32	28	36
2 hours	43	38	33	40	43	37	32	38

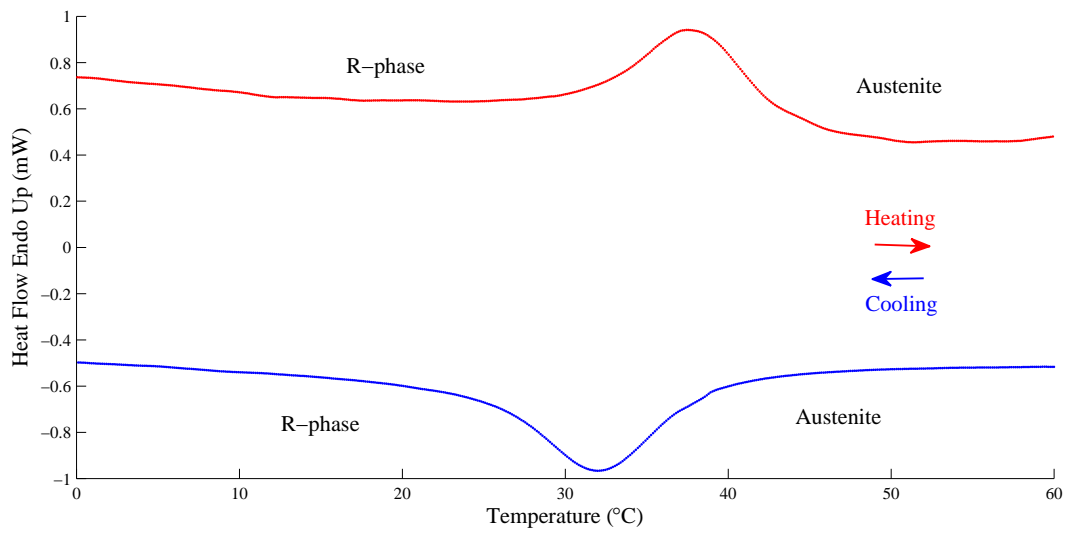
Table 6.5: Transformation temperatures of annealed superelastic Nitinol from DSC analysis

The results show a transformation from a lower temperature state, assumed to be the R-phase based on the low hysteresis, to the higher temperature austenite state beginning at approximately 35°C on heating. There is very little difference between the DSC thermograms of the one hour and two hour annealed samples for both scan rates. These results suggest that the change in Nitinol microstructure or transformation temperature shift do not significantly depend on the duration of the applied annealing treatment, which is consistent with other studies [92].

The temperature in the chamber was monitored using a thermocouple (type-K) during the electrical impedance analysis. It was found that the resonant frequencies of the superelastic Nitinol cymbal transducer increased until approximately 44°C. On first inspection, the A_F transformation temperature result from DSC is consistent

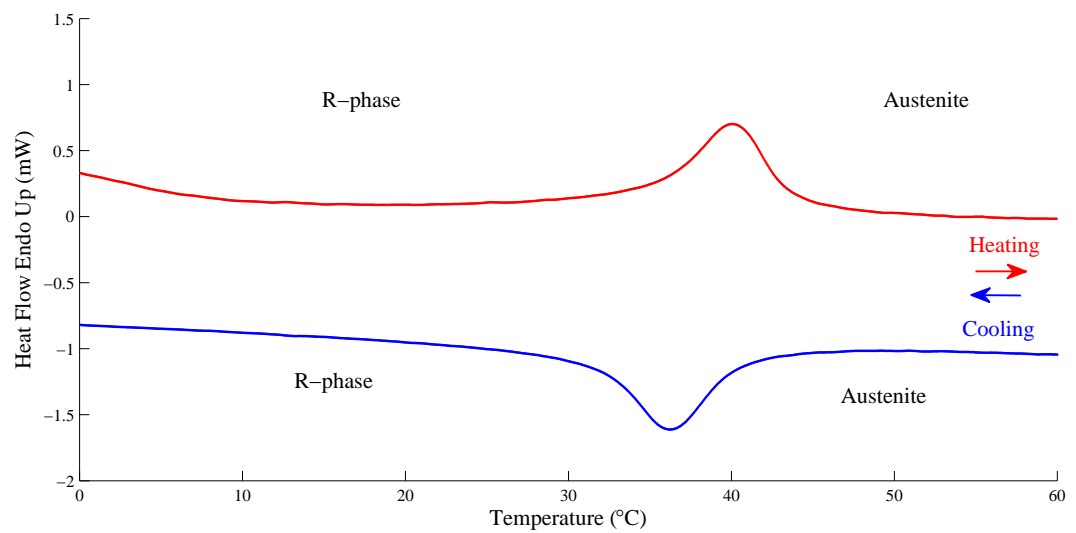


(a)

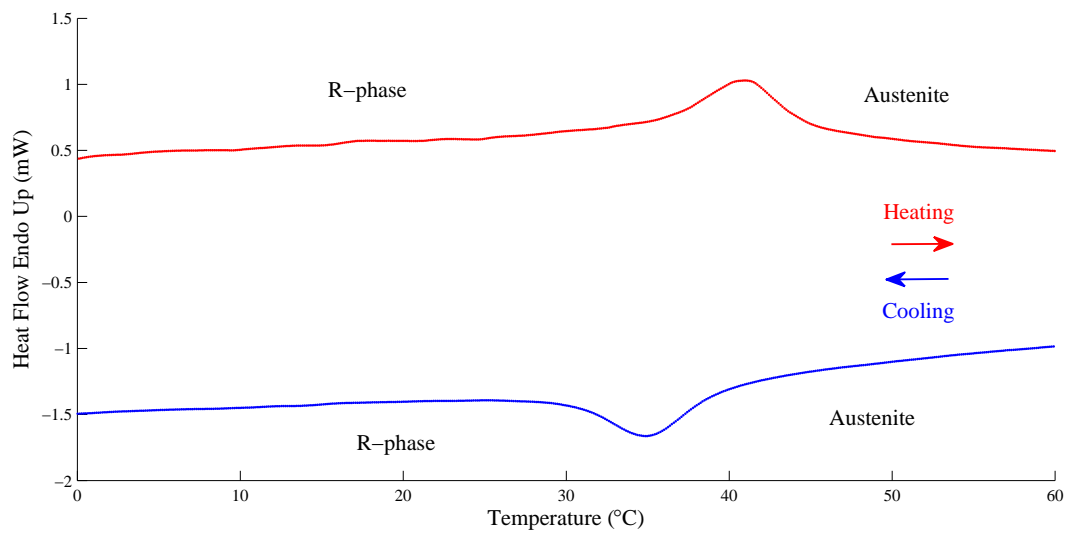


(b)

Figure 6.10: DSC thermograms of superelastic Nitinol annealed for one hour at scan rates of (a) 10°C/min and (b) 20°C/min



(a)



(b)

Figure 6.11: DSC thermograms of superelastic Nitinol annealed for two hours at scan rates of (a) 10°C/min and (b) 20°C/min

with the temperature required in electrical impedance analysis to increase the resonant frequencies of the superelastic Nitinol cymbal transducer fabricated using the untreated end-caps. The DSC results for both annealing durations, as shown in Table 6.5, are similar. The results show the A_F transformation temperature of the annealed superelastic Nitinol at approximately 41-43°C, close to where the untreated superelastic Nitinol transforms to austenite. It has been argued in the literature that the temperature of the heat treatment can significantly affect the transformation behaviour of Nitinol [68]. However, in this research, the untreated superelastic Nitinol appears to transform around the same temperature as the annealed superelastic Nitinol. Dynamic characterisation of an annealed superelastic Nitinol cymbal transducer would provide further evidence for this. It is most likely that the annealing process results in release of the residual stresses in the material, hence reducing the distortion of the transformation temperature estimations in the DSC thermograms. Previous reports have suggested that residual stress can affect DSC thermogram results [91], and that DSC is more suited to fully annealed Nitinol rather than cold worked [74]. However, another study has suggested that an annealing temperature of 450°C may not be sufficient to relieve all stress [92], and so it is therefore likely that a proportion of austenite in the lower temperature state exists.

6.3.2 Resonant frequency characterisation

A cymbal transducer was assembled using the end-caps which were annealed for two hours. The end-caps which were annealed for one hour were not of sufficient quality for use in transducer fabrication, since the applied mechanical abrasion removed too much material from the end-caps. The resonant frequencies of the annealed superelastic Nitinol cymbal transducer were first measured using electrical impedance analysis at approximately 19.7°C, the results of which are shown in Figure 6.12.

Only one resonant frequency is displayed in the frequency response, suggesting a high degree of symmetry in the fabricated transducer. There is an indication that two closely coupled resonant frequency responses exist, seen as a slight double-peak within the single response curve. However, when electrical impedance measurements were recorded at a higher temperature, two distinct resonant frequencies were exhibited in

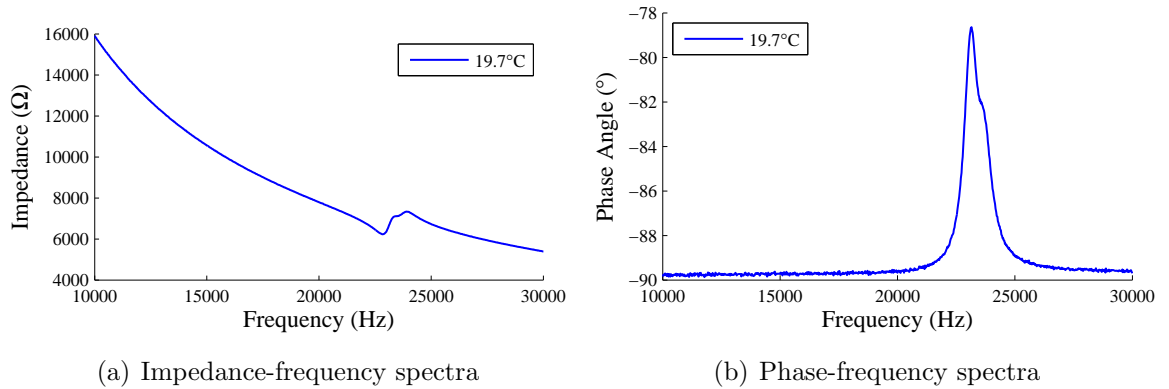


Figure 6.12: Initial resonant frequency characterisation of the annealed superelastic Nitinol cymbal transducer at 19.7°C showing the measured (a) impedance-frequency and (b) phase-frequency spectra

the frequency response. The transducer at 55.7°C was allowed to cool back to room temperature and then the impedance-frequency and phase-frequency spectra at both temperatures were re-measured. This time it was found that the transducer exhibited two resonant frequencies at both temperatures, as shown in Figure 6.13. It is possible that a small change in one of the epoxy bond layers as a result of heating contributed to asymmetry in the transducer, or the epoxy resin may have not fully cured when the data in Figure 6.12 was measured. Table 6.6 shows the resonant frequency change for each mode between the two temperatures.

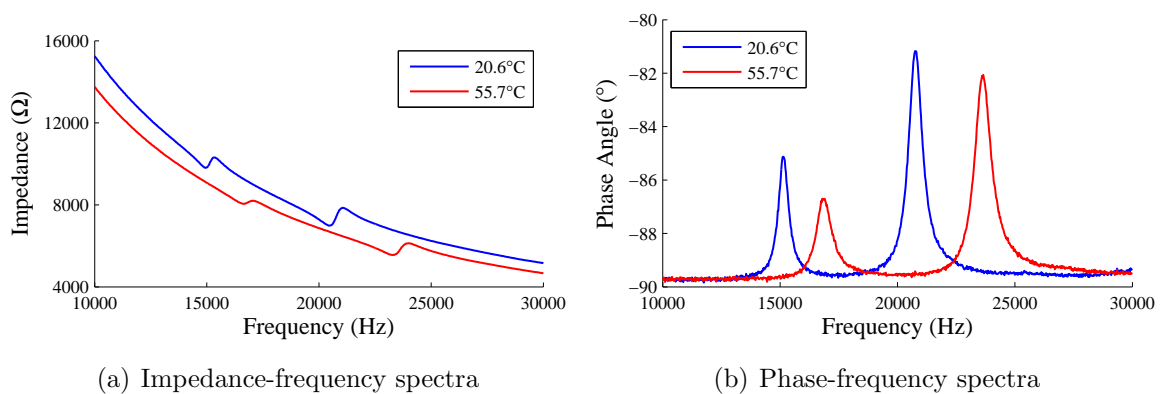


Figure 6.13: Final resonant frequency characterisation of the annealed superelastic Nitinol cymbal transducer showing the measured (a) impedance-frequency and (b) phase-frequency spectra

The measurements from the electrical impedance analysis confirm that the resonant frequencies of the annealed superelastic Nitinol transducer could be controlled at

	f_r at 20.6°C (Hz)	f_r at 55.7°C (Hz)	Difference (Hz)	Change (%)
Mode 1	14925	16600	+1675	+11.22
Mode 2	20475	23375	+2900	+14.16

Table 6.6: Resonant frequency shifts of the annealed superelastic Nitinol cymbal transducer

temperatures consistent with the DSC. This demonstrates that by annealing the superelastic Nitinol, the DSC analysis could be reliably used for transformation temperature estimation of each phase of the Nitinol.

6.3.3 Modal behaviour

There were problems when conducting the EMA of the annealed transducer, principally because of the low reflectivity of the annealed surfaces of the end-caps. It is possible to rectify the problem by applying a reflective agent to the surface of the material or by mechanical abrasion, but these approaches were avoided, as they would likely change the resonant frequencies of the transducer. The EMA results of the annealed superelastic Nitinol cymbal transducer measured at 21.5°C were therefore identified from the measurement of the axial response, and are shown in Figure 6.14.

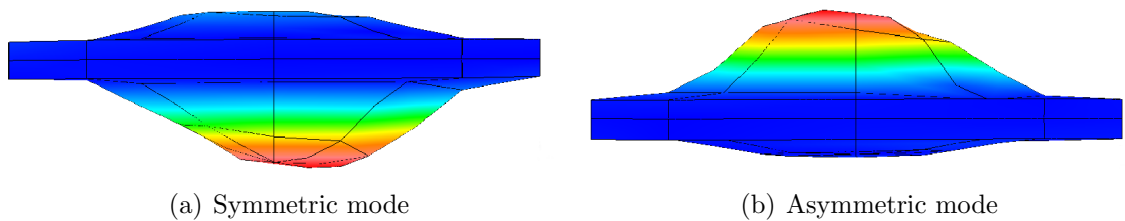


Figure 6.14: Modes of the annealed superelastic Nitinol cymbal transducer, showing (a) the symmetric mode at 15029Hz, and (b) the asymmetric mode at 20519Hz, measured at 21.5°C

6.3.4 Vibration resonance response characterisation

The displacement amplitude responses of each mode of the transducer for two temperatures are shown in Figures 6.15 and 6.16. It is noticeable that for both modes of the transducer with end-caps in the austenite phase, modulations in the displacement

response are exhibited, and are more pronounced than for both the asymmetric cymbal transducer.

The displacement amplitudes are higher for the transducer with end-caps in the stiff austenite phase compared to the softer R-phase. This seems unusual, but the consistency of this phenomenon with the other Nitinol transducers studied in this research suggests that a significant difference in damping capacity of Nitinol between the two phases. A high level of correlation between the transformation temperatures estimated from DSC analysis and the temperature required to induce a shift in resonant frequency estimated from the dynamic characterisation process has been achieved. The resonant frequencies measured using all the dynamic characterisation methods are shown in Figure 6.17.

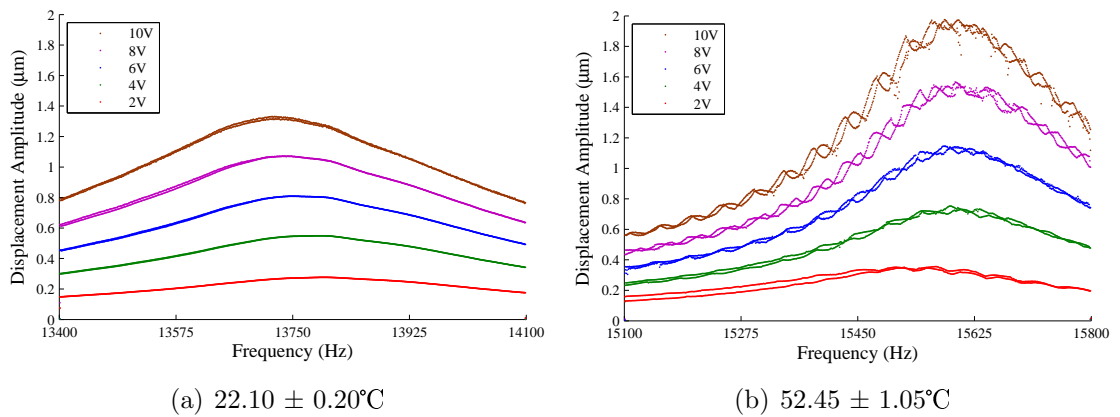


Figure 6.15: Plots showing the (a) R-phase and (b) austenite responses of the symmetric mode of the annealed superelastic Nitinol cymbal transducer

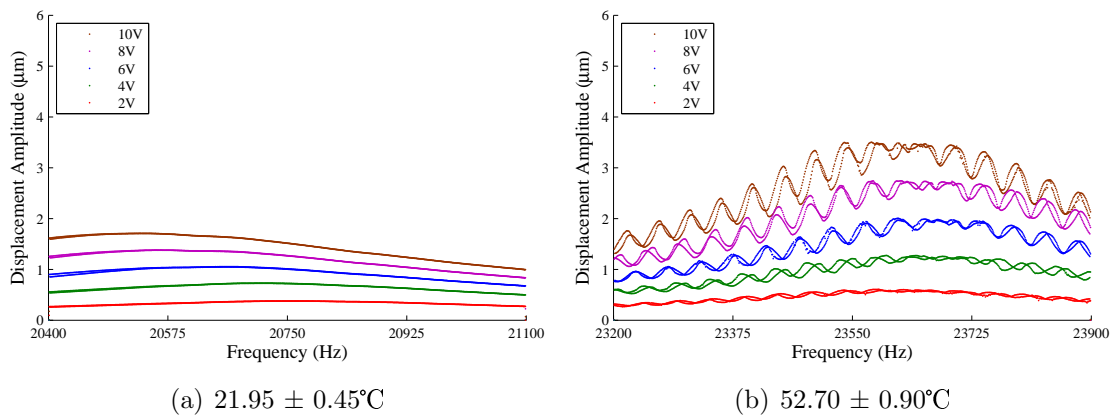


Figure 6.16: Plots showing the (a) R-phase and (b) austenite responses of the asymmetric mode of the annealed superelastic Nitinol cymbal transducer

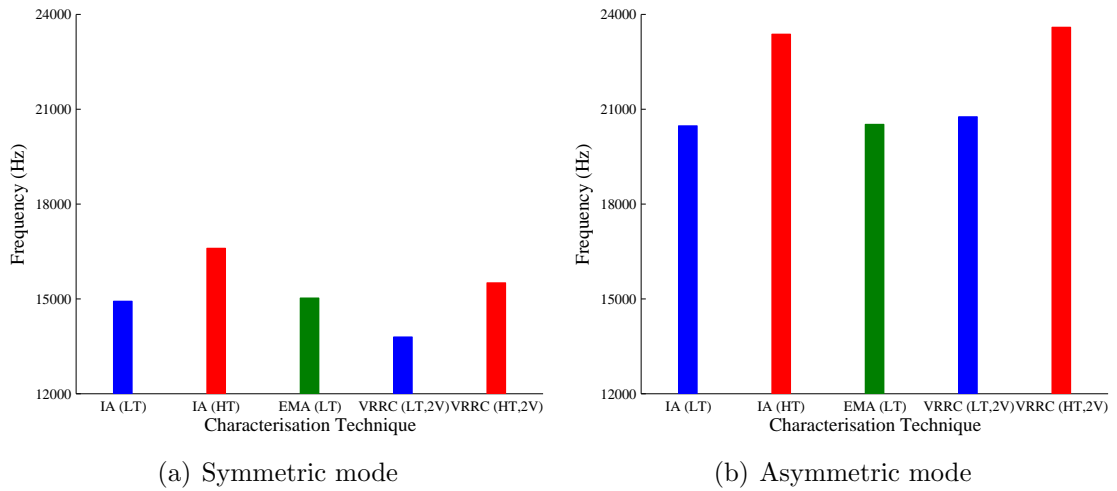


Figure 6.17: Resonant frequencies measured using the three dynamic characterisation techniques for the annealed superelastic Nitinol cymbal transducer

The effect of the annealing heat treatment on the transformation temperatures is still unclear. However, a shift of the transformation temperatures has been measured, and it is also probable that the heat treatment has relieved a proportion of the residual stress in the Nitinol end-caps. It has been postulated in the literature that residual stresses in Nitinol are a contributory factor to the inaccuracy of DSC analysis, and that the cutting of Nitinol induces localised martensitic transformations which affect the quality of DSC measurements [91]. This could be significant for this research, as materials which exist as austenite around the cutting temperature would experience localised transitions to stress-induced martensite at the regions of high deformation. Nitinol with A_S and A_F transformation temperatures far above room temperature are not likely to be affected by these localised transformations, since cutting would normally be performed at room temperature. This may be a reason why DSC is more reliable for shape memory Nitinol.

6.4 Evidence of the superelastic effect

There was no definitive evidence found from the dynamic characterisation results of the first superelastic Nitinol transducer that there were any contributions from superelasticity to the displacement amplitude response in either mode. This means that the stress in the end-caps was not sufficient to generate stress-induced martensite in the

end-caps in the austenite phase. It would be useful if the stress required to generate stress-induced martensite could be determined using mechanical tensile testing, but the difficulties were described in detail in Chapter 4. However, an indication of the stress levels in the transducer was found in Chapter 5, where the stress for a 2V input voltage could reach approximately 3.36MPa. The unreliability of mechanical testing in this case is exacerbated by the significant difference in stress-strain response of a standard test specimen and a Nitinol end-cap.

The mode shape of the transducer with end-caps in the austenite phase which exhibits the highest displacement amplitude for a 2V input voltage is first determined. The austenite state must be generated in the end-caps, otherwise stress-induced martensite cannot be produced. The voltage to the transducer is increased in steps of 20V until either the transducer fails, or a significant change in the displacement amplitude response of the transducer occurs. It is assumed that the entirety of each end-cap would not transform to martensite upon the generation of stress-induced martensite, because a cymbal transducer under cyclic loading experiences non-uniform stress distribution. The regions of higher stress concentration are around both the end-cap base and the apex surface, as shown in Figure 5.18 from the FEA of Chapter 5. The affected end-cap is more likely to exhibit a local emergence of martensite, as has been reported in the literature [228,229]. To investigate the superelastic effect further, a cymbal transducer was fabricated using untreated superelastic Nitinol end-caps.

6.4.1 Resonant frequencies and modal behaviour

The resonant frequencies of the transducer in both the lower and higher temperature states, assumed to generate the R-phase and austenite phase respectively in the end-caps, are shown in Figure 6.18.

There are more than two peaks in the frequency response spectrum, where two of the peaks will be the symmetric and asymmetric modes of vibration of the transducer. At this stage, it is not possible to determine which peaks in the frequency response spectra are the symmetric and asymmetric modes of vibration. The mode shapes and modal frequencies can be found using EMA. Two points close to the conductive epoxy region on one of the end-caps were excluded from the analysis as the measurements recorded

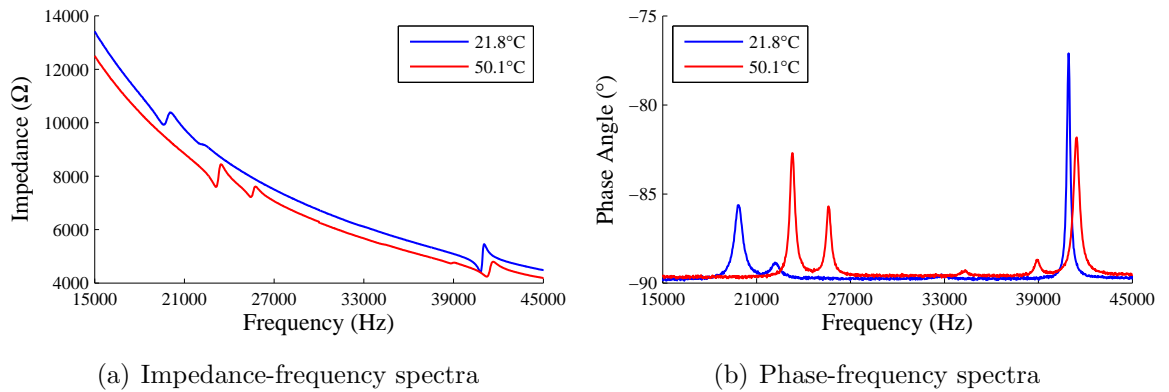


Figure 6.18: Resonant frequency characterisation of the third superelastic Nitinol cymbal transducer showing the measured (a) impedance-frequency and (b) phase-frequency spectra

at those points were noisy, but in spite of this, a complete 3-D EMA is presented. The mode shapes, measured at 20.4°C, are shown in Figure 6.19.

The presence of the multiple peaks in the impedance spectra of the transducer shows the importance of the EMA method in the characterisation of cymbal transducers. The symmetric and asymmetric modes of vibration were determined using EMA, but there is a large difference between the resonant frequencies at which the modes appear. The large difference in resonant frequency is not common for cymbal transducers, however the mode shapes found from EMA clearly demonstrate that the resonant frequencies shown in Table 6.7 correspond to the asymmetric and symmetric modes of vibration.

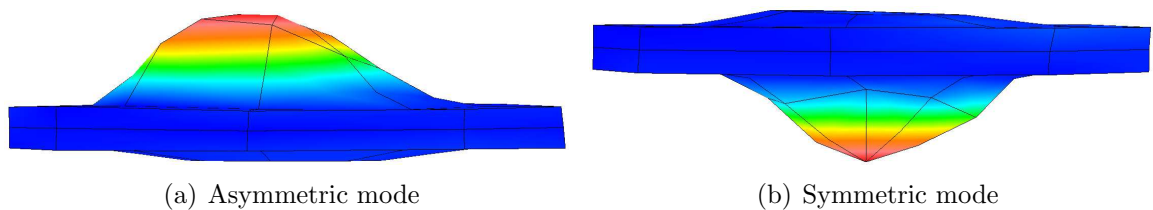


Figure 6.19: Modes of the third superelastic Nitinol cymbal transducer, showing (a) the asymmetric mode at 19466Hz, and (b) the symmetric mode at 40543Hz, measured at 20.4°C

It was stated earlier in the chapter that the geometrical dimensions of the superelastic end-caps were not all equal, upon inspection using the Mitutoyo digital callipers. A large difference in resonant frequency between modes could be attributed to the variation in the geometrical dimensions between the end-caps, and also unequal epoxy bond layer profiles in the transducer. Table 6.7 shows a summary of the difference

	f_r at 21.8°C (Hz)	f_r at 50.1°C (Hz)	Difference (Hz)	Change (%)
Asymmetric	19525	23050	+3525	+18.05
Symmetric	40750	41175	+425	+1.04

Table 6.7: Resonant frequency shifts of the third superelastic Nitinol cymbal transducer between the resonant frequency measured at the higher temperature compared to the lower temperature for the asymmetric and symmetric modes of vibration. The shift in resonant frequency measured for the asymmetric mode is much greater than that of the symmetric mode.

6.4.2 Vibration resonance response characterisation

The mode of vibration which exhibited the highest displacement amplitude for a 2V voltage was first determined, before higher voltages were applied to the transducer. The result of this experiment is shown in Figure 6.20.

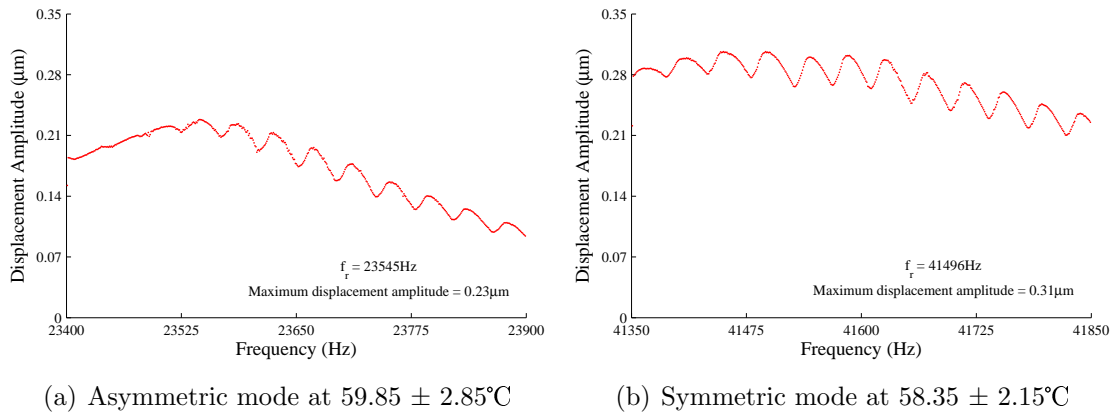


Figure 6.20: Measurement of the maximum displacement amplitude of the third superelastic Nitinol cymbal transducer in the austenite phase for 2V input voltage

For the experiment, the transducer was excited in the symmetric mode, which had the higher displacement amplitude for a 2V input voltage. The displacement amplitude response was measured around resonance for increasing voltages in 20V increments, starting from 20V. The transducer was heated to generate the austenite phase microstructure in the Nitinol end-caps, and only an upwards frequency sweep was used. Figure 6.21 shows the result of this experiment.

The results show that the transducer exhibits modulations in the displacement

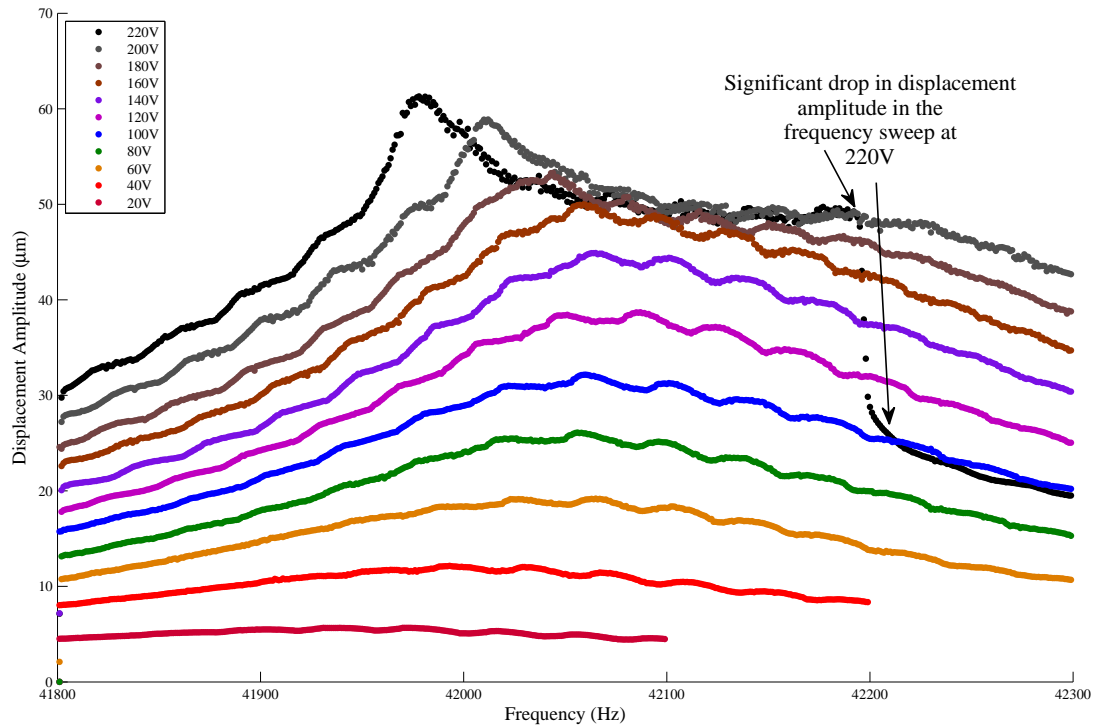


Figure 6.21: Vibration response of the third superelastic Nitinol cymbal transducer at increasing voltage, measured in the austenite state at $57.90 \pm 4.10^\circ\text{C}$

amplitude response for each voltage level, similar to the behaviour exhibited by other transducers studied in this research, with the exception of the shape memory Nitinol transducers. The resonant frequency increases with voltage up to 140V, characteristic of a hardening nonlinearity. Above 140V, the resonant frequency decreases with voltage. Although it is unclear why the response hardens up to 140V and then softens, it could be that the increase in stress on the epoxy bond layers is causing them to vibrate differently. During the frequency sweep with a 220V input voltage, a significant drop in displacement amplitude occurred, which is a result of failure of one of the epoxy bond layers in the transducer.

The origin of the modulations in the displacement amplitude response remain unclear. However, for each transducer in which the modulation occurs, there is no evidence of modulation in the displacement amplitude response when the transducer is operated at the lower of the two test temperatures. At the higher temperature it is likely that the epoxy resin has softened such that it behaves differently in response to ultrasonic vibration.

There is no strong evidence from the results in Figure 6.21 to suggest that stress-induced martensite has contributed to the displacement amplitude response between 20V and 220V. Localised transformations to martensite in the Nitinol may produce significant drops in resonant frequency as the modulus of the material softens. No significant drop in resonant frequency has been measured in this experiment. The significant reduction in displacement amplitude during the frequency sweep at 220V can be more attributed to a failure of one or both of the epoxy bond layers than an indicator of the emergence of localised transformation to martensite in the Nitinol end-cap. In order to properly assess any localised transformation to martensite, a technique such as XRD would be useful to identify the crystallography of the Nitinol microstructure, and DIC would be beneficial to study the generation of the localised phase transformations in the Nitinol end-cap.

6.5 Chapter conclusions

Experimental evidence has been produced which confirms the ineffectiveness of DSC for the accurate estimation of transformation temperatures of superelastic Nitinol. In particular, it was found that the A_F transformation temperature of untreated superelastic Nitinol estimated from DSC did not correlate well with the temperature required to increase the resonant frequencies of the superelastic Nitinol transducer in the electrical impedance analysis and VRRC dynamic characterisation procedures. The resonant frequencies of the transducer increased as the temperature was raised until approximately 40°C, however the estimation of the A_F transformation temperature from DSC was approximately 25°C. The discrepancy between the DSC estimation of the A_F transformation temperature for the superelastic Nitinol and the temperature required to increase the resonant frequencies of the superelastic Nitinol cymbal transducer has been attributed to the unsuitability of DSC analysis for Nitinol which possesses residual stresses, for example from cold working.

It was found that by annealing the superelastic Nitinol at 450°C for durations of one and two hours followed by immediate water quenching, the DSC estimation of the A_F transformation temperature of the annealed superelastic Nitinol correlates well with

the temperature required to raise the resonant frequency of a transducer fabricated using annealed superelastic Nitinol end-caps in the dynamic characterisation process. If untreated superelastic Nitinol is used in the design and fabrication of a tuneable cymbal transducer, then DSC would not be a reliable method for estimating the transformation temperatures. Examples of more suitable approaches for estimating the transformation temperatures of superelastic Nitinol are by employing a temperature-controlled resonant frequency experiment or an active A_F test.

In terms of the superelasticity of Nitinol above the A_F transformation temperature, there was no conclusive evidence that stress-induced martensite was generated in any of the experiments, and it is likely that the stress levels in the end-caps were not sufficient to cause this effect. This chapter has discussed the implications on the design and characterisation of transducers which incorporate superelastic Nitinol. For Nitinol to exist as austenite around room temperature, with an A_F transformation temperature of around 20°C, the A_S transformation temperature could be as low as 0°C, meaning that the martensite phase would exist at sub-zero temperatures. However, for tuneable frequency applications at temperatures below room temperature, superelastic Nitinol would be a viable choice of end-cap material.

Chapter 7

A tuneable prototype device

It has been demonstrated in Chapters 5 and 6 how Nitinol can be used in the design and fabrication of tuneable cymbal transducers, and there is strong evidence that the resonant frequencies can be tuned in response to modest changes in temperature, although it appears that the epoxy bond layers restrict the mechanical performance of this transducer configuration. In this chapter, a shape memory Nitinol cymbal transducer is modified to incorporate added masses in the form of steel cylinders attached to the end-caps. These cylinders are included to represent the addition of an end-effector to the transducer, such as a cutting tool. The cylinders are affixed to the apex of each transducer end-cap to produce a basic configuration of a tuneable prototype actuator. The objective is to investigate how the mass loading affects the tuneability of the resonant frequencies.

The effect of mass addition to a cymbal transducer end-cap has been reported in the literature [130], however it is unknown how a shape memory Nitinol transducer is affected. It is expected that mass added to the end-cap will affect the transformation of the shape memory Nitinol between R-phase and austenite, since the transformation temperatures are stress dependent. The increased load will generate higher stresses in the Nitinol end-caps, particularly around the edge of the base of the end-cap cavity, as shown in Figure 5.18. For higher stress, a further increase in temperature may be required to generate the required phase transformation in the shape memory Nitinol from R-phase to austenite, based on the relationship shown in Figure 1.7.

To investigate these effects of added mass, two tuneable prototype actuator devices

were fabricated. Each prototype device is based on a cymbal transducer with shape memory Nitinol end-caps. A silver steel cylinder was attached to the apex surface of each end-cap with a cyanoacrylate adhesive, after which the devices were characterised using experimental techniques comprising electrical impedance analysis, EMA and VRRC.

7.1 Characterisation of the transducer

A shape memory Nitinol cymbal transducer was fabricated and characterised using electrical impedance measurements and EMA. VRRC was not used in the characterisation of the transducer alone so that stresses which cause damage in the epoxy bond layers of the transducer could be avoided. Only the resonant frequencies and mode shapes of the transducer were of interest at this stage, to provide a baseline characterisation from which added mass effects could be evaluated.

7.1.1 Resonant frequency characterisation

The resonant frequencies of the shape memory Nitinol transducer were measured using impedance analysis, the results of which are shown in Figure 7.1.

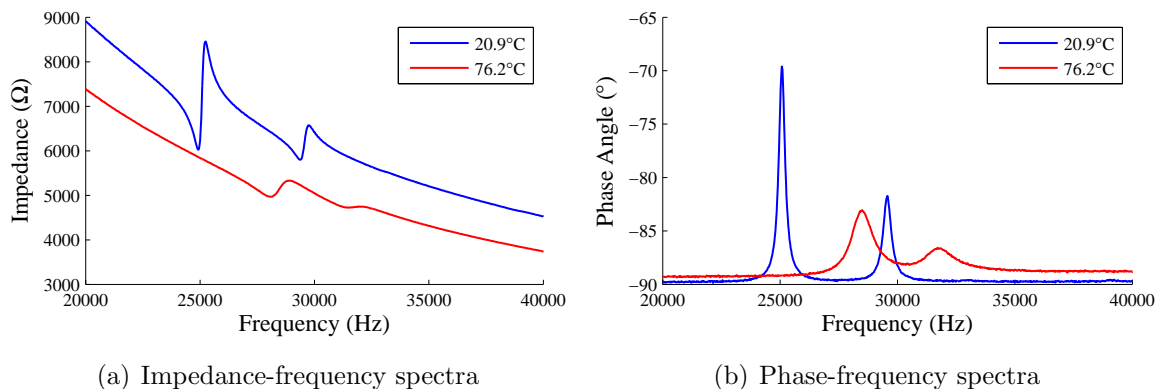


Figure 7.1: Resonant frequency characterisation of the shape memory Nitinol cymbal transducer showing the measured (a) impedance-frequency and (b) phase-frequency spectra

The double-peak in the frequency response spectrum signifies the existence of a symmetric and asymmetric mode of vibration for the transducer. The resonant

frequencies of the transducer for two different temperatures are summarised in Table 7.1, in addition to the frequency shifts in response to the temperature change. The lower temperature causes the formation of an R-phase microstructure in the Nitinol end-caps, while the austenite phase is generated at the higher temperature, based on the DSC estimations of the shape memory Nitinol shown in Chapter 5. The data in Table 7.1 shows the increase in resonant frequency for both the symmetric and asymmetric modes of vibration between the two temperatures.

	f_r at 20.9°C (Hz)	f_r at 76.2°C (Hz)	Difference (Hz)	Change (%)
Mode 1	24850	28025	+3175	+12.78
Mode 2	29375	31275	+1900	+6.47

Table 7.1: Resonant frequency shifts of the shape memory Nitinol cymbal transducer

7.1.2 Modal behaviour

The EMA was conducted with the shape memory Nitinol end-caps in the lower temperature R-phase state. The transducer was supported by the electrode wires in the experiment so that the vibration response of the entire end-cap surfaces could be measured with the 3-D LDV. The results of the EMA at 20.2°C are shown in Figure 7.2.

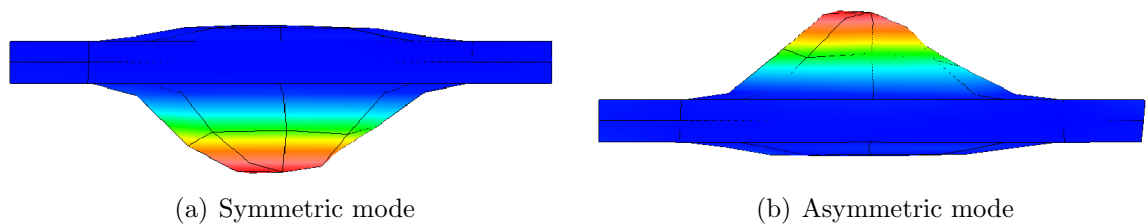


Figure 7.2: Modes of the shape memory Nitinol cymbal transducer, showing (a) the symmetric mode at 24662Hz, and (b) the asymmetric mode at 29421Hz, measured at 20.2°C

The EMA results shown in Figure 7.2 are 3-D since the noise levels for each measurement point in all three coordinates during the EMA were sufficiently low. The results show that the symmetric mode is mode 1 identified by impedance analysis and mode 2 is the higher-frequency asymmetric mode.

7.2 Characterisation of the prototype device

Resonant frequency is dependent on mass, and so a steel cylinder affixed to the apex of each end-cap will cause a reduction in the resonant frequencies. The dimensions of the larger steel cylinders used for the first prototype device are shown in Table 7.2. The geometrical dimensions were measured with the Mitutoyo digital callipers, and the mass of each cylinder was measured using a standard scale (EPS-302, County Scales Ltd). There were small differences in mass and geometrical dimensions of the cylinders which were available.

Dimension	Cyl_{L1}	Cyl_{L2}
Diameter, ϕ , (mm)	4.54	4.46
Length, l (mm)	5.91	5.79
Mass, m (g)	0.73	0.69

Table 7.2: Dimensions of the larger steel cylinders

A cylinder was attached to each end-cap apex surface with a small amount of cyanoacrylate adhesive (Loctite). The mating of the cylinders to the apex of the end-caps was as precise and even as possible, achieved by holding each cylinder in place during adhesive curing, so as not to induce further asymmetry to the device, although this was very difficult to control. Figure 7.3 shows the assembled prototype device with the larger steel cylinders affixed to the end-caps.



Figure 7.3: The prototype device with larger cylinders

The resonant frequencies of the prototype device were measured using electrical impedance analysis for two different temperatures. The measured impedance-frequency and phase-frequency spectra are shown in Figure 7.4.

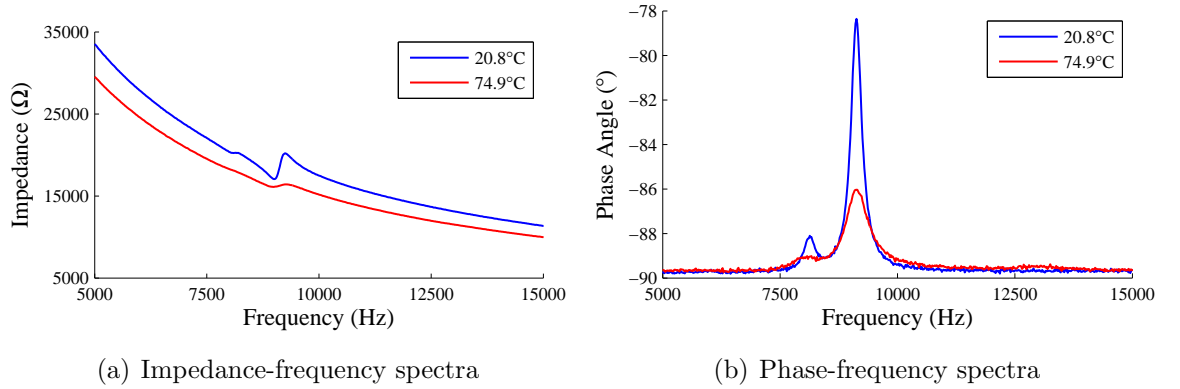


Figure 7.4: Resonant frequency characterisation of the larger shape memory Nitinol prototype device showing the measured (a) impedance-frequency and (b) phase-frequency spectra

The resonant frequencies of the prototype device are significantly lower than those of the transducer, due to the added mass of the cylinders. There is no clear change in the resonant frequencies of the prototype device at the lower and higher temperatures. The added mass of each cylinder increases the total stress in the Nitinol end-caps when in operation, and this affects the phase transformation of the shape memory Nitinol at the temperatures estimated by DSC analysis, since the transformation temperatures are dependent on stress. It is possible that by decreasing the mass of the cylinders, the phase transformation of the shape memory Nitinol will be able to be activated by the temperature change, even though the transformation temperatures will be different to those measured by DSC. Smaller steel cylinders were therefore used to fabricate a smaller prototype device, the dimensions of which are shown in Table 7.3.

Dimension	Cyl_{S1}	Cyl_{S2}
ϕ (mm)	4.48	4.48
l (mm)	2.04	1.79
m (g)	0.25	0.23

Table 7.3: Dimensions of the smaller steel cylinders

Cyl_{S1} was affixed using the cyanoacrylate adhesive to the end-cap which exhibited the higher amplitude from the EMA result of the symmetric mode at 24662Hz, and Cyl_{S2} was connected to the end-cap which displayed the higher amplitude in the asymmetric mode at 29421Hz, based on the EMA results of the transducer. The

smaller prototype device is shown in Figure 7.5.

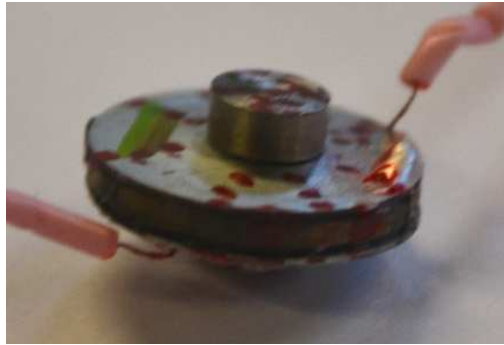


Figure 7.5: The prototype device with smaller cylinders

7.2.1 Resonant frequency characterisation

The resonant frequencies of the prototype device with smaller cylinders and the associated shifts in frequency for two different temperatures were measured using electrical impedance analysis. The measured impedance-frequency and phase-frequency spectra are shown in Figure 7.6.

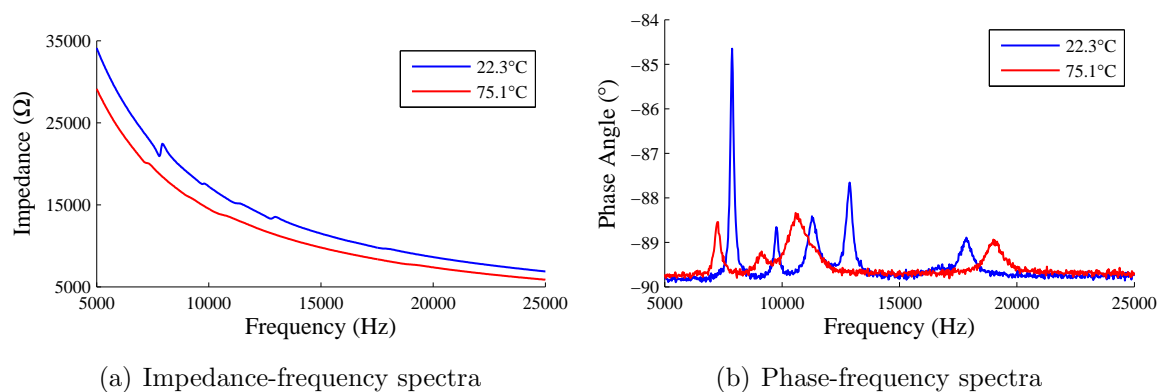


Figure 7.6: Resonant frequency characterisation of the smaller shape memory Nitinol prototype device showing the measured (a) impedance-frequency spectra and (b) phase-frequency spectra

The frequencies of the prototype device with smaller cylinders are higher than those of the prototype with larger cylinders. The results show that there is a change in the frequency of the peaks which are exhibited in the frequency response spectrum between the two temperatures. This suggests that the mass of the steel cylinders affixed to the shape memory Nitinol transducer is low enough such that the phase transformation of

the Nitinol for a change in temperature has occurred. There are more frequency peaks exhibited in the frequency response spectrum whose associated modal behaviour are unknown. Although there is evidence of resonant frequency change, it is not possible at this stage to determine the influence of the Nitinol phase transformation.

7.2.2 Modal behaviour

EMA was conducted to determine the symmetric and asymmetric modes of vibration of the prototype device. The EMA measurement grid for the cymbal transducer was modified to incorporate the geometry of the steel cylinder on the apex of each transducer end-cap. The adapted measurement grid is shown in Figure 7.7, and the EMA was conducted with the Nitinol end-caps in the lower temperature R-phase state. The symmetric and asymmetric modes found from EMA at 20.1°C are shown in Figure 7.8, and the mode shapes which exhibited bending in the transducer are shown in Figure 7.9.

Unlike for the EMA of the transducer without steel cylinders attached, the higher noise levels encountered during the EMA measurements meant that the results presented in Figures 7.8 and 7.9 are taken from the axial measurements only, perpendicular to the apex of the prototype device. The mode shapes which were found that exhibited bending in the prototype device shown in Figure 7.9 are labelled as either symmetric or asymmetric, to differentiate the mode shapes with respect to the phase of the vibrating end-caps of the device.

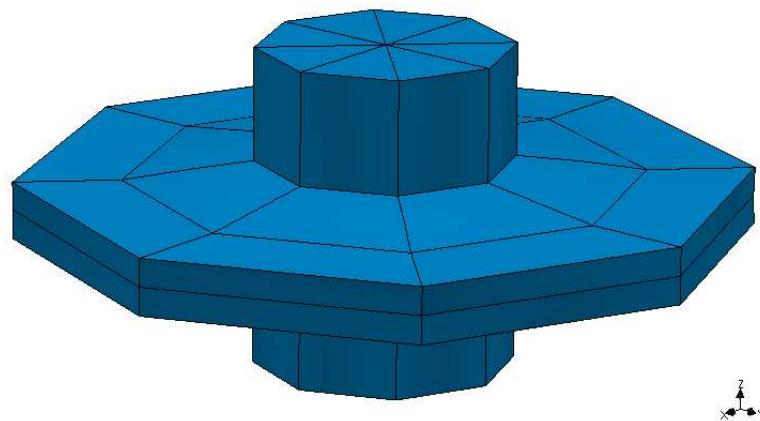


Figure 7.7: The measurement grid for the prototype device with smaller cylinders

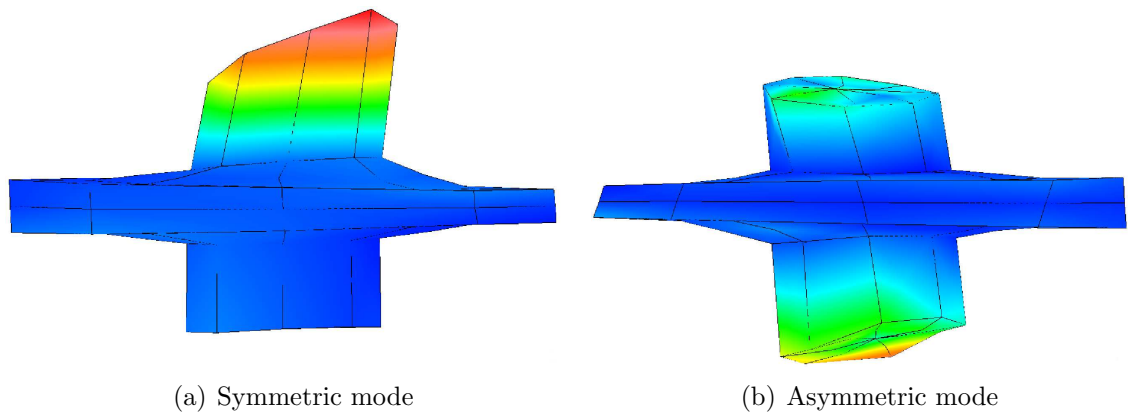


Figure 7.8: Modes of the smaller shape memory Nitinol prototype device, showing (a) the symmetric mode at 7922Hz, and (b) the asymmetric mode at 11099Hz, measured at 20.1°C

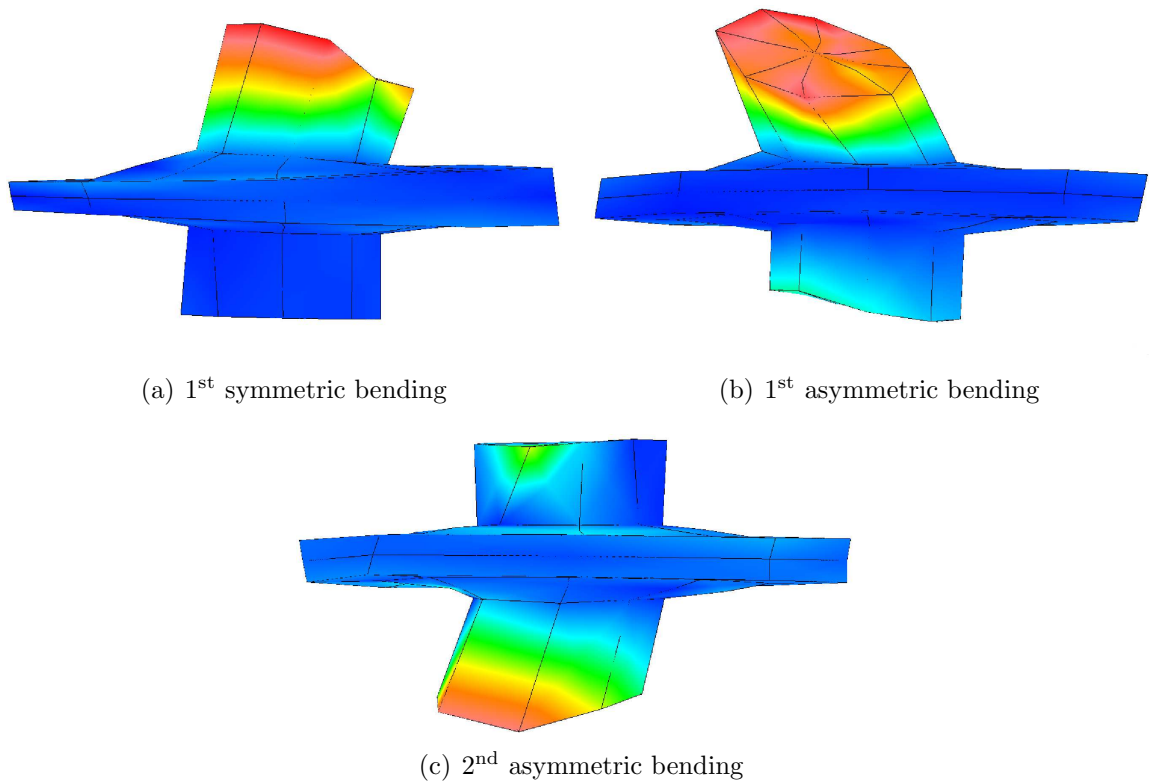


Figure 7.9: Bending modes of the smaller shape memory Nitinol prototype device, showing (a) the first symmetric bending mode at 9732Hz, (b) the first asymmetric bending mode at 12782Hz, and (c) the second asymmetric bending mode at 17642Hz, measured at 20.1°C

Not enough is known about the mechanical coupling in the device or the characteristics of the bond between the steel cylinders and the Nitinol end-caps. Also, it is not fully understood how the stress in the Nitinol is affecting the vibration behaviour of the device. The complications involved in accurately modelling a prototype device with cylinder attachments meant that a reliable FEM could not be produced. However, FEA was used to demonstrate that whilst the addition of mass does reduce resonant frequency, the relationship between cylinder length (and hence mass) and frequency is not linear. This is shown in Figure 7.10, which shows the relationship between device resonant frequency and cylinder length as calculated using FEA, for a transducer FEM similar to that shown in Chapter 5, but with thinner epoxy resin bond layers. The geometrical dimensions of the end-caps were the same as for the FEM of Chapter 5. The FEA was conducted for different lengths of silver steel cylinder attached. The resonant frequency for each data point represents that of the symmetric mode of vibration.

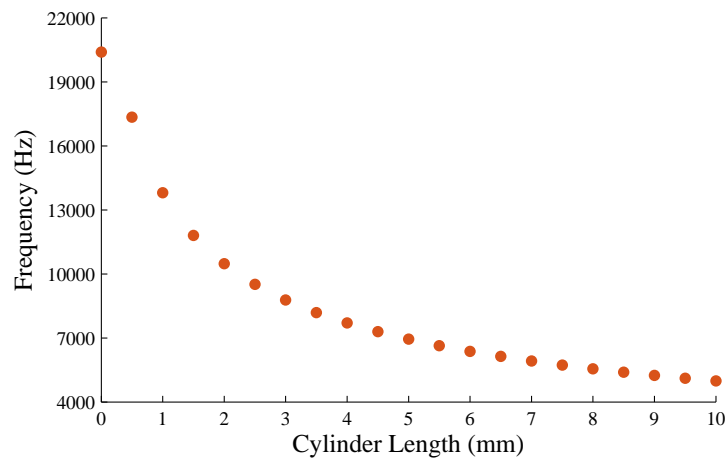


Figure 7.10: The change in resonant frequency of a cymbal transducer for the symmetric mode of vibration for different lengths of silver steel cylinder, calculated from FEA

It is clear from the simulation results that in theory, the length of the attached tool does not significantly affect the resonant frequencies of the device, after a threshold attachment length is passed. The practical implication of this is that it may be possible to develop a tuneable device which can drive a number of attachments of different mass, without causing a significant reduction of the resonant frequency.

7.2.3 Vibration resonance response characterisation

VRRC was performed on the prototype device for two different temperatures, where the R-phase microstructure was generated in the end-caps at the lower temperature, and the austenite phase was generated in the end-caps at the higher temperature. However, before VRRC was conducted, the resonant frequencies of the device were re-measured using electrical impedance analysis. This is because at the time, the frequency response of the device had been measured at different temperatures on multiple occasions. It was necessary to ensure the device remained operational. The results of this experiment are shown in Figure 7.11.

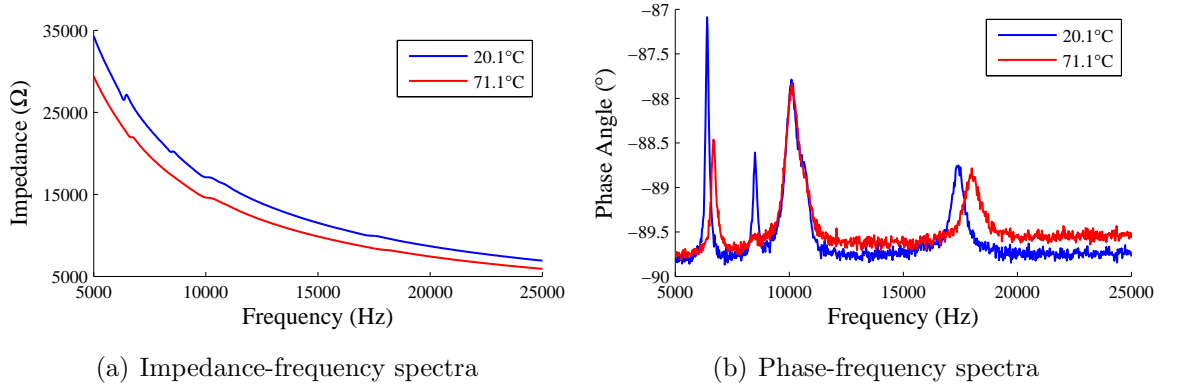


Figure 7.11: Repeated resonant frequency characterisation of the smaller shape memory Nitinol prototype device showing the measured (a) impedance-frequency spectra and (b) phase-frequency spectra

The resonant frequencies are generally lower than those found in the original impedance measurements for this device. This can be attributed to a softening or cracking of the epoxy bond layers as a result of extended periods of use in different vibration and temperature conditions. The resonant frequencies of both the symmetric and asymmetric modes of vibration for the prototype device at two different temperatures are summarised in Table 7.4.

	f_r at 20.1°C (Hz)	f_r at 71.1°C (Hz)	Difference (Hz)	Change (%)
Symmetric mode	6350	6675	+325	+5.12
Asymmetric mode	9875	10000	+125	+1.27

Table 7.4: Resonant frequency shifts of the smaller prototype device

This data can be used to show how the resonant frequency shifts of the symmetric and asymmetric modes for the smaller prototype device compare to those of the transducer alone, as a result of the phase transformation of the shape memory Nitinol. Table 7.5 shows this comparison, where f_{HT} denotes the resonant frequency at the higher temperature, f_{LT} is the resonant frequency of the transducer at the lower temperature, and $\Delta\%$ is the percentage change between the resonant frequency of the transducer or device at the lower and higher temperatures.

Device	Symmetric, $f_{HT}-f_{LT}$ (Hz)	$\Delta\%$	Asymmetric, $f_{HT}-f_{LT}$ (Hz)	$\Delta\%$
Transducer	3175	12.78	1900	6.47
Prototype device	325	5.12	125	1.27

Table 7.5: Comparison of the shift of resonant frequency for each mode of the transducer and the smaller prototype device, where LT signifies the resonant frequency in the low temperature state, and HT represents the resonant frequency in the high temperature state

The results demonstrate that the frequency shift is significantly lower for the prototype device compared to the transducer. This suggests that the increased mass from the steel cylinders affects the phase transformation of the shape memory Nitinol. It is probable that a higher temperature is required to generate the phase transformation due to the increased stress in the Nitinol end-caps. Although a significant resonant frequency change has not been exhibited by the prototype device, the results demonstrate that the tuneability of resonant frequency for a prototype device fabricated with shape memory Nitinol is possible. After the electrical impedance analysis was repeated, the VRRC was conducted. The displacement amplitude responses were measured perpendicular to and at the centre of the apex surface of each steel cylinder. The displacement amplitude response data obtained from driving the prototype device around the resonant frequency of the symmetric mode at two different temperatures is shown in Figure 7.12.

The maximum displacement amplitude of the symmetric mode for the Nitinol end-caps in the R-phase state was found to be around 6500Hz, and the results are shown in Figure 7.12(a). The displacement amplitude response of the prototype device at the lower temperature for the symmetric mode is shown in Figure 7.12(b). This data

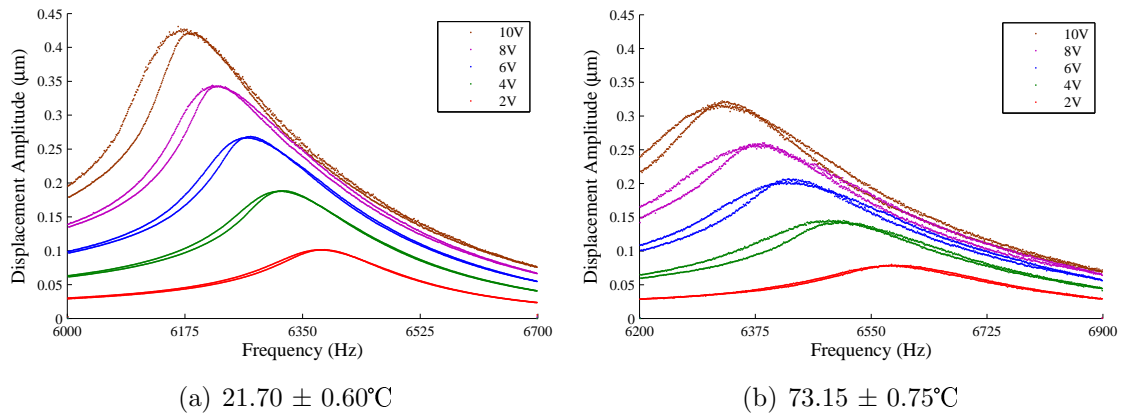


Figure 7.12: Plots showing the symmetric mode responses at (a) lower temperature and (b) higher temperature for the smaller prototype device

shows that, consistent with the results from the electrical impedance measurements, there was an increase in resonant frequency of this mode as a result of the transition of the Nitinol end-caps from R-phase to austenite. The displacement amplitude response of the prototype device for the asymmetric mode is shown in Figure 7.13.

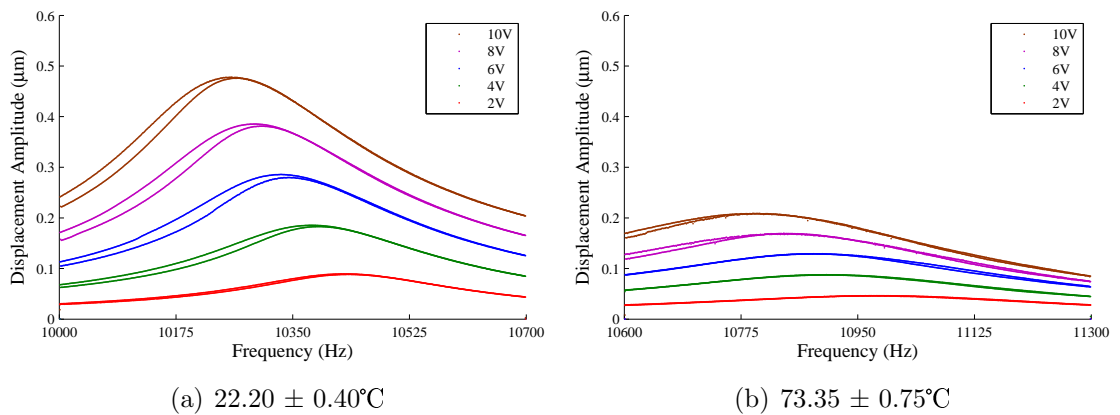


Figure 7.13: Plots showing the asymmetric mode responses at (a) lower temperature and (b) higher temperature for the smaller prototype device

The results shown in Figure 7.13(a) indicate that again, consistency has been achieved between the resonant frequencies identified from the displacement amplitude response of the asymmetric mode of the prototype device with end-caps in the R-phase state, with those from the electrical impedance analysis, the results of which are shown in Figure 7.11. The displacement amplitude response of the prototype device with end-caps in the austenite phase is shown in Figure 7.13(b), demonstrating that the resonant frequency of the mode has increased in response to the temperature change.

There was an approximate frequency increase of 600Hz from the lower to the higher temperature for the asymmetric mode, indicating the transition from the R-phase state to the austenite phase.

For this prototype device, softening nonlinear behaviour is exhibited in the displacement amplitude response of both modes of vibration shown in Figures 7.12 and 7.13 at both temperatures. There is also further asymmetry in the prototype, because the steel cylinders and their positioning are not exactly equal. As a consequence, the displacement amplitude response depends on the measurement location on the end of the cylinder. The displacement amplitude response of the asymmetric mode of the device in the austenite phase has been used to demonstrate this. Measurement locations were specified on one of the steel cylinders and designated as Edge 1 and Edge 2, as shown in Figure 7.14. Edge 1 and Edge 2 are measurement locations which are diametrically opposite one another.

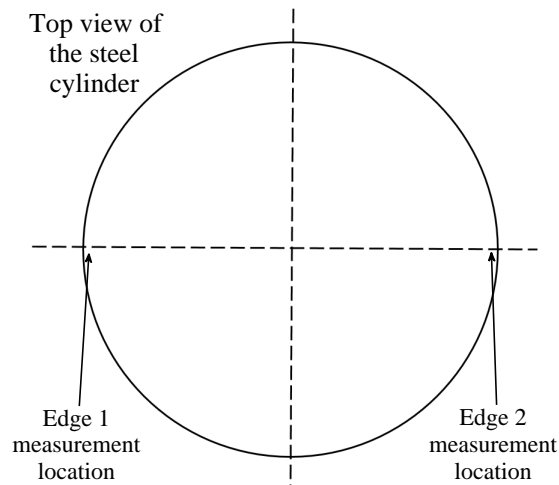


Figure 7.14: Measurement points on the apex surface of the steel cylinder

The results shown in Figure 7.15 are the displacement amplitudes measured at the different locations. The experiment was conducted with the Nitinol end-caps of the device in the austenite phase, and the device vibrating in the asymmetric mode of vibration.

Significant differences in displacement amplitude are measured depending on the measurement point on the steel cylinder. It is also noticeable that the displacement amplitude responses of the prototype device with end-caps in the austenite state

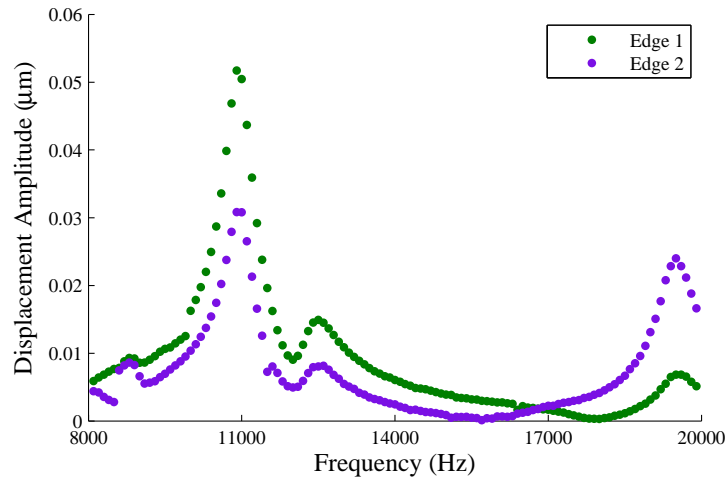


Figure 7.15: The displacement amplitude responses for each measurement location using experimental VRRC data, measured at 72.90°C

are lower than for the device with end-caps in the R-phase state. The effect of the steel cylinders on the displacement amplitude response of the device requires further investigation. Comparison of the resonant frequencies of the symmetric and asymmetric modes of vibration for the prototype device measured using the different dynamic characterisation processes is shown in Figure 7.16.

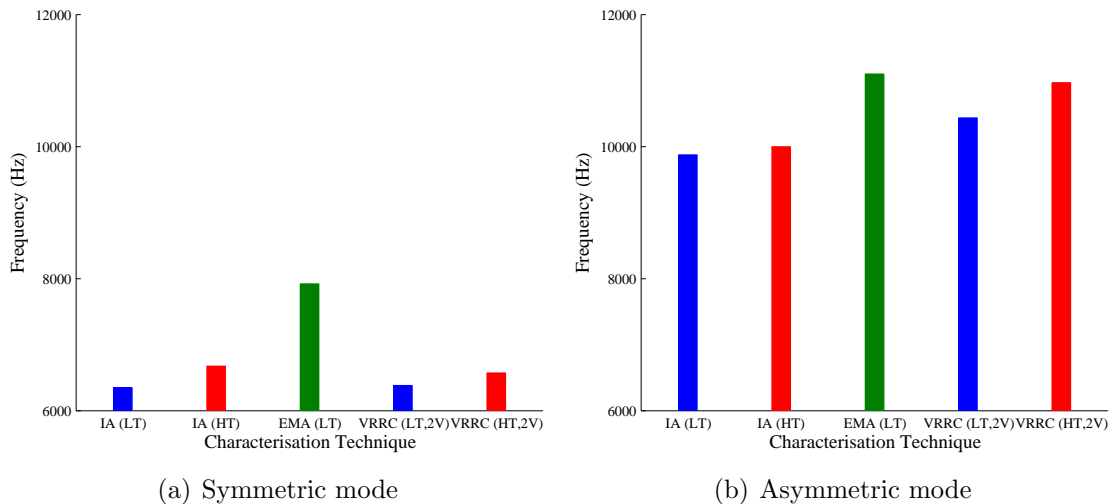


Figure 7.16: Comparison of resonant frequencies measured using the three dynamic characterisation techniques for the smaller shape memory Nitinol prototype device

The resonant frequencies from the EMA do not correlate closely with those found from VRRC and electrical impedance analysis. This can be explained by the fact that the EMA was conducted before the device was subjected to the vibration levels of

VRRC, which are higher than those of electrical impedance analysis and EMA. The resonant frequencies of the prototype device noticeably decreased after only a small number of VRRC experiments, suggesting that there is a severe limitation on fatigue life imposed by the epoxy bond layers, making the behaviour of these devices very difficult to predict. Devices which do not contain epoxy bond layers as the method of mechanical coupling should be considered in future.

7.3 Chapter conclusions

This chapter has demonstrated the successful development of an initial tuneable prototype actuator using shape memory Nitinol. The resonant frequencies of the prototype could be tuned by a change to the temperature of the device. However, it was found that when two steel cylinders of approximately 0.7g in mass were attached to the end-caps, no significant shift in resonant frequency could be measured. Although it may be possible that the deformation of each end-cap apex was limited by the presence of the cylinder, thus lowering the stress at the apex, the lack of a shift in resonant frequency was attributed to a restriction on the ability of the Nitinol end-caps to transform phase when the end-caps experience additional stress.

A device was then constructed using smaller length steel cylinders which were each approximately 0.25g in mass. The resonant frequencies of this prototype device could be tuned by changing the temperature of the device, but again the increased mass did limit the ability to tune the resonant frequency. A major limitation of the transducer configuration identified in this research relates to the mechanical coupling conferred by the epoxy bond layers. A clearer understanding of the mechanical limits of Nitinol in ultrasonic vibration in terms of its capacity to be tuned through a phase change with a tool attached would be beneficial for future device design.

Chapter 8

Conclusions

This research has reported on the design and characterisation of tuneable cymbal transducers, by incorporating Nitinol into the cymbal transducer as the end-cap material. It has been demonstrated that the resonant frequencies of the symmetric and asymmetric modes of a cymbal transducer fabricated with Nitinol end-caps can be tuned as a result of a temperature change. It has also been shown how there are critical design and analysis factors which must be considered if this research is to be developed in the future.

In 1997, research was conducted which reported on the development of a cymbal transducer exhibiting two different resonant frequencies, based on the selection of end-cap geometry and material [41]. The capacitance and admittance spectra, as a function of frequency, showed that dual resonance could be achieved [41]. The research presented in Chapter 3 has extended this by the characterisation of an asymmetric cymbal transducer at different temperatures. The transducer was fabricated using metal end-caps, one being steel and the other titanium. The transducer was characterised using EMA and VRRRC in addition to electrical impedance measurements. It was demonstrated how FEA could be used to predict the mode shapes, resonant frequencies and displacement amplitudes of an asymmetric cymbal transducer with accuracy. It was demonstrated how a dual frequency transducer could be designed by using end-caps fabricated from two different materials. To tune between the resonant frequencies for a practical application, such as driving an end-effector for cutting, a different side of the transducer would have to be used. The disadvantage of this is that for some applications, the removal of the transducer to switch the position of the end-effector would be inconvenient. An active tuning capability would therefore be more

desirable, and the incorporation of an SMA into the cymbal transducer configuration was subsequently investigated.

SMA's are materials which exhibit a phase change capability. Nitinol is one such SMA, whose elastic properties such as modulus can be tuned over a temperature range. For a cymbal transducer end-cap, a change in elastic modulus causes a change in resonant frequency. Therefore, Nitinol was used to fabricate end-caps to develop and characterise Nitinol cymbal transducers. Awareness of the effects of stress and temperature on the mechanical properties of Nitinol is important. Also, the influence of chemical composition, heat treatment and cold working on the transformation temperatures must also be considered. The elastic modulus is a very useful property for transducer design. Although the understanding of the mechanical behaviour of Nitinol has greatly improved in recent years, the measurement of the modulus in each phase has been shown in the literature to be problematic, affecting the ability to develop robust numerical models of Nitinol behaviour. In recent years, the research activity in the design and characterisation of a shape memory Nitinol cymbal transducer has been very limited. However, research was conducted in 2000 regarding the design and resonance analysis of a Nitinol cymbal transducer which exhibited shifts in resonant frequency depending on its temperature, and could repair itself if damaged via the SME [67]. The change in resonant frequency was measured using electrical impedance measurements over a fixed temperature range [67]. This research has extended this in two ways. The first is the adoption of DSC to estimate the transformation temperatures. This information was used to define the temperatures at which the Nitinol cymbal transducers were operated, in order to generate the desired microstructure phase in the end-caps. Secondly, in addition to electrical impedance measurements, EMA and VRRC were employed in the characterisation of each transducer for two different temperatures. The temperature in the vibration characterisation procedures was measured using a thermocouple. It was found that the temperature required to increase the resonant frequencies of each transducer closely correlated with the A_F transformation temperature estimated using DSC. This signified the change in phase of the Nitinol end-caps from a microstructure dominated by R-phase to a microstructure principally consisting of austenite. However, it is apparent that there remain limitations

with the current measurement setup. Nitinol is very sensitive to stress and temperature changes, and it was not possible to correlate the required dynamic characterisation temperature with the A_F transformation temperature estimated by DSC to a very high accuracy. It was also not possible to record the precise change in microstructure between the two temperatures.

The mechanical coupling conferred by the epoxy bond layers was found to be a major limitation of the cymbal transducer. It was not possible to accurately control the deposition of the epoxy resin in the assembly of each transducer, and it has been argued that the softening of the epoxy bond layers in the transducers as a result of an increase in temperature contributed to changes in displacement amplitude. Although the epoxy bond layers can also be affected by stress from transducer vibration, the mechanical behaviour of the epoxy bond layers at higher temperatures is still not fully understood. Modulations in the displacement amplitude responses of a number of the transducers studied in this research were found, occurring only for the VRRC at the higher of the two temperatures applied to each affected transducer. The source of the modulations remains unclear, but it is known that the storage and flexural moduli of certain epoxies can decrease at raised temperatures [185]. Therefore it is likely that the mechanical properties of the bond layers are being affected as the transducer, and hence epoxy resin, temperature is increased.

Prior to this research, the effects of superelasticity on the vibration response of an ultrasonic transducer had not received significant attention. End-caps were fabricated from superelastic Nitinol, where the transformation to austenite in the Nitinol was specified to occur between 20-25°C. It was found that DSC was unsuitable for the estimation of the transformation temperatures of superelastic Nitinol. It has been reported that the unsuitability of DSC for measuring the transformation temperatures of superelastic Nitinol is a consequence of the required cold working process for the fabrication of the material. Although the limitation of DSC for the analysis of superelastic Nitinol has previously been demonstrated in the literature, the supportive experimental evidence is not substantial. There was a poor correlation between the A_F transformation temperature estimated from DSC and the temperature at which the resonant frequencies of the superelastic Nitinol cymbal transducer

stopped increasing, measured using a thermocouple in the electrical impedance analysis procedure. It is likely that at approximately 20-25°C, the superelastic Nitinol was below the A_F transformation temperature, but above the A_S transformation temperature. The stiffness of the end-cap in this temperature range was physically inspected to be indicative of a stiff cubic austenite structure, based on its relatively high resistance to deformation. The microstructure of the Nitinol between the A_S and A_F transformation temperatures contains a proportion of both low and high temperature phase microstructures, which are R-phase and austenite respectively. As the superelastic Nitinol is heated, the modulus of each end-cap continues to increase until A_F is passed. This was reflected in the electrical impedance analysis, where the resonant frequencies of the superelastic Nitinol cymbal transducer increased until approximately 45°C, indicating that the A_F transformation temperature had been reached. This confirmed the inaccuracy of the DSC method for the superelastic Nitinol.

To investigate the limitation of the DSC method for estimating the transformation temperatures of superelastic Nitinol further, superelastic Nitinol end-caps were annealed to relieve stress in the end-caps from cold working incurred in the fabrication of the end-caps. The end-caps were softer at ambient conditions after annealing, based on physical inspection. A cymbal transducer was also constructed using annealed Nitinol end-caps. The electrical impedance measurements of the transducer were recorded between two different temperatures, where the temperature was monitored with a thermocouple. It was found that the resonant frequencies stopped increasing at a temperature consistent with the A_F transformation temperature estimated from DSC. Reports in the literature attribute the limitation of DSC for transformation temperature estimation of superelastic Nitinol to the presence of residual stresses or localised plasticity. It is therefore likely that residual stresses in the material have been either partially or fully relieved. It is uncertain why DSC was suitable for the shape memory Nitinol but not superelastic Nitinol, despite both being from configurations of similar shape. It is likely that the manufacture of shape memory Nitinol differs to that of superelastic Nitinol, which can be optimised for superelasticity via specific chemical composition, cold working and heat treatments. Cold working can cause residual stresses [77], and it has been reported that Nitinol fabricated for

superelastic performance are often subjected to high cold working [226], and that the heat treatments which are used to induce changes to superelastic behaviour can affect residual stresses [230]. Therefore if there are residual stresses present in superelastic Nitinol, then this could affect the accuracy of DSC. The contribution of residual stresses to the distortion of DSC results has been recognised [59], and it has been reported that XRD can be used to profile the residual stress level in Nitinol [230]. There appears to be a strong influence on the accuracy of transformation temperatures estimated using DSC from the fabrication of the Nitinol.

VRRC was also conducted on a superelastic Nitinol cymbal transducer to investigate if there were any contributions to the vibration response of the transducer from superelasticity of the Nitinol end-caps. There was no conclusive evidence of contributions from the superelasticity of the end-caps, suggesting that the stress in the end-caps was probably not sufficient to generate stress-induced martensite. VRRC was repeated on a separate superelastic Nitinol cymbal transducer at higher voltages. Although a failure in the mechanical coupling occurred, this could not be attributed to an emergence of superelasticity in the end-caps. Also, modulations in the displacement amplitude responses were found, and were not exclusive to the superelastic Nitinol cymbal transducers, as the phenomenon also occurred in the response of the asymmetric cymbal transducer.

The final step in the research concerned the characterisation of a tuneable prototype device. A driver transducer was assembled using shape memory Nitinol end-caps, to which two steel cylinders were attached. The resonant frequencies of the device were able to be changed between two temperatures over a modest temperature range. VRRC showed that the displacement amplitude of the device with austenitic end-caps was lower at resonance than that of the device with R-phase end-caps. The displacement amplitudes of a transducer whose end-caps exist as stiff austenite should in principle be lower than those of a less stiff phase such as R-phase, and the behaviour exhibited by the prototype was consistent with this premise. However, the damping capacity of Nitinol in either the martensite or R-phase states is higher than austenitic Nitinol, and so the energy required to produce the same displacement amplitude will be greater. A number of the VRRC results presented in Chapters 5 and 6 exhibited lower

displacement amplitudes for transducers with R-phase Nitinol end-caps compared to those with austenitic Nitinol end-caps. The difference in damping between the two Nitinol phases would account for this observation. It was also found that the resonant frequency shift was not exhibited by a prototype device with larger steel cylinders affixed to the driver transducer. This could be attributed to the stress dependency of Nitinol phase transformations, but further research is required.

This research has demonstrated that there is significant potential for Nitinol to be successfully incorporated into ultrasonic devices as a means of resonant frequency control. There is scope for wider investigation, especially in relation to the difficulties of material property characterisation, and the behaviour of the material in ultrasonic vibration. These are just two of the challenges which must be addressed in the future design and fabrication of tuneable ultrasonic devices.

Chapter 9

Future research and development

Unfortunately, the research and development of SMAs remains relatively esoteric [226], and this has a significant impact on the number of applications in which Nitinol is utilised. For example, it is not known how the fatigue life of Nitinol is affected at sustained ultrasonic vibration. Another significant reason restricting the incorporation of SMAs such as Nitinol into a wider range of applications is the sensitivity of the transformation temperatures to thermomechanical processing [226]. These processes include cold working or heat treatments such as ageing. Traditionally, Nitinol has only been available in very simple configurations such as wire, ribbon or plate formations due to its poor workability [226], and the fabrication of more complex geometrical configurations often incur great expense. It is evident that there remains a high interest in tuneable and multiple frequency technology, and developing this area of scientific research is of great importance. Whilst progress has been made in the development of tuneable cymbal transducers, there are avenues of further research which have been identified:

1. A greater understanding of the characteristics and measurement of the mechanical properties of Nitinol, such as the stress and temperature dependent elastic modulus, for the transducer design process
2. Fabrication of SMAs into more complex configurations for a range of transducer designs
3. Further development of numerical models, the simulations of which can be used to validate and verify experimental data

There are experimental techniques which could be adopted to investigate the mechanical behaviour of Nitinol, for example in a cymbal-shape. XRD measurements could be conducted over complete experimental thermal and mechanical loading cycles to show the crystallography of the Nitinol phase transformations. It would also be possible to determine how the phase of Nitinol transforms in a defined period of time for a power ultrasonic application. DIC could be adopted for this purpose. DIC has recently been successfully implemented for analysing both the superelastic and SME responses of Nitinol wires [231]. It is still not understood how local phase transformations would propagate in Nitinol at ultrasonic frequencies. Further investigation would also be useful into the mechanical behaviour of Nitinol in the R-phase. It has already been demonstrated that a functional actuator can be developed by utilising the phase transformation between austenite and the R-phase, and so knowledge of the R-phase properties and how they can be measured are of great importance for tuneable Nitinol transducer design.

The integration of SMAs into different ultrasonic transducers would be advantageous to help promote the expansion of the number of applications in which SMAs are used. For example, the vibration behaviour of a tuneable Langevin-type transducer with a Nitinol horn would be interesting to investigate, where the longitudinal mode of the transducer could be tuned by generating austenite and martensite phases of Nitinol. Flextensional transducer configurations which could be further developed are those proposed by Lin [23] and Bejarano et al. [24, 25], and it would be desirable to utilise transducers which do not require epoxy bond layers. This research has demonstrated the limitations of the epoxy bond layers both in the fabrication of a cymbal transducer and in a transducer under ultrasonic vibration. It would be desirable to eliminate the need for the epoxy bond layer as the mechanical coupling mechanism.

There are various SMAs which can be exploited for different applications, and experimentation with other types of SMA would be beneficial. In medical devices such as biomedical stents, Nitinol is preferred because of its excellent strength and fatigue resistance, as well as biocompatibility. However, some SMAs are inexpensive compared to nickel-titanium alloys, such as those which are copper-based. Copper alloys are generally used at higher temperatures [63]. As an example of a recent development,

Song et al. [87] reported on the performance of a $Zn_{45}Au_{30}Cu_{25}$ alloy in 2013. It was demonstrated that the thermal hysteresis of this material is far lower than that of nickel-titanium alloys, and that there was not as severe a shift in the transformation temperatures as a result of thermal cycling [87].

The numerical modelling and simulation of SMA behaviour should also be further developed. The modelling of the phase transitions in an SMA is complex due to the dependence of the transformation behaviour on a number of parameters such as the applied heat treatment and the cold working. As an example, the microstructure of Nitinol will contain a mixture of different phases during a phase transformation, or before the final transformation temperature of a phase has been passed. This makes the modelling of Nitinol very complicated, and it would be of interest to be able to accurately simulate changing material properties, for example with respect to stress and temperature.

The number of applications for which tuneable and multiple frequency technology using SMAs could be adopted is vast. For example, a Nitinol transducer could be used for tuneable surgical cutting, or projection and receiver systems could be developed where one tuned frequency could be used for the projection signal, and another tuned frequency of the same device could act as the receiving frequency. The effect of temperature on the damping of Nitinol should also be considered, as it has been reported that alterations in temperature can significantly affect damping, and thus impact on the useful energy which is conferred to the SMA [232]. The damping capacity of Nitinol in the martensite phase and also as stress-induced martensite is very high compared to that in the austenite phase [221]. This means that for a Nitinol transducer, a greater energy input would likely be required to generate a displacement amplitude if the Nitinol exists in the martensite phase compared to the same displacement amplitude for the material in the austenite phase. Electrical circuits could also be developed which match the impedance between a tuneable device and the driving system, thus optimising the energy transfer. However, in order to achieve this, it is evident that further financial investment is required if these recommendations can be properly developed.

Appendix A

List of publications

Peer-reviewed, journal

1. A. Feeney and M. Lucas, “Smart cymbal transducers with nitinol end caps tunable to multiple operating frequencies,” (Invited), *IEEE Transactions on Ultrasonics, Ferroelectrics and Frequency Control*, vol. 61, no. 10, pp. 1709-1719, 2014.
2. P. Harkness, M. McRobb, P. Lützkendorf, R. Milligan, A. Feeney, and C. Clark, “Development status of AEOLDOS - a deorbit module for small satellites,” *Advances in Space Research*, vol. 54, no. 1, pp. 82-91, 2014.
3. F. Bejarano, A. Feeney, and M. Lucas, “A cymbal transducer for power ultrasonics applications,” *Sensors and Actuators A: Physical*, vol. 210, pp. 182-189, 2014.

Conference

1. A. Feeney and M. Lucas, “Characterisation of nitinol for the design of tuneable transducers,” *Proceedings of the 2014 International Conference on Experimental Mechanics*, University of Cambridge, Cambridge, UK, July 2014.
2. A. Feeney and M. Lucas, “Nitinol cymbal transducers for power ultrasonics applications,” *Proceedings of the 9th International Conference on Advances in Experimental Mechanics*, the British Society for Strain Measurement, University of Cardiff, Wales, United Kingdom, September 2013.

3. M. Lucas and A. Feeney, "Smart cymbal transducers with nitinol end-caps for power ultrasonics applications," *Proceedings of the 2013 Joint UFFC, EFTF, and PFM Symposium*, Prague, Czech Republic, pp. 1440-1443, July 2013.
4. A. Feeney and M. Lucas, "An investigation of the vibration response of a superelastic nitinol cymbal transducer," *Proceedings of the 2013 International Congress on Ultrasonics*, Singapore, pp. 321-326, May 2013.
5. F. Bejarano, A. Feeney, and M. Lucas, "Vibration characterisation of cymbal transducers for power ultrasonics applications," *Journal of Physics: Conference Series*, IOP Publishing, vol. 382, no. 1, p. 012063, 2012.
6. F. Bejarano, A. Feeney, and M. Lucas, "Optimisation of a cymbal transducer for its use as driver of a high-power ultrasonic cutting device for bone surgery," *Proceedings of the 41st UIA Symposium*, San Francisco, USA, April 2012.
7. A. Feeney, F. Bejarano, and M. Lucas, "Dynamics characterisation of cymbal transducers for power ultrasonics applications," *Proceedings of the 41st UIA Symposium*, San Francisco, USA, April 2012.
8. T. Sinn, M. McRobb, A. Wujek, J. Skogby, M. Zhang, M. Vasile, G. Tibert, J. Wepler, A. Feeney, J. Russell, F. Rogberg, and J. Wang, "REXUS 12 Suaineadh experiment: deployment of a web in microgravity conditions using centrifugal forces," *IAC 2011: Proceedings of the 62nd International Astronautical Congress*, IAC-11-A2.3.7, Paper ID 9425, September 2011.

References

- [1] T. D. Rossing, *Introduction to acoustics*. Springer Handbook of Acoustics, Springer, 2007.
- [2] S. Paul and M. M. Richter, “A dynamic automatic noisy speech recognition (DANSR) system for a single-channel hybrid noisy industrial environment,” *Proceedings of Meetings on Acoustics, Acoustical Society of America*, vol. 19, no. 1, pp. 1–9, 2013.
- [3] W. J. Gastmeier and B. Howe, “Recent studies of infrasound from industrial sources,” *Canadian Acoustics*, vol. 36, no. 3, pp. 58–59, 2008.
- [4] V. Anes, D. Montalvão, A. Ribiero, M. Freitas, and M. Fonte, “Design and instrumentation of an ultrasonic fatigue testing machine,” *Proceedings of the 5th International Conference on Very High Cycle Fatigue, Berlin, Germany*, pp. 421–426, 2011.
- [5] J. Zhang, W. J. Hughes, R. J. Meyer, Jr., K. Uchino, and R. E. Newnham, “Cymbal array: a broad band sound projector,” *Ultrasonics*, vol. 37, no. 8, pp. 523–529, 2000.
- [6] R. J. Meyer, Jr., W. J. Hughes, T. C. Montgomery, D. C. Markley, and R. E. Newnham, “Design of and fabrication improvements to the cymbal transducer aided by finite element analysis,” *Journal of Electroceramics*, vol. 8, no. 2, pp. 163–174, 2002.
- [7] C. Kannan, R. Dhilsha, P. M. Rajeshwari, S. Jacob, and M. A. Atmanand, “Performance evaluation of cymbal hydrophones for underwater applications,” *International Journal of Mechanical Engineering and Applications*, vol. 1, no. 2, pp. 43–48, 2013.

- [8] A. L. Kholkin, N. A. Pertsev, and A. V. Goltsev, *Piezoelectricity and crystal symmetry*. Piezoelectric and Acoustic Materials for Transducer Applications, Springer, 2008.
- [9] S. O. R. Moheimani and A. J. Fleming, *Piezoelectric Transducers for Vibration Control and Damping*. Springer, 2006.
- [10] J. Zhang, A.-C. Hladky-Hennion, W. J. Hughes, and R. E. Newnham, “Modeling and underwater characterization of cymbal transducers and arrays,” *IEEE Transactions on Ultrasonics, Ferroelectrics and Frequency Control*, vol. 48, pp. 560–568, March 2001.
- [11] J. Zhang, W. J. Hughes, P. Bouchilloux, R. J. Meyer, Jr., K. Uchino, and R. E. Newnham, “A class V flextensional transducer: the cymbal,” *Ultrasonics*, vol. 37, no. 6, pp. 387–393, 1999.
- [12] R. J. Meyer, Jr., A. Dogan, C. Yoon, S. M. Pilgrim, and R. E. Newnham, “Displacement amplification of electroactive materials using the cymbal extensional transducer,” *Sensors and Actuators A: Physical*, vol. 87, no. 3, pp. 157–162, 2001.
- [13] J. F. Tressler, R. E. Newnham, and W. J. Hughes, “Capped ceramic underwater sound projector: the “cymbal” transducer,” *Journal of the Acoustical Society of America*, vol. 105, pp. 591–600, February 1999.
- [14] J. F. Tressler, W. Cao, K. Uchino, and R. E. Newnham, “Finite element analysis of the cymbal-type flextensional transducer,” *IEEE Transactions on Ultrasonics, Ferroelectrics and Frequency Control*, vol. 45, pp. 1363–1369, September 1998.
- [15] A. Dogan and E. Uzgur, “Size and material effects on cymbal transducer for actuator applications,” *Ferroelectrics*, vol. 331, no. 1, pp. 53–63, 2006.
- [16] R. E. Newnham, J. Zhang, and R. Meyer, Jr., “Cymbal transducers: a review,” *Proceedings of the IEEE International Symposium on Applied Ferroelectrics*, pp. 29–32, 2000.

- [17] P. Ochoa, M. Villegas, J. L. Pons, P. Leidinger, and J. F. Fernández, “Tunability of cymbals as piezocomposite transducers,” *Journal of Electroceramics*, vol. 14, no. 3, pp. 221–229, 2005.
- [18] C.-L. Sun, S. S. Guo, W. P. Li, Z. B. Xing, G. C. Liu, and X.-Z. Zhao, “Displacement amplification and resonance characteristics of the cymbal transducers,” *Sensors and Actuators A: Physical*, vol. 121, no. 1, pp. 213–220, 2005.
- [19] R. E. Newnham, J. Zhang, S. Alkoy, R. Meyer, W. J. Hughes, A.-C. Hladky-Hennion, J. Cochran, and D. Markley, “Cymbal and BB underwater transducers and arrays,” *Materials Research Innovations*, vol. 6, no. 3, pp. 89–91, 2002.
- [20] A. C. Mathieson, *Nonlinear characterisation of power ultrasonic devices used in bone surgery*. PhD thesis, University of Glasgow, 2012.
- [21] R. E. Newnham, S. Alkoy, A.-C. Hladky, W. J. Hughes, D. C. Markley, R. J. Meyer, Jr., and J. Zhang, “Underwater flat-panel transducer arrays,” *OCEANS, 2001, MTS/IEEE Conference and Exhibition*, vol. 3, pp. 1529–1535, 2001.
- [22] P. Ochoa, J. L. Pons, M. Villegas, and J. F. Fernandez, “Effect of bonding layer on the electromechanical response of the cymbal metal-ceramic piezocomposite,” *Journal of the European Ceramic Society*, vol. 27, no. 2-3, pp. 1143–1149, 2007.
- [23] S. Lin, “An improved cymbal transducer with combined piezoelectric ceramic ring and metal ring,” *Sensors and Actuators A: Physical*, vol. 163, no. 1, pp. 266–276, 2010.
- [24] F. Bejarano, A. Feeney, and M. Lucas, “Vibration characterisation of cymbal transducers for power ultrasonics applications,” *Journal of Physics: Conference Series, IOP Publishing*, vol. 382, no. 1, p. 012063, 2012.
- [25] F. Bejarano, A. Feeney, and M. Lucas, “A cymbal transducer for power ultrasonics applications,” *Sensors and Actuators A: Physical*, vol. 210, pp. 182–189, 2014.

- [26] E. Maione, K. K. Shung, R. J. Meyer, Jr., J. W. Hughes, R. E. Newnham, and N. B. Smith, "Transducer design for a portable ultrasound enhanced transdermal drug-delivery system," *IEEE Transactions on Ultrasonics, Ferroelectrics and Frequency Control*, vol. 49, pp. 1430–1436, October 2002.
- [27] N. B. Smith, S. Lee, E. Maione, R. B. Roy, S. McElligott, and K. K. Shung, "Ultrasound-mediated transdermal transport of insulin in vitro through human skin using novel transducer designs," *Ultrasound in Medicine & Biology*, vol. 29, no. 2, pp. 311–317, 2003.
- [28] S. Lee, R. E. Newnham, and N. B. Smith, "Short ultrasound exposure times for noninvasive insulin delivery in rats using the lightweight cymbal array," *IEEE Transactions on Ultrasonics, Ferroelectrics and Frequency Control*, vol. 51, pp. 176–180, February 2004.
- [29] E. J. Park, J. Werner, and N. B. Smith, "Ultrasound mediated transdermal insulin delivery in pigs using a lightweight transducer," *Pharmaceutical Research*, vol. 24, no. 7, pp. 1396–1401, 2007.
- [30] M. R. Prausnitz and R. Langer, "Transdermal drug delivery," *Nature Biotechnology*, vol. 26, no. 11, pp. 1261–1268, 2008.
- [31] C.-L. Sun, K. H. Lam, S. H. Choy, H. L. W. Chan, X.-Z. Zhao, and C. L. Choy, "High sensitivity cymbal-based accelerometer," *Review of Scientific Instruments*, vol. 77, no. 3, p. 036109, 2006.
- [32] L. Shuang, L. Denghua, and G. Xiangyu, "Non-linear error compensation of voltage sensitivity for vibration accelerometer based on cymbal transducer," *8th International Conference in Electronic Measurement and Instruments, IEEE, 2007*, pp. 563–566, 2007.
- [33] L. Denghua, G. Xiangyu, Z. Feng, and Z. Zhixin, "Research on nonlinearity property of piezoelectric vibration accelerometer based on cymbal transducer," *Proceedings of the 2010 IEEE International Conference on Information and Automation (ICIA)*, pp. 930–934, 2010.

- [34] H. W. Kim, S. Priya, K. Uchino, and R. E. Newnham, “Piezoelectric energy harvesting under high pre-stressed cyclic vibrations,” *Journal of Electroceramics*, vol. 15, no. 1, pp. 27–34, 2005.
- [35] S. R. Anton and H. A. Sodano, “A review of power harvesting using piezoelectric material (2003-2006),” *Smart Materials and Structures*, vol. 16, no. 3, pp. R1–R21, 2007.
- [36] J. b. Yuan, X. b. Shan, T. Xie, and W. s. Chen, “Energy harvesting with a slotted-cymbal transducer,” *Journal of Zhejiang University SCIENCE A*, vol. 10, no. 8, pp. 1187–1190, 2009.
- [37] J. Yuan, X. Shan, T. Xie, and W. Chen, “Modeling and improvement of a cymbal transducer in energy harvesting,” *Journal of Intelligent Material Systems and Structures*, vol. 21, no. 8, pp. 765–771, 2010.
- [38] X. Li, M. Guo, and S. Dong, “A flex-compressive-mode piezoelectric transducer for mechanical vibration/strain energy harvesting,” *IEEE Transactions on Ultrasonics, Ferroelectrics and Frequency Control*, vol. 58, pp. 698–703, April 2011.
- [39] C. Mo, D. Arnold, W. C. Kinsel, and W. W. Clark, “Modeling and experimental validation of unimorph piezoelectric cymbal design in energy harvesting,” *Journal of Intelligent Material Systems and Structures*, vol. 24, no. 7, pp. 828–836, 2012.
- [40] J. Palosaari, M. Leinonen, J. Hannu, J. Juuti, and H. Jantunen, “Energy harvesting with a cymbal type piezoelectric transducer from low frequency compression,” *Journal of Electroceramics*, vol. 28, no. 4, pp. 214–219, 2012.
- [41] J. F. Tressler and R. E. Newnham, “Doubly resonant cymbal-type transducers,” *IEEE Transactions on Ultrasonics, Ferroelectrics and Frequency Control*, vol. 44, pp. 1175–1177, September 1997.
- [42] J. J. Vaitekunas, F. B. Stulen, and E. S. Grood, “Effects of frequency on the cutting ability of an ultrasonic surgical instrument,” *Proceedings of the 31st*

- Annual Ultrasonic Industry Association Symposium, Atlanta, USA*, pp. 1–10, October 2001.
- [43] G. McGuinness, J. A. McGeough, G. Gavin, and B. O’Daly, “Surgical cutting and ablation by energy based devices: principles and applications,” *Dublin Institute of Technology Conference Papers*, pp. 1–12, June 2011.
- [44] G. Pavlíková, R. Foltán, M. Burian, E. Horká, S. Adámek, A. Hejčl, T. Hanzelka, and J. Šedý, “Piezosurgery prevents brain tissue damage: an experimental study on a new rat model,” *International Journal of Oral and Maxillofacial Surgery*, vol. 40, pp. 840–844, 2011.
- [45] G. C. Robertson, “Ultrasonic surgical instrument blades,” US Patent 8,057,498 B2, 2011.
- [46] K. L. Houser, “Ultrasonic surgical instrument and cartilage and bone shaping blades therefor,” US Patent 8,236,019 B2, 2012.
- [47] M. C. Sharp, “Ultrasonic dental scaler selectively tunable either manually or automatically,” US Patent 6,190,167 B1, 2001.
- [48] P. W. Lorraine, “Ultrasonic transducer with selectable center frequency,” US Patent 5,381,068, 1995.
- [49] M. S. Seyed-Bolorforosh, M. Greenstein, T. R. Gururaja, and H. Yoshida, “Tunable acoustic resonator for clinical ultrasonic transducers,” US Patent 5,438,554, 1995.
- [50] R. Feng, Y. Zhao, C. Zhu, and T. J. Mason, “Enhancement of ultrasonic cavitation yield by multi-frequency sonication,” *Ultrasonics Sonochemistry*, vol. 9, no. 5, pp. 231–236, 2002.
- [51] P. A. Tatake and A. B. Pandit, “Modelling and experimental investigation into cavity dynamics and cavitation yield: influence of dual frequency ultrasound sources,” *Chemical Engineering Science*, vol. 57, no. 22, pp. 4987–4995, 2002.

- [52] G. Servant, J. L. Laborde, A. Hita, J. P. Caltagirone, and A. Gérard, “On the interaction between ultrasound waves and bubble clouds in mono- and dual-frequency sonoreactors,” *Ultrasonics Sonochemistry*, vol. 10, no. 6, pp. 347–355, 2003.
- [53] A. H. Barati, M. Mokhtari-Dizaji, H. Mozdarani, Z. Bathaie, and Z. M. Hassan, “Effect of exposure parameters on cavitation induced by low-level dual-frequency ultrasound,” *Ultrasonics Sonochemistry*, vol. 14, no. 6, pp. 783–789, 2007.
- [54] H.-L. Liu and C.-M. Hsieh, “Single-transducer dual-frequency ultrasound generation to enhance acoustic cavitation,” *Ultrasonics Sonochemistry*, vol. 16, no. 3, pp. 431–438, 2009.
- [55] V. S. Moholkar, “Mechanistic optimization of a dual frequency sonochemical reactor,” *Chemical Engineering Science*, vol. 64, no. 24, pp. 5255–5267, 2009.
- [56] S. A. Thompson, “An overview of nickel-titanium alloys used in dentistry,” *International Endodontic Journal*, vol. 33, no. 4, pp. 297–310, 2000.
- [57] R. E. Newnham, “Piezoelectric sensors and actuators: smart materials,” *Proceedings of the 46th IEEE Frequency Control Symposium, 1992*, pp. 513–524, 1992.
- [58] T. A. Hall, “Joint, a laminate, and a method of preparing a nickel-titanium alloy member surface for bonding to another layer of metal,” US Patent 5,242,759, 1993.
- [59] J. A. Shaw, C. B. Churchill, and M. A. Iadicola, “Tips and tricks for characterizing shape memory alloy wire: part 1 - differential scanning calorimetry and basic phenomena,” *Experimental Techniques*, vol. 32, no. 5, pp. 55–62, 2008.
- [60] J. V. Humbeeck, “Non-medical applications of shape memory alloys,” *Materials Science and Engineering: A*, vol. 273, pp. 134–148, 1999.
- [61] J. Chen, Z. Li, and Y. Y. Zhao, “A high-working-temperature CuAlMnZr shape memory alloy,” *Journal of Alloys and Compounds*, vol. 480, no. 2, pp. 481–484, 2009.

- [62] C. Bach, M. N. Kabir, A. Goyal, R. Malliwal, S. Kachrilas, M. E. E. Howairis, J. Masood, N. Buchholz, and I. Junaid, "A self-expanding thermolabile nitinol stent as a minimally invasive treatment alternative for ureteral strictures in renal transplant patients," *Journal of Endourology*, vol. 27, no. 12, pp. 1543–1545, 2013.
- [63] P. K. Kumar and D. C. Lagoudas, *Introduction to shape memory alloys*. Shape memory alloys - modeling and engineering applications, Springer, 2008.
- [64] S. Daly, G. Ravichandran, and K. Bhattacharya, "Stress-induced martensitic phase transformation in thin sheets of nitinol," *Acta Materialia*, vol. 55, no. 10, pp. 3593–3600, 2007.
- [65] A. S. Paula, J. P. H. G. Canejo, R. M. S. Martins, and F. M. B. Fernandes, "Effect of thermal cycling on the transformation temperature ranges of a Ni-Ti shape memory alloy," *Materials Science and Engineering: A*, vol. 378, no. 1, pp. 92–96, 2004.
- [66] J. M. McNaney, V. Imbeni, Y. Jung, P. Papadopoulos, and R. O. Ritchie, "An experimental study of the superelastic effect in a shape-memory nitinol alloy under biaxial loading," *Mechanics of Materials*, vol. 35, no. 10, pp. 969–986, 2003.
- [67] R. J. Meyer, Jr. and R. E. Newnham, "Flextensional transducers with shape memory caps for tunable devices," *Journal of Intelligent Material Systems and Structures*, vol. 11, no. 3, pp. 199–205, March 2000.
- [68] X. Huang and Y. Liu, "Effect of annealing on the transformation behaviour and superelasticity of NiTi shape memory alloy," *Scripta Materialia*, vol. 45, no. 2, pp. 153–160, 2001.
- [69] D. Stöckel, "Nitinol - a material with unusual properties," *Endovascular Update*, no. 1, pp. 1–8, 1998.
- [70] P. Poncet, "Nitinol medical device design considerations," *Strain*, vol. 2, no. 4, pp. 1–12, 2000.

- [71] A. R. Pelton, J. DiCello, and S. Miyazaki, "Optimisation of processing and properties of medical grade nitinol wire," *Minimally Invasive Therapy & Allied Technologies*, vol. 9, no. 1, pp. 107–118, 2000.
- [72] Correspondence between A. Feeney and M. Ehrlinspiel (*Memry GmbH*), 4th December 2013.
- [73] A. L. McKelvey and R. O. Ritchie, "On the temperature dependence of the superelastic strength and the prediction of the theoretical uniaxial transformation strain in nitinol," *Philosophical Magazine A*, vol. 80, no. 8, pp. 1759–1768, 2000.
- [74] T. Duerig, "Shape memory alloys, in ASM Handbook, Volume 23: Materials for Medical Devices," *ASM International*, pp. 237–250, June 2012.
- [75] V. V. Rubanik, Jr., V. V. Rubanik, and V. V. Klubovich, "The influence of ultrasound on shape memory behavior," *Materials Science and Engineering: A*, vol. 481, pp. 620–622, 2008.
- [76] S. Belyaev, A. Volkov, and N. Resnina, "Alternate stresses and temperature variation as factors of influence of ultrasonic vibration on mechanical and functional properties of shape memory alloys," *Ultrasonics*, vol. 54, no. 1, pp. 84–89, 2014.
- [77] G. Kuhn and L. Jordan, "Fatigue and mechanical properties of nickel-titanium endodontic instruments," *Journal of Endodontics*, vol. 28, no. 10, pp. 716–720, 2002.
- [78] A. R. Pelton, S. M. Russell, and J. DiCello, "The physical metallurgy of nitinol for medical applications," *Journal of Metals*, vol. 55, no. 5, pp. 33–37, 2003.
- [79] M. Narayanan, R. W. Schwartz, and D. Zhou, "Stress-biased cymbals using shape memory alloys," *Journal of the American Ceramic Society*, vol. 90, no. 4, pp. 1122–1129, 2007.
- [80] J. M. G. Fuentes, P. Gumpel, and J. Strittmatter, "Phase change behavior of nitinol shape memory alloys," *Advanced Engineering Materials*, vol. 4, no. 7, pp. 437–452, 2002.

- [81] D. D. Shin, K. P. Mohanchandra, and G. P. Carman, “High frequency actuation of thin film NiTi,” *Sensors and Actuators A: Physical*, vol. 111, no. 2, pp. 166–171, 2004.
- [82] T. M. Adams, S. R. Kirkpatrick, Z. Wang, and A. Siahmakoun, “NiTi shape memory alloy thin films deposited by co-evaporation,” *Materials Letters*, vol. 59, no. 10, pp. 1161–1164, 2005.
- [83] R. M. S. Martins, N. Schell, R. J. C. Silva, and F. M. B. Fernandes, “Structural in situ studies of shape memory alloy (SMA) Ni-Ti thin films,” *Nuclear Instruments and Methods in Physics Research B: Beam Interactions with Materials and Atoms*, vol. 238, no. 1, pp. 319–322, 2005.
- [84] K. Otsuka and X. Ren, “Recent developments in the research of shape memory alloys,” *Intermetallics*, vol. 7, no. 5, pp. 511–528, 1999.
- [85] T. Tadaki, Y. Nakata, and K. Shimizu, “Thermal cycling effects in an aged Ni-rich Ti-Ni shape memory alloy,” *Transactions of the Japan Institute of Metals*, vol. 28, no. 11, pp. 883–890, 1987.
- [86] R. Zarnetta, R. Takahashi, M. L. Young, A. Savan, Y. Furuya, S. Thienhaus, B. Maaß, M. Rahim, J. Frenzel, H. Brunken, Y. S. Chu, V. Srivastava, R. D. James, I. Takeuchi, G. Eggeler, and A. Ludwig, “Identification of quaternary shape memory alloys with near-zero thermal hysteresis and unprecedented functional stability,” *Advanced Functional Materials*, vol. 20, no. 12, pp. 1917–1923, 2010.
- [87] Y. Song, X. Chen, V. Dabade, T. W. Shield, and R. D. James, “Enhanced reversibility and unusual microstructure of a phase-transforming material,” *Nature*, vol. 502, no. 7469, pp. 85–88, 2013.
- [88] H. C. Ling and R. Kaplow, “Stress-induced shape changes and shape memory in the r and martensite transformations in equiatomic NiTi,” *Metallurgical Transactions A*, vol. 12, no. 12, pp. 2101–2111, 1981.

- [89] S. Miyazaki and K. Otsuka, "Deformation and transition behavior associated with the R-phase in Ti-Ni alloys," *Metallurgical Transactions A*, vol. 17, no. 1, pp. 53–63, 1986.
- [90] J. Uchil, K. P. Mohanchandra, K. K. Mahesh, and K. G. Kumara, "Thermal and electrical characterization of r-phase dependence on heat-treat temperature in nitinol," *Physica B: Condensed Matter*, vol. 253, no. 1, pp. 83–89, 1998.
- [91] J. Eaton-Evans, J. M. Dulieu-Barton, E. G. Little, and I. A. Brown, "Observations during mechanical testing of nitinol," *Proceedings of the Institution of Mechanical Engineers, Part C: Journal of Mechanical Engineering Science*, vol. 222, no. 2, pp. 97–105, 2008.
- [92] L. Xu and R. Wang, "The effect of annealing and cold-drawing on the super-elasticity of the Ni-Ti shape memory alloy wire," *Modern Applied Science*, vol. 4, pp. 109–115, December 2010.
- [93] D. Guyomar, N. Aurelle, C. Richard, P. Gonnard, and L. Eyraud, "Nonlinearities in Langevin transducers," *Proceedings of the IEEE Ultrasonics Symposium*, vol. 2, pp. 925–928, 1994.
- [94] N. Aurelle, D. Guyomar, C. Richard, P. Gonnard, and L. Eyraud, "Nonlinear behaviour of an ultrasonic transducer," *Ultrasonics*, vol. 34, no. 2, pp. 187–191, 1996.
- [95] M. Arafa and A. Baz, "On the nonlinear behavior of piezoelectric actuators," *Journal of Vibration and Control*, vol. 10, no. 3, pp. 387–398, 2004.
- [96] M. Cartmell, *Introduction to Linear, Parametric and Nonlinear Vibrations*. Chapman and Hall, 1st ed., 1990.
- [97] T. J. Royston and B. H. Houston, "Modeling and measurement of nonlinear dynamic behavior in piezoelectric ceramics with application to 1-3 composites," *The Journal of the Acoustical Society of America*, vol. 104, no. 5, pp. 2814–2827, 1998.

- [98] I. S. Caleon and R. Subramaniam, "From pythagoras to sauveur: tracing the history of ideas about the nature of sound," *Physics Education*, vol. 42, pp. 173–179, March 2007.
- [99] T. L. Szabo, *Diagnostic Ultrasound Imaging, Inside Out*. Elsevier Inc., 2004.
- [100] W. P. Mason, "Sonics and ultrasonics: early history and applications," *IEEE Transactions on Sonics and Ultrasonics*, vol. SU-23, no. 4, pp. 224–232, July 1976.
- [101] C. H. Sherman and J. L. Butler, *Transducers and arrays for underwater sound*. Springer, 2007.
- [102] R. Goldman, *Ultrasonic Technology*. New York, Reinhold Publishing Corporation, 1962.
- [103] A. P. Cracknell, *Ultrasonics*. Wykeham Publications, 1980.
- [104] E. G. Richardson, *Ultrasonic Physics*. Elsevier Publishing Company, 1962.
- [105] J. Blitz, *Fundamentals of Ultrasonics*. Butterworth & Co. (Publishers) Ltd., 1963.
- [106] D. Knorr, M. Zenker, V. Heinz, and D.-U. Lee, "Applications and potential of ultrasonics in food processing," *Trends in Food Science & Technology*, vol. 15, no. 5, pp. 261–266, 2004.
- [107] I. Donald and U. Abdulla, "Further advances in ultrasonic diagnosis," *Ultrasonics*, vol. 5, pp. 8–12, January 1967.
- [108] I. Donald, "Sonar - the story of an experiment," *Ultrasound in Medicine & Biology*, vol. 1, pp. 109–117, 1974.
- [109] K. D. Rolt, "History of the flextensional electroacoustic transducer," *The Journal of the Acoustical Society of America*, vol. 87, no. 3, pp. 1340–1349, 1990.
- [110] L. H. Royster, "The flextensional concept: a new approach to the design of underwater acoustic transducers," *Applied Acoustics*, vol. 3, pp. 117–126, 1970.

- [111] J. F. Lindberg, “Material challenges for transducer designers in the 21st century,” *Proceedings of SPIE*, vol. 4699, pp. 485–498, 2002.
- [112] B. P. Naidu, A. B. Rao, N. S. Prasad, and K. Trinath, “Modal analysis of class V flextensional transducer,” *Proceedings of the 2009 IEEE International Symposium on Ocean Electronics (SYMPOLE)*, pp. 122–127, 2009.
- [113] J. Zhang, *Miniaturized flextensional transducers and arrays*. PhD thesis, The Pennsylvania State University, 2000.
- [114] G. Brigham and B. Glass, “Present status in flextensional transducer technology,” *The Journal of the Acoustical Society of America*, vol. 68, no. 4, pp. 1046–1052, 1980.
- [115] A. Dogan, K. Uchino, and R. E. Newnham, “Composite piezoelectric transducer with truncated conical endcaps “cymbal”,” *IEEE Transactions on Ultrasonics, F*, vol. 44, pp. 597–605, May 1997.
- [116] J. F. Tressler, S. Alkoy, A. Dogan, and R. E. Newnham, “Functional composites for sensors, actuators and transducers,” *Composites Part A: Applied Science and Manufacturing*, vol. 30, no. 4, pp. 477–482, 1999.
- [117] E. C. N. Silva, S. Nishiwaki, and N. Kikuchi, “Design of piezocomposite materials and piezoelectric transducers using topology optimization - part II,” *Archives of Computational Methods in Engineering*, vol. 6, no. 3, pp. 191–215, 1999.
- [118] J. F. Fernández, A. Dogan, J. T. Fielding, K. Uchino, and R. E. Newnham, “Tailoring the performance of ceramic-metal piezocomposite actuators, ‘cymbals’,” *Sensors and Actuators A: Physical*, vol. 65, no. 2, pp. 228–237, 1998.
- [119] J. Zhang, A.-C. Hladky-Hennion, W. J. Hughes, and R. E. Newnham, “A miniature class V flextensional cymbal transducer with directional beam patterns: the double-driver,” *Ultrasonics*, vol. 39, no. 2, pp. 91–95, 2001.
- [120] T. R. Howarth and J. F. Tressler, “Thin, lightweight, low frequency acoustic projectors for shallow water environments,” *AeroSense 2000, International Society for Optics and Photonics*, pp. 1510–1517, 2000.

- [121] J. F. Tressler, T. R. Howarth, and D. Huang, "A comparison of the underwater acoustic performance of single crystal vs. piezoelectric ceramic based cymbal projectors," *Proceedings of OCEANS 2003, IEEE*, vol. 5, pp. 2372–2379, 2003.
- [122] A. Dogan, J. F. Fernandez, K. Uchino, and R. E. Newnham, "The "cymbal" electromechanical actuator," *Proceedings of the Tenth IEEE International Symposium on Applications of Ferroelectrics, ISAF'96*, vol. 1, pp. 213–216, 1996.
- [123] A. Dogan, E. Uzgur, D. C. Markley, R. J. Meyer, Jr., A.-C. Hladky-Hennion, and R. E. Newnham, "Materials for high performance cymbal transducers," *Journal of Electroceramics*, vol. 13, no. 1-3, pp. 403–407, 2004.
- [124] J. Zhang, W. J. Hughes, A.-C. Hladky-Hennion, and R. E. Newnham, "Concave cymbal transducers," *Material Research Innovations*, vol. 2, no. 5, pp. 252–255, 1999.
- [125] O. A. Ganilova, M. Lucas, and A. Cardoni, "An analytical model of cymbal transducer dynamics. Radial vibration of a piezoelectric disc," *Proceedings of the Institution of Mechanical Engineers, Part C: Journal of Mechanical Engineering Science*, vol. 225, no. 5, pp. 1077–1086, 2011.
- [126] E. Uzgur, D. C. Markley, M. Guo, B. Snyder, R. J. Meyer, Jr., A. Dogan, and R. E. Newnham, "Pressure dependence of cymbal transducers," *IEEE Journal of Oceanic Engineering*, vol. 32, pp. 408–415, April 2007.
- [127] J. Zhang and R. E. Newnham, "Class V flexensional transducer with directional beam patterns," US Patent 6,614,143 B2, 2003.
- [128] K. H. Lam, X. X. Wang, and H. L. W. Chan, "Lead-free piezoceramic cymbal actuator," *Sensors and Actuators A: Physical*, vol. 125, no. 2, pp. 393–397, 2006.
- [129] P. Ochoa, M. Villegas, and J. F. Fernández, "Resonant frequency response of cymbal transducer," *Ferroelectrics*, vol. 273, no. 1, pp. 321–326, 2002.
- [130] P. Ochoa, J. L. Pons, M. Villegas, and J. F. Fernandez, "Advantages and limitations of cymbals for sensor and actuator applications," *Sensors and Actuators A: Physical*, vol. 132, no. 1, pp. 63–69, 2006.

- [131] Y. Ke, T. Guo, and J. Li, “A new-style, slotted-cymbal transducer with large displacement and high energy transmission,” *IEEE Transactions on Ultrasonics, Ferroelectrics and Frequency Control*, vol. 51, pp. 1171–1177, September 2004.
- [132] M. Narayanan and R. W. Schwartz, “Design, fabrication and finite element modeling of a new wagon wheel flextensional transducer,” *Journal of Electroceramics*, vol. 24, no. 3, pp. 205–213, 2008.
- [133] M. Narayanan and R. W. Schwartz, “Stress-biased cymbals incorporating a shape memory alloy,” US Patent 2009/0303839 A1, 2009.
- [134] L. Luo, Y. Tang, F. Wang, C. He, and H. Luo, “Displacement amplification and electric characteristics of modified rectangular cymbal transducers using electroactive materials,” *Solid State Communications*, vol. 143, no. 6-7, pp. 321–325, 2007.
- [135] S. Wu, Q. Zhang, Z. Huang, and J. Xiong, “Research on frequency characteristics of spherical-cymbal transducers,” *2009 International Conference on Measuring Technology and Mechatronics Automation, IEEE*, vol. 1, pp. 514–518, 2009.
- [136] T. R. Howarth, “Piezoelectric generator and method,” US Patent 8,030,825 B2, 2011.
- [137] P. Ochoa, J. L. Pons, M. Villegas, and J. F. Fernandez, “Mechanical stress and electric potential in cymbal piezoceramics by FEA,” *Journal of the European Ceramic Society*, vol. 25, no. 12, pp. 2457–2461, 2005.
- [138] O. Kastner, *First principles modelling of shape memory alloys*. Springer, 2012.
- [139] F. J. Gil and J. A. Planell, “Shape memory alloys for medical applications,” *Proceedings of the Institution of Mechanical Engineers, Part H: Journal of Engineering in Medicine*, vol. 212, no. 6, pp. 473–488, 1998.
- [140] B. Donohue, “Developing a good memory: Nitinol shape memory alloy,” *Today’s Machining World*, pp. 42–48, March 2009.

- [141] S. Saadat, J. Salichs, M. Noori, Z. Hou, H. Davoodi, I. Bar-on, Y. Suzuki, and A. Masuda, “An overview of vibration and seismic applications of NiTi shape memory alloy,” *Smart Materials and Structures*, vol. 11, no. 2, pp. 218–229, 2002.
- [142] D. Stoeckel, “The shape memory effect - phenomenon, alloys and applications,” *Proceedings: Shape Memory Alloys for Power Systems EPRI*, no. 1, pp. 1–13, 1995.
- [143] T. Duerig, A. Pelton, and D. Stöckel, “An overview of nitinol medical applications,” *Materials Science and Engineering: A*, vol. 273, pp. 149–160, 1999.
- [144] D. Stoeckel, “Nitinol medical devices and implants,” *Minimally Invasive Therapy & Allied Technologies*, vol. 9, no. 2, pp. 81–88, 2000.
- [145] T. Duerig, D. Stoeckel, and D. Johnson, “SMA - smart materials for medical applications,” *Proceedings of SPIE, European Workshop on Smart Structures in Engineering and Technology, International Society for Optics and Photonics*, vol. 4763, pp. 7–15, 2003.
- [146] D. Stoeckel, A. Pelton, and T. Duerig, “Self-expanding nitinol stents: material and design considerations,” *European Radiology*, vol. 14, no. 2, pp. 292–301, 2004.
- [147] X. Liu, Y. Wang, D. Yang, and M. Qi, “The effect of ageing treatment on shape-setting and superelasticity of a nitinol stent,” *Materials Characterization*, vol. 59, no. 4, pp. 402–406, 2008.
- [148] S. B. Alapati, W. A. Brantley, M. Iijima, W. A. T. Clark, L. Kovarik, C. Buie, J. Liu, and W. B. Johnson, “Metallurgical characterization of a new nickel-titanium wire for rotary endodontic instruments,” *Journal of Endodontics*, vol. 35, no. 11, pp. 1589–1593, 2009.
- [149] A. Jalaeefar and B. Asgarian, “Experimental investigation of mechanical properties of nitinol, structural steel, and their hybrid component,” *Journal of Materials in Civil Engineering*, vol. 25, no. 10, pp. 1498–1505, 2012.

- [150] F. M. B. Fernandes, K. K. Mahesh, and A. dos Santos Paula, "Thermomechanical treatments for Ni-Ti alloys," *Shape Memory Alloys-Processing, Characterization and Applications, InTech*, 2013.
- [151] T. W. Duerig, "Some unsolved aspects of nitinol," *Materials Science and Engineering: A*, vol. 438-440, pp. 69–74, 2006.
- [152] T. Breczko, V. V. Rubanik, and V. V. Rubanik, Jr., "Study of behaviour NiTi-alloy under action of ultrasound," *International Workshop on Nondestructive Testing and Computer Simulations in Science and Engineering, International Society for Optics and Photonics, SPIE*, vol. 3687, pp. 310–312, 1999.
- [153] H.-C. Kim, Y.-I. Yoo, and J.-J. Lee, "Development of a NiTi actuator using a two-way shape memory effect induced by compressive loading cycles," *Sensors and Actuators A: Physical*, vol. 148, no. 2, pp. 437–442, 2008.
- [154] C. Tang, W. M. Huang, C. C. Wang, and H. Purnawali, "The triple-shape memory effect in NiTi shape memory alloys," *Smart Materials and Structures*, vol. 21, no. 8, p. 085022, 2012.
- [155] T. C. Madison and H. G. Frey, "Multiple-frequency transducer," US Patent 3,952,216, 1976.
- [156] J. F. Lindberg, "Parametric dual mode transducer," US Patent 4,373,143, 1983.
- [157] S. C. Thompson, "Broadband radial vibrator transducer with multiple resonant frequencies," US Patent 4,604,542, 1986.
- [158] S. C. Thompson, "Broadband multi-resonant longitudinal vibrator transducer," US Patent 4,633,119, 1986.
- [159] C. M. Stearns, D. J. Erickson, and L. M. Izzo, "Dual frequency sonar transducer assembly," US Patent 5,515,342, 1996.
- [160] P. Mauchamp and A. Flesch, "Multi-purpose ultrasonic slotted array transducer," US Patent 6,537,224 B2, 2003.
- [161] R. Porzio, "Multiple frequency sonar transducer," US Patent 7,535,801 B1, 2009.

- [162] J. Chen, Q. C. Xu, M. Blaszkievicz, R. J. Meyer, Jr., and R. E. Newnham, "Lead zirconate titanate films on nickel-titanium shape memory alloys: SMARTIES," *Journal of the American Ceramic Society*, vol. 75, no. 10, pp. 2891–2892, 1992.
- [163] R. E. Newnham, Q. C. Xu, and M. Blaszkievicz, "Frequency agile sonic transducer," US Patent 5,166,907, 1992.
- [164] H. A. B. Alwi, B. V. Smith, and J. R. Carey, "Factors which determine the tunable frequency range of tunable transducers," *The Journal of the Acoustical Society of America*, vol. 100, no. 2, pp. 840–847, 1996.
- [165] K. A. Williams, G. T.-C. Chiu, and R. J. Bernhard, "Passive-adaptive vibration absorbers using shape memory alloys," *Proceedings of SPIE*, vol. 3668, pp. 630–641, 1999.
- [166] A. B. Flatau, M. J. Dapino, and F. T. Calkins, "High bandwidth tunability in a smart vibration absorber," *Journal of Intelligent Material Systems and Structures*, vol. 11, pp. 923–929, December 2000.
- [167] G. R. Ashurst, "Ambient temperature shape memory alloy actuator," US Patent 6,427,712 B1, 2002.
- [168] P. Fenton, F. Harrington, and P. Westhaver, "Disposable ultrasonic soft tissue cutting and coagulation systems," US Patent 2003/0212332 A1, 2003.
- [169] M. Mertmann and G. Vergani, "Design and application of shape memory actuators," *The European Physical Journal Special Topics*, vol. 158, no. 1, pp. 221–230, 2008.
- [170] C. Peters, D. Maurath, W. Schock, and Y. Manoli, "Novel electrically tunable mechanical resonator for energy harvesting," *Proceedings of PowerMEMS*, pp. 253–256, 2008.
- [171] M. Li, Y. Wen, P. Li, and J. Yang, "A magnetostrictive/piezoelectric laminate transducer based vibration energy harvester with resonance frequency tunability," *Sensors, 2011 IEEE*, pp. 1768–1771, 2011.

- [172] N. V. Datla, M. Honarvar, T. M. Nguyen, B. Konh, K. Darvish, Y. Yu, A. P. Dicker, T. K. Podder, and P. Hutapea, "Towards a nitinol actuator for an active surgical needle," *Proceedings of the ASME 2012 Conference on Smart Materials, Adaptive Structures and Intelligent Systems, American Society of Mechanical Engineers*, pp. 265–269, 2012.
- [173] R. E. Newnham, A. Dogan, D. C. Markley, J. F. Tressler, J. Zhang, E. Uzgur, R. J. Meyer, Jr., A.-C. Hladky-Hennion, and W. J. Hughes, "Size effects in capped ceramic underwater sound projectors," *OCEANS'02 MTS/IEEE*, vol. 4, pp. 2315–2321, 2002.
- [174] <http://uk.rs-online.com/web/p/steel-rods-bars-tubes-hexagonals/4377168/>.
- [175] M. Niinomi, "Mechanical properties of biomedical titanium alloys," *Materials Science and Engineering: A*, vol. 243, no. 1, pp. 231–236, 1998.
- [176] L. Rubio, J. Fernández-Sáez, and C. Navarro, "Determination of dynamic fracture-initiation toughness using three-point bending tests in a modified hopkinson pressure bar," *Experimental Mechanics*, vol. 43, no. 4, pp. 379–386, 2003.
- [177] J. Y. Kao, C. C. Tsao, S. S. Wang, and C. Y. Hsu, "Optimization of the EDM parameters on machining Ti-6Al-4V with multiple quality characteristics," *The International Journal of Advanced Manufacturing Technology*, vol. 47, no. 1-4, pp. 395–402, 2010.
- [178] S. Arbós-Torrent, B. Ganapathisubramani, and R. Palacios, "Leading- and trailing-edge effects on the aeromechanics of membrane aerofoils," *Journal of Fluids and Structures*, vol. 38, pp. 107–126, 2013.
- [179] C. Casavola, C. Pappalettere, and F. Tattoli, "Experimental and numerical study of static and fatigue properties of titanium alloy welded joints," *Mechanics of Materials*, vol. 41, no. 3, pp. 231–243, 2009.
- [180] H. D. Al-Budairi, *Design and analysis of ultrasonic horns operating in longitudinal and torsional vibration*. PhD thesis, University of Glasgow, 2012.

- [181] “Piezoelectric ceramics, Morgan Electro Ceramics.” Booklet, November 2007.
- [182] <http://piezomat.org/materials/52>.
- [183] A. V. Carazo, *Novel piezoelectric transducers for high voltage measurements*. PhD thesis, Universitat Politècnica de Catalunya, 2000.
- [184] R. A. R. Rashid, S. Sun, G. Wang, and M. S. Dargusch, “An investigation of cutting forces and cutting temperatures during laser-assisted machining of the Ti6Cr5Mo5V4Al beta titanium alloy,” *International Journal of Machine Tools & Manufacture*, vol. 63, pp. 58–69, 2012.
- [185] I. Harismendy, R. Miner, A. Valea, R. Llano-Ponte, F. Mujika, and I. Mondragon, “Strain rate and temperature effects on the mechanical behaviour of epoxy mixtures with different crosslink densities,” *Polymer*, vol. 38, no. 22, pp. 5573–5577, 1997.
- [186] K. B. Gatzwiller, K. B. Ginn, A. Betts, and S. Morel, “Practical aspects of successful laser Doppler vibrometry based measurements,” *Fortschritte der Akustik*, vol. 29, pp. 873–879, 2003.
- [187] M. Umeda, S. Takahashi, Y. Sasaki, and S. U. K. Nakamura, “Vibration stress and temperature dependence of piezoelectric resonators with lead-zirconate-titanate ceramics,” *Electronics and Communications in Japan (Part II: Electronics)*, vol. 83, no. 9, pp. 1–7, 2000.
- [188] N. M. M. Maia and J. M. M. Silva, “Modal analysis identification techniques,” *Philosophical Transactions of the Royal Society A: Mathematical, Physical and Engineering Sciences*, vol. 359, no. 1778, pp. 29–40, 2001.
- [189] <http://www.polytec.com/uk/solutions/vibration-measurement/basic-principles-of-vibrometry/>.
- [190] A. Cardoni, *Characterising the dynamic response of ultrasonic cutting devices*. PhD thesis, University of Glasgow, 2003.

- [191] Y.-S. Lee, C.-H. Ryu, H.-S. Kim, and Y.-J. Choi, "A study on the free drop impact of a cask using commercial FEA codes," *Nuclear Engineering and Design*, vol. 235, no. 20, pp. 2219–2226, 2005.
- [192] G. Nader, E. C. N. Silva, and J. C. Adamowski, "Effective damping value of piezoelectric transducer determined by experimental techniques and numerical analysis," *ABCM Symposium Series in Mechatronics*, vol. 1, pp. 271–279, 2004.
- [193] V. J. Logeeswaran, F. E. H. Tay, M. L. Chan, F. S. Chau, and Y. C. Liang, "First harmonic (2f) characterisation of resonant frequency and Q-factor of micromechanical transducers," *Analog Integrated Circuits and Signal Processing*, vol. 37, no. 1, pp. 17–33, 2003.
- [194] T. W. Duerig and A. R. Pelton, "Ti-Ni shape memory alloys," *Materials Properties Handbook: Titanium Alloys*, pp. 1035–1048, 1994.
- [195] <http://jmmedical.com/resources/211/Measuring-Transformation-Temperatures-in-Nitinol-Alloys.html>, Accessed 17th February 2014.
- [196] V. Antonucci, G. Faiella, M. Giordano, F. Mennella, and L. Nicolais, "Electrical resistivity study and characterization during NiTi phase transformations," *Thermochimica Acta*, vol. 462, no. 1, pp. 64–69, 2007.
- [197] R. Brammajyosula, V. Buravalla, and A. Khandelwal, "Model for resistance evolution in shape memory alloys including R-phase," *Smart Materials and Structures*, vol. 20, no. 3, p. 035015, 2011.
- [198] Thass, "Understanding unexpected results by DSC," *Application Note AN 34, SII Nanotechnology Inc*, pp. 1–2.
- [199] C. G. Slough, "A study of the nitinol solid-solid transition by DSC," *TA Instruments, Inc., TA 346*, pp. 1–5, 2007.
- [200] D. W. Berzins and H. W. Roberts, "Phase transformation changes in thermocycled nickel-titanium orthodontic wires," *Dental Materials*, vol. 26, no. 7, pp. 666–674, 2010.

- [201] M. Drexel, G. Selvaduray, and A. Pelton, “The effects of cold work and heat treatment on the properties of nitinol wire,” *Medical Device Materials IV: Proceedings from the Materials & Processes for Medical Devices Conference 2007*, pp. 114–119, 2008.
- [202] K. Kus and T. Brezko, “DSC-investigations of the effect of annealing temperature on the phase transformation behaviour in Ni-Ti shape memory alloy,” *Materials Physics and Mechanics*, vol. 9, no. 1, pp. 75–83, 2010.
- [203] “Perkin Elmer Diamond DSC - Quick Reference Guide, Engineering Instrument Pool.” Booklet.
- [204] N. Gao, M. J. Starink, and T. G. Langdon, “Using differential scanning calorimetry as an analytical tool for ultrafine-grained metals processed by severe plastic deformation,” *Materials Science and Technology*, vol. 25, no. 6, pp. 687–698, 2009.
- [205] “User’s Manual, FLIR B Series and FLIR T Series, FLIR.” Booklet, February 2010.
- [206] Y. Liu and H. Xiang, “Apparent modulus of elasticity of near-equiatomic NiTi,” *Journal of Alloys and Compounds*, vol. 270, no. 1, pp. 154–159, 1998.
- [207] R. R. Adharapurapu, *Phase transformations in nickel-rich nickel-titanium alloys: influence of strain-rate, temperature, thermomechanical treatment and nickel composition on the shape memory and superelastic characteristics*. PhD thesis, University of California, San Diego, 2007.
- [208] D. Favier, Y. Liu, L. Orgéas, A. Sandel, L. Debove, and P. Comte-Gaz, “Influence of thermomechanical processing on the superelastic properties of a ni-rich nitinol shape memory alloy,” *Materials Science and Engineering: A*, vol. 429, no. 1-2, pp. 130–136, 2006.
- [209] S. Rajagopalan, A. L. Little, M. A. M. Bourke, and R. Vaidyanathan, “Elastic modulus of shape-memory NiTi from in situ neutron diffraction during

- macroscopic loading, instrumented indentation, and extensometry,” *Applied Physics Letters*, vol. 86, no. 8, p. 081901, 2005.
- [210] K. E. Perry and P. E. Labossiere, “Phase transformations in nitinol and challenges for numerical modeling,” *Medical Device Materials II, ASM International*, pp. 131–134, 2004.
- [211] J. Olbricht, A. Yawny, J. L. Pelegrina, A. Dlouhy, and G. Eggeler, “On the stress-induced formation of R-phase in ultra-fine-grained ni-rich NiTi shape memory alloys,” *Metallurgical and Materials Transactions A*, vol. 42, no. 9, pp. 2556–2574, 2011.
- [212] D. Z. Li and Z. C. Feng, “Dynamic properties of pseudoelastic shape memory alloys,” *Smart Structures and Materials’ 97, International Society for Optics and Photonics*, pp. 715–725, 1997.
- [213] X. M. Wang and Z. F. Yue, “FEM prediction of the pseudoelastic behavior of NiTi SMA at different temperatures with one temperature testing results,” *Computational Materials Science*, vol. 39, no. 3, pp. 697–704, 2007.
- [214] N. Vidal, E. Asua, J. Feuchtwanger, A. Garcia-Arribas, J. Gutierrez, and J. M. Barandiaran, “FEM simulation of the nitinol wire,” *The European Physical Journal Special Topics*, vol. 158, no. 1, pp. 39–44, 2008.
- [215] <http://memry.com/nitinol-iq/nitinol-fundamentals/fabrication-heat-treatment>.
- [216] <http://memry.com/products-services/melting/nitinol-alloys>.
- [217] T. L. Turner, “Thermomechanical response of shape memory alloy hybrid composites,” *NASA/TM-2001-210656*, January 2001.
- [218] T. L. Turner, “Structural acoustic response of a shape memory alloy hybrid composite panel (lessons learned),” *SPIE’s 9th Annual International Symposium on Smart Structures and Materials, International Society for Optics and Photonics*, vol. 4701, pp. 592–603, 2002.

- [219] K. Wu, S. K. Dalip, Y. Liu, and Z. Pu, “Damping characteristics of r-phase NiTi shape memory alloys,” *In Smart Structures & Materials '95, International Society for Optics and Photonics*, pp. 139–148, 1995.
- [220] H.-C. Kim, J. Yum, B. Hur, and G. S.-P. Cheung, “Cyclic fatigue and fracture characteristics of ground and twisted nickel-titanium rotary files,” *Journal of Endodontics*, vol. 36, no. 1, pp. 147–152, 2010.
- [221] M. C. Piedboeuf, R. Gauvin, and M. Thomas, “Damping behaviour of shape memory alloys: strain amplitude, frequency and temperature effects,” *Journal of Sound and Vibration*, vol. 214, no. 5, pp. 885–901, 1998.
- [222] S. K. Wu and H. C. Lin, “Damping characteristics of TiNi binary and ternary shape memory alloys,” *Journal of Alloys and Compounds*, vol. 355, no. 1, pp. 72–78, 2003.
- [223] <http://memry.com/nitinol-iq/nitinol-fundamentals/physical-properties>.
- [224] <http://jmmedical.com/resources/120/Nitinol-Specification-Guidelines.html>.
- [225] E. Abel, H. Luo, M. Pridham, and A. Slade, “Issues concerning the measurement of transformation temperatures of NiTi alloys,” *Smart Materials and Structures*, vol. 13, no. 5, pp. 1110–1117, 2004.
- [226] N. Morgan, *The stability of NiTi shape memory alloys and actuator applications*. PhD thesis, Cranfield University, 1999.
- [227] M. H. Wu, “Fabrication of nitinol materials and components,” *Proceedings of the International Conference on Shape Memory and Superelastic Technologies*, pp. 285–292, 2001.
- [228] S. W. Robertson, *On the mechanical properties and microstructure of Nitinol for biomedical stent applications*. PhD thesis, University of California, Berkeley, 2006.
- [229] B. S. Shariat, Y. Liu, and G. Rio, “Finite element computational modelling and experimental investigation of perforated NiTi plates under tension,” *Materials Research Bulletin*, vol. 48, no. 12, pp. 5099–5104, 2013.

- [230] T. A. Thayer, M. D. Bagby, R. N. Moore, and R. J. DeAngelis, “X-ray diffraction of nitinol orthodontic arch wires,” *American Journal of Orthodontics and Dentofacial Orthopedics*, vol. 107, no. 6, pp. 604–612, 1995.
- [231] B. Reedlunn, S. Daly, L. Hector, Jr., P. Zavattieri, and J. Shaw, “Tips and tricks for characterizing shape memory wire part 5: full-field strain measurement by digital image correlation,” *Experimental Techniques*, vol. 37, no. 3, pp. 62–78, 2013.
- [232] S.-Y. Cha, S.-Y. Jeong, J. H. Park, S. E. Park, J. K. Park, and C. R. Cho, “Thermodynamic and structural characterization of high- and low- temperature nitinol,” *Journal of the Korean Physical Society*, vol. 49, pp. S580–S583, December 2006.